UNIVERSIDAD NACIONAL AUTÓNOMA DE MÉXICO

PROGRAMA DE DOCTORADO EN CIENCIAS BIOMÉDICAS
INSTITUTO DE FISIOLOGÍA CELULAR

"AUMENTO EN LA ACTIVIDAD DE LA EXPORTINA 1/CRM1 EN NEURONAS CONTRIBUYE CON LA DISFUNCIÓN AUTOFAGICA Y EL ESTABLECIMIENTO DE LA SENESCENCIA NEURONAL EN EL ENVEJECIMIENTO"

TESIS
QUE PARA OPTAR POR EL GRADO DE:
DOCTORA EN CIENCIAS BIOMÉDICAS

PRESENTA:
GENTLY ELISA GOROSTIETA SALAS

DIRECTORA DE TESIS:
DRA. SUSANA CASTRO OBREGÓN
INSTITUTO DE FISIOLOGÍA CEULAR

COMITÉ TUTOR:
DRA. ANA BRÍGIDA CLORINDA ARIAS ÁLVAREZ
INSTITUTO DE INVESTIGACIONES BIOMÉDICAS
DR. MARTIN GUSTAVO PEDRAZA ALVA
INSTITUTO DE BIOTECNOLOGÍA

CIUDAD DE MÉXICO, SEPTIEMBRE 2021.

El presente trabajo fue realizado en el departamento de Neurodesarrollo y Fisiología, en la División de Neurosciencias del Instituto de Fisiología Celular, bajo la guía de la Dra. Susana Castro Obregón, y con financiamiento de los proyectos CONACyT FC921 y PAPIIT-UNAM IN206518. Gracias al apoyo económico brindado por la beca CONACyT 58932 y la "Red colaborativa de Investigación Traslacional para el Envejecimiento Saludable de la Ciudad de México (RECITES)" fue posible la culminación de este proyecto.

“Why would we choose to focus on problems that impact small groups of people if we could address the problem that impacts everyone—especially if, in doing so, we could significantly impact all those other, smaller problems?”

— David A. Sinclair

AGRADECIMIENTOS

A la Dra. Beatriz Aguilar Maldonado por el apoyo técnico brindando a lo largo de este proyecto.

A la Bióloga Teresa Montiel Montes por toda la guía y apoyo técnico.

Al Dr. Abraham Rosas Arellano y la Dra. Ruth Rincón Heredia de la Unidad de Microscopia del IFC por toda su ayuda en la obtención y análisis de imágenes de microscopia confocal.

A la M.V.Z Claudia Rivera Cerecedo y la Unidad del Bioterio del IFC.

A Sandra Daniela Rodríguez Montaño de la Unidad de Histología del IFC.

A la M.C. Ana María Escalante y Francisco Pérez de la Unidad de Computo del IFC.

A los ingenieros Aurey Galván Lobato y Manuel Ortínez Benavides del Taller de Mantenimiento.

AGRADECIMIENTOS PERSONALES

A la Dra. Susana Castro Obregón por abrirme las puertas de su laboratorio, por compartir sus ideas, conocimientos y experiencia. Por guiarme en el desarrollo de este proyecto y de otras ideas, pero especialmente, gracias por enseñarme que “el diablo está en los detalles”.

A mis compañeros y amigos. Daniel, Cristian, Pilar, Gabriel, Miguel, Jorge, Melanie y Bety. Hicieron que todo fuera más simple, más lógico y más divertido durante estos años. Gracias por su apoyo y por todos los buenos momentos que compartimos.

A Abraham, por compartir sus conocimientos y su tiempo conmigo, gracias por ser tan paciente.

DEDICATORIA

A mi familia, gracias por su apoyo no solo en este proceso sino a lo largo de mi vida. A mis padres a quienes nunca voy a terminar de agradecerles su cariño y comprensión. A mis hermanos, Isaac, Angélica y David porque siempre encuentro consejo, apoyo, risas y mucho amor a su lado, son el mejor equipo. A Sebas por llegar a esta familia y ser mi compañero de travesuras.

INDICE

Enhanced activity of exportin-1/ CRM1 in neurons contributes to autophagy dysfunction and senescent features in old mouse brain.

Abstract

Aging affects all living species at different rates and seems to be a consequence of a combined action of a set of different molecular and cellular mechanisms, including autophagy failure and cellular senescence. In the brain, dysfunctional autophagy is related with loss of cognitive abilities. While autophagy can either promote or suppress cellular senescence in proliferating cells, in postmitotic cells such as neurons, autophagy impairment promotes cellular senescence. Exportin-1/CRM1 (Chromosomal region Maintenance 1) regulates nucleocytoplasmic traffic of hundreds of proteins, including TFEB, the principal transcription factor involved in autophagy and lysosomal genes expression, as well as STAT3, another modulator of autophagy. Accordingly, reduction of CRM1 expression promotes autophagy, extends lifespan in worms and protects from neurodegeneration in flies, via TFEB nuclear enrichment. Interestingly, enhanced CRM1 activity is observed in skin fibroblast from Hutchingson-Gilford progeria syndrome patients and old healthy individuals, and its overexpression induces cellular senescence in normal fibroblasts.

In this work we tested the hypothesis that impaired autophagic flux during brain aging could be due to an Exportin-1/CRM1 accumulation, and hence cytoplasmic localization of autophagy promoting transcription factors such as TFEB and STAT3. We found enhanced Exportin-1/CRM1 activity concomitant with an increase of cytoplasmic TFEB and STAT3 in senescent neurons having autophagic flux impairment in old mice brains. We demonstrated that CRM1 inhibition on an *in vitro* model of neuronal senescence restored nuclear TFEB localization, improved autophagic flux and reduced a senescent marker in neurons. Collectively, our data suggest that enhanced CRM1-mediated export of proteins during brain aging contributes to autophagy impairment and triggers neuronal senescence.

Key words: Autophagy, TFEB, CRM1/EXPORTIN-1/XPO1, Neuronal Senescence, Aging, mammalian brain.

Aumento en la actividad de la exportina 1/CRM1 en neuronas contribuye con la disfunción autofágica y el establecimiento de la senescencia neuronal en el envejecimiento

Resumen

El envejecimiento afecta a todos los organismos en diferentes grados y tazas, y es caracterizado por diversos cambios celulares y moleculares que en conjunto se conocen como “signos” del envejecimiento, entre ellos una autofagia disfuncional y senescencia celular. En el cerebro, la disfunción autofágica se relaciona con la pérdida de las capacidades cognitivas. Mientras que la autofagia puede promover o evitar la senescencia celular en células mitóticas, en células postmitóticas como las neuronas las fallas en la autofagia promueven la senescencia celular. La exportina-1/CRM1 (Chromosomal region Maintenance 1) transporta del núcleo al citoplasma cientos de proteínas, incluyendo TFEB, el principal factor de transcripción involucrado en la expresión de genes de proteínas lisosomales y de la autofagia. De igual forma, transporta STAT3 del núcleo al citoplasma, otro modulador de la autofagia. Consistentemente, reducir la expresión de CRM1 activa el flujo autofágico, extiende la esperanza de vida en nemátodos y evita la neurodegeneración en moscas, todo vía el enriquecimiento nuclear de TFEB. De forma interesante, fibroblastos de piel de pacientes con progeria de Hutchinson-Gilford y fibroblastos de donadores saludables de edad avanzada muestran un aumento en los niveles y la actividad de CRM1; además, la sobreexpresión de CRM1 induce senescencia celular en fibroblastos de piel de personas jóvenes.

En este trabajo, probamos la hipótesis de que las fallas en la autofagia durante el envejecimiento del cerebro podrían ser causadas por la acumulación de CRM1, que altera la localización subcelular de factores de transcripción necesarios para el inicio de la autofagia como TFEB y STAT3. Encontramos que, en el cerebro de ratones viejos, el incremento en la actividad de CRM1 es acompañada por un incremento en la localización citosólica de TFEB y STAT3 en neuronas senescentes que tienen alterado el flujo autofagico. Demostramos que la inhibición farmacológica de CRM1 en un modelo *in vitro* de senescencia neuronal restaura la localización nuclear de TFEB, mejora el flujo autofagico y reduce una de las características de senescencia en las neuronas. En conjunto, nuestros datos confirman un aumento en la actividad de CRM1 en el envejecimiento y sugieren que esto promueve el exporte de proteínas pro-autofágicas, con lo que contribuye a la disfunción autofágica y la inducción de la senescencia neuronal.

Palabras clave: Autofagia, TFEB, CRM1/EXPORTINA-1/XPO1, senescencia neuronal, envejecimiento, cerebro de mamífero.

Abreviaturas

AD	Enfermedad de Alzheimer (del inglés Alzheimer´s disease)
ALS	Esclerosis lateral amiotrófica (del inglés Amyotrofic lateral sclerosis)
ALR	Regeneración autofágica de los lisosomas (del inglés Autophagic lysosome reformation)
AP1	Proteína activadora 1 (del inglés Activator protein 1)
ATG	Gen relacionado a **a**u**t**ofa**g**ia (del inglés Autophagy related genes)
ATM	Ataxia telangiectasia mutado (del inglés Ataxia-telangiectasia mutated)
ATR	Ataxia telagiectasia RAD3 relacionada (del inglés Ataxia telangiectasia and Rad3-related protein)
BSA	Albúmina de suero bovino (del inglés Bovine serum albumin)
CA3	Cuerno de Amón 3
CCF	Fragmentos de cromatina en el citoplasma (del inglés Cytoplasmic chromatin fragments)
CDK	Cinasa dependiente de ciclina (del inglés Cyclin dependent protein kinase)
CMA	Autofagia mediada por chaperonas (del inglés Chaperon mediated autophagy)
CRM1	Proteína de mantenimiento cromosómico 1 (del inglés Chromosomal region maintenance 1)
CLEAR	Red de expresión y regulación coordinada de lisosomas (del inglés Coordinated lysosomal expression and regulation)
CQ	Cloroquina
DIV	Días *in vitro*
FIP200	Proteína de interacción focal (del inglés Focal interacting protein of 200 kD)
GEF	Factor intercambiador de guanina (del inglés Guanine exchange factor)
GFP	Proteína verde fluorescente (del inglés Green fluorescent protein)
H3k9me	Histona 3 trimetilada en lisina 9
HGPS	Progeria de Hutchinson-Gilford (del inglés Hutchinson-Gilford progeria syndrome)
HP1	Proteína de heterocromatina 1 (del inglés Heterochromatin protein 1)
Hsc	Proteína de choqué térmico citosólica (del inglés Heat shock cognate)
IL6	Interleucina 6
IL8	Interleucina 8
LAMP2	Proteína de membrana asociada a lisosoma tipo 2 (del inglés Lysosome-associated membrane protein 2)
LC3	Proteína de cadena ligera 3 asociada a microtúbulos
LMB	Leptomicina B
MAPK	Proteínas cinasas activadas por mitógenos
NES	Señal de exporte nuclear (del inglés Nuclear export signal)
NLS	Señal de importe nuclear (del inglés Nuclear localization signal)
NPC	Complejo del poro nuclear (del inglés Nuclear pore complex)
NTRs	Receptores nucleares (del Inglés Nuclear transport receptors)
Nup	Nucleoporina
mHTT	Huntingtina mutante (del inglés Mutant Huntingtin)
mTOR	Blanco de la rapamicina
NF-κB	Factor nuclear kappa B
PD	Enfermedad de Parkinson (del inglés Parkinson´s disease)
PI3KC3	Fosfatidil-inositol-3-cinasa clase 3

P53BP	Proteína de unión a p53
PE	Fosfatidiletanolamina
PFA	Paraformaldehido
PLL	Poli-L-lisina
PBS	Tampón fosfato salino (del inglés Phosphate-buffered saline)
PP2A	Fosfatasa 2
PRC1	Complejo represor polycomb 1 (del inglés Polycomb represor complex 1)
PRh	Perirhinal
ROS	Especies reactivas de oxígeno (del inglés Reactive Oxygen species)
SA-β-gal	β-galactosidasa asociada a senescencia
SAHF	Focos de heterocromatina asociados a senescencia (del inglés Senescence associated heterochomatin foci)
SASP	Fenotipo de secreción asociado a senescencia (del inglés Senescence associated secretory phenotype)
SNARE	Receptor de la proteína unida a NSF soluble
STX17	Sintaxina 17
TFEB	Factor de transcripción EB
TUJ-1	Anticuerpo anti-beta-III-tubulin
ULK	Cinasa tipo UNC-51

1. Introducción

1.1. *Envejecimiento*

El envejecimiento se define como la pérdida progresiva de las funciones biológicas, que afecta a todos los organismos en diferentes grados y que aumentan la probabilidad de muerte. El proceso de envejecimiento se caracteriza por diversos cambios moleculares y celulares que en conjunto se denominan “signos del envejecimiento”. Entre ellos se encuentran la inestabilidad genómica, acortamiento y daño a los telóremos, cambios epigenéticos, perdida de proteostasis, alteraciones en la regulación de nutrimentos, disfunción mitocondrial, senescencia celular, agotamiento de células troncales y comunicación intracelular alterada [1]. Además, estudios recientes demuestran que durante el envejecimiento hay una disminución en la permeabilidad de la membrana nuclear y aumento en el transporte núcleo-citoplasma [2–4], apuntando a nuevos marcadores asociados con el envejecimiento.

Aunque el envejecimiento no es considerado una enfermedad, si es el principal factor de riesgo para padecer diversas enfermedades crónicas como el cáncer, enfermedades cardiovasculares, metabólicas como la diabetes y enfermedades neurodegenerativas [5]. En la actualidad, la esperanza de vida de las personas sigue en aumento, aunque no se acompaña por un aumento en la esperanza de vida saludable. Esto, favorece que las personas mayores padezcan varias enfermedades de manera simultánea, por más de una década. En este sentido, comprender los mecanismos celulares y moleculares que subyacen al proceso de envejecimiento resulta de particular relevancia para el desarrollo de estrategias terapéuticas que permitan reducir o retrasar dichos cambios.

El cerebro, al igual que otros órganos es afectado por el envejecimiento. La pérdida de las habilidades cognitivas que incluyen la disminución en la capacidad de aprendizaje y la memoria, se asocian con fallas en la proteostasis, en especial con una macroautofagia disfuncional, así como con la acumulación de células senescentes. Esta relación ha sido observada tanto en el envejecimiento fisiológico como patológico del cerebro [6,7]. En este contexto, diversas estrategias experimentales que activan la autofagia o eliminan células senescentes en el cerebro, aumentan la esperanza de vida [8] y mejoran la memoria [7,9,10].

El mecanismo que desencadena las fallas en la autofagia y la senescencia celular durante el envejecimiento del cerebro, sigue bajo estudio. Sin embargo, el aumento en el transporte núcleo-citoplasma se ha propuesto como un candidato que podría explicar las fallas en la autofagia y el establecimiento del fenotipo senescente [2,11].

1.1.1. *Autofagia*

La autofagia es un proceso catabólico altamente conservado que dirige la degradación de componentes intracelulares dentro del lisosoma. De acuerdo al mecanismo utilizado para llevar los cargos hasta el lumen del lisosoma, la autofagia en mamíferos se ha clasificado en: microautofagia, autofagia mediada por chaperonas y macroautofagia [12].

1.1.2. *Microautofagia*

La microautofagia es la forma menos estudiada de autofagia y en mamíferos se refiere a la degradación de componentes intracelulares que son engullidos directamente en endosomas tardíos y cuerpos mutivesiculares en lugar de lisosomas [12,13]. En cambio, en hongos y plantas la microautofagia ocurre en la vacuola, organelo equivalente a los lisosomas.

1.1.3. *Autofagia mediada por chaperonas*

Durante la autofagia mediada por chaperonas (CMA por sus siglas en inglés de chaperon mediated autophagy), las proteínas seleccionadas para su degradación son asistidas por un complejo de chaperonas. Una vez identificados los cargos, estos son translocados a través de la membrana lisosomal y degradados. La CMA puede dividirse en 3 pasos: 1) reconocimiento, 2) translocación y desdoblamiento y 3) degradación [14] .

Para que se lleve a cabo el reconocimiento, las proteínas blanco deben ser identificadas por la chaperona citosolica Hsc70 en un motivo de 5 aminoácidos conocido como KFERQ (Lys-Phe-Glu-Arg-Gln). Este motivo, incluye un residuo de glutamina (Q), un residuo cargado positivamente como lisina (K) o arginina (R), un aminoácido hidrofóbico que puede ser fenilalanina (F) o valina (V), leucina (L) o isoleucina (I) y un residuo cargado negativamente como ácido glutámico (E) o ácido aspártico (D). Una vez que el cargo es reconocido, se forma un complejo proteína/Hsc70. Este complejo se une a la proteína de membrana asociada a lisosoma (LAMP2, por sus siglas en inglés de lysosome associated membrane protein 2) y como resultado de esta unión, LAMP2 se multimeriza formando un canal a través del cual las proteínas cargo serán desplegadas e importadas al lumen lisosomal. Finalmente, el cargo es degradado por el contacto con las hidrolasas lisosomales. Es interesante que el motivo KFERQ se puede crear por modificaciones post-traduccionales que incorporen cargas negativas por ejemplo a través de la fosforilación o acetilación. Esto aumenta el número de proteínas que pueden ser degradadas por esta vía [13,15].

Este tipo de autofagia también se atrofia con el envejecimiento, y podría estar relacionada a la inducción de la senescencia celular, como proponemos en la revisión que se presenta en el anexo 1 [15].

1.1.4. *Macroautofagia*

Este es el tipo de autofagia mejor caracterizado. En esta, los componentes intracelulares seleccionados para degradación son engullidos y dirigidos al lisosoma por una vesícula de doble membrana llamada autofagosoma [12]. Al inicio, se pensó que la macroautofagia era un proceso catabólico que solo se activaba en respuesta a la falta de nutrimentos y que tenía como función proporcionar a la célula biomoléculas esenciales a partir de la degradación de componentes intracelulares. Sin embargo, actualmente sabemos que la macroautofagia está involucrada en la regulación de diversos procesos celulares como el recambio de proteínas, la degradación de organelos dañados, la respuesta inflamatoria, la secreción no convencional [16], la integración del metabolismo [17] y el desarrollo de sinapsis en el caso del sistema nervioso [18,19].

1.1.5. *Mecanismo molecular de la macroautofagia*

La macroautofagia (en adelante autofagia) es un proceso complejo que requiere de la participación de diversas proteínas conocidas como ATG (gen relacionado a autofagia, por sus siglas en inglés). Cuando una señal de activación se presenta, estas proteínas trabajan en complejos y son reclutadas a una localización subcelular específica para dirigir la formación del autofagosoma y su eventual fusión con el lisosoma. Para comprender este proceso a detalle, se ha divido en 4 etapas [20,21]:

1. **Inicio:** Para que el proceso de la autofagia comience, es necesaria la activación del complejo ULK1/2. Este complejo, está formado por las proteínas ATG13, ATG101 y FIP200. En condiciones en las que la célula tiene nutrimentos y factores de crecimiento, el complejo mTORC1 está activo e inhibe por fosforilación al complejo ULK. Pero, en respuesta a estímulos como el estrés nutricional, ULK1/2 puede activarse por autofosforilacion, esto genera un cambio conformacional que permite la disociación del complejo mTORC1 y la defosforilación en sitios represores. Una vez que ULK se encuentra activo, puede fosforilar y activar al complejo de la fosfatidilinositol 3 cinasa de clase III (PI3KC3), esta proteína pertenece a su vez a un complejo formado por las proteínas PI3KC3, BECN1, AMBRA1 y ATG14. Cuando está activo, el complejo PI3KC3 produce fosfatidilinositiol 3-fosfato [PI(3)P] en la superficie de la membrana y recluta a proteínas de la familia WIPI que dan lugar a la formación del fagóforo (Figura 1).

2. **Elongación:** Para promover la elongación del fagóforo alrededor del cargo seleccionado para degradación, dos complejos tipo ubiquitina son necesarios. El primero, es el complejo ATG5-ATG12. Para que este complejo se forme se requiere la unión covalente de ATG12 a ATG5 y esta reacción es catalizada por una enzima tipo E1, la ATG7 y una enzima tipo E2, la ATG10. El complejo ATG5-ATG12, se forma constitutivamente después de la traducción de ATG5 y ATG12. Sin embargo, cuando se presenta un estímulo que activa la autofagia, ATG12-ATG5 interactúan con ATG16L formando un complejo multiproteico que es reclutado al fagóforo. El complejo ATG5-ATG12-ATG16L recién formado actúa como una enzima ligasa E3

y permitirá la segunda reacción de conjugación para lipidar a LC3-II. Por su parte, la proteína pro-LC3, es cortada por la proteasa de cisteína ATG4, produciendo la isoforma LC3-I. Cuando la autofagia se activa, la proteína LC3-I se une covalentemente a la fosfatidiletanolamina (PE), es decir se lipida en la superficie de la membrana del fagóforo. La forma lipidada de la proteína LC3-I es conocida como LC3-II y esta conjugación es catalizada primero por la enzima tipo E1, ATG7, luego por la enzima tipo E2, ATG3 y finalmente por el complejo ATG5-ATG12-ATG16L que actúa como una E3 ligasa. La proteína LC3-II es de relevancia particular para monitorear la vía autofágica porque se queda anclada a la membrana interna y externa del autofagosoma, de tal forma que su abundancia nos brinda información sobre la formación de nuevos autofagosomas (Figura 1). De hecho, la proteína verde fluorescente (GFP), fusionada a LC3 es usada ampliamente para el análisis de la formación de autofagosomas que se detectan como puntos en la célula. Como se mencionó anteriormente, el reconocimiento de cargos sucede durante la elongación del fagóforo. La proteína LC3 tiene un dominio de unión a receptores autofágicos como la proteína p62/SQSTM1. Por su parte, estos receptores autofágicos reconocen alguna marca molecular en el material a degradar, por ejemplo, proteínas ubiquitinadas, funcionando como un puente entre LC3 y los cargos a degradar. El papel de los receptores autofágicos es por tanto favorecer el reconocimiento de cargos y el crecimiento del fagóforo alrededor de ellos. Una vez que los extremos de esta doble membrana se cierran, se completa la formación del autofagosoma y la proteasa ATG4 remueve LC3-II de la membrana externa del autofagosoma, permitiendo la fusión con el lisosoma.

3. **Fusión:** La fusión del autofagosoma maduro con el lisosoma, requiere primero que estos se movilicen dentro de la célula para estar cerca físicamente. El transporte sucede a través de los microtúbulos y es mediado por la dineína. Mutaciones en la dineína que impiden el transporte resultan en una disminución en la fusión autofagosoma-lisosoma [22]. Pero, cuando autofagosoma y el lisosoma se encuentran en el mismo espacio, la fusión es mediada por RAB7, HPOS y proteínas Q-SNARE como sintaxina 17 (STX17) [23].

4. **Degradación y reciclaje:** Al completarse la fusión, el contenido del autofagosoma incluyendo el cargo, los receptores autofagicos como p62/SQSTM1 y LC3-II entran en contacto con las hidrolasas del lisosoma y son degradados. Los productos de la degradación incluyendo aminoácidos, azucares y ácidos grasos son transportados fuera del autolisosoma y liberados al citosol para ser reciclados en caso de que el estímulo inductor sea la falta de nutrimentos. Los autolisosomas son estructuras que se desintegran una vez que la autofagia ha terminado, a este paso se le conoce como ALR (regeneración autofagica de los lisosomas por sus siglas en inglés de autophagic lysosome reformation). Durante la ALR, la membrana del lisosoma es reciclada a través de la formación de estructuras tubulares compuestos de la membrana originalmente lisosomal; a partir de estas estructuras, los lisosomas se forman nuevamente a través de un proceso de escisión/gemación asistido por proteínas como clatrina que promueve la gemación, KIF5B que dirige la elongación y dinamina 2 cuya función es promover la escisión del proto-lisosoma (Figura 2) [24]. Inicialmente, estos nuevos lisosomas no son funcionales y su maduración

depende de la síntesis de nuevas enzimas lisosomales. Para este paso la actividad del factor de trascripción EF (TFEB) es determinante [25].

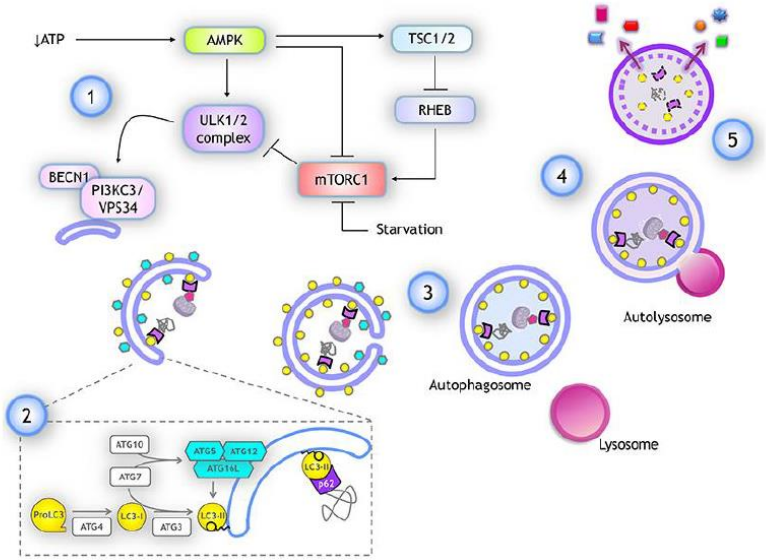

Figura 1. Mecanismo molecular de la macroautofagia. (*tomado de Acevo-Rodríguez et al., 2020)*

1.1.6. *Regulación transcripional de la autofagia*

El factor de transcripción EB (TFEB) es un miembro de la familia de factores de trascripción asociados a microftalmia (familia MiT). Es un regulador maestro que controla la expresión de genes lisosomales y asociados a la autofagia. En presencia de nutrientes, mTORC1 regula negativamente a TFEB. Cuando el complejo mTORC1 fosforila a TFEB en los residuos de serina 142 (S142) y serina 211 (S211), lo retiene en el citoplasma. La fosforilación en S211 es reconocida como un sitio de unión para proteínas 14-3-3 (unión que evita su transporte al núcleo), pero aún no está claro como la fosforilación en S142 retiene a TFEB en el citosol [26]. Sin embargo, la falta de nutrimentos o el estrés lisosomal, inhiben a mTORC1 y permiten que TFEB sea desfosforilado por la proteína fosfatasa 2A (PP2A). La forma desfosforilada de TFEB puede entonces ser importada al núcleo en donde lleva a cabo su actividad transcripcional [27,28].

En el núcleo, TFEB se une al motivo CLEAR (siglas en inglés que hacen referencia a la red de expresión y regulación coordinada lisosomal), favoreciendo la expresión de diversos genes lisosomales incluyendo hidrolasas y proteínas de la membrana lisosomal. Además, genes de la autofagia como *secuestrosoma* 1, *Becn1* y *Map1lc3a* son blancos de TFEB [29,30]. Otras modificaciones postraduccionales de TFEB como la acetilación y

desacetilación también regulan su actividad transcripcional. Cuando TFEB está en el núcleo, SIRT1 promueve su desacetilación en el residuo de lisina 116 (K116R) y esto aumenta la unión de TFEB a sus genes blanco [31].

En cuanto al mecanismo de degradación, no está claro si esta ocurre en el núcleo o únicamente en el citoplasma. Sin embargo, sabemos que en el citoplasma la forma fosforilada de TFEB (inactiva) es ubiqutinada por STUB1, una proteína E3 ligasa que promueve su degradación vía proteasoma [32]

El potencial terapéutico de TFEB como inductor de autofagia está en exploración y estrategias experimentales que aumentan su localización nuclear y por lo tanto promueven su actividad transcripcional, resultan en un aumento del flujo autofágico y mayor degradación de agregados proteicos tanto en modelos *in vivo* como *in vitro* [33,34].

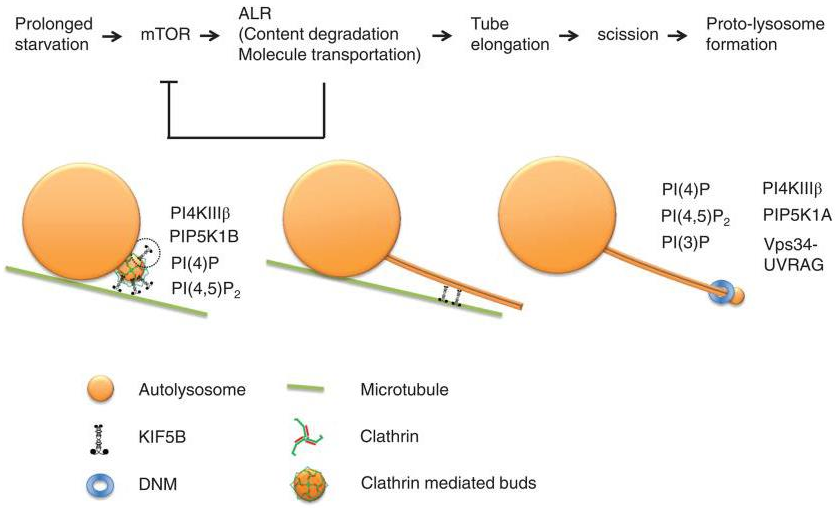

Figura 2. Reciclaje de lisosomas (tomando de *Chen & Yu., 2017)*

1.1.7. *Funciones de la autofagia*

La autofagia es un proceso constantemente activo en las células, identificado como autofagia basal y de particular relevancia para las células mitóticas y post-mitoticas porque favorece la homeostasis celular. Por ejemplo, se encarga de la degradación de organelos dañados como las mitocondrias, a esta forma de autofagia se le conoce como mitofagia [35]. La disfunción mitocondrial, es un signo del envejecimiento y se asocia con enfermedades neurodegenerativas como la enfermedad de Parkinson (PD por Parkinson´s disease) y Alzheimer (AD por Alzheimer´s disease) [36]. Aumentar la mitofagia en modelos de la AD, disminuye el estrés oxidante y mejora las habilidades cognitivas [37]. Por otro lado, la autofagia es un mecanismo con el que cuentan las células eucariontes para degradar agregados proteicos, a esta forma de autofagia se le denomina agrefagia y cuando es deficiente, los agregados se acumulan y resultan tóxicos para la célula. En particular, las células postmitoticas como las neuronas son susceptibles a la disfunción

autofagica en general, porque al no poder diluir insultos a través de la división celular, dependen totalmente de este mecanismo para mantener la homeostasis y evitar el daño [38]. Además, la autofagia también es relevante en el desarrollo y envejecimiento del cerebro. Una autofagia activa y funcional es necesaria para la formación de nuevas memorias. De hecho, su activación farmacológica en el hipocampo de ratones envejecidos, revierte los déficits cognitivos en parte, promoviendo la formación de nuevas espinas dendríticas (sitios postsinápticos de las neuronas) [7].

Las fallas en la autofagia en modelos experimento, se asocian a enfermedades neurodegenerativas (PD y AD), enfermedades metabólicas y cáncer. Aumentar el flujo autofagico tiene un efecto benéfico sobre la esperanza de vida en estos modelos [39]. En este sentido, Fernández et al., 2018 mostraron que al inhibir la formación del complejo BECN1-BCL-2 en ratones, la forma libre de BECN1 aumenta la autofagia basal, extendiendo la esperanza de vida y la vida saludable de machos y hembras [40]. Además, al analizar el transcriptoma de 76 centenarios (personas mayores de 100 años con vida saludable), se encontró un aumento en la expresión de genes asociados a la vía autofágica [41]. Estos resultados demuestran que mantener la autofagia basal tiene un potencial papel anti-envejecimiento y se sugiere que, en parte, este efecto benéfico es el resultado de mantener la homeostasis y retrasando así el establecimiento del fenotipo senescente [42].

1.2. *Senescencia celular*

La senescencia celular es un fenotipo que se ha descrito en el contexto del envejecimiento, el desarrollo embrionario y la cicatrización. En el desarrollo embrionario, la senescencia programada contribuye a la diferenciación y la muerte celular programada, favoreciendo por ejemplo el desarrollo de la medula espinal [43].Por otro lado, durante envejecimiento las células adquieren el fenotipo senescente en respuesta a diferentes estímulos dañinos y se caracterizan por la falta de respuesta a estímulos mitóticos y apoptoticos que es acompañada por la detención del ciclo celular y el desarrollo de un fenotipo secretor asociado a la senescencia conocido como SASP, por sus siglas en inglés. En condiciones fisiológicas, las células senescentes son retiradas del tejido por el sistema inmune. Sin embargo, durante el envejecimiento hay una acumulación perdurable de estas células que, al continuar secretando moléculas que modifican el tejido circundante, promueven un ambiente proinflamatorio y reducen la capacidad regenerativa de los tejidos [44].

El mecanismo molecular que dirige el desarrollo del fenotipo senescente durante el envejecimiento no se entiende del todo, pero diversos tipos de estrés como el daño al DNA, el estrés oxidante, la activación de oncogenes, el daño a los telómeros y las fallas en la autofagia, promueven este fenotipo. Las características que definen a las células senescentes se describen a continuación:

1. **Expresión de inhibidores del ciclo celular**. Las cinasas dependientes de ciclinas involucradas en el arresto del ciclo celular durante la senescencia son: $p16^{INK4a}$ y $p21^{CIP/WAFI}$, codificadas por los genes *Cdkn2a* y *Cdkn1a* respectivamente. $p16^{INK4a}$, se utiliza como un marcador de senescencia celular y su expresión puede ser regulada por cambios epigenéticos y por factores de transcripción como Sp1, ETS y AP1. Adicionalmente, la degradación de PRC1 (complejo represor Polycomb 1),

que secuestra al promotor de *Cdkn2a*, también aumenta su expresión [45]. Por su parte, la expresión de *Cdkn1a* puede estar regulada por la actividad de p53 y la respuesta de daño al DNA, así como por otros factores de transcripción como SP1 y TNF-β. De forma interesante, se ha confirmado que tanto la expresión de $p16^{INK4a}$ como la de $p21^{CIP/WAFI}$ aumentan en células mitóticas y también en celulas postmitóticas cuando éstas desarrollan el fenotipo senescente [46,47].

2. **Incremento del contenido lisosomal y aumento de la actividad β-galactosidasa asociada a senescencia (SA-β-gal).** Las células senescentes exhiben un aumento del contenido lisosomal, en particular la actividad de la enzima β-galactosidasa aumenta de tal suerte que puede ser detectada a un pH suboptimo de 6.0, que se conoce como actividad β-galactosidasa asociada a senescencia (SA-β-gal, del inglés senescente associated). Aunque la detección de la actividad SA-β-gal se utiliza como un marcador de senescencia, esta no es determinante para el establecimiento de este fenotipo, pues células que tiene mutación nula en el gen que codifica para ella pueden establecer el fenotipo senescente [48].

3. **Alteraciones nucleares.** Uno de los cambios comúnmente observados en la senescencia celular, es la desestabilización de la integridad nuclear. Esto, debido a cambios en las proteínas de la envoltura nuclear como lamina B1, el receptor de lamina B1 (LBR) y lamina A/C. La reducción de la lamina B1 y su receptor se asocia con la reorganización de la cromatina, específicamente con la pérdida de heterocromatina constitutiva y con aumento de fragmentos de cromatina en el citoplasma (CCFs por cytoplasmic chromatin fragmets) [49]. En el caso de lamina A/C, se ha observado que cuando p53 aumenta en el núcleo, este interactúa físicamente con la lamina A/C. Esta interacción estabiliza a la lamina A/C, favoreciendo la degradación de PRC1 y en consecuencia aumentando la expresión de *Cdkn2a (*$p16^{INK4a}$) [45].

4. **Resistencia a la apoptosis.** Las células senescentes son resistentes a la apoptosis. Cuando estas células son tratadas con inductores de la apoptosis, no regulan a la baja a la proteína anti-apoptotica BCL-2. Otros miembros de la familia BCL-2 como BCL-XL y BCL-W, también confieren resistencia a la apoptosis. Por otro lado, se ha descrito que cuando la proteína $p21^{CIP/WAFI}$ se encuentra en el citoplasma, protege a las células senescentes de la apoptosis al restringir la señalización de las caspasas cuando hay daño persistente al DNA [50,51].

5. **Focos de heterocromatina.** La senescencia celular está asociada a cambios globales en la organización de la cromatina. Dichos cambios corresponden a una inversión en la localización de la heterochromatina y eucromatina. Normalmente, la heterochromatina se ubica en la periferia del núcleo y se encuentra en contacto con la lamina B1, mientras tanto la eucomatrina se ubica al centro del núcleo. Sin embargo, en las células senescentes y sin importar el estímulo que las induzca a este fenotipo, la heterochomatina y eucromatina se invierten [52]. Adicionalmente, las células que entran en senescencia forman focos de heterocromatina visibles al microscopio, a estos se les conoce como SAHF (Senescence associated heterochromatin foci). Los focos están enriquecidos en marcadores de heterocromatina como H3K9me3 (la historia h3 tri-metilada en la lisina 9) y la histona macroH2A, una variante de histona asociada con el silenciamiento de genes. Se

piensa que los SAHF representan regiones que son transcripcionalmente inactivas, pero no todas las células senescentes presentan estos focos [53].

6. **Fenotipo secretor asociado a senescencia (SASP).** Las células senescentes se caracterizan por desarrollar en fenotipo secretor. Estas pueden secretar todo un set de moléculas que alteran el microambiente circundante, por ejemplo, citocinas, quimiocinas, factores de crecimiento, proteasas e incluso especies reactivas de oxígeno. Si el efecto de la secreción de estas moléculas es positivo o negativo, dependerá del contexto en el que se secretaron. En algunos casos estas favorecen la remodelación de tejidos y el cierre de heridas, pero en el caso del cáncer, podrían favorecer la progresión y durante el envejecimiento, promueven la inflamación. El SASP es un programa transcripcional mediado por la activación del factor de transcripción NF-κB, como resultado del daño al DNA. Otros factores de transcripción involucrados en el desarrollo del SASP como GATA4 y C/EBPβ ya fueron descritos. Además, se propone que el SASP puede depender también de cambios epigenéticos que incluyen la reducción de la H3K9me en promotores de genes como IL6 e IL8, dos componentes importantes del SASP [54].

7. **Daño al DNA y respuesta de daño al DNA.** El daño al DNA es uno de los principales inductores del fenotipo senescente. El acortamiento de telómeros y las rupturas de doble cadena, desencadenan una respuesta rápida de daño al DNA. Los principales mediadores de esta respuesta de daño al DNA son las proteínas ATM, ATR, CHK1, CHK2, que fosforilan y activan proteínas de ciclo celular incluyendo p53. Cuando p53 se activa, favorece la expresión de proteínas como $p21^{CIP/WAFI}$. Las células senescentes se caracterizan por tener una respuesta sostenida de daño al DNA que puede ser evaluada a través de la fosforilación de la histona H2AX (γH2AX) [55].

8. **Acumulación de lipofuscina.** Durante el envejecimiento y la senescencia celular, se ha observado que las células acumulan lipofuscina, un material autofluorescente. Esta lipofuscina se acumula en los lisosomas y se forma por el entrecruzamiento de proteínas oxidadas, lípidos y metales que no pueden ser degradados por las hidrolasas, afectando la capacidad degradativa del lisosoma [56].

No se cuenta con un marcador único y específico para detectar a las células senescentes. De hecho, se requiere la detección simultánea de diversas características descritas arriba para definir que una célula ha adquirido dicho fenotipo [54,57–59].

1.2.1. *Senescencia celular y envejecimiento*

Aunque la senescencia celular tiene un papel benéfico durante el desarrollo y la regeneración de tejidos [60], en el envejecimiento, la acumulación de estas células es deletérea porque altera la estructura y función de los tejidos. Esta idea fue demostrada al remover selectivamente células senescentes, cuando se desarrolló una línea de ratones transgénicos con la construcción INK-ATTAC que expresa una variante de la caspasa 8 bajo el control del promotor de *Cdkn2a* (que codifica para $p16^{INK4a}$), permitiendo así la eliminación selectiva de células que expresan $p16^{INK4a}$. Como resultado, en los ratones en que se eliminaron células senescentes, se observó un retraso en el desarrollo de tumores,

preservación la funcionalidad del glomérulo, extensión en la esperanza de vida saludable y un aumento en la esperanza de vida [61,62]. Además, el uso de senolíticos como navitoclax (moléculas pequeñas que promueven la muerte de las células senescentes), previene la perdida de la capacidad cognitiva asociada a la muerte neuronal en un modelo de neurodegeneración. Ratones con la mutación MAPT P301S desarrollan marañas neurofibrilares formadas por la proteína Tau hiperfosforilada, así como acumulación de glía senescente y gliosis reactiva. El tratamiento con navitoclax, reduce la astrogliosis, microgliosis y la formación de marañas neurofibrilares, disminuyendo la muerte neuronal [6]. Estas evidencias demuestran que las células senescentes tienen un papel importante promoviendo la perdida de función y estructura de los tejidos, durante el envejecimiento. Por ello, actualmente se siguen investigando estrategias que eviten la senescencia celular o favorezcan la eliminación de células con este fenotipo.

1.3. *Autofagia y senescencia celular*

La relación entre la autofagia disfuncional y la conversión al fenotipo senescente se ha descrito de manera amplia. Por ejemplo, el silenciamiento de los genes *ATG12, ATG7 y LAMP2,* en fibroblastos humanos, promueven un fenotipo senescente, caracterizado por el aumento en la actividad SA-β-gal, acumulación de lipofuscina, arresto del ciclo celular, morfología alargada y aumento del contenido lisosomal y mitocondrial. En este modelo, las fallas en la autofagia promueven la acumulación de mitocondrias dañadas, que a su vez aumentan la producción de ROS y el estrés oxidante. El daño oxidante en consecuencia promueve la activación de p53 y el aumento en la expresión de $p16^{INK4a}$ y $p21^{CIP/WAFI}$ [63]. Por otro lado, activar el flujo autofagico en células satélite musculares de ratones envejecidos, evita la transición de quiescencia a senescencia, un fenómeno característico de la sarcopenia y que limita la capacidad regenerativa del musculo [64]. Esta evidencia apunta a que la disfunción autofagica promueve la senescencia en células mitóticas y postmitoticas.

En el caso del cerebro, sabemos que neuronas y astrocitos muestran aumento de características senescentes durante el envejecimiento. Por ejemplo, las células de Purkinje de ratones viejos exhiben aumento de lipofuscina, actividad SA-β-gal y una respuesta sostenida de daño al DNA [65]. Además, cerebros *post-mortem* de pacientes con esclerosis lateral amiotrófica (ALS, por amyotrofic lateral sclerosis), mostraron un aumento de $p16^{INK4a}$ y $p21^{CIP/WAFI}$ en el núcleo de astrocitos, así como incremento de $p21^{CIP/WAFI}$ en el citoplasma de las neuronas [66]. Las neuronas son células con una autofagia basal alta y al igual que en otras células, una autofagia disfuncional caracterizada por una baja degradación y acumulación de autofagosomas, favorece la senescencia neuronal en modelos *in vitro*. Acorde, el tratamiento con inductores de autofagia como la rapamicina (inhibidor de mTOR) y la trehalosa (un inductor de autofagia independiente de mTOR), previenen el fenotipo senescente en neuronas [46,47].

Si bien, se ha demostrado que mantener activa la autofagia basal es una estrategia que previene la senescencia tanto en células mitóticas como postmitoticas, la pregunta de ¿Por qué falla la autofagia en el envejecimiento?, sigue vigente. Algunas hipótesis apuntan al aumento en la actividad de mTORC1 durante el envejecimiento, como el factor más importante en la regulación de la autofagia. Sin embargo, evidencia reciente demuestra que el aumento en el exporte nuclear del factor de trascripción EB, podría ser un elemento clave en la disfunción autofagica observada durante el envejecimiento [11].

1.4. Transporte núcleo-citoplasma

Las células eucariontes están compartamentalizadas, pero han desarrollado sistemas de transporte que permiten la comunicación intracelular. El transporte núcleo-citoplasma es un sistema que conecta funcionalmente los procesos que ocurren en el núcleo con los del citoplasma, por ejemplo, la transcripción y traducción. La importación y exportación nuclear ocurre a través de un complejo de proteínas llamado el complejo del poro nuclear (NPC, por sus siglas en inglés de nuclear pore complex). Este complejo atraviesa la membrana nuclear y permite el transporte activo y pasivo de proteínas. Cuando las proteínas son menores a 40 kDa (kilodaltones) pueden atravesar por difusión el NPC, pero cuando son mayores a 40 kDa requieren un transporte activo que involucra la actividad de receptores nucleares (NTRs, por sus siglas en inglés de nuclear transport receptors) [67].

Los NTRs, son proteínas solubles que pertenecen a la familia de receptores nucleares carioferinas-β, y se encargan de transportar diferentes proteínas y algunos tipos de RNAs a través del NPC. Los receptores a cargo del importe se conocen como importinas e interactúan con sus cargos a partir del reconocimiento de una señal de importe nuclear conocida como señal de localización nuclear (NLS, por sus siglas en inglés de nuclear localization signal) que es una secuencia corta de 1 a 8 aminoácidos, rica en lisinas (K) y argininas (R). Por su parte, los receptores que facilitan el exporte, se conocen como exportinas y reconocen sus cargos a partir de una señal de exporte nuclear llamada NES (por sus siglas en inglés de nuclear export signal), rica en residuos hidrofóbicos como Leucina. La exportina mejor descrita hasta el momento es la exportina-1/CRM1 [67,68].

Para que el transporte activo se lleve a cabo, se requiere de la interacción transitoria de los NTRs con el NPC, esta interacción facilita el transporte a través de la envoltura nuclear y necesita la participación de pequeñas proteínas G monoméricas llamadas GTPasas Ran. Las proteínas Ran, son un “switch” molecular que puede existir en dos estados conformacionales unidos a GDP o GTP. La conversión Ran-GTP/Ran-GDP se promueve por las proteínas GAP (proteínas activadoras de GTPasas) que dirigen la hidrólisis del GTP y comúnmente se localizan en el citoplasma. Por otro lado, la conversión Ran-GDP/Ran-GTP es regulada por las proteínas GEF (factor intercambiador de nucleótido de guanina), localizadas en el núcleo.

El gradiente de Ran-GTP/Ran-GDP favorece el importe y el exporte nuclear. Cuando se ha formado el complejo importina-cargo-Ran-GDP, este alcanza el núcleo y una vez ahí, las proteínas GEF intercambian GDP por GTP provocando un cambio conformacional que libera al cargo. En contraste, el exporte requiere la formación del complejo Ran GTP-exportina- cargo. Cuando este complejo alcanza el citoplasma, se hidroliza el GTP unido a Ran-GTP y esto produce un cambio conformacional que libera al cargo de la exportina (figura 2), permitiendo así que el ciclo de exporte e importe continúe [68].

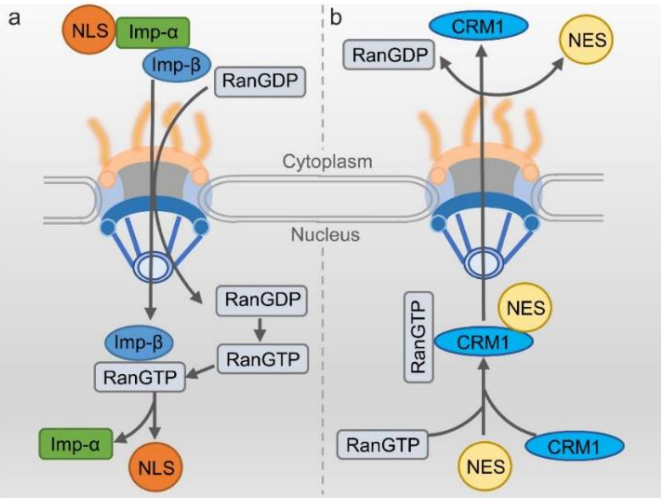

Figura 3. Esquema del transporte núcleo-citoplasma (*tomada de Fu et al., 2018*). Detalles en el texto.

1.4.1. *Alteraciones del transporte núcleo-citoplasma durante el envejecimiento*

¿Por qué cambia el exporte y el importe nuclear en el envejecimiento? Es una pregunta tan reciente como lo son las observaciones que nos llevaron a plantearla. Aunque los mecanismos moleculares son desconocidos, se ha encontrado evidencia de un transporte núcleo-citoplasma alterado tanto en el envejecimiento fisiológico como patológico. Por ejemplo, en el cerebro y en fibroblastos de donadores de diferentes edades, se identificó que la proteína RanBp17 (importina-β) disminuye en donadores viejos respecto a los jóvenes [4]. Mientras que en el cerebro de ratas viejas al menos 7 proteínas mostraron cambios en su localización subcelular, entre ellas la exportina-5 con una mayor abundancia en el citoplasma [69]. Estos datos surgieren que durante el envejecimiento las proteínas encargadas del transporte núcleo-citoplasma podrían tener una función alterada.

Por otro lado, en modelos *in vitro* y murinos de esclerosis lateral amiotrofica (ALS), la expansión anormal del hexanucleótido G4C2 en el gen *C9orf72*, se asocia con un transporte núcleo-citoplasma deficiente, caracterizado por la acumulación citosolica de la proteína TDP-43 (proteína de unión a RNA), y la nucleoporina 205 o NUP205 (una proteína del poro nuclear que favorece el transporte activo de proteínas). Además, se observa la pérdida del gradiente de Ran, causado por la acumulación citosolica de RanGAP1 [70–72]. Estas observaciones fueron confirmadas en cerebros *post mortem* de pacientes con ALS [71,73]. Por su parte, la sobreexpresión de la Huntingtina mutante (mHTT), inhibe el exporte de RNAs mensajeros a través del secuestro de RanGAP1 y Gle1 (un componente clave en el exporte del mRNA) [74]. Mientras tanto, NUP62 una proteína relevante en el control de la permeabilidad nuclear y el tráfico de macromoléculas al núcleo, se acumula en el citosol de neuronas, en un modelo murino de la enfermedad de Huntington [75].

De forma interesante, el uso de inhibidores selectivos de la exportina-1/CRM1, llamados compuestos SINE, han mostrado tener efectos neuroprotectores en diferentes

condiciones. En este aspecto, KPT-335 (Verdinexor), reduce la muerte neuronal causada por la sobrexpresion de TDP-43 [70] y el tratamiento con KTP-276 retrasa la neurodegeneración en un modelo de ALS en *Drosophila melanogaster* [72]. Por su parte, KPT-350 reduce de manera significativa la muerte de neuronas corticales transfectadas con mHTT, restaurando el trafico núcleo-citoplasma [75]. Se ha especulado que los efectos neuroprotectores de los compuestos SINE son el resultado de inhibir el exporte de factores de transcripción con funciones neuroprotectoras como NRF2 [76] o TFEB [11].

1.5. *Antecedentes*

El papel de CRM1 durante el envejecimiento fue confirmado en el nematodo *C. elegans*. Distintas cepas mutantes de *C. elegans* que muestran extensión en la esperanza de vida comparten como característica el enriquecimiento nuclear de la proteína HLH-30 ortólogo de TFEB [77]. En la búsqueda de nuevos blancos que pudieran regular la localización subcelular de HLH-30/TFEB se identificó que al silenciar a CRM1, no solo se favorece la localización nuclear de HLH-30/TFEB, sino que se observa un aumento en la actividad autofágica y en la esperanza de vida; estos efectos son independientes de la actividad de mTOR. Además, en un modelo de ALS en moscas, se observó que el silenciamiento de CRM1 restaura el flujo autofágico aumentando la transcripción de genes blanco de MITF/TFEB. De forma interesante, sobreexpresar Mitf/TFEB no es suficiente para aliviar las fallas en la autofagia causadas por el hexanucleótido G4C2 [78]. Resultados similares se han observado en células Hela al inhibir farmacológicamente a CRM1, sugiriendo que esta vía está conservada [11].

Otros reguladores de la autofagia como proteínas de la familia FOXO y STAT3 también se han identificado como blancos de CRM1. La localización nuclear de las proteínas FOXO promueve la autofagia porque favorecen la expresión de genes como *Ulk1/2, Atg4 y Atg14* [79]. En contraste, la localización citoplasmatica de STAT3 inhibe la autofagia porque se une a PKR, que interfiere con la fosforilación eIF2α, un paso necesario para el inicio de la autofagia [80].

De forma interesante, García-Aguirre et., 2019 observaron que los niveles y la actividad de la proteína CRM1 aumentan en los fibroblastos humanos de pacientes con progeria Hutchinson-Gilford (HGPS, una condición genética caracterizada por la expresión de una proteína llamada progerina y envejecimiento acelerado), y en fibroblastos de personas de 80-90 años. En este estudio, además se identificó que la expresión ectópica de progerina en fibroblastos humanos jóvenes es suficiente para aumentar la unión del factor de transcripción NF-YA con el promotor de CRM1, aumentando así su expresión. Sin embargo, el mecanismo que regula el aumento de CRM1 durante el envejecimiento fisiológico, sigue bajo investigación. Además, el aumento en CRM1 es una característica observada en diferentes células cancerosas. En este contexto el aumento en su actividad se asocia con supresores tumorales y oncoproteinas localizadas de manera aberrante [81]. El mecanismo que induce un aumento en la expresión de CRM1 en el cáncer no está claro pero se ha propuesto que está relacionado con factores de transcripción como p53, cMyc y Sp1 [82].

¿Cómo afecta a las células el aumento de CRM1?, este hecho no está claro, pero la sobrexpresión de CRM1 en fibroblastos jóvenes promueve el desarrollo de la senescencia celular. Por el contrario, al inhibir la actividad de CRM1 en fibroblastos HGPS que desarrollan senescencia de forma prematura, se reducen características del fenotipo senescente incluyendo la actividad SA-β-gal y se previene la pérdida de la lamina B1 [2].

En conjunto, estos datos sugieren que las alteraciones en el flujo autofágico típicamente observadas en el envejecimiento, podrían deberse a un incremento en la actividad de CRM1. Trabajo previo de nuestro laboratorio describió que las disfunciones en el flujo autofágico favorecen la senescencia en neuronas en un modelo *in vitro* [47]. Sin embargo, el papel de CRM1 en el envejecimiento neuronal aún no ha sido explorado, ni el rol de esta exportina en la regulación de la autofagia y el fenotipo senescente en neuronas. Por tanto, en este trabajo nos enfocamos en explorar el papel de CRM1 en el envejecimiento neuronal.

2. Justificación

El presente proyecto de investigación está encaminado a dilucidar los mecanismos moleculares que participan en el establecimiento de la senescencia neuronal. Si encontramos una relación inversa entre la actividad de CRM1 y el flujo autofágico, contribuiremos a la búsqueda de blancos terapéuticos dirigidos a mantener funcional la autofagia basal en las neuronas y así prevenir el establecimiento de la senescencia neuronal que conlleva la pérdida de las capacidades cognitivas asociadas al envejecimiento.

3. Hipótesis

El aumento de CRM1 en neuronas, disminuye el flujo autofágico y promueve la senescencia durante el envejecimiento.

4. Objetivo general

Analizar si los niveles de la proteína CRM1 correlaciona con la disfunción autofágica durante el envejecimiento neuronal y determinar si la reducción farmacológica de la actividad de CRM1 restaura el flujo autofágico y disminuye la senescencia neuronal.

5. Objetivos particulares

- Evaluar el flujo autofagico en neuronas jóvenes y envejecidas de corteza e hipocampo.
- Estudiar marcadores de senescencia en neuronas
- Evaluar el papel de CRM1 en el flujo autofagico y el establecimiento de la senescencia neuronal.

6. Materiales y métodos

6.1. *Animales*

1) Ratas de la cepa Wistar obtenidas en el vivario del Instituto de Fisiología Celular de la Universidad Nacional Autónoma de México (UNAM) y fueron alojadas con un ciclo de luz/obscuridad de 12 horas a 22°C y con acceso libre a agua y comida.
2) Ratones de la cepa C57BL/6J [ratón internacional, fuente (IMSR) catalogo 143 # JAX:000664, RRID:IMSR_JAX:000664], fueron obtenidos de Laboratorios Jackson y mantenidos en la Universidad Mayor de Chile. Los ratones transgénicos C57BL/6J, con el gen reportero GFP-LC3 fueron amablemente donados por la Dra. Sandra Cabrera y mantenidos en el vivario del Instituto de Fisiología Celular de la Universidad Nacional Autónoma de México (UNAM). Todos los animales fueron alojados con un ciclo luz/obscuridad de 12 horas a 22°C y con acceso libre a agua y comida.

Los animales usados en este estudio fueron manejados y cuidados de acuerdo a la legislación ética de cuidado animal. Todos los procedimientos fueron aprobados por el Comité Interno para el Cuidado y Uso de Animales de Laboratorio del Instituto de Fisiología Celular (IFC-SCO51-18), al igual que por el SAG de Chile (RUP: 13.1.07.0018).

6.2. *Cultivos corticales primarios, tratamiento con Leptomicina B y cloroquina.*

Los cultivos celulares se realizaron de acuerdo al protocolo estandarizado y publicado [47]. La corteza de embriones de ratas de la cepa Wistar de 17 días de gestación, fue disectada evitando tomar las meninges. Una vez aislado el tejido, este fue disgregado utilizando Tripsina-EDTA al 0.005% (15400054, Invitrogen/Gibco, Grand Island, NY, USA) y pipeta Pasteur. La suspensión fue filtrada utilizando una malla para disociar PGC Scientifics Cat. 34-1800-01 a fin de eliminar agregados y se centrifugó a 300 rpm por 3 minutos. Se desechó el sobrenadante y el pellet fue suspendido en medio Neurobasal (21103049, Invitrogen/Gibco Grand Island, NY, USA) suplementando con 2% de B27 (17504044, Invitrogen/Gibco, Grand Island NY, USA), GlutamaMax ™ 200 mM (35050061, Gibco Life Technologies, Grand Island, NY, USA) y 0.02mg/ml de Gentamicina (15710064, Invitrogen/Gibco, Grand Island, NY, USA).

Las células fueron contadas utilizando una cámara de Neubauer y sembradas en cajas de 12 pozos a una densidad de 100,000 células por cm^2 o en cajas Petri de 10 cm. Las cajas de cultivo deben ser pre-incubadas durante 24 horas con XPoly-L-lisina (0.01 mg/ml) (P1524,Sigma-Aldrich St. Louis, Mo, USA). Las células son cultivadas por 26 días *in vitro* (26 D*IV*) a 37°C y 5% CO_2. La mitad del medio de cultivo se cambió cada 6 días. Las células fueron tratadas con 5 nM de Leptomicina, cuyo vehículo es etanol (LMB; Sigma-Aldrich) por 24 horas (comenzando en 25 D*IV*) o 4 días (comenzando a 23 D*IV*). Para corroborar el flujo autofagico las células fueron tratadas con 20 μM Cloroquina (C-6628 Sigma-Aldrich, St. Louis, MO, USA) por 4 horas. El medio de cultivo contiene los suplementos necesarios para mantener los cultivos neuronales a largo plazo.

6.2.1. *Viabilidad Celular*

La viabilidad celular fue estimada por tinción con LIVE/DEAD viability/cytotoxicity kit (INVITROGEN/GIBCO, Grand Island, NY, USA). Las células vivas se tiñeron con calceína, mientras que las células muertas fueron teñidas con homodímero de etidio, siguiendo las instrucciones del fabricante. Solo se cuantificaron las células con morfología nuclear sana. Las imágenes fueron obtenidas en el microscopio invertido Nikon ECLIPSE Ti-U y el programa de análisis de imágenes NIS Elements. Cinco imágenes por experimento fueron analizadas. Se realizaron 3 experimentos independientes por condición.

6.3. *Western blot*

6.3.1. *Lisado completo*

Los animales fueron tratados por eutanasia usando utilizando una sobredosis de pentobarbital sódico (90 mg/kg). Se extrajeron el hipocampo y la corteza cerebral de 6 ratones silvestres jóvenes (3 a 6 meses), 6 adultos (14 a 17 meses) y 6 viejos (24 a 28 meses), estas áreas cerebrales se homogenizaron en buffer de lisis (Tris-HCl pH 8.0 mM, NaCl 150 mM, Triton X-100 1%, Desoxicolato de sodio 0.5% y SDS 2% e inhibidor de proteasas Complete). Se utilizaron 30 μg de muestra para los ensayos de electroforesis en geles de poliacrilamida (SDS-PAGE), los cuales fueron transferidos utilizando membranas de polivinilideno (PDVF) (Milipore). Las membranas fueron bloqueadas utilizando leche descremada (Bio-Rad Cat. #170-6404) al 3% en TTBS (Trizma 50 mM pH 7.6, NaCl 150 mM, Tween 0.1%) por una hora a temperatura ambiente (TA). Los siguientes anticuerpos primarios fueron incubados toda la noche a 4°C, conejo anti-CRM1 (1:1000, Novus 100-79802, Centennial-CO, USA), conejo anti-Lamina B1 (1:1000, Abcam 32454, Cambrigde, MA, USA), ratón anti-Lamina A/C (1:1000, Santa Cruz Biotechnology 376248, Dallas, Tx, USA) y ratón anti-β-actina (1:5000, Sigma A3682, Saint, Louis, USA), en una solución TTBS/BSA 3%. Después de 3 lavados de 5 minutos cada uno con TTBS, los siguientes anticuerpos secundarios se incubaron por 1 hora a TA; cabra anti-ratón IgG (1:5000, Sigma A0545, Saint, Louis, USA), o cabra anti-conejo IgG (1:5000, Sigma A0545, Saint, Louis, USA). Los anticuerpos secundarios fueron preparados en una solución TTBS/leche 3%. Después de 3 lavados de 5 minutos con TTBS, las membranas fueron reveladas utilizando sustrato quimioluminiscente de HRP (Milipore Cat. WBKLS0100, Billerica, Ma, USA) y la señal fue escaneada en el equipo C-Digit Blot (LI-COR).

6.3.2. *Fracciones celulares*

Para las fracciones celulares, el tejido fue disectado y homogenizado usando un buffer hipotónico (Hepes 10 mM, $MgCl_2$ 1.5 mM, KCl 10 mM, pH 7.4 e inhibidor de proteasas Complete). Después de ser homogenizados, los tejidos fueron incubados por 5 minutos a 4°C y centrifugados a 11,000 rpm por 1 minuto a 4°C. El sobrenadante (proteínas citosólicas) fue recolectado y se centrifugó a 4,000 rpm por 10 minutos a 4°C. El pellet fue descartado y el sobrenadante recuperado, las proteínas citosólicas fueron precipitadas agregando una mezcla metanol/cloroformo (5:1) en una proporción 1:1 y centrifugando a 14,000 rpm por 5 minutos a 4°C. El pellet fue posteriormente resuspendido en buffer de lisis (Tris-HCl pH 8.0 mM, NaCl 150 mM, Triton X-100 1%, Desoxicolato de sodio 0.5% y SDS 2%). El pellet obtenido en la primera centrifugación (proteínas nucleares) fue re-suspendido en buffer de lisis. Se utilizaron 30 μg de la fracción nuclear y de la citosólica para la electroforesis en geles de poliacrilamida. Los geles se transfirieron en membranas de polivinilideno (PVDF) (Milipore). Las membranas fueron bloqueadas utilizando leche sin grasa (Bio-Rad Cat. #170-6404) al 3% en TTBS (Trizma 50 mM pH 7.6, NaCl 150 mM, Tween 0.1%) por una hora a temperatura ambiente (TA). Los siguientes anticuerpos primarios fueron incubados toda la noche a 4°C; conejo anti-TFEB (1:1000, Mybiosure MBS716265, San Diego, CA, USA), conejo anti-GADPH (1:8000, Cell Signaling Technology, Mab2128, MA, USA), conejo anti-Fibrilarina (1:1000, Abcam 5821 Cambridge, MA, USA). Todos los anticuerpos primarios fueron preparados en una solución TTBS/BSA 3%. Después de 3 lavados de 5 minutos cada uno con TTBS, las membranas fuero incubadas con anticuerpo secundario por 1 hora a TA. cabra anti-ratón IgG (1:5000, Sigma A0545, Saint, Louis, USA), o cabra anti-conejo IgG (1:5000, Sigma A0545, Saint, Louis, USA). Los anticuerpos secundarios fueron preparados en una solución TTBS/leche 3%. Después de 3 lavados de 5 minutos con TTBS, las membranas fueron reveladas utilizando sustrato quimioluminiscente de HRP (Milipore Cat. WBKLS0100, Billerica, Ma, USA) y la señal fue escaneada en el equipo C-Digit Blot (LI-COR).

6.3.3. *Cultivo primario*

Las células fueron lisadas en un buffer de extracción que contiene 62.5mM Tris, 2% SDS y 2 mg/ml de inhibidor de proteasas Complete. 30 μg de proteína fueron utilizados para la electroforesis en geles de poliacrilamida. Las proteínas fueron transferidas en membranas PVDF-FL (Millipore). Después de secar las membranas por una hora a TA, protegidas del polvo, reactivadas utilizando metanol y lavadas con agua destilada. Posteriormente, las membranas fueron incubadas con anticuerpo primario a 4°C durante toda la noche. Los anticuerpos primarios conejo anti-LC3 (1:2000, MBL PD014, Nagoya, Japan), conejo anti-Lamina B1 (1:1000, Abcam 32454, Cambridge, MA, USA), ratón anti-Lamina A/C (1:1000 Santa Cruz Biotechnology 376248, Dallas, Tx, USA) y ratón anti-β actina fueron diluidos en TTBS/BSA 3%. Después de 3 lavados con TTBS, los siguientes anticuerpos secundarios fueron incubados TA por 1 hora; IRDye® 680RD cabra anti-conejo (925-68071, LI-COR) o IRDye® 800CW cabra anti-ratón (925-32210, LI-COR), utilizando una dilución de 1:5000 en TTBS. Las membranas fueron escaneadas usando el escáner Clx de LI-COr y las imágenes fueron analizando utilizando Image Studio Software 5.2.5.

6.4. *Inmunofluorescencia*

6.4.1. *Rebanadas de cerebro*

Las ratas o ratones transgénicos GFP-LC3 fueron anestesiados utilizando pentobarbital 39 mg/kg y perfundidos transcardialmente con PBS y paraformaldehido (PFA) al 4%. Los cerebros fueron post-fijados con PFA al 4% por 24 horas a 4°C y crioprotegidos con 30% sacarosa disuelta en PBS por 48 horas. Se realizaron cortes coronales de 40 μm del hipocampo y la corteza perirhinal (PRh) y posteriormente se montaron en laminillas. Las rebanadas de hipocampo o PRh fueron lavadas 3 veces por 10 minutos con PBS, incubadas por 15 minutos con glicina 0.01% /PBS para apagar la fluorescencia causada por el proceso de fijación. El proceso de permeabilización y bloqueo se realizó de manera simultánea incubando las rebanadas con PBS/Tween 0.5%/ BSA 5% por 30 minutos a TA. Después de un lavado de 10 minutos con PBS/ Tween 0.5%, el anticuerpo primario fue incubado toda la noche a 4°C en PBS/Tween 0.5%/Triton 0.1%. Después de 3 lavados de 10 minutos con PBS/Tween 0.5% las rebanadas fueron incubadas con anticuerpo secundario a TA durante 2 horas o 12 hrs a 4°C. El anticuerpo secundario AlexaFlour anti-ratón IgG, anti-conejo IgG o anti-cabra IgG (1:400 Life Technologies, Oregon, USA) fue preparado en PBS/Tween 0.5%/Triton 0.1%/BSA 2%; los núcleos fueron teñidos con DAPI (1μg/ml). Al terminar la inmunofluorescencia y para apagar la señal autofluorescente causada por la lipofuscina, las rebanadas fueron incubadas con Sudan Black B por 3 minutos. Se utilizaron los siguientes anticuerpos: conejo anti-CRM1 (1:500,Novus NB100-79802, Centennial-CO, USA), conejo anti-TFEB (1: 400, Mybiosure MBS716265, San Diego, CA, USA), ratón anti-p62 (1:300, Abcam 56416, Cambridge, MA, USA), ratón anti-Lamin A/C (1:1000, Santa Cruz Biotechnology 376248, Dallas, Tx, USA), conejo anti-p21 (1:200, abcam 109199 Cambridge, MA, USA), ratón anti-p16 (1:200, Santa Cruz Biotechnology sc1661, Dallas, Tx, USA), ratón anti- β-Tubulina clase III (1:1000, Abcam 14545, Cambridge, MA, USA), conejo anti- β-Tubulina class III (1:1000, abcam 18207, Cambridge, MA, USA) y conejo anti-MAP2 (1:500 abcam 32454 Cambridge, MA, USA), ratón anti-GFAP (1:400, SIGMA-ALDRICH G3893, St. Louis, MO, USA), ratón anti-STAT3 (1:100 Santa Cruz Biotechnology 482, Dallas, Tx, USA). La adquisición de las imagines se llevó a cabo en un microscopio confocal Zeiss LSM 800; y en todos los casos las imágenes fueron procesadas y cuantificadas utilizando el software Fiji, asignándoles pseudolores. Para cada individuo se obtuvieron de 3 a 4 imágenes por región, para cada una de las fotos la intensidad de fluorescencia corregida se obtuvo restando la fluorescencia del fondo a la fluorescencia total. El promedio de la intensidad de fluorescencia de 3 o 4 imágenes por región por individuo fue representado en los gráficos como un punto.

6.4.2. *Cultivos primarios*

Las células fueron fijadas con 100% metanol en hielo por 20 minutos y luego enjuagadas con PBS y permeabilizadas con PBS/Tritón 0.5% por 5 minutos y se bloquearon con PBS/BSA 5% por 30 minutos. Los anticuerpos primarios fueron incubados durante toda la noche a 4°C. Después de 3 lavados con PBS, las células se incubaron con anticuerpo secundario por una hora a TA. Los anticuerpos secundarios Alexa Fluor (1:1000 Life Technologies, Oregón, USA) fueron diluidos en PBS/BSA 2%. los núcleos fueron teñidos con DAPI (1μg/ml). Los anticuerpos primarios se usaron como se describe a continuación: Conejo anti-CRM1 (1:400, Novus NB100-79802, Centennial-CO, USA), conejo anti-TFEB (1: 500, Mybiosure MBS716265, San Diego, CA, USA), ratón anti-p62 (1:500, Abcam

56416, Cambridge, MA, USA), conejo anti-LAMP1 (1:1000, SIGMA-ALDRICH L1418, St. Louis, MO, USA), ratón anti-Lamin A/C (1:1000, Santa Cruz Biotechnology 376248, Dallas, Tx, USA), conejo anti-Lamin B1 (1:1000, Abcam 32454, Cambridge, MA, USA), ratón anti $p16^{INK4a}$ (1:1000, Santa Cruz Biotechnology sc1661, Dallas, Tx, USA), ratón anti β-Tubulina clase III (1:1000, Abcam 14545, Cambridge, MA, USA) y conejo anti β-Tubulina clase III (1:1000, abcam 18207, Cambridge, MA, USA). Las imágenes fueron adquiridas utilizando un microscopio confocal Zeiss LSM 800 y procesadas utilizando el Software Fiji. Al menos 300 células fueron cuantificadas, 100 células por experimento, 3 experimentos independientes fueron realizados cada célula es representada como un punto en los graficos.

6.5. *Cuantificación de lisosomas pequeños o alargados*

Las imágenes de inmunofluorescencia de LAMP1 fueron binarizadas en el software Fiji y sometidas al análisis de partículas. Utilizando el plugging de Fiji, se contaron las partículas con un área de 10 μm^2 o menor, el índice de circularidad se estableció en 0.60. Los lisosomas con estas características fueron considerados lisosomas pequeños o funcionales. Las partículas con un tamaño mayor a 10 μm^2 de área o un índice de circularidad de 1 fueron considerados lisosomas alargados o no funcionales. El área ocupada por los lisosomas alargados y los pequeños es considerada el área total equivalente al 100 %. Este análisis explica qué porcentaje del área total está siendo ocupada por lisosomas pequeños o alargados.

6.6. *Tinción SA-β-galactosidasa*

6.6.1. *Rebanadas de Cerebro*

El protocolo para la tinción SA-β-galactosidasa se realizó de acuerdo al método previamente publicado [83]. El cerebro fue fijado utilizando paraformaldehido al 4% y crioprotegido con sacarosa al 30% (disuelta en PBS) por 48 horas. Se realizaron cortes coronales que fueron lavados con PBS por 10 minutos e incubados con una solución que contiene 20 mg/ml de X-gal (IBI SCIENTIFIC, IB02260), diluido en dimetilformamida. La solución X-gal es posteriormente diluida en un buffer de ácido cítrico/fosfato de sodio 0.2 M (a pH=6 importante), ferrocianuro de potasio 100 mM, ferricianuro de potasio 100 mM, cloruro de sodio 5 M y cloruro de magnesio 1 M. El pH fue ajustado a 6, como indica el protocolo para detectar actividad β-galactosidasa asociada a senescencia. Al asegurarse que las rebanadas están completamente sumergidas en la solución x-gal se incubaron por 16 h a 37 °C sin CO_2. Posteriormente, se realizó un lavado de 5 minutos con PBS y se detuvo la reacción incubando las rebanadas con 1ml de metanol por 1 minuto. Se retiró el metanol y después de un lavado de 5 minutos con PBS, se montaron las laminillas. Las imágenes de hipocampo y Prh se obtuvieron utilizando el microscopio confocal Zeiss LSM 800, un objetivo 40x e iluminación con luz trasmitida.

6.6.2. *Cuantificación de la señal SA-β-galactosidasa*

Después de adquirir las imágenes, estas fueron cuantificadas utilizando IsoData como umbral y el análisis de partículas del software Fiji. Para obtener el porcentaje del área SA-β-gal positiva, primero se cuantificó el área total ocupada por las partículas SA-β-gal positiva y finalmente el área total de la foto. Partículas SA-β-gal positivas fueron consideradas a partir de una circularidad 0.20 y un tamaño de 10 μm^2. El porcentaje del área positiva a la señal SA-β-galactosidasa fue cuantificada usando imágenes del hipocampo y la PRh de ambos hemisferios cerebrales de 3 animales diferentes por grupo.

6.6.3. *Cultivo celular*

El protocolo para la tinción SA-β-galactosidasa se realizó de acuerdo al método publicado [83]. Las células se fijaron con 2% de formaldehído + 0.2 % de glutaraldehído durante 5 min, se lavaron con PBS y se tiñeron con la solución de tinción X-gal descrita arriba. Los cubreobjetos con células fueron incubados por 16 horas a 37°C sin CO_2. Las células positivas a la tinción de X-gal se detectaron utilizando un microscopio confocal LSM 800 y el objetivo de 63x de acuerdo al método descrito por Levistsky et al., 2013 [84].

Para la cuantifiación de la señal SA-β-galactosidasa se obtuvieron imágenes de 3 experimentos independientes y se cuantificó el porcentaje de área positiva a la tinción SA-β-galactosidasa después de binarizar las imágenes, aplicar el umbral (treshold) IsoData y utilizar el puggling análisis de partículas del software Fiji. Para normalizar el grafico, se dividió el área SA-β-gal positiva entre el número total de núcleos para cada experimento.

6.7. *Análisis Estadístico*

Todos los datos fueron analizados y graficados utilizando el programa Prisma 6 (GraphPad Software Inc. La Jolla, CA, USA). Los análisis estadísticos se realizaron de acuerdo a cada experimento y se indican en el pie de figura correspondiente.

7. Resultados

7.1. *Neuronas con autofagia atrofiada se acumulan en el hipocampo y corteza de ratas viejas.*

Tomando en cuenta que las alteraciones en el flujo autofagico favorecen la senescencia celular tanto en células mitóticas como postmitoticas [47], nosotros nos preguntamos si las neuronas de ratas viejas (25 meses) que mostraban alteraciones en el flujo autofagico también mostraban marcadores de senescencia, indicando así una correlación *in vivo*. Analizamos las neuronas de la región CA3 del hipocampo y la corteza entorrinal que forman parte de la vía perforante. Esta vía es la principal entrada de información del hipocampo y dichas estructuras fueron seleccionadas porque tienen un papel relevante en los procesos de aprendizaje y memoria y muestran alteraciones funcionales y estructurales tanto en el envejecimiento fisiológico como patológico, tal es el caso de la enfermedad de Alzheimer [85,86]Confirmamos que las neuronas de la región CA3 del hipocampo y la corteza, en los cerebros de ratas de 25 meses mostraron acumulación de la proteína LC3 indicativa de autofagosomas (Figura 4a,b,c). De igual forma, los puntos de p62/SQSTM1 por célula incrementan comparadas con sus controles jóvenes (Figura 4a,b,d). Estos resultados sugieren, que el flujo autofágico está disminuido en neuronas de hipocampo y corteza en ratas viejas.

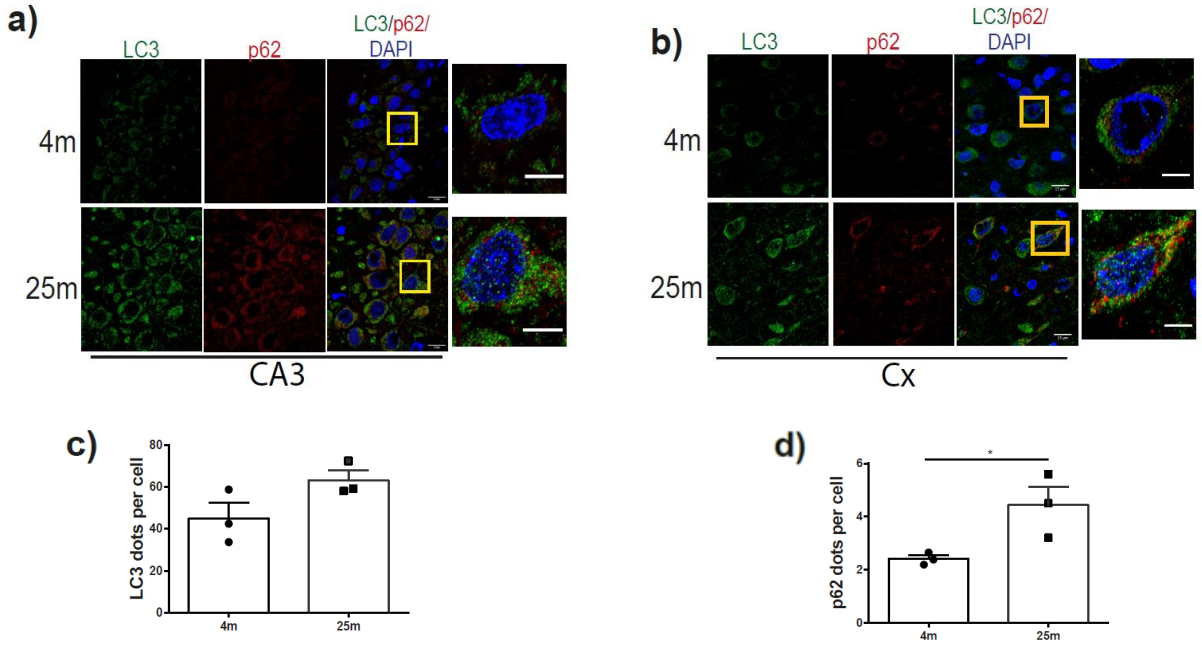

Figura 4. LC3 y p62/SQSTM1 se acumulan en las células durante el envejecimiento del cerebro de rata. (a,b) Inmunofluorescencia de LC3 (verde) y p62/SQSTM1 (rojo) en células de las regiones del cerebro indicadas CA3 (cuerno de Amón 3) y Cx (Corteza entorrinal). La barra representa 15 μm. (c,d) Las gráficas muestran la cuantificación de los puntos de LC3 y p62/SQMST1 por célula en la región CA3 del hipocampo. Las barras corresponden a la media ± SEM de tres experimentos independientes. t- Student; *p <0.05. Tres o cuatro campos por región por edad fueron analizados. A la derecha se muestra una célula representativa con barra de escala correspondiente a 5 μm.

7.2. Disminución de TFEB en neuronas de hipocampo y corteza de ratas envejecidas.

Fallas en el flujo autofágico son asociadas a una disminución en la actividad transcripcional de TFEB en diversos modelos de neurodegeneración [87]. Para determinar si TFEB está relacionado con las fallas en la autofagia durante el envejecimiento fisiológico, evaluamos su abundancia y localización subcelular. Observamos, que las neuronas de 25 meses de la región CA3 del hipocampo de rata mostraron una disminución de TFEB total, así como una menor localización nuclear en comparación con neuronas jóvenes (Figura 5a,c). De acuerdo con estos datos, sugerimos que la disminución del flujo autofágico está asociada a una disminución en la actividad de TFEB en el hipocampo. No se observaron cambios en la corteza (Figura 5b,d).

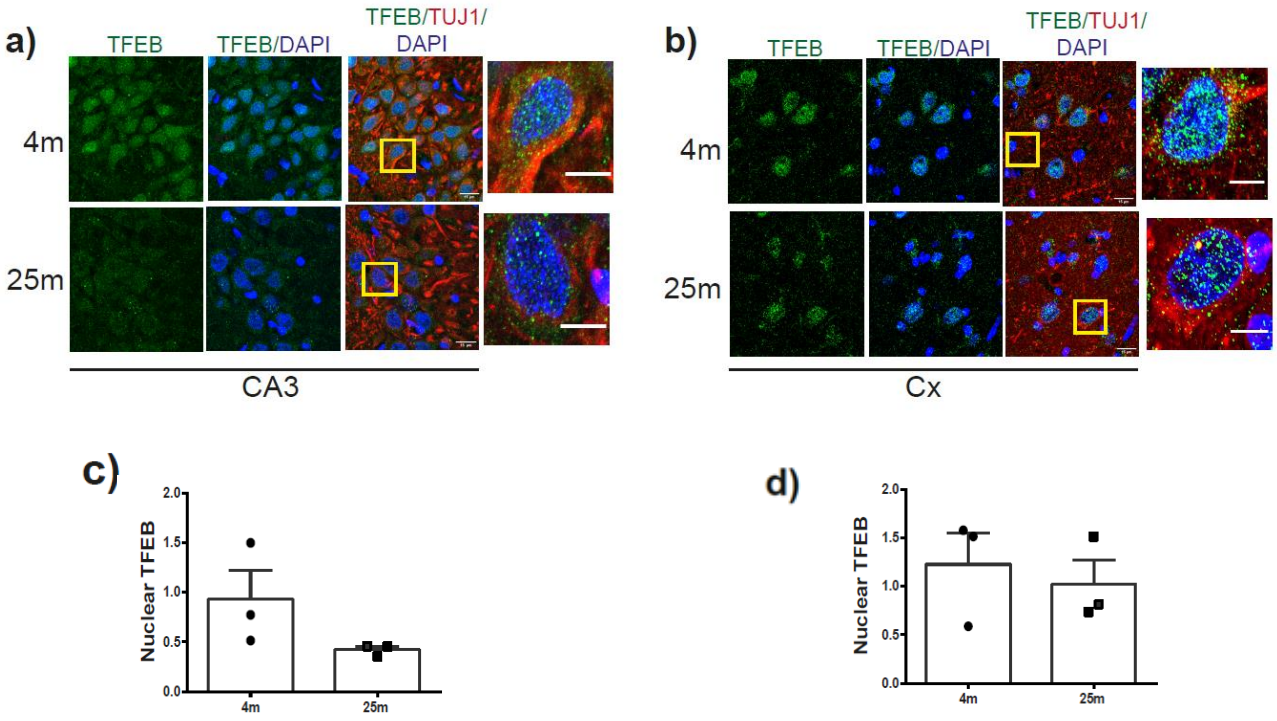

Figura 5. Las neuronas de la región CA3 del hipocampo muestran una disminución de TFEB nuclear. (a,b) Detección de TFEB por inmunofluorescencia en neuronas (células que expresan TUJ1) en las regiones indicadas. La barra de escala corresponde a 15 µm y una neurona representativa se muestra a la derecha. (c,b) Las gráficas muestran la densidad de pixeles de TFEB en el núcleo de neuronas. Las barras corresponden a la media ± SD de tres experimentos independientes. Tres o cuatro campos por región por edad fueron analizados.

7.3. *Neuronas senescentes se acumulan en el hipocampo y corteza durante el envejecimiento.*

Demostramos (anexo 3) que la disfunción autofágica promueve el fenotipo senescente en neuronas en un modelo *in vitro* de senescencia neuronal. De acuerdo con esta observación, encontramos que las neuronas de ratas de 25 meses de la región CA3 del hipocampo y de la corteza muestran fallas en la autofagia y también exhiben marcadores típicos de la senescencia celular, tales como un aumento de la actividad SA- β-gal (Figura 6a, b, d, e) y acumulación de lipofuscina (Figura 6a, b, c, f) (datos publicados en referencia 45). Los resultados aquí obtenidos, asemejan a aquellos encontrados en ratones viejos [88], sugiriendo que tanto las fallas en la autofagia como la senescencia celular son fenómenos propios del envejecimiento del cerebro sin importar la especie y los datos que a continuación se presentan sugieren que la relación mecanistica entre las fallas en la autofagia y la senescencia podrían estar mediadas por CRM1. Para abordar esta hipótesis, evaluamos los niveles de CRM1 en neuronas de la región CA3 (Figura 6g) y encontramos que las neuronas de ratas de 25 meses muestran un aumento de la proteína CRM1, en comparación con neuronas de ratas de 4 meses. De forma interesante, observamos que las neuronas jóvenes muestran a CRM1 en una localización perinuclear mientras que, en las neuronas de 25 meses, CRM1 se concentra al interior del núcleo.

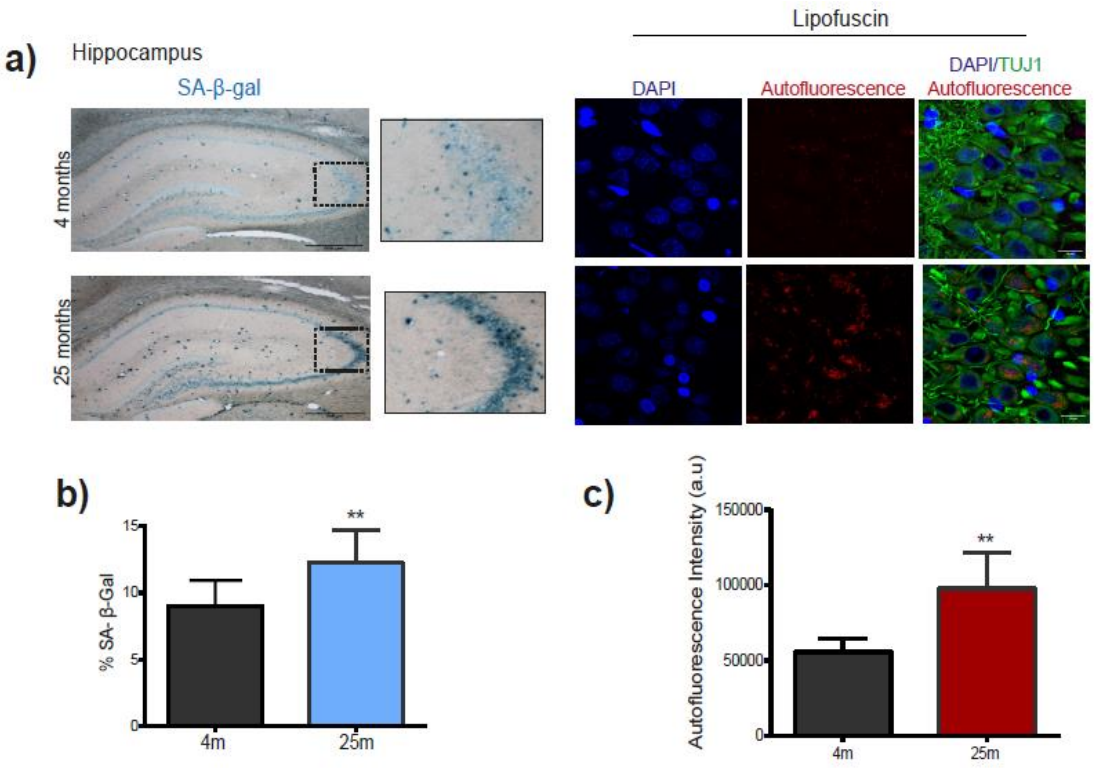

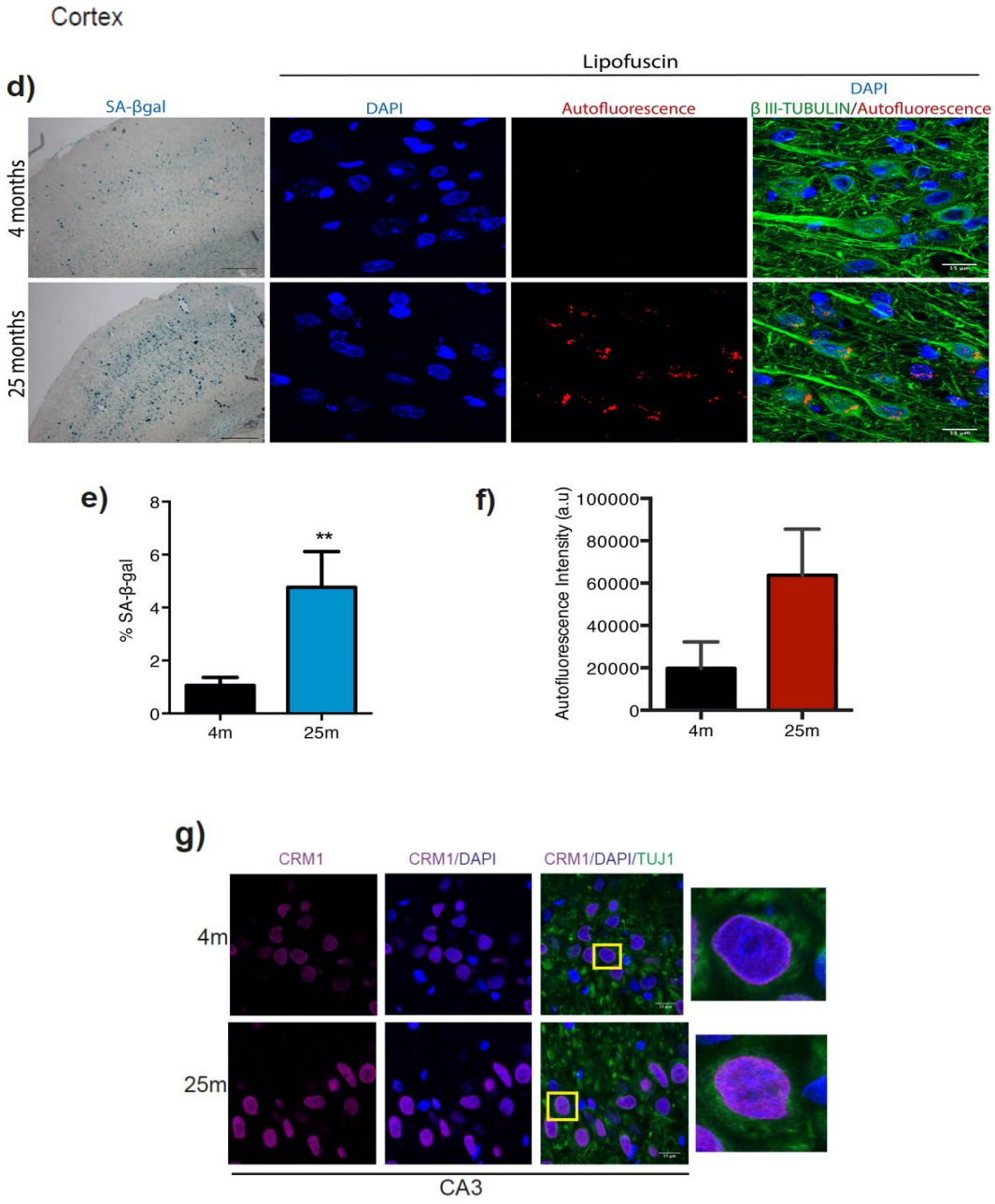

Figura 6. Neuronas con características senescentes se acumulan en el hipocampo y corteza de ratas de 25 meses. (a,b,d,e) Se muestra el porcentaje de área SA-β-gal positiva en el hipocampo y la corteza de ratas de 4 y 25 meses. Las barras corresponden a la media ± SD de tres experimentos independientes, las diferencias significativas se determinaron usando t-Test Student *p <0.05. La barra de escala representa 500 µm en ambos casos. (c,f) La acumulación de lipofuscina fue determinada a partir de la señal obtenida a 560nm en el microscopio confocal en células TUJ1 positivas. La grafica muestra la cuantificación de la intensidad de autofluorescencia obtenida y las barras corresponden a la media ± SD de tres experimentos. (g) Detección de CRM1 en neuronas (Tuj1 positivas), en la región CA3 del hipocampo, la barra de escala corresponde a 15 µm y se muestra una neurona representativa a la derecha.

7.4. *CRM1 se acumula en neuronas del hipocampo y corteza perirhinal de ratones viejos.*

Para establecer si los niveles de la exportina-1/CRM1 también cambian durante el envejecimiento fisiológico del cerebro de ratones, comparamos la expresión de esta proteína en el hipocampo y corteza de ratones jóvenes, adultos y viejos. Estas regiones fueron seleccionadas por la importancia de la vía perforante en los procesos de memoria y aprendizaje y mostraron cambios relevantes en el modelo de envejecimiento fisiológico de rata. Para corroborar que estos cambios asociados al envejecimiento podrían mantenerse en diversos modelos murinos, evaluamos dichas regiones en un modelo de ratón. El análisis por Western blot de lisados totales mostró que existe un aumento significativo de CRM1 en el hipocampo de ratones viejos (24-28 meses) y en la corteza de ratones adultos (14-17 meses), en comparación con ratones jóvenes (3-6 meses) (Figura 7 a,b) tanto para el hipocampo de ratones viejos (24-28 meses) como para la corteza de ratones adultos (14-17 meses). Al analizar por inmunofluroescencia regiones específicas del hipocampo (CA3 e Hilus) y corteza perirhinal (PRh), confirmamos que la acumulación de CRM1 ocurre en las neuronas de ratones viejos comparado con sus controles, y tal como se observó previamente para ratas de 25 meses, CRM1 pierde su localización perinuclear para concentrarse en el núcleo. Además, se observa un aumento de la localización citosolica de CRM1. En particular, las neuronas de la región CA3 del hipocampo mostraron que CRM1 aumenta significativamente, mientras que en el Hilus y la PRh únicamente encontramos una tendencia (Figura 7c, d, e). Nos preguntamos si otros tipos celulares, además de las neuronas también muestran cambios en la expresión de CRM1 y encontramos que, los astrocitos de 25 meses exhiben un aumento significativo de CRM1 (Figura 7f) en comparación con astrocitos de 4 meses. Para corroborar que el aumento de CRM1 no estaba relacionado con cambios en el tamaño de las neuronas, evaluamos el área de los núcleos y citoplasma de las neuronas. No se observamos diferencias significativas (Figura 8a, b).

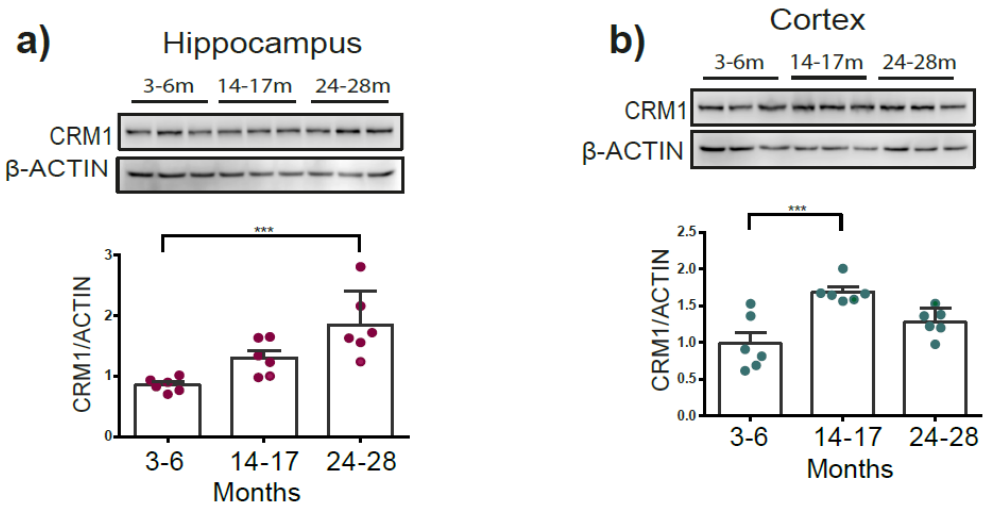

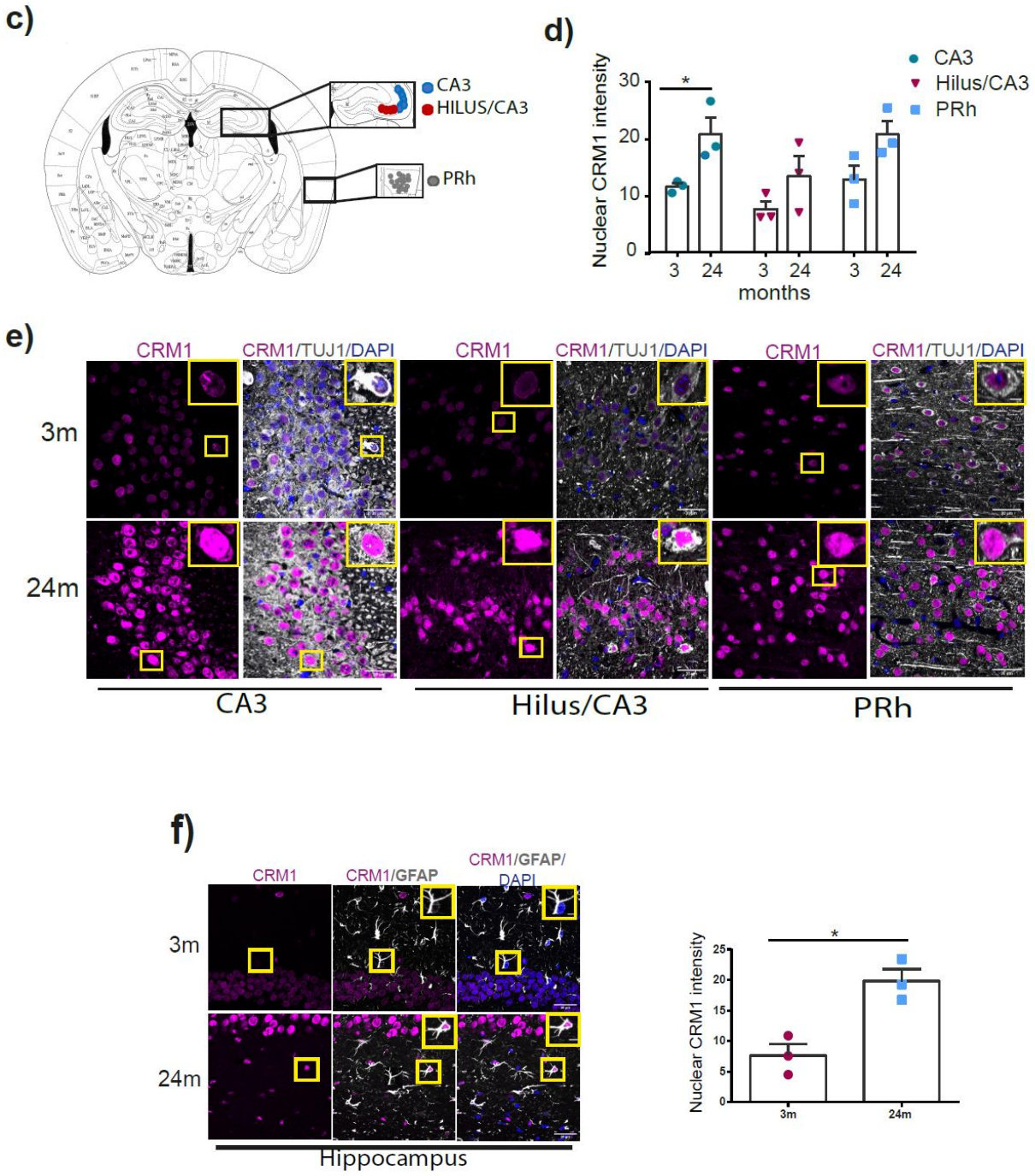

Figura 7. CRM1 se acumula en las neuronas durante el envejecimiento del cerebro. (a,b) El análisis por Western Blot muestra que la expresión de la proteína CRM1 aumenta en el hipocampo y corteza de ratones silvestres en las edades avanzadas. Se analizaron 6 animales por grupo, las gráficas representan la media ± SEM, Anova de una vía y Dunnet como post hoc test *p <0.05. (c) Diagrama anatómico para localizar las regiones analizados en este trabajo. La grafica representa la densidad de pixeles de CRM1 en el núcleo de las neuronas de ratones de acuerdo a la edad indicada, detectado por inmunofluorescencia. Las barras representan la media ± SEM de 3 experimentos independientes, las diferencias significativas fueron determinadas por t-Student para datos no pareados, *p <0.05. Tres o cuatro campos por región fueron analizados. Para cada región

se consideraron de 70 a 100 neuronas por edad: para CA3, n=300 neuronas por cada edad; Hilus, n=274 neuronas de 3 meses y n=263 neuronas de 24 meses; para la corteza PRh, n=115 neuronas de 3 meses y n= 139 neuronas de 24 meses. (e) Imágenes representativas de la inmunofluorescencia para detectar CRM1 en neuronas (identificadas por la expresión de TUJ1) en el hipocampo (CA3 e Hilus) y en la corteza perirhinal (PRh) de ratones jóvenes (3 meses) y viejos (24 meses). La barra de escala representa 30 µm. (f) Coinmunodetección de CRM1 en astrocitos (células GFAP positivas) en el hipocampo. La grafica muestra la densidad de pixeles de CRM1 en los núcleos de los astrocitos. Las barras representan la media ± SEM de 3 experimentos. Las diferencias significativas se determinaron usando t-Test Student *p <0.05. Los núcleos fueron teñidos con Dapi. Los cuadros amarillos muestran una amplificación de neuronas representativas.

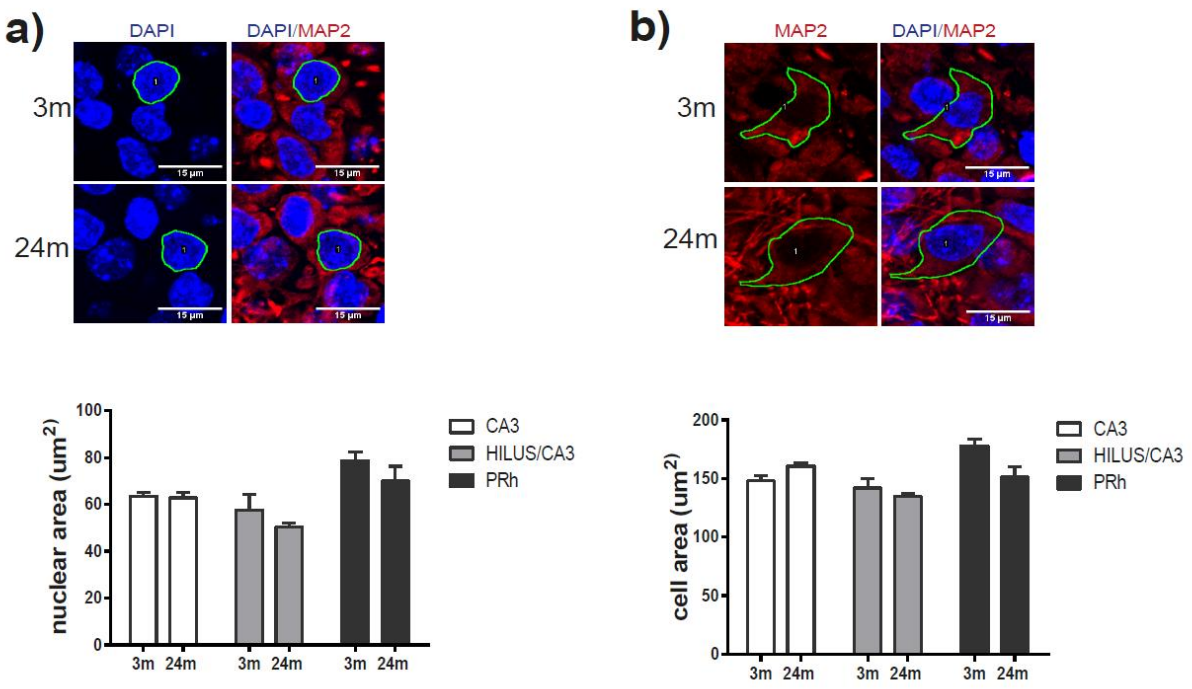

Figure 8. El tamaño de las neuronas no cambia con el envejecimiento. (a) El área del núcleo y (b) citoplasma expresada en µm^2 es similar en las neuronas (identificadas por MAP2) que fueron cuantificadas en el hipocampo y corteza de ratones de 3 y 24 meses. Las gráficas representan la media ± SEM. No se observaron diferencias significativas al realizar el análisis t-Test para muestras no pareadas. El total de neuronas analizadas por región corresponde a: CA3, n= 248 de 3 meses y n= 203 de 24 meses, Hilus, n= 248 de 3 meses y n=132 de 24 meses; PRh, n= 133 de 3 meses y n=133 de 24 meses. Neuronas representativas de la región CA3 se muestran con una barra de escala de 15 µm.

7.5. *Las neuronas que tienen CRM1 aumentado también muestran un aumento en el exporte nuclear de TFEB y STAT3 en ratones viejos.*

Para determinar si el aumento en los niveles de CRM1 acompaña un aumento en su actividad, estudiamos la localización subcelular de TFEB y STAT3. El exporte de estos factores de transcripción depende de la actividad de CRM1 y cuando su ubicación es citosólica, contribuyen a la inhibición del flujo autofagico [11,89,90]. Como se muestra en la figura 8a, b, las neuronas de la región CA3 del hipocampo de ratones viejos muestran una disminución significativa en la localización nuclear de ambas proteínas, TFEB y STAT3. Esto sugiere que en la región CA3 el aumento de CRM1 también involucra un aumento en su actividad. Sin embargo, en el caso del Hilus y la PRh no se observaron diferencias significativas en la abundancia en el núcleo con respecto al citoplasma para estas proteínas. Al analizar los niveles totales de las proteínas TFEB y STAT3, encontramos que la abundancia de ambas disminuyó en las neuronas de ratones viejos, en las regiones estudiadas (Figura 9a, b). Para corroborar la distribución intracelular de estas proteínas, analizamos por Western blot las fracciones celulares correspondientes a núcleo y citoplasma del hipocampo y la corteza. Efectivamente, encontramos una disminución significativa de TFEB en el núcleo, así como una disminución en los niveles totales de la proteína (Figura 9c). En conjunto, estos datos sugieren un aumento en la actividad de la proteína CRM1 en la región CA3 del hipocampo. Estudios adicionales se requieren para identificar si otros blancos de CRM1 que regulan también la autofagia, como las proteínas FOXO, también son exportados del núcleo al citoplasma.

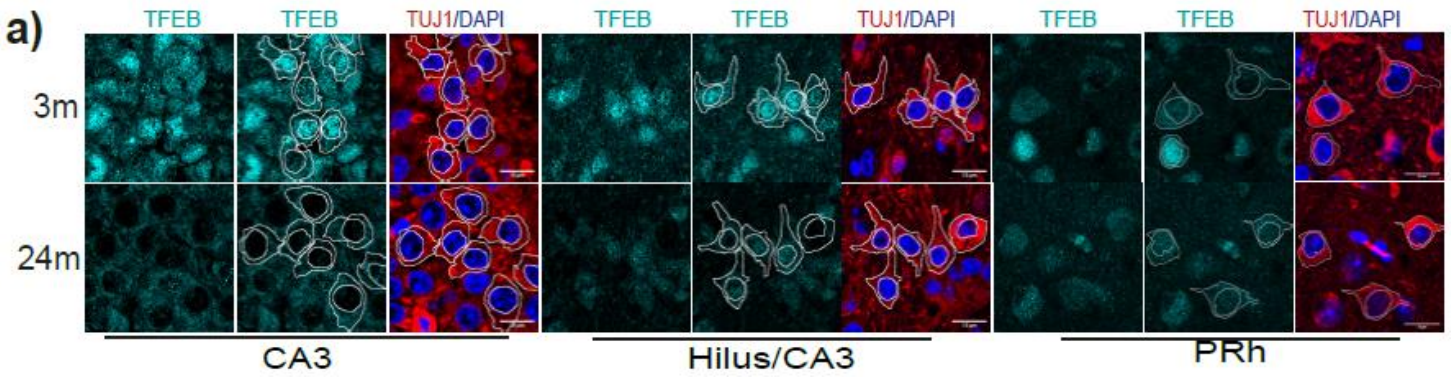

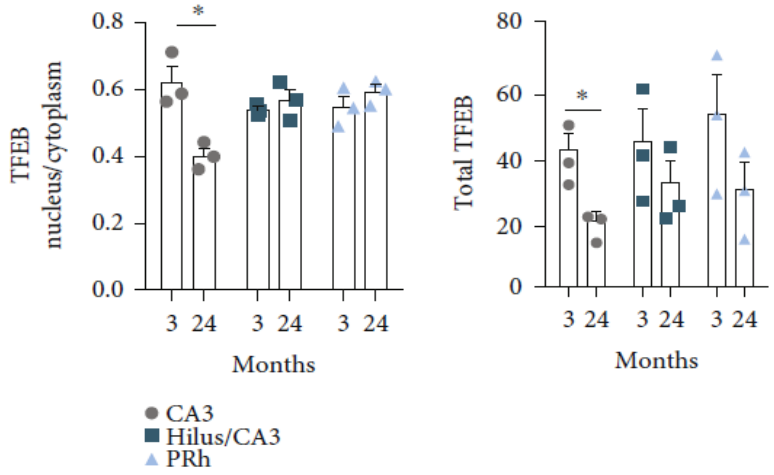
TFEB nucleus/cytoplasm
0.8
0.6
0.4
0.2
0.0
*
3 24 3 24 3 24
Months
Total TFEB
80
60
40
20
0
*
3 24 3 24 3 24
Months
CA3
Hilus/CA3
PRh

b)

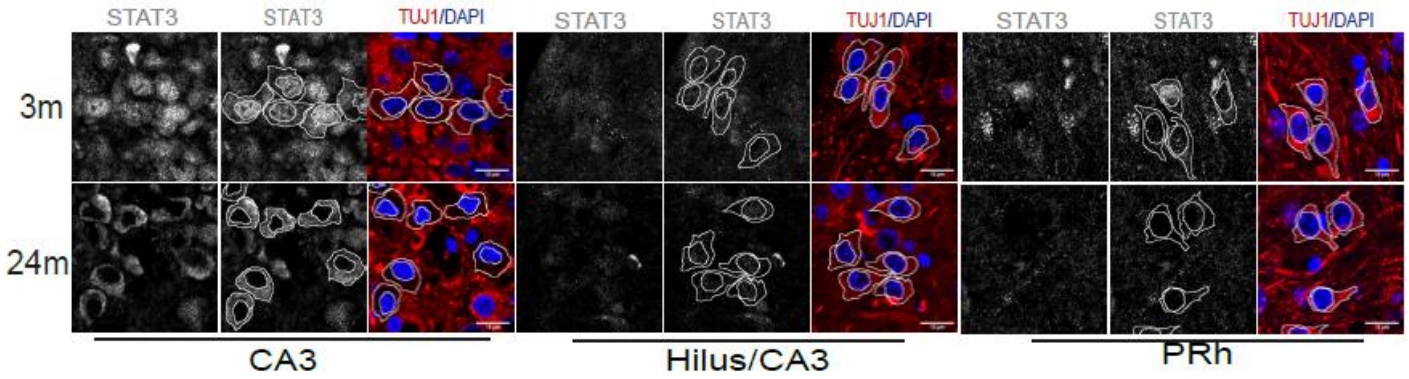
STAT3
STAT3
TUJ1/DAPI
STAT3
STAT3
TUJ1/DAPI
STAT3
STAT3
TUJ1/DAPI
3m
24m
CA3
Hilus/CA3
PRh

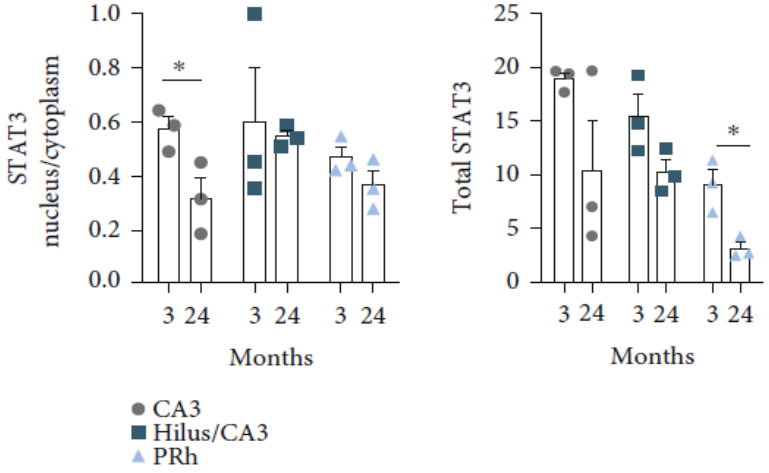
STAT3 nucleus/cytoplasm
1.0
0.8
0.6
0.4
0.2
0.0
*
3 24 3 24 3 24
Months
Total STAT3
25
20
15
10
5
0
*
3 24 3 24 3 24
Months
CA3
Hilus/CA3
PRh

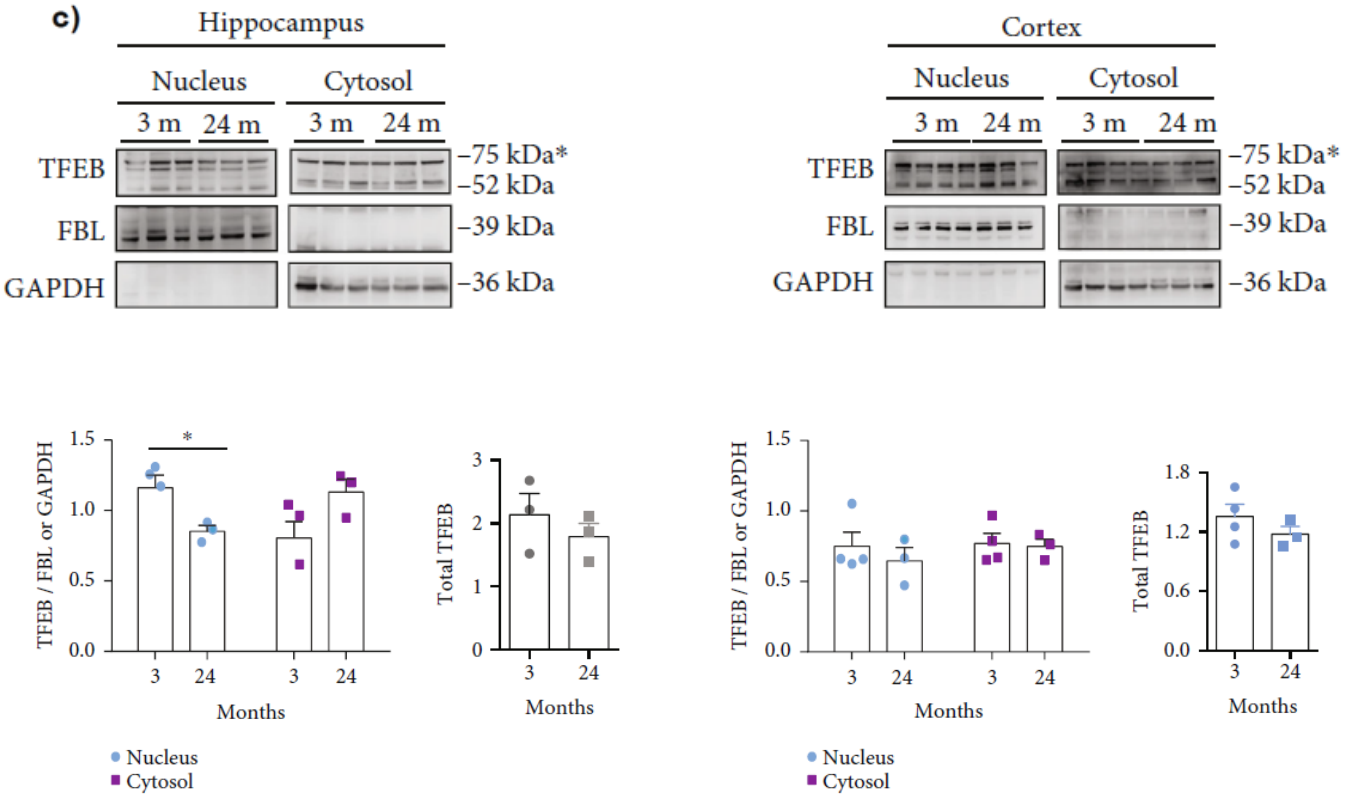

Figura 9. Aumentó el exporte nuclear de TFEB y STAT3 en neuronas de la región CA3 en el envejecimiento de ratones. (a,b) Detección de TFEB y STAT3 por inmunofluorescencia en neuronas (identificadas por la expresión de TUJ1), en la región CA3, hilus y PRh de ratones de 3 y 24 meses. La barra de escala representa 15 µm. Los núcleos fueron teñidos con DAPI. La densidad de pixeles de TFEB o STAT3 fue cuantificada en el núcleo y citoplasma de las células TUJ1 positivas, de acuerdo a como lo indican las líneas blancas. Las gráficas de la izquierda representan la relación núcleo/citoplasma encontrada en cada región para cada edad; las gráficas de la derecha representan el total de la señal (núcleo más citoplasma); las barras representan la media ± SEM. Tres o cuatro campos por región, por animal fueron cuantificados. El número de neuronas contadas fue: CA3, n=150 neuronas de 3 meses y n=120 neuronas de 24 meses; Hilus, n=86 neuronas de 3 meses, n= 70 neuronas de 24 meses; corteza PRh, n=75 neuronas de 3 meses y n=77 neuronas de 24 meses. Las diferencias significativas fueron determinadas con un análisis t-Test Student *p <0.05. (c) Distribución subcelular de TFEB analizada por Western blot en el hipocampo y corteza de ratones en las edades indicadas. GADPH y fibrilarina (FBL) se usaron como controles de carga para la fracción citoplásico o nuclear, respectivamente. Las gráficas representan la media ± SEM obtenida en el análisis de la densitometria de la banda de 75 kDa de tres experimentos independientes. Las diferencias significativas fueron determinadas con un análisis t-Test Student; *p <0.05. Los niveles totales de la proteína TFEB y STAT3 fueron obtenidos sumando la fracción nuclear y citosolica de los lisados totales, como lo indican las gráficas de la derecha.

7.6. *La acumulación de p62/SQSTM1 en neuronas de ratones envejecidos, indicativo de interrupción del flujo autofágico, correlaciona con el aumento de CRM1.*

Debido a que el aumento de TFEB y STAT3 en el citoplasma de neuronas viejas podría llevar a alteraciones en el flujo autofágico [91], analizamos a la proteína p62/SQSTM1 cuya acumulación es indicativa de un flujo autofágico. De manera consistente, observamos que p62/SQSTM1 se acumula en el cerebro de ratones de 24 meses, siendo significativa en las neuronas de la corteza PRh (Figura 10a, b). Analizamos si las mismas células que acumulan p62/SQSTM1 también tienen mayor cantidad de CRM1. La detección simultanea de p62/SQSTM1 y CRM1 mostró una correlación positiva entre el aumento de CRM1 y la acumulación de puntos de p62/SQSQTM1 en las neuronas de la región CA3 (Figura 10 c). Sin embargo, cuando analizamos la distribución intracelular de GFP-LC3 no encontramos una mayor acumulación de GFP-LC3 punteada (indicativo de acumulación de autofagosomas) con diferencias significativas con la edad, en las regiones evaluadas (Figura 10 d).

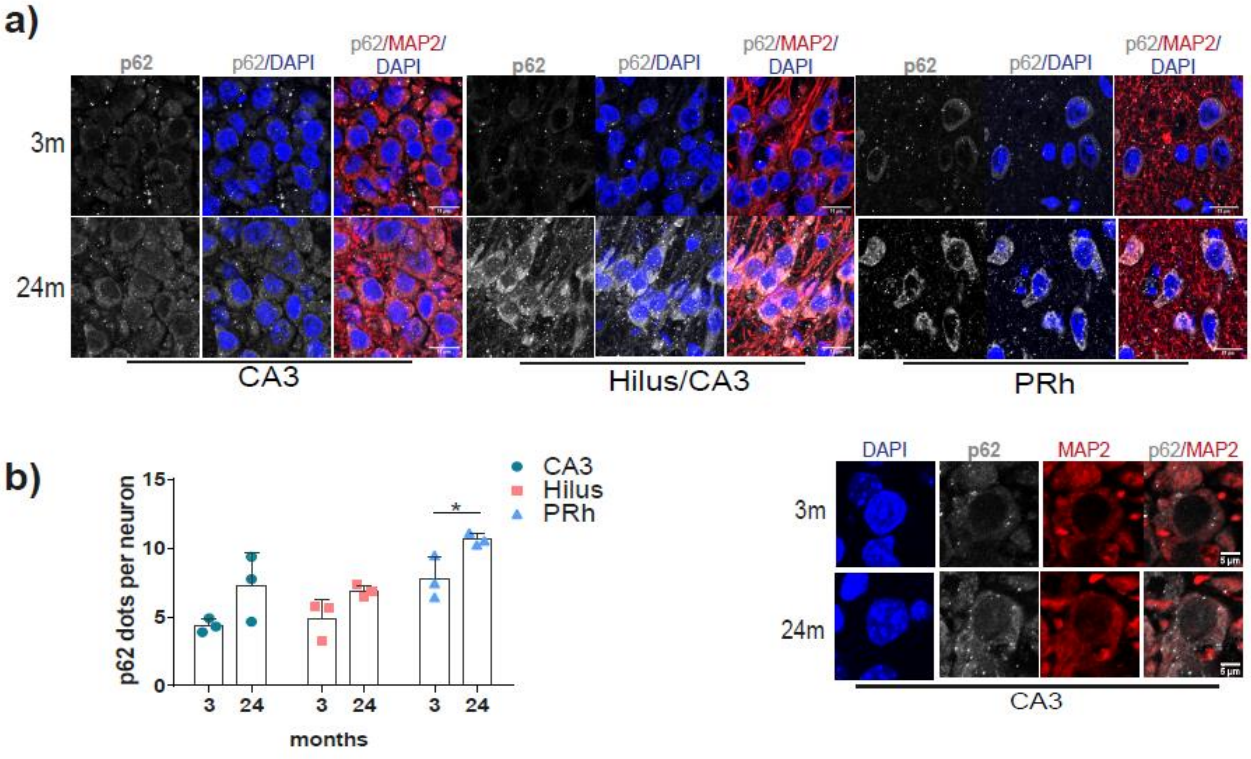

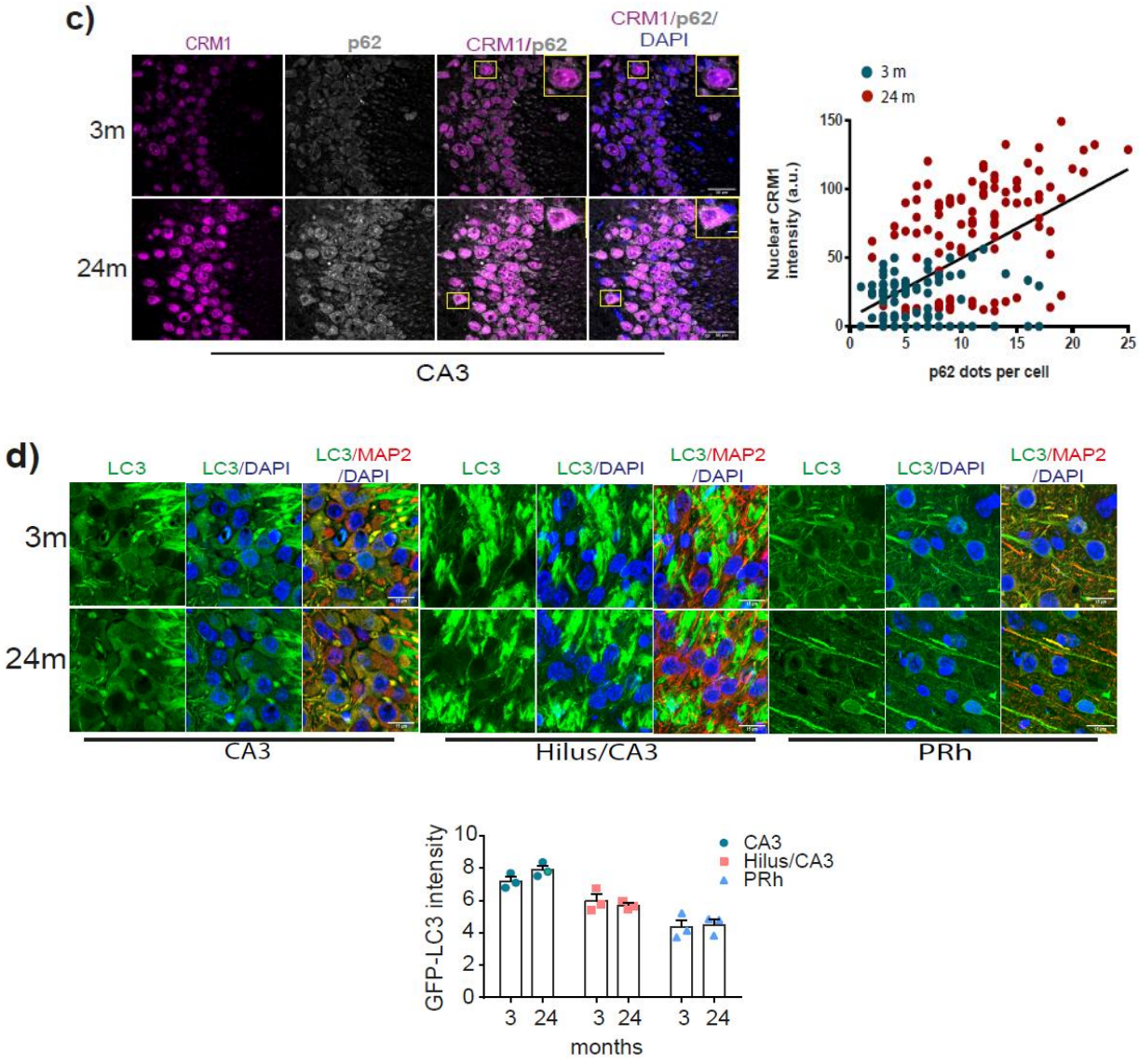

Figura 10. La acumulación de p62/SQSTM1 correlaciona con el aumento en CRM1 nuclear en las neuronas de la región CA3 de ratones envejecidos. (a.b) Inmunofluorescencia de p62/SQSTM1 en neuronas (identificadas porque expresan MAP2), en las regiones del cerebro indicadas. La barra representa 15 μm y las gráficas muestran la cuantificación de los puntos de p62/SQMST1 por neurona. Las barras corresponden a la media ± SEM de tres experimentos independientes. t-Test Student; *p <0.05. Tres o cuatro campos por región por edad fueron analizados. El número total de neuronas contadas fue: CA3, n=187 de 3 meses, n=201 de 24 meses; Hilus, n=161 de 3 meses y n=285 de 24 meses; Corteza PRh, n=113 de 3 meses y n=124 de 24 meses. Abajo a la derecha se muestra una amplificación de las neuronas de la región CA3. (c) Detección simultanea de p62/SQSTM1 y CRM1 en la región CA3 del hipocampo de ratones de 3 y 24 meses. La barra de escala representa 30 μm. El grafico muestra un análisis de regresión lineal con una correlación positiva entre los niveles de CRM1 nuclear y los puntos de p62/SQSTM1 por célula (r= 5985, n=100 neuronas de 3 meses y n=102 neuronas de 24 meses. p<0.0001). (d) Imágenes confocales que muestran la señal GFP-LC3 en neuronas del hipocampo y PRh de ratones GFP-LC3 transgénicos de 3 y 24 meses. La grafica muestra la densidad de pixeles de GFP-LC3, las barras representan la media ± SEM.

7.7. *El aumento en la expresión de CRM1 correlaciona con un aumento de neuronas senescentes en ratones viejos.*

En fibroblastos de personas jóvenes, la sobrexpresión de CRM1 promueve el fenotipo senescente, caracterizado por una disminución de la lamina B1 y H3k9m3 (marca de heterochromatina) [2]. Ya que la disfunción del flujo autofágico contribuye al establecimiento del fenotipo senescente en neuronas [15,92], nosotros nos preguntamos si el aumento en los niveles y la actividad de CRM1 observados en el cerebro de ratones viejos podría contribuir a la senescencia neuronal durante el envejecimiento fisiológico. Para responder esta pregunta, evaluamos la presencia de neuronas senescentes en el cerebro de ratones jóvenes y viejos. Observamos que la actividad SA-β-gal aumentó en el hipocampo y corteza de ratones de 24 meses comparado con ratones de 4 meses (Figura 11a). Otra característica de las células senescentes es que adquieren una morfología nuclear aberrante, resultado de alteraciones en las proteínas que conforman la envoltura nuclear; de acuerdo con esta idea, encontramos que lamina B1 disminuye en la corteza, mientras que la lamina A/C aumenta en el hipocampo (Figura 11b,c). Sin embargo, el análisis por Western blot no mostró cambios significativos para la lamina B1 en el hipocampo o lamina A/C en la corteza. Al cuantificar los niveles de lamina AC específicamente en las neuronas de la región CA3, Hilus y corteza PRh, observamos un aumento en las neuronas excepto para el hilus (Figura 11d). En células senescentes el aumento de la proteína p53 en el núcleo también favorece la estabilización de la lamina A/C a través de la interacción entre estas proteínas. A su vez, el aumento en la lamina A/C favorece la degradación del complejo PCR1 y en consecuencia la expresión de $p16^{INK4a}$ [45]. Por ello, estudiamos si los animales viejos mostraban cambios en la expresión de este inhibidor de ciclo celular. Consistentemente, encontramos un aumento en la expresión de $p16^{INK4a}$ en células de la región CA3 y de la corteza PRh en el cerebro de ratones de 24 meses (Figura 12a, b). Si bien encontramos en la región CA3 estás células que expresan $p16^{INK4a}$ en ratones jóvenes, tienen una intensidad menor a la encontrada en células que son positivas a los 24 meses (Figura 12c). Además, la detección simultanea de CRM1 y $p16^{INK4a}$ mostró que los niveles de expresión de CRM1 correlacionan con los niveles de expresión de $p16^{INK4a}$ (Figura 12d). La expresión de $p16^{INK4a}$ fue confirmada en neuronas a través de una doble inmunofluorescencia para detectar a MAP2 (Figura 12e). Estos resultados nos permitieron especular que el aumento en el nivel de CRM1 podría estar relacionada con la senescencia neuronal. Aunque más estudios se requieren para determinar la causalidad, nosotros proponemos que CRM1 podría promover la senescencia al generar fallas en la autofagia, al exportar al citoplasma proteínas como TFEB y STAT3.

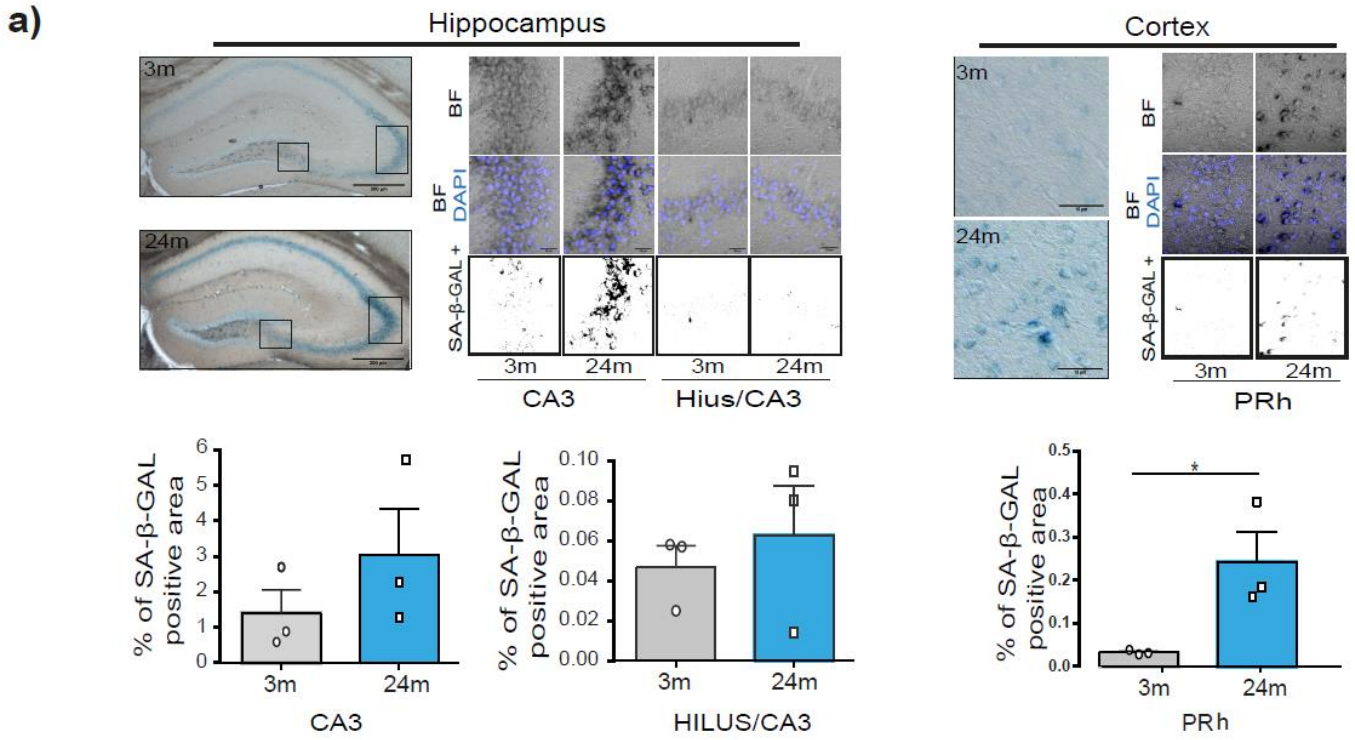
a)
Hippocampus
Cortex
3m
24m
BF
BF DAPI
SA-β-GAL +
CA3
Hius/CA3
PRh
% of SA-β-GAL positive area
HILUS/CA3

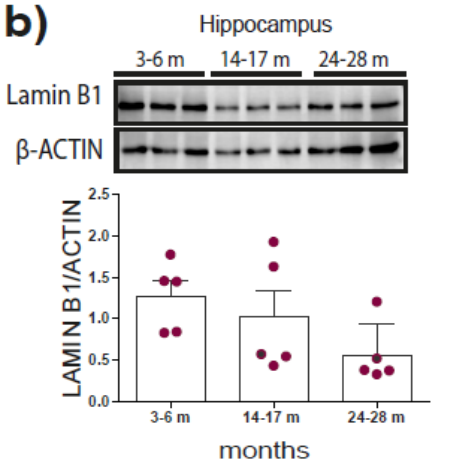
b)
Hippocampus
Cortex
3-6 m
14-17 m
24-28 m
Lamin B1
β-ACTIN
LAMIN B1/ACTIN
months

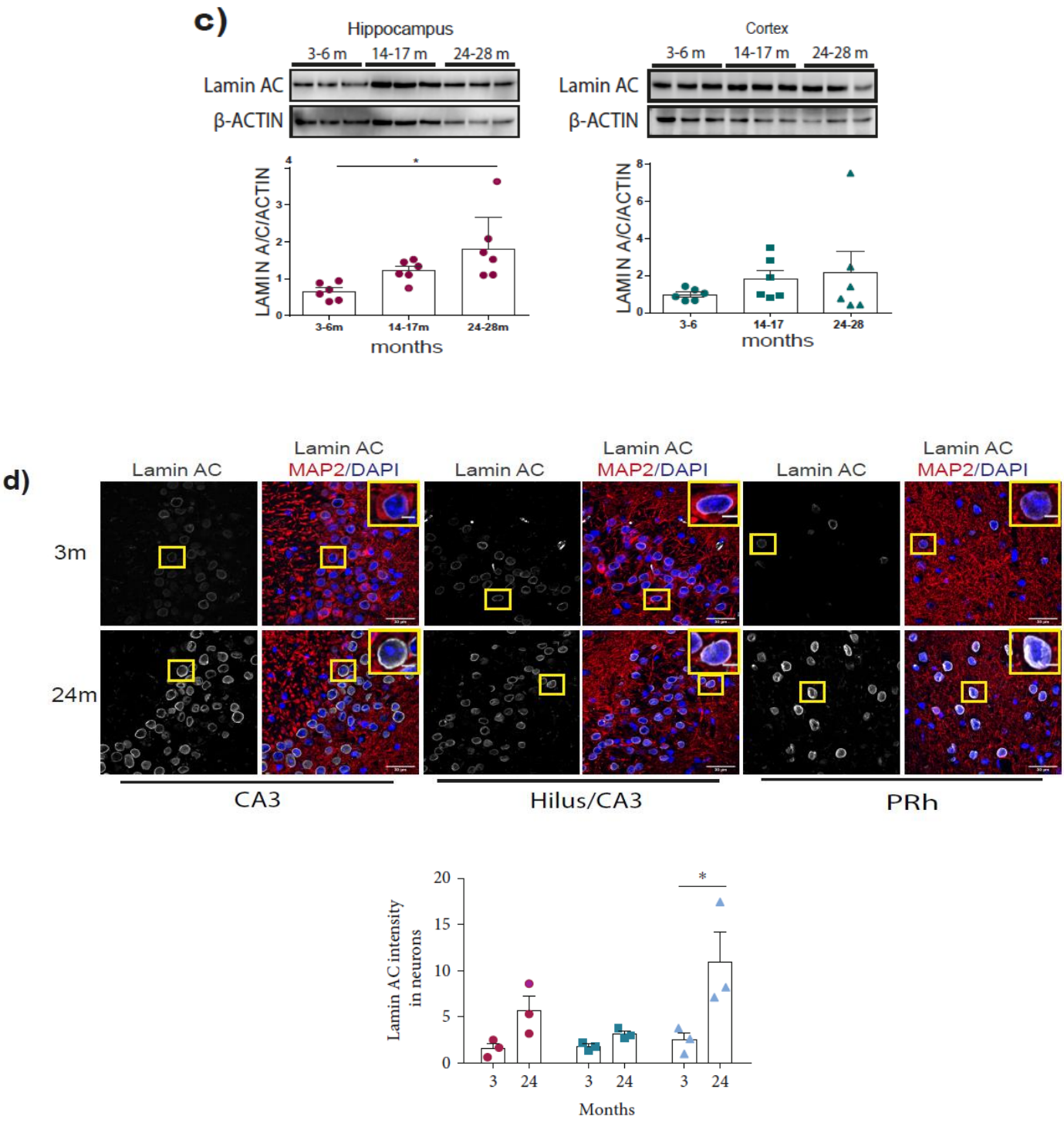

Figura 11. Neuronas con características senescentes se acumulan en el hipocampo y corteza perirhinal en ratones de 24 meses. (a) La actividad SA-β-gal fue cuantificada en el hipocampo y corteza de ratones de 3 y 24 meses como se indica en los métodos. Las gráficas muestran el porcentaje de área SA-β-gal positiva en cada región analizada. Las barras corresponden a la media ± SEM de tres experimentos independientes, las diferencias significativas se determinaron usando t-Test Student *p <0.05. (b, c) Western blot para detectar la expresión de lamina B1 y lamina A/C en el hipocampo y corteza de ratones de las edades indicadas. Las gráficas representan el análisis de la densitometría de 5 ó 6 experimentos independientes. Las barras representan la media ± SEM, las diferencias significativas se calcularon con Anova de una vía y Dunnet´s como test post hoc; *p <0.05, **p<0.01. (d.) Inmunofluorescencia para detectar lamina A/C en neuronas (identificadas porque expresan MAP2) en las

áreas indicadas de ratones de 3 y 24 meses. Las gráficas muestran la densidad de pixeles de lamina A/C en las áreas del cerebro indicas. Las barras presentan la media ± SEM de tres experimentos independientes, con diferencias significativas calculadas con Anova de dos vías y Sidak como test post hoc, * p <0.05.

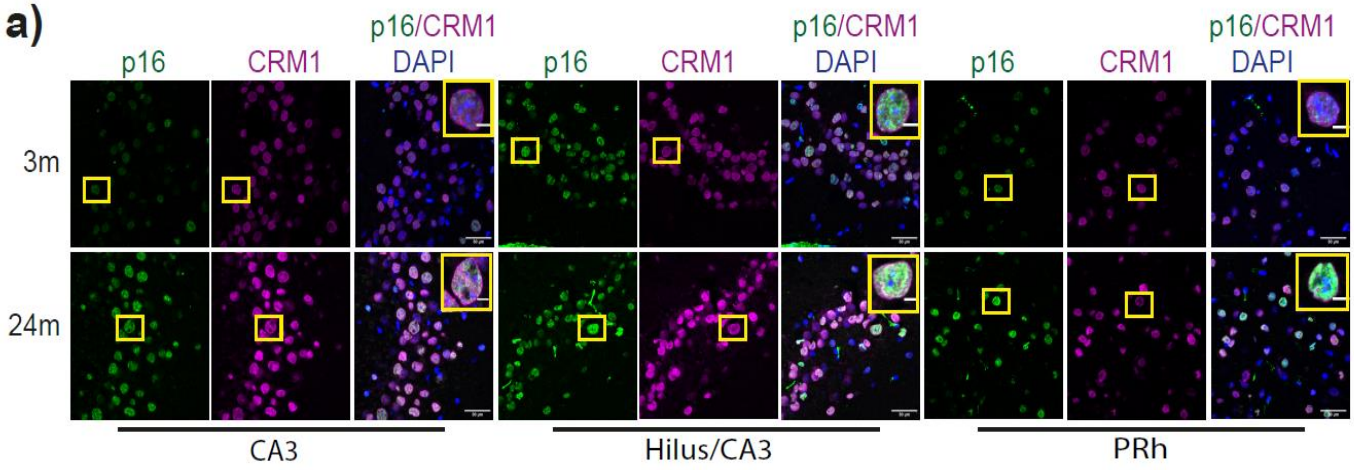

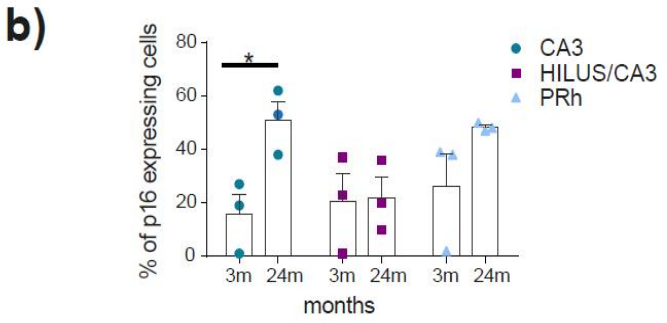

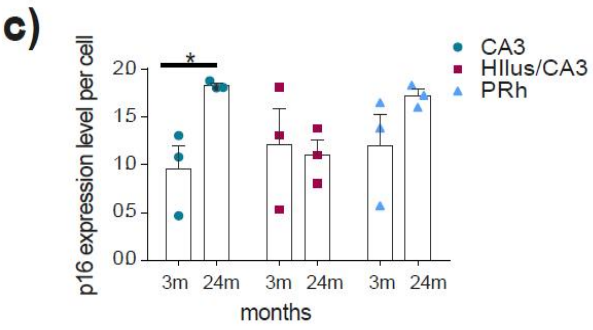

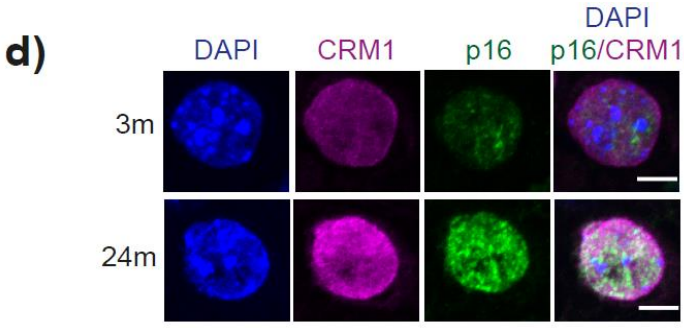

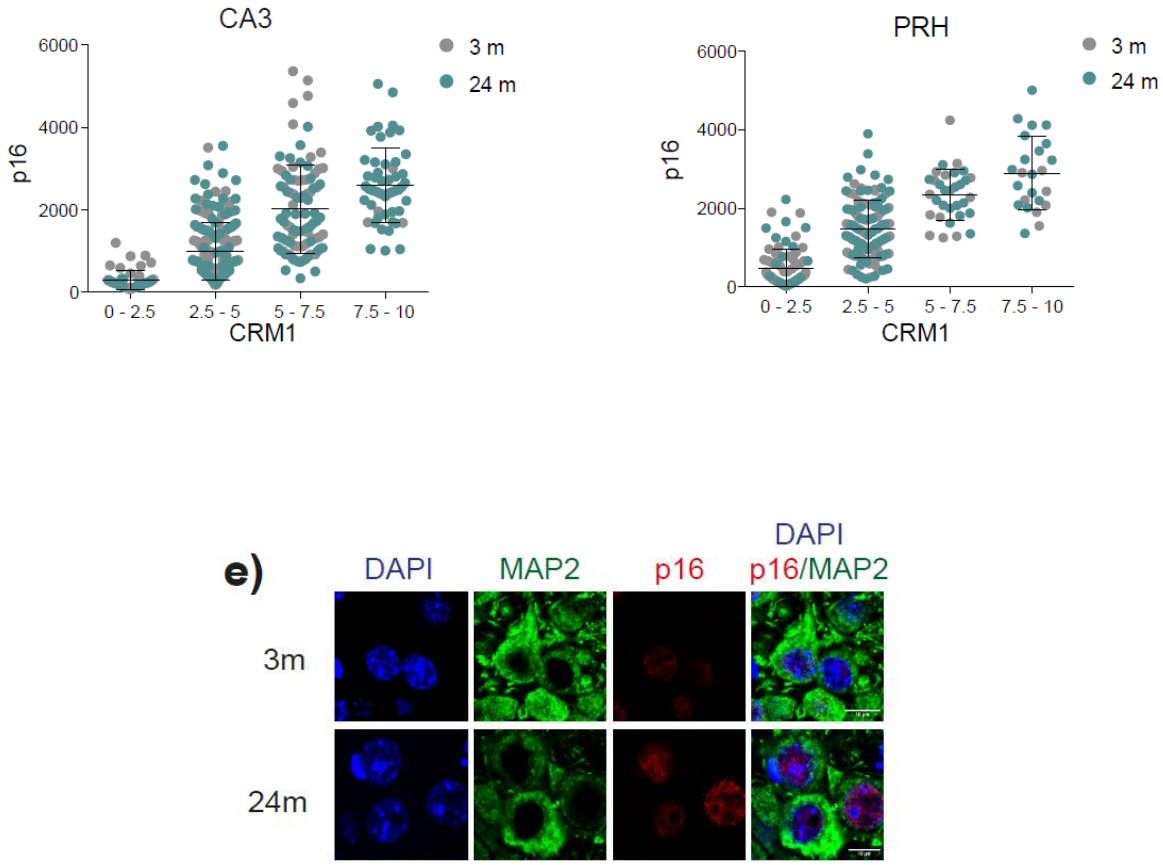

Figura 12. Un aumento en la expresión de p16^{INK4a} en células de la región CA3 y la corteza PRh de ratones de 24 meses correlaciona con el aumento de CRM1 nuclear. (a.) Inmunofluorescencia para detectar a p16^{INK4a} y CRM1 en la región CA3, hilus y corteza perirhinal (PRh), de ratones jóvenes (3 meses) y de ratones viejos (24 meses). Los cuadros amarillos muestran una célula representativa (b) Las gráficas representan el porcentaje de células con núcleos p16^{INK4a} positivos, o la densidad de pixeles de la señal p16^{INK4a} nuclear como se indica. n=3. Las barras representan la media ± SEM, t-Test Student *p <0.05. (c) El gráfico presenta la densidad de pixeles de p16^{INK4a} nuclear, el resultado se expresa como la media ± SEM, t-Test Student *p <0.05. Para (b) y (c) el número de células contadas fue: CA3, n=233 para 3 meses y n=221 para 24 meses; Hilus, n=134 de 3 meses y n=159 de 24 meses; corteza PRh, n=168 de 3 meses y n=151 de 24 meses. (d) Imagen representativa de la doble inmunotinción p16^{INK4a}-CRM1; la barra de escala representa 5µm. La cuantificación de la densidad de pixeles de p16^{INK4a} fue graficada contra la densidad de pixeles nuclear de CRM1 en la región CA3, n=190 de 3 meses y n=200 de 24 meses y corteza PRh, n=125 de 3 meses y n=132 de 24 meses. (e) Iinmunofluorescencia representativa de p16^{INK4a} en neuronas identificadas por su expresión de MAP2 en la región CA3 del hipocampo de 3 y 24 meses

7.8. *La inhibición farmacológica de CRM1 incrementa TFEB nuclear y promueve el flujo autofágico en un modelo de senescencia neuronal in vitro.*

Para evaluar la relación entre el aumento de CMR1 y las alteraciones del flujo autofágico, trabajamos con un modelo de senescencia neuronal *in vitro*. Como se muestra en Moreno-Blas et al.,2019, neuronas corticales embrionarias que son cultivadas durante 26 días *in vitro* (26 D*IV)*, desarrollan un fenotipo senescente acompañado por una autofagia disfuncional. En este modelo, las neuronas de 26 D*IV* logran recapitular características de la senescencia neuronal observada *in vivo* en el envejecimiento fisiológico que mostramos arriba [47]. Observamos que a 26 D*IV* las neuronas muestran acumulación de CRM1 comparadas con sus controles jóvenes de 6 D*IV* (Figura 13a, b). Además, la mitad de las neuronas también presentaron invaginaciones nucleares enriquecidas de CRM1 (Figura 13a, c). De manera interesante, la presencia de estas estructuras intranucleares ha sido reportada en senescencia inducida por radiación. Sin embargo, no está claro cuál es el papel de estas estructuras durante la senescencia [93]. Consistente con los resultados observados *in vivo*, encontramos una disminución de TFEB nuclear en neuronas senescentes de 26 D*IV* (Figura 13d, e). Para saber si la actividad de CRM1 causa el exporte de TFEB del núcleo, tratamos a las células con leptomicina B, una molécula que se une covalentemente a un residuo de cisteína en la región central conservada de CRM1, inhibiendo así su actividad [94]. Observamos un aumento significativo en los niveles de TFEB nuclear después de 24 horas de tratamiento, este efecto se conserva tanto en neuronas de 6 D*IV* (jóvenes) como en neuronas de 26 D*IV* (viejas) (Figura 13f, g). El aumento de TFEB nuclear reduce la acumulación de p62/SQSTM1 y LC3 observada en células de 26 D*IV,* después de 4 días de tratamiento, sin afectar la viabilidad celular (Figura 14a-c). Con el fin de confirmar el aumento en el flujo autofágico, las células fueron tratadas con LMB en presencia de cloroquina (CQ), un fármaco que reduce el flujo autofágico evitando la fusión del autofagosoma con el lisosoma [95]. Observamos que el tratamiento con CQ aumenta la cantidad de puntos de p62/SQMST1 por célula y la señal de LC3; dicho aumento supera los niveles de los controles de 26 D*IV,* sugiriendo que el tratamiento con LMB aumenta el flujo autofágico (Figura 14a-c). Adicionalmente, estudiamos la morfología de los lisosomas como una evidencia complementaria de un flujo autofágico activo. Cuando los lisosomas tienen una tasa de degradación baja, se alargan (crecen) y acumulan agregados protéicos; esta es una característica de las células senescentes [96–98]. Identificamos que los lisosomas de neuronas de 26 D*IV* (neuronas senescentes), muestran un aumento significativo de los lisosomas alargados (Figura 14d-f). Acorde a nuestra hipótesis, en respuesta al tratamiento con LMB la morfología de los lisosomas se recuperá, aumentando parcialmente el porcentaje de lisosomas pequeños o funcionales. Estos resultados muestran que la inhibición farmacología de CRM1 es capaz de aumentar los niveles de TFEB nuclear y en consecuencia aumentar el flujo autofágico en neuronas senescentes.

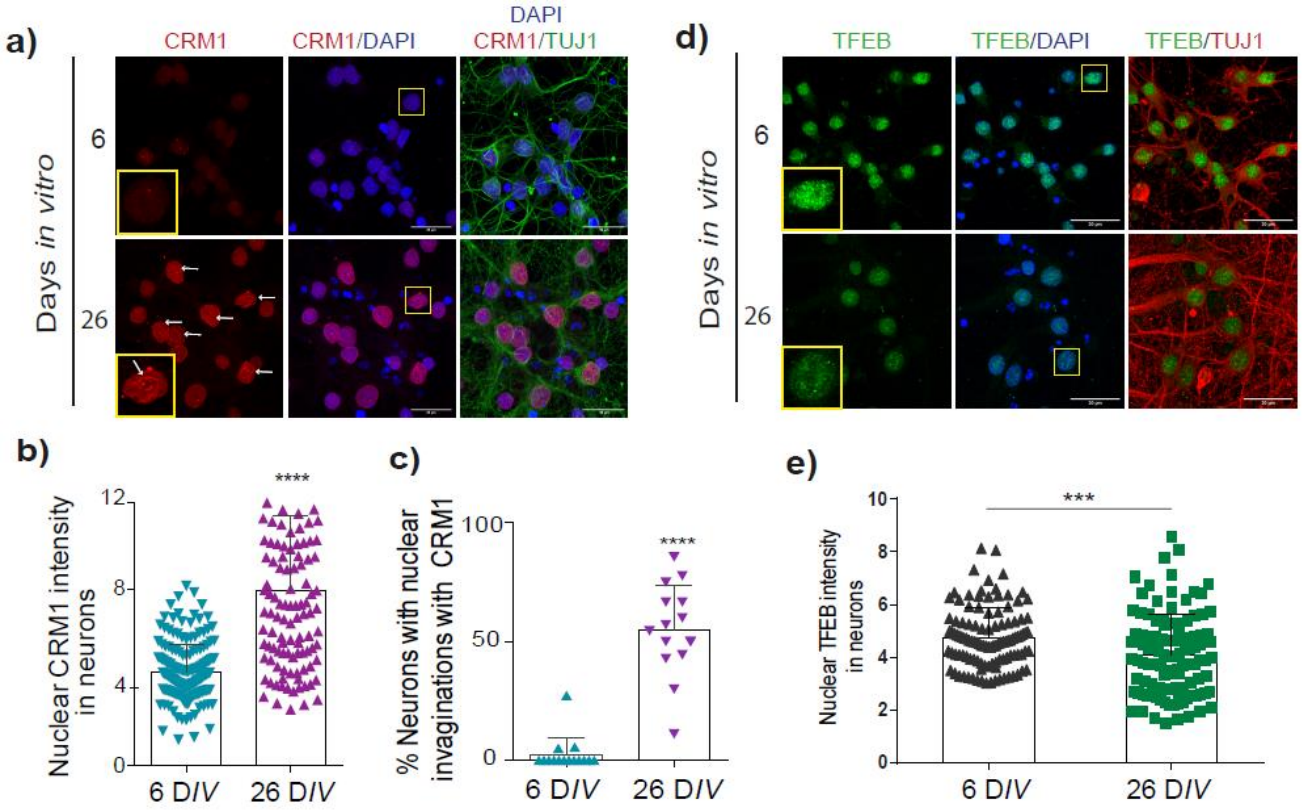
a)
CRM1
CRM1/DAPI
DAPI
CRM1/TUJ1
Days in vitro
6
26
d)
TFEB
TFEB/DAPI
TFEB/TUJ1
b)
Nuclear CRM1 intensity in neurons
****
6 DIV
26 DIV
c)
% Neurons with nuclear invaginations with CRM1
e)
Nuclear TFEB intensity in neurons
***

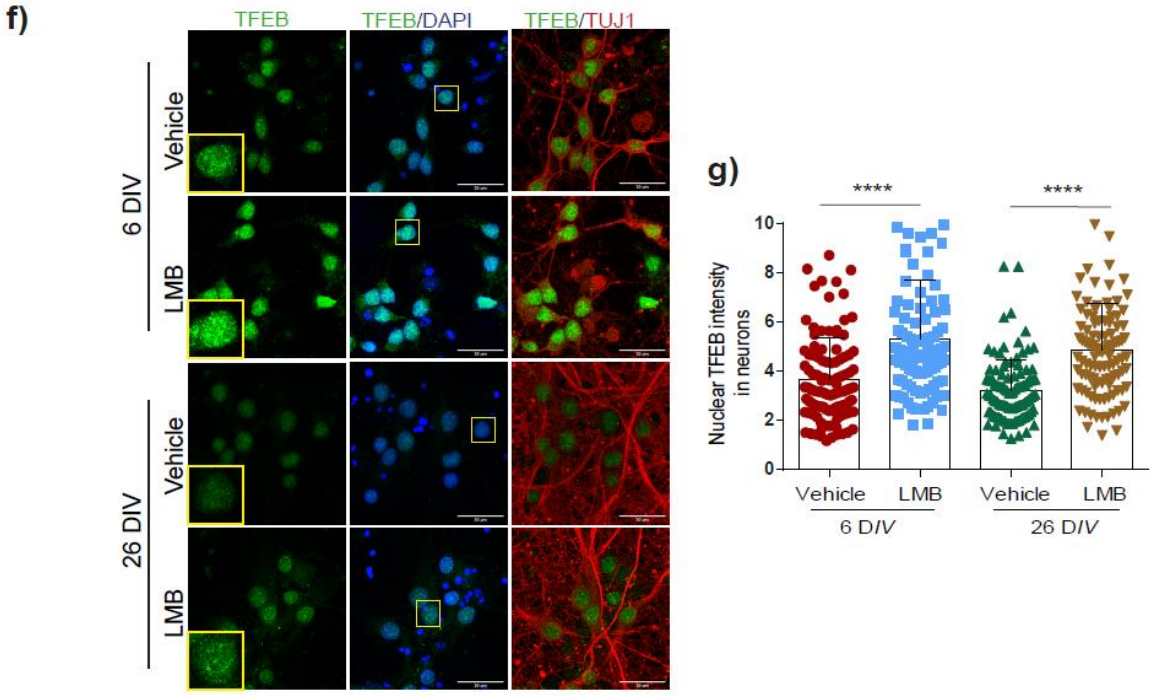
f)
TFEB
TFEB/DAPI
TFEB/TUJ1
6 DIV
26 DIV
Vehicle
LMB
g)
Nuclear TFEB intensity in neurons
****
Vehicle
LMB
6 DIV
26 DIV

Figura 13. CRM1 se acumula en neuronas senescentes *in vitro* y la inhibición farmacológica de CRM1 aumenta la localización nuclear de TFEB. (a.) Inmunofluorescencia para detectar CRM1 en neuronas (identificadas por expresar TUJ1) en un cultivo primario de corteza por los días indicados. Las flechas indican que CRM1 está enriquecido en invaginaciones de la envoltura nuclear. La barra de escala representa 25 µm (b.) La gráfica muestra la densidad de pixeles de CRM1 en el núcleo, cada punto representa una célula, 100 células por condiciones fueron incluidas(c.) La gráfica representa el porcentaje de neuronas con invaginaciones nucleares enriquecidas en CRM1 sobre el total de células, fueron cuantificadas al menos 100 células por grupo, de 3 experimentos independientes; t-Student **** p<0.0001. (d) Inmunofluorescencia para detectar TFEB en las neuronas (identificadas por expresar TUJ1); la barra de escala representa 30 µm. (e) Las gráficas muestran la densidad de pixeles de TFEB nuclear en neuronas corticales incubadas durante los días indicados. Las barras representan la media ± SD (n=100 células por experimento, por grupo, de tres experimentos independientes), t-Student ***p<0.001. (f) Células corticales cultivadas por 6 o 26 D*IV* y tratadas por 24 hrs con leptomicina (LMB) a una concentración de 5nM o vehículo para detectar TFEB. (g) Las gráficas representan la densidad de pixeles de TFEB nuclear, las barras corresponden a la media ± SD (n=100 células por grupo, por experimento de tres experimentos independientes), con diferencias significativas determinadas con t-Student, ****p<0.0001.

.

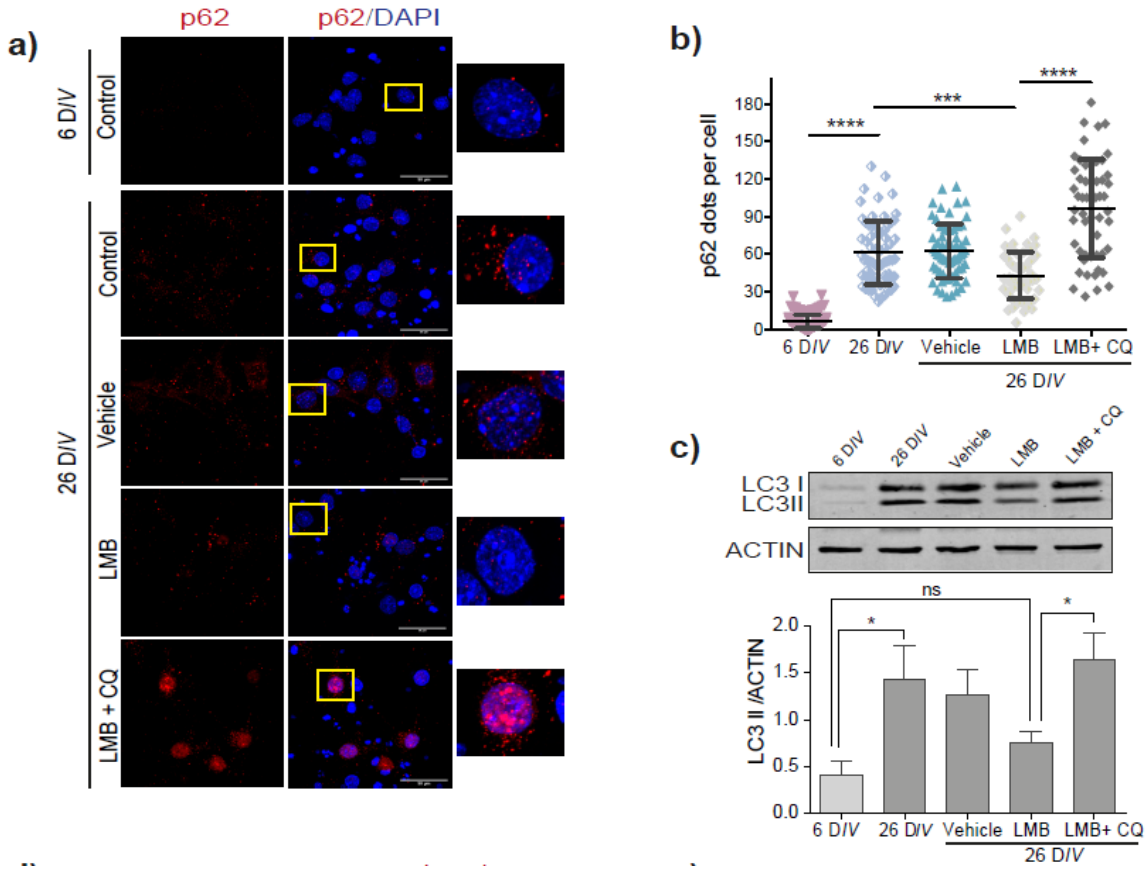

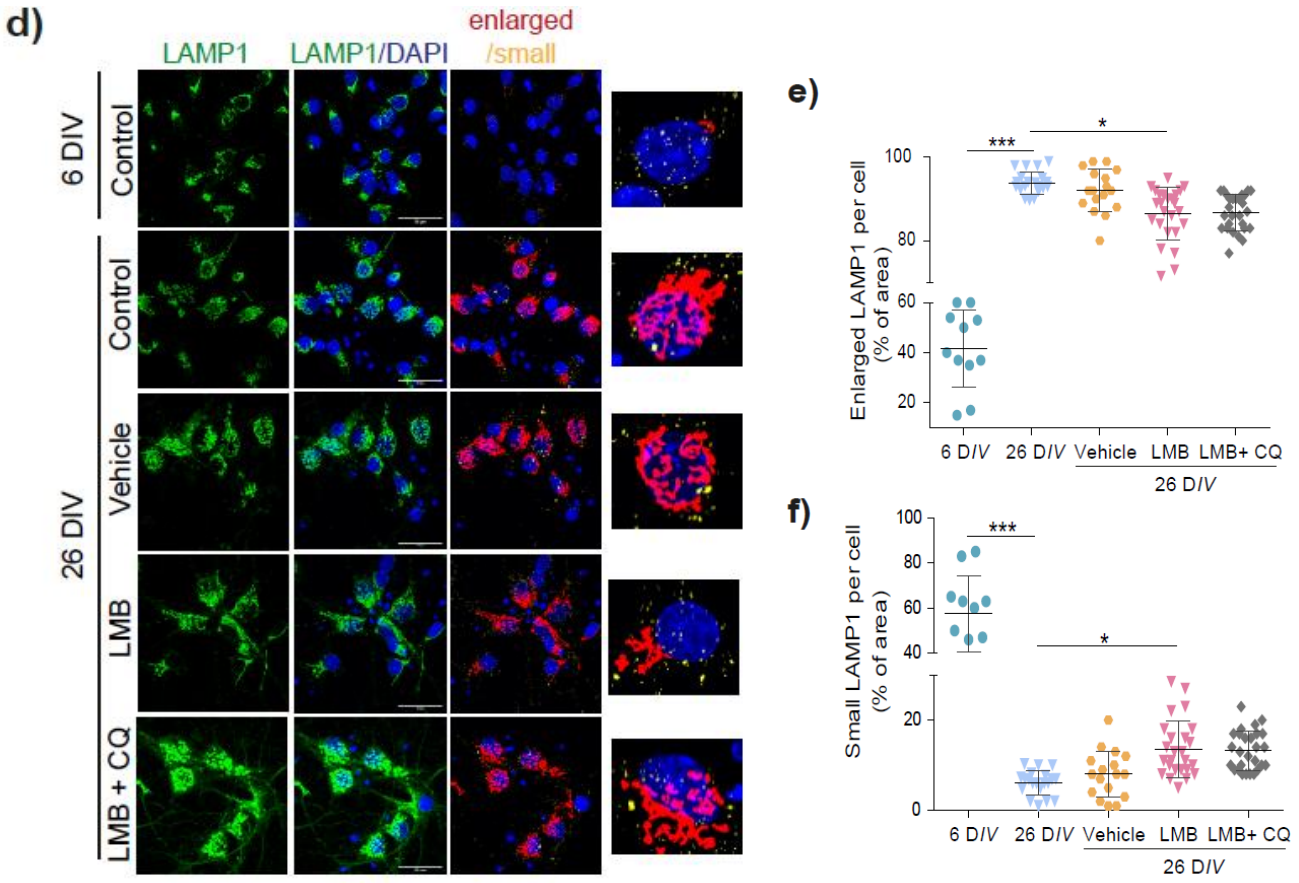

Figura 14. La inhibición de CRM1 restaura el flujo autofágico en neuronas de 26 D*IV*. Neuronas corticales de 26 D*IV* fueron tratadas LMB 5 nM durante 4 días (empezando en 22 D*IV*) y con CQ 20 µM o vehículo durante 4 horas. (a) Inmunofluorescencia para detectar p62/SQSTM1; la barra de escala representa 30µm, una amplificación de una célula representativa se muestra a la derecha. (b) Las gráficas muestran la cuantificación de los puntos de p62/SQSTM1 por célula, las barras muestran la media ± SD de tres experimentos independientes, las diferencias significativas fueron evaluados utilizando Anova de una vía y comparación múltiple de Tuckey, ***p<0.001, **** p<0.0001. (c) Western blot para detectar LC3 y ACTINA. Las gráficas muestran el análisis de densitometría de LC3-II normalizado con ACTINA; las barras representan la media ± SEM. El análisis Anova de dos vías seguida por comparación múltiple de Holm-Sidak; *p <0.05, ns=no. (d) Inmunofluorescencia para LAMP1. (e) Se muestra el número de lisosomas alargados por célula. (f) Se muestra el número de lisosomas pequeños por célula. El método de cuantificación se describe la sección de métodos. Las barras representan la media ± SD, con diferencias significativos calculadas por Anova de una vía seguida por comparación múltiple de Sidak, *p<0.05, **** p<0.0001.

7.9. *Inhibir a CRM1 reduce la actividad SA-β-gal, pero no recupera las alteraciones de la envoltura nuclear*

La actividad aumentada de CRM1 durante el envejecimiento disminuye la localización nuclear de TFEB y altera el flujo autofágico. Una autofagia deficiente promueve el establecimiento de la senescencia celular en neuronas [46,47], por ello exploramos la posibilidad de que este aumento en la proteína CRM1 también correlaciona con la senescencia neuronal. Evaluamos cuatro marcadores de senescencia: la estabilización de la lamina A/C, expresión de $p16^{INK4a}$, reducción de la lamina B1 y la actividad SA-β-gal. Tal como se observó en el cerebro *in vivo,* encontramos un aumento en la expresión de $p16^{INK4a}$ en neuronas de 26 D*IV*, además este aumento correlaciona de forma positiva con el incremento en los niveles de CRM1 (Figura 15a). En el caso de las laminas, observamos que lamina A/C aumenta y este aumento también correlaciona con el incremento en la señal de CRM1 (Figura 15b). Por su parte, la lamina B1 disminuye en neuronas de 26 D*IV (*Figura 15c). En conjunto, estos datos sugieren que las células corticales de 26 D*IV* muestran características del fenotipo senescente que podrían estar asociadas con el aumento en la expresión de CRM1. Para corroborar esta idea, los cultivos fueron tratados durante 4 días (de 23 D*IV* a 26 D*IV*) con LMB. La viabilidad celular fue corroborada utilizando una tinción de calceina y homodímero de etidio. No se observó una disminución significativa en la viabilidad celular tal como se muestra en la Figura 16a. Notablemente, la inhibición de CRM1 durante 4 días previo a la evaluación redujo significativamente la actividad SA-β-gal (Figura 17a). Sin embargo, no encontramos cambios en los niveles de lamina A/C o Lamina B1 en respuesta al tratamiento con LMB (Figura 17b, c).

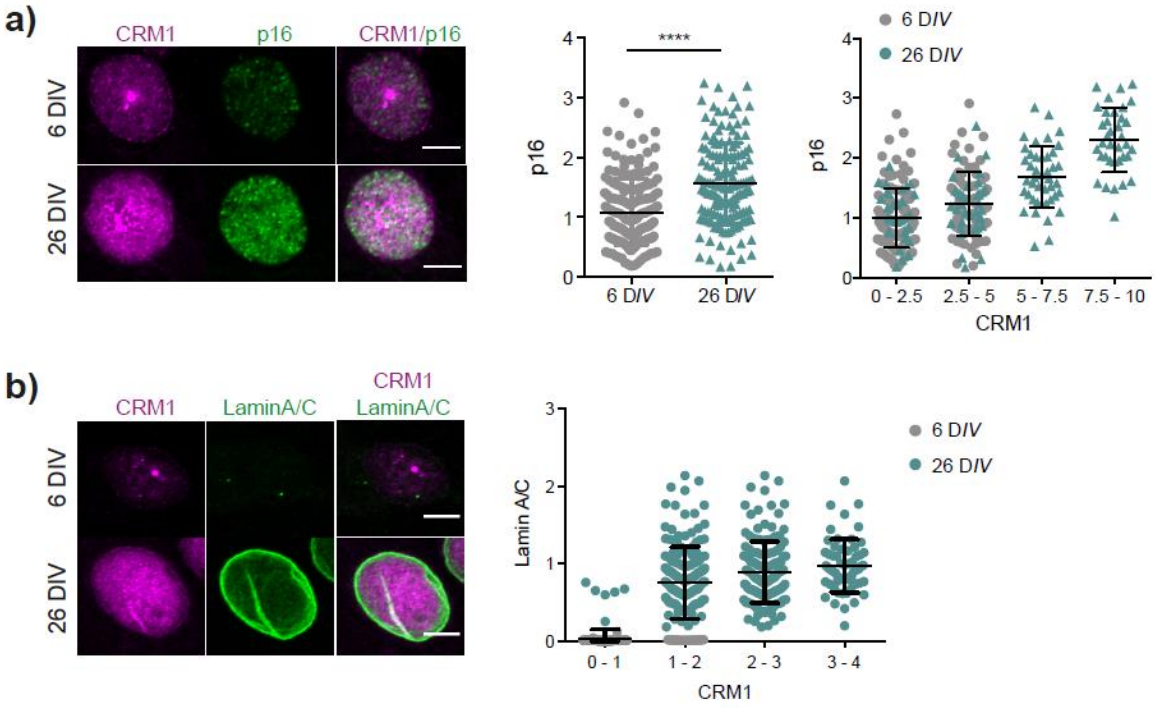

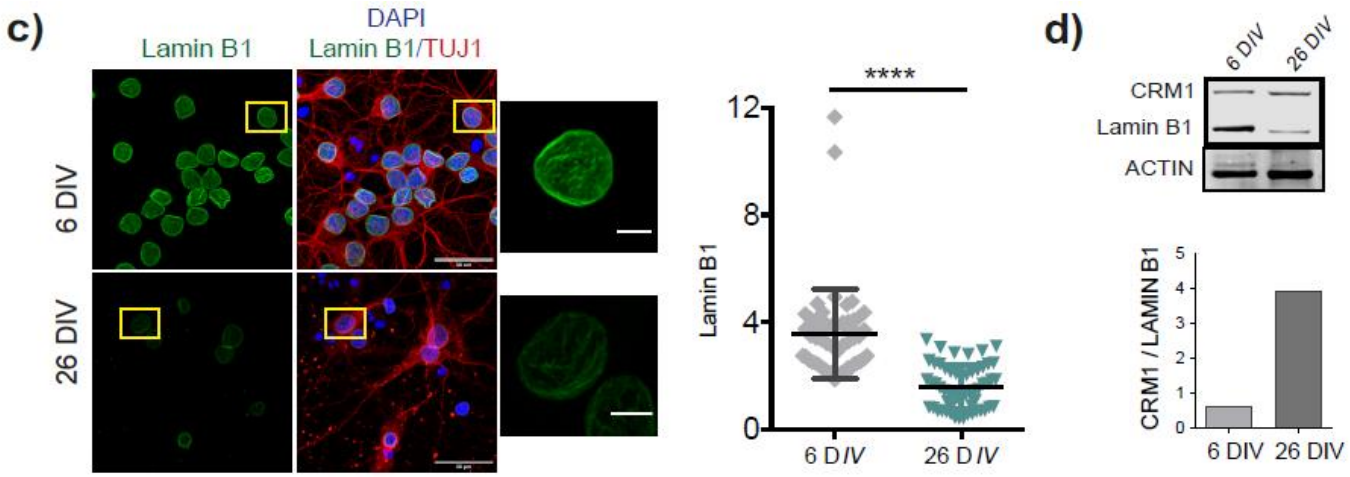

Figura 15. Un aumento en los niveles de CRM1 nuclear correlacionan con marcadores de senescencia neuronal *in vitro.* (a) Inmunofluorescencia para identificar p16^{INK4a} y CRM1 en cultivos primarios corticales de 6 o 26 D*IV*. La barra de escala representa 30 µm. Los núcleos fueron teñidos con DAPI. Las gráficas a la izquierda muestran la densidad de pixeles de p16^{INK4a} en el núcleo de células corticales; el grafico a la derecha muestra la correlación entre los niveles de expresión de p16 ^{INK4a} y CRM1. Las barras representan la media ± SD de tres experimentos independientes con diferencias significativas determinadas por t-Student ****p<0.0001. Las células de 26 D*IV* muestran mayor expresión de CRM1 y de p16 ^{INK4a} comparadas con las células de 6 D*IV*. (b) Doble inmunofluorescencia para detectar CRM1 y lamina A/C. La barra de escala representa 5 µm. El gráfico muestra la cuantificación de la intensidad de la lamina A/C *versus* la intensidad de CRM1. Las barras representan la media ± SD de 3 experimentos independientes. (c) Inmunodetección de lamina B1 en neuronas (identificadas por expresar TUJ1) de 6 o 26 *DIV.* La barra de escala representa 30µm. Los cuadros amarillos sobre las imágenes, muestran una amplificación. La gráfica representa la intensidad de fluorescencia de la señal de la lamina B1 nuclear. Las barras muestran la media ± SD de 3 experimentos independientes con diferencias significativas determinadas por t-Student, ****p<0.0001. Cada punto en la gráfica representa una célula y se incluyen 3 experimentos independientes. (d) Western blot de lisados totales de células corticales cultivas por el tiempo indicado. La relación CRM1 sobre lamina B1 (ambas previamente normalizadas con actina), es comparada la gráfica, n=2.

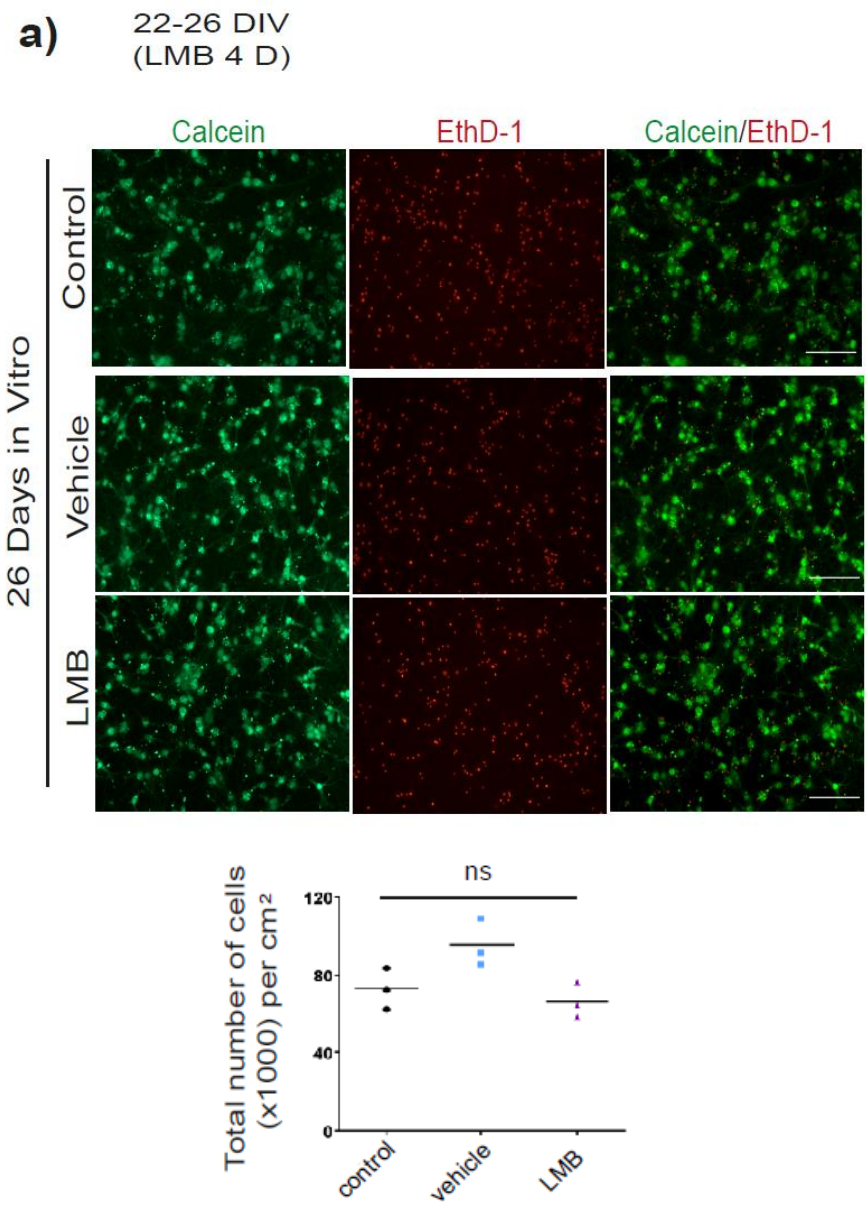

Figura 16. Las células corticales son viables después del tratamiento con leptomicina (LMB). (a) La viabilidad celular fue evaluada utilizando el kit LIVE/DEAD. Las células vivas fueron teñidas con calceina (verde) y las células muertas con homodímero de etidio (rojo). La barra de escala representa 500 µm. La gráfica representa el número total de células por cm^2 después del tratamiento con LMB o vehículo por 4 días. Se realizaron 3 experimentos independientes, el punto representa el promedio de 5 imágenes por experimento. Anova de una vía y comparación múltiple de Tukey como prueba post hoc.

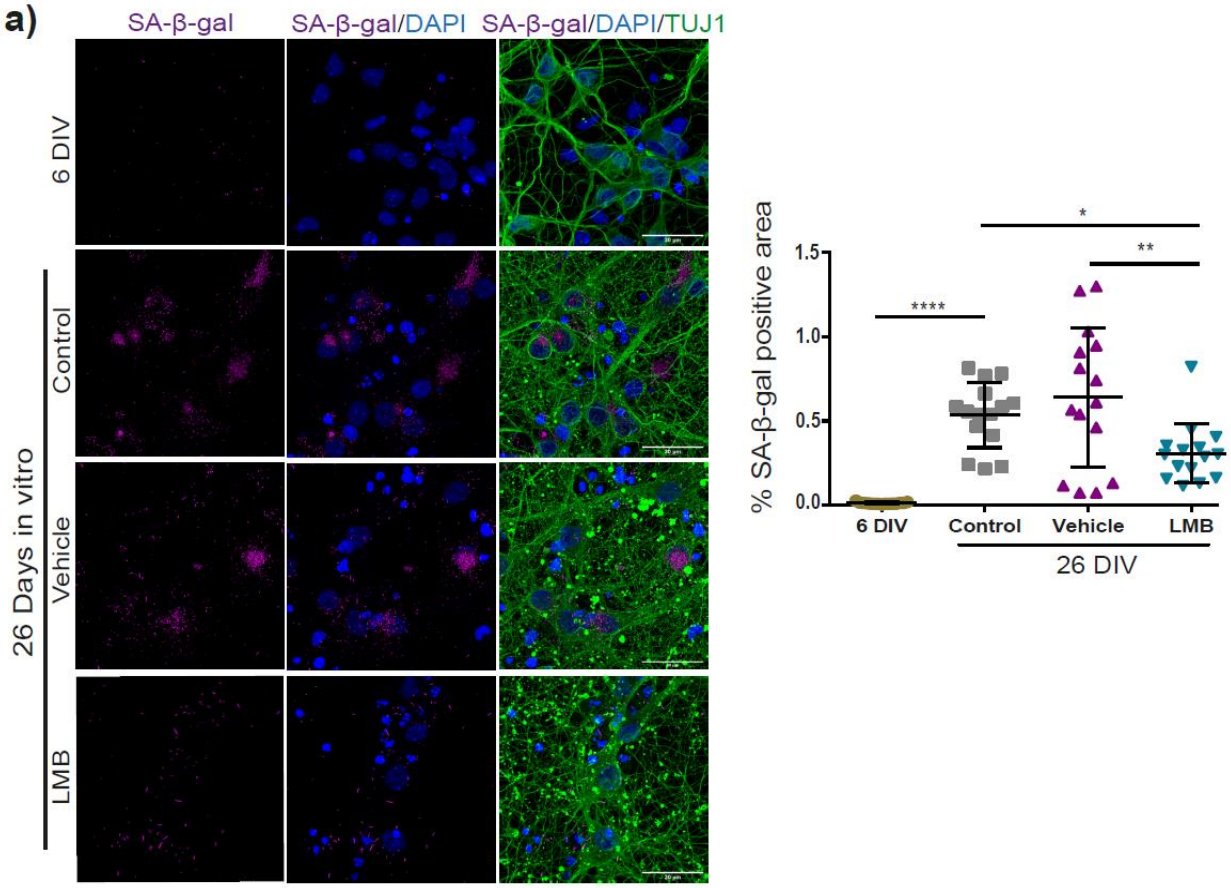
a)
SA-β-gal
SA-β-gal/DAPI
SA-β-gal/DAPI/TUJ1
6 DIV
26 Days in vitro
Control
Vehicle
LMB
% SA-β-gal positive area
1.5
1.0
0.5
0.0
****
*
**
6 DIV
Control
Vehicle
LMB
26 DIV

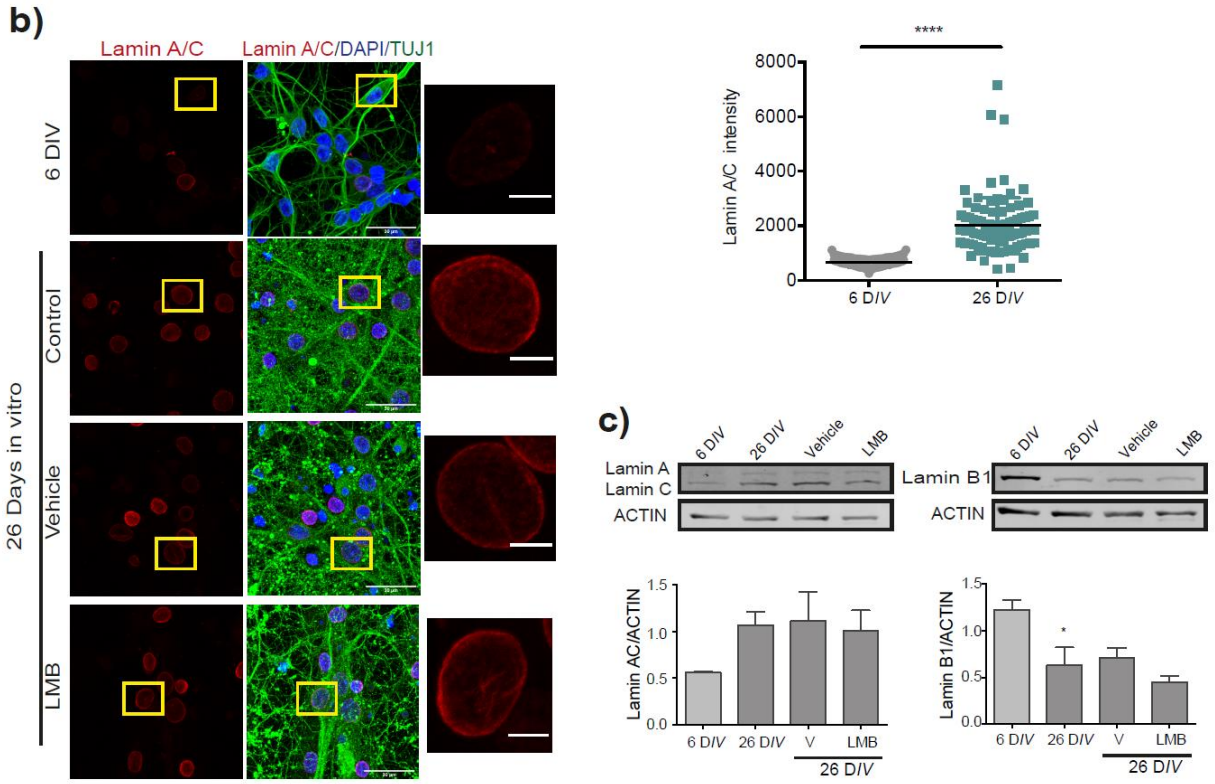

Figura 17. La inhibición de CRM1 reduce la actividad SA-β-gal, pero no revierte las alteraciones de la envoltura nuclear en neuronas senescentes *in vitro*. (a.) Detección de la actividad SA-β-gal (por microscopia confocal) en neuronas (identificadas por expresar TUJ1) de cultivos corticales de 26 *DIV* tratadas por 4 con 5μM LMB o vehículo. La barra de escala representa 30 μm. Las gráficas muestran el porcentaje del área SA-β-gal positiva. Cinco campos de tres experimentos independientes fueron cuantificados. Las barras representan la media ± SD de 3 experimentos independientes con diferencias significativas determinadas por Anova de una vía, con Comparación mutiple de Holm-Sidak, test *p <0.05; **p <0.01; ****p <0.0001. El tratamiento con LMB reduce significativamente el porcentaje de área SA-β-gal positiva. (b) Inmunofluorescencia para detectar Lamina AC en neuronas corticales de 6 y 26 *DIV,* tratadas con 5 nM LMB o vehículo por 4 días. La gráfica muestra la intensidad de lamina A/C en neuronas de 6 y 26 D*IV,* t-Student ****p<0.0001. (c.) Análisis por Western blot para detectar la expresión de lamina A/C o lamina B1 en cultivos primarios de células corticales de 6 y 26 D*IV*, tratadas o no con LMB, n=3. Las barras representan la media ± SEM. Anova de una vía y comparación múltiple de Holm-Sidak, *p <0.05.

8. Discusión

Durante el envejecimiento del cerebro, alteraciones en el flujo autofágico y la senescencia celular se relacionan con la pérdida de las habilidades cognitivas en mamíferos. El objetivo de este trabajo fue determinar si en el cerebro de ratas y ratones ocurren fallas en la autofagia que favorecen el establecimiento de la senescencia neuronal, y de ser así, si son causadas por un aumento en la actividad de la exportina-1/CRM1. El tráfico de proteínas entre el núcleo y el citoplasma es regulado por el complejo del poro nuclear (NPC), las importinas y las exportinas. De forma interesante, cambios en la actividad de estas proteínas se relacionan con el envejecimiento [4]. Por su parte, la proteína CRM1 es la exportina mejor estudiada y entre sus blancos se encuentran factores de transcripción necesarios para el buen funcionamiento de la autofagia, como TFEB [11,99] Debido a esta relación, nosotros nos preguntamos si el aumento en la actividad de CRM1 en neuronas podría dirigir las fallas en la autofagia y en consecuencia promover la senescencia neuronal que efectivamente encontramos en corteza e hipocampo de cerebros viejos. De forma consistente, observamos que la proteína CRM1 aumenta en neuronas del hipocampo y corteza en ratones de 24 meses y este cambio es acompañado por una disminución en la localización nuclear de TFEB, sugiriendo un aumento en su exporte. El aumento de CRM1 media la disminución de TFEB en el núcleo y promueve una autofagia disfuncional en la región CA3 del hipocampo de ratones de 24 meses, tal como sugiere la acumulación de p62/SQSTM1 en neuronas que correlaciona positivamente con el aumento de CRM1. Fortaleciendo nuestra hipótesis, la inhibición farmacológica de CRM1 en un modelo *in vitro,* aumenta la localización nuclear de TFEB en neuronas, y este cambio es acompañado por el aumento del flujo autofágico caracterizado por la disminución de p62/SQSTM1 y LC3. Adicionalmente, observamos disminución de la morfología alargada de los lisosomas en neuronas de 26 D*IV*. Estos resultados son consistentes con los datos obtenidos en un modelo de ALS, en el que se observan alteraciones en el flujo autofágico relacionados con la disminución de TFEB en el núcleo [78].

Trastornos genéticos que causan envejecimiento prematuro como el síndrome de Hutchinson-Gilford y el síndrome de Weber, se caracterizan por presentar alteraciones en proteínas de la envoltura nuclear. Dichas alteraciones se asocian con inestabilidad genómica y defectos en el transporte núcleo-citoplasma [2,100]. Recientemente, se ha observado que estos cambios también ocurren en enfermedades neurodegenerativas y en el envejecimiento fisiológico. Por ejemplo, en las demencias causadas por hiper-fosforilación de Tau y en modelos de la enfermedad de Huntington y ALS se presentan disfunciones en el transporte núcleo-citoplasma [72,75,78,101,102] mientras que en cerebros *post mortem* de pacientes con la enfermedad de Alzheimer se encuentran alteradas las laminas nucleares [103]. Por nuestra parte, nosotros observamos que CRM1 está enriquecido en neuronas senescentes tanto *in vivo* como *in vitro*. De forma interesante observamos que CRM1 pierde su localización perinuclear en neuronas senescentes tanto *in vivo* como *in vitro*. Dado que CRM1 tiene un papel relevante en mantener la estructura y organización del genoma [104], es posible que los cambios en su localización estén relacionados con la reorganización del genoma reportada en células senescentes. Además, *in vitro* observamos que la acumulación de CRM1 ocurre especialmente en invaginaciones nucleares, que podrían estar relacionadas con la compartamentalización del NPC, aumentado la cinética de exporte de CRM1, tal como se ha observado para el exporte del mRNA a través de las invaginaciones nucleares causadas por Tauopatías [105]. Adicionalmente, en senescencia celular inducida por oncogenes se observa un incremento en la transcripción de rRNA inmediatamente después de la inducción a senescencia. De

forma interesante la proteína CRM1 regula el exporte de rRNA [106,107]. Por otro lado, las fallas en la autofagia durante el envejecimiento contribuyen a la formación de agregados proteicos que son característicos de enfermedades neurodegenerativas y que son conocidos por dañar el NPC, la permeabilidad del núcleo y por tanto el tráfico de proteínas a través del NPC. El aumento en la actividad de CRM1 observado en fibroblastos de piel de pacientes con HGPS es el resultado de un aumento en la expresión de CRM1 que es dirigido por el factor de transcripción NF-YA [2]. Además, la expresión de CRM1 también aumenta en diversos tipos de cáncer, en este contexto p53 y el factor de transcripción SP1, también activan su expresión [108]. Sin embargo, más estudios son necesarios para determinar si el aumento de CRM1 en neuronas durante el envejecimiento está asociado a un aumento en su expresión o fallas en su degradación.

Intervenciones farmacológicas o genéticas que reducen la actividad de CRM1 demuestran ser eficientes reduciendo la muerte neuronal y restaurando el transporte núcleo-citoplasma tanto en modelos de la enfermedad de Huntington [75], como de esclerosis lateral amiotrofica [78], demencias frontotemporales [72] y en un modelo de taupatias en moscas [105]. En este trabajo, observamos que el tratamiento con Leptomicina B que reduce la actividad de CRM1, también mejora el flujo autofagico a través del enriquecimiento de TFEB en el núcleo. Esta evidencia nos permite especular que la inhibición de CRM1 favorece la actividad transcripcional de TFEB tal como se ha observado en otros modelos [11,78]. Otras proteínas blanco de CRM1 como STAT3, podrían también contribuir a promover la autofagia y retrasar la senescencia. De forma interesante, encontramos que el tratamiento con Leptomicina B parece prevenir la aparición de algunas características del fenotipo senescente, como es el caso de la actividad SA-β-gal. Sin embargo, nosotros no observamos cambios en los niveles de lamina B1 o lamina A/C en respuesta al tratamiento con LMB, lo cual sugiere que las alteraciones en la envoltura nuclear no pueden ser revertidas en estas células, una vez que se han establecido. Estos resultados parecen ser contrarios a aquellos observados en fibroblastos HGPS senescentes [2]. Pero, sugerimos que la reducción en el número de fibroblastos senescentes después del tratamiento con LMB podría ser explicado por la naturaleza proliferativa de estas células, en contraste con las neuronas. En este sentido, es posible que una subpoblación de fibroblastos que no han adquirido el fenotipo senescente en el momento en que son tratados con LMB, prolifere y que, al mismo tiempo, el tratamiento con LMB prevenga la geroconversion de estas células proliferativas. Adicionalmente, trabajo previo de nuestro laboratorio observó que el tratamiento con trehalosa, un inductor de autofagia que promueve la localización nuclear de TFEB, reduce las invaginaciones nucleares de lamina A/C, en neuronas de 26 DIV cuando son tratadas en ventanas temporales más largas a las usadas en el presente trabajo. Por ello, más experimentos son necesarios para comprender si el efecto de inhibir CRM1 está relacionado con la prevención o con la reversión del fenotipo senescente.

En conjunto, nuestros datos demuestran que los niveles de la proteína CRM1 y su actividad aumentan en las neuronas y este aumento es dependiente del envejecimiento. La actividad aumentada de CRM1 es un mecanismo que podría perturbar la homeostasis neuronal contribuyendo a las fallas en la autofagia que, a su vez, favorecen la senescencia neuronal. Por lo tanto, CRM1 representa un blanco terapéutico y disminuir su actividad podría tener efectos benéficos en el envejecimiento fisiológico del cerebro y diferentes enfermedades neurodegenerativas.

9. Conclusión

El desarrollo de este trabajo nos permitió aportar información nueva al campo del envejecimiento neuronal. Descubrimos que en la corteza e hipocampo de ratas y ratones envejecidos se acumulan neuronas senescentes con la autofagia atrofiada. Comprendimos que una parte del mecanismo involucrado en las fallas de la autofagia se asocia con el aumento en los niveles y actividad de la proteína CRM1. Además, proponemos que el aumento en el exporte nuclear dirigido por CRM1 altera la homeostasis neuronal durante el envejecimiento. Por lo tanto, es relevante considerar a las fallas en el transporte núcleo-citoplasma como una nueva característica del envejecimiento en el sistema nervioso central, de tal forma que se impulse la identificación de estrategias terapéuticas para evitar los efectos deletéreos asociados al aumento de CRM1, con el objetivo de retrasar el envejecimiento neuronal.

Perspectivas

1. Evaluar si el tratamiento con inhibidores de CRM1 menos tóxicos que permitan modular su actividad de manera que se restablezca la localización nuclear de los factores de transcripción pro-autofágicos.

En este proyecto implementamos el uso de las ventanas temporales de 7 días comenzando con el tratamiento de 19 a 26 D*IV.* Sin embargo, en esta condición observamos que LMB es tóxica y disminuye la viabilidad celular. La alta citotoxicidad de la LMB es resultado de la permanente inhibición de CRM1 mediada por una unión covalente.

Proponemos como alternativa implementar el uso de Selinexor (KTP-330) como inhibidor de CRM1, en un esquema de tratamiento similar al usado con trehalosa [47], tal como se muestra en la figura 18c. Selinexor pertenece a una serie de compuestos de segunda generación diseñados para inhibir a CRM1. Estas moléculas conocidas como compuestos SINE muestran una menor toxicidad. El mecanismo por el cual Selinexor inhibe la actividad de CRM1 involucra una unión de naturaleza covalente pero que es reversible, razón por la cual este compuesto es menos toxico. Además, KTP-330 promueve la degradación de la proteína CRM1 [109]. De forma interesante este compuesto y otros compuesto SINE, se encuentran en fases clínicas como auxiliar en el tratamiento de cáncer. Si el uso de KTP-330 no disminuye la viabilidad neuronal en respuesta a un tratamiento prolongado, se sugiere evaluar la potencia de este compuesto como un agente en la prevención de la senescencia neuronal. Adicionalmente, es importante considerar que CRM1 regula el exporte de alrededor de 200 proteínas y rRNAs de tal forma que es importante buscar otras vías relacionadas con el establecimiento de la senescencia neuronal que puedan ser reguladas por CRM1, además de las fallas en la autofagia ya evaluadas.

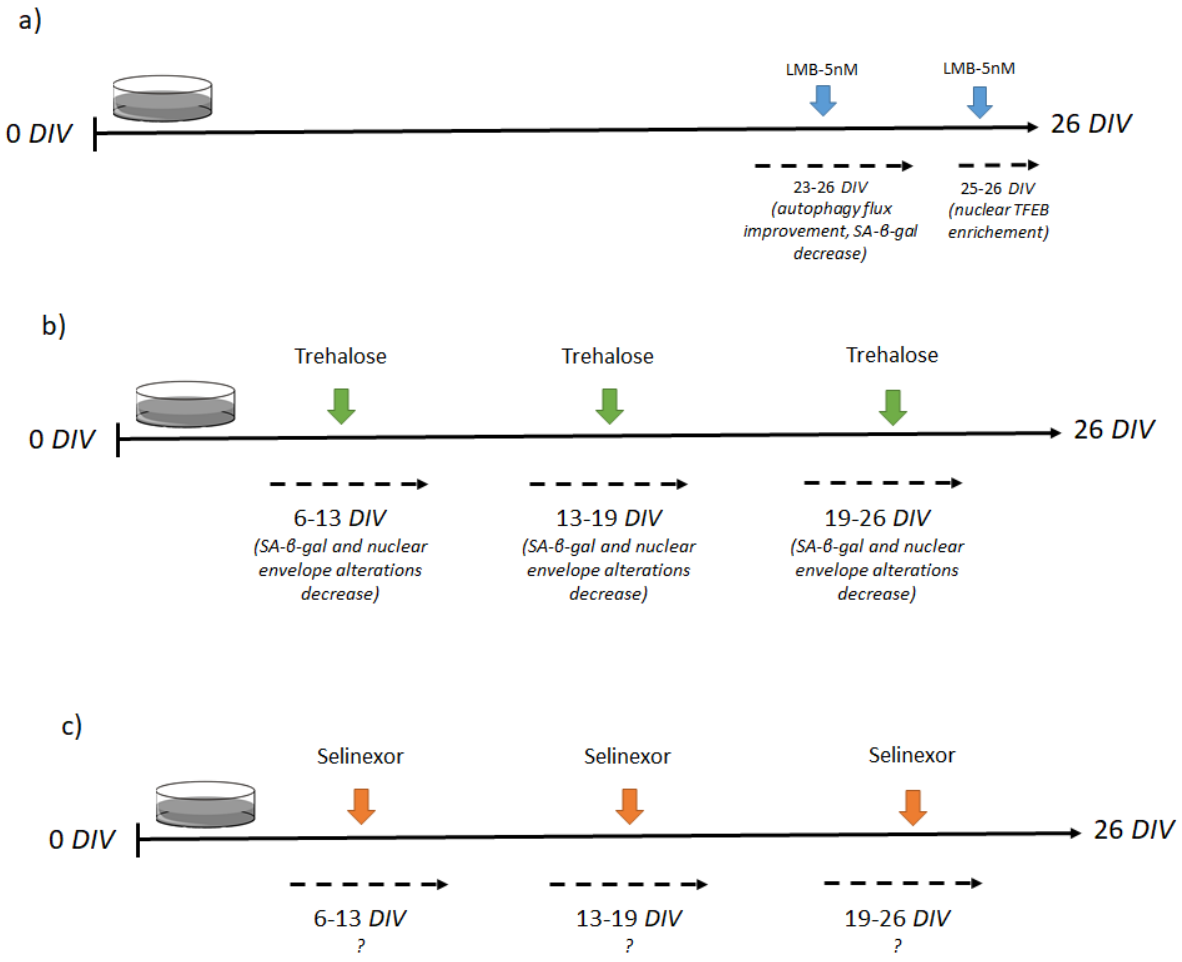

Figura 18. Esquemas de tratamiento para la inhibición de CRM1 y el aumento del flujo autofágico en neuronas, un modelo *in vitro*. (a.) Ventanas de tratamiento utilizadas para inhibir CRM1 con LMB 5nM, durante 24 horas y 4 días según se indica. La inducción de la autofagia y características del fenotipo senescente fueron evaluadas a 26 D*IV* en todos los casos. (b) Esquema de tratamiento desarrollado por Moreno-Blas et al., 2019 para el uso de trehalosa como inductor de autofagia. Las ventanas de tratamiento corresponden a 7 días y cada una de ellas aumenta la actividad autofagia y previene el establecimiento de la senescencia neuronal evaluada a 26 D*IV*. (c) Modelo de tratamiento sugerido para el compuesto Selinexor en el modelo de senescencia neuronal in vitro. Se sugiere un tiempo de 7 días para cada ventana temporal, así como la evaluación de la viabilidad celular, inducción de autofagia y características del fenotipo senescente en neuronas de 26 *DIV*.

10. Referencias

1. López-otín C, Blasco MA, Partridge L, Serrano M. The Hallmarks of Aging. 2013; 153: 1194–217. Available from: doi:https://doi.org/10.1016/j.cell.2013.05.039

2. García-Aguirre I, Alamillo-Iniesta A, Rodríguez-Pérez R, Vélez-Aguilera G, Amaro-Encarnación E, Jiménez-Gutiérrez E, Vásquez-Limeta A, Samuel Laredo-Cisneros M, Morales-Lázaro SL, Tiburcio-Félix R, Ortega A, Magaña JJ, Winder SJ, et al. Enhanced nuclear protein export in premature aging and rescue of the progeria phenotype by modulation of CRM1 activity. Aging Cell [Internet]. 2019; 18: 1–14. Available from: https://doi.org/10.1111/acel.13002

3. Cho UH, Hetzer MW. Nuclear Periphery Takes Center Stage : The Role of Nuclear Pore Complexes in Cell Identity and Aging. Neuron [Internet]. Elsevier Inc.; 2020; 106: 899–911. Available from: https://doi.org/10.1016/j.neuron.2020.05.031

4. Defects RAN, Mertens J, Ku M, Yao J, Hetzer MW, Gage FH, Paquola CM, Ku M, Hatch E, Bo L, Mertens J. Directly Reprogrammed Human Neurons Retain Aging-Associated Transcriptomic Signatures and Article Directly Reprogrammed Human Neurons Retain Aging-Associated Transcriptomic Signatures and Reveal Age-Related Nucleocytoplasmic Defects. 2015; : 705–18.

5. Aunan JR, Watson MM, Hagland HR, Søreide K. Molecular and biological hallmarks of ageing. Br J Surg. 2016; 103: e29–46.

6. Bussian TJ, Aziz A, Meyer CF, Swenson BL, Baker DJ, Clinic M, Clinic M. Clearance of senescent glial cells prevents tau-dependent pathology and cognitive decline. Nature [Internet]. 2019; 562: 578–82. Available from: https://doi.org/10.1038/s41586-018-0543-y

7. Glatigny M, Moriceau S, Rivagorda M, Ramos-Brossier M, Nascimbeni AC, Lante F, Shanley MR, Boudarene N, Rousseaud A, Friedman AK, Settembre C, Kuperwasser N, Friedlander G, et al. Autophagy Is Required for Memory Formation and Reverses Age-Related Memory Decline. Curr Biol. 2019; 29: 435-448.e8.

8. Simonsen A, Cumming RC, Brech A, Isakson P, Schubert DR, Finley KD. Promoting basal levels of autophagy in the nervous system enhances longevity and oxidant resistance in adult Drosophila. Autophagy. 2008; 4: 176–84.

9. Zhang P, Kishimoto Y, Grammatikakis I, Gottimukkala K, Cutler RG, Zhang S, Abdelmohsen K, Bohr VA, Sen JM, Gorospe M, Mattson MP. oligodendrocyte progenitor cell senescence and cognitive deficits in an Alzheimer ' s disease model. Nat Neurosci [Internet]. Springer US; 2019; 22. Available from: http://dx.doi.org/10.1038/s41593-019-0372-9

10. Risi M De, Torromino G, Tufano M, Moriceau S, Pignataro A, Rivagorda M, Carrano N, Middei S, Settembre C, Ammassari-teule M, Gardoni F, Mele A, Oury F, et al. Mechanisms by which autophagy regulates memory capacity in ageing. 2020; : 1–15.

11. Silvestrini MJ, Johnson JR, Kumar A V., Thakurta TG, Blais K, Neill ZA, Marion SW, St. Amand V, Reenan RA, Lapierre LR. Nuclear Export Inhibition Enhances HLH-30/TFEB Activity, Autophagy, and Lifespan. Cell Rep [Internet]. ElsevierCompany.; 2018; 23: 1915–21. Available from: https://doi.org/10.1016/j.celrep.2018.04.063

12. Galluzzi L, Baehrecke EH, Ballabio A, Boya P, Manuel J. Molecular definitions of autophagy and related processes. 2017; 36: 1811–36.

13. Tekirdag K, Cuervo AM. Chaperone-mediated autophagy and endosomal microautophagy: Joint by a chaperone. J Biol Chem. 2018; 293: 5414–24.

14. Kaushik S, Cuervo AM. The coming of age of chaperone-mediated autophagy. Nat Rev Mol Cell Biol [Internet]. Springer US; 2018; 19: 365–81. Available from: http://dx.doi.org/10.1038/s41580-018-0001-6

15. Moreno-Blas D, Gorostieta-Salas E, Castro-Obregón S. Connecting chaperone-mediated autophagy dysfunction to cellular senescence. Ageing Res Rev [Internet]. Elsevier B.V.; 2018; 41: 34–41. Available from: http://dx.doi.org/10.1016/j.arr.2017.11.001

16. Ponpuak M, Mandell MA, Kimura T, Chauhan S, Cleyrat C, Deretic V. Secretory autophagy. Curr Opin Cell Biol. 2015; 35: 106–16.

17. Kaur J, Debnath J. Autophagy at the crossroads of catabolism and anabolism. Nat Rev Mol Cell Biol. Nature Publishing Group; 2015; 16: 461–72.

18. Bento CF, Renna M, Ghislat G, Puri C, Ashkenazi A, Vicinanza M, Menzies FM, Rubinsztein DC. Mammalian Autophagy: How Does It Work? Annu Rev Biochem [Internet]. 2016; 85: 685–713. Available from: http://www.annualreviews.org/doi/10.1146/annurev-biochem-060815-014556

19. Shen W, Ganetzky B. Autophagy promotes synapse development in Drosophila. J Cell Biol. 2009; 187: 71–9.

20. Acevo-rodríguez PS, Maldonado G, Castro-obregón S. Autophagy Regulation by the Translation Machinery and Its Implications in Cancer. 2020; 10: 1–17.

21. Dikic I, Elazar Z. Mechanism and medical implications of mammalian autophagy. Nat Rev Mol Cell Biol [Internet]. Springer US; 2018; 19: 349–64. Available from: http://dx.doi.org/10.1038/s41580-018-0003-4

22. Kimura S, Noda T, Yoshimori T. Dynein-dependent Movement of Autophagosomes Mediates Efficient Encounters with Lysosomes. 2008; 122: 109–22.

23. Yu L, Chen Y, Tooze SA. Autophagy pathway: Cellular and molecular mechanisms. Autophagy. 2018; 14: 207–15.

24. Chen Y, Yu L. Recent progress in autophagic lysosome reformation. Traffic. 2017; 18: 358–61.

25. Yu L, Mcphee CK, Zheng L, Mardones GA, Rong Y, Peng J, Mi N, Zhao Y, Liu Z, Wan F, Hailey DW, Oorschot V, Klumperman J, et al. Termination of autophagy and

reformation of lysosomes regulated by mTOR. 2010; 465: 942–7.

26. Napolitano G, Esposito A, Choi H, Matarese M, Benedetti V, Di Malta C, Monfregola J, Medina DL, Lippincott-Schwartz J, Ballabio A. mTOR-dependent phosphorylation controls TFEB nuclear export. Nat Commun [Internet]. Springer US; 2018; 9. Available from: http://dx.doi.org/10.1038/s41467-018-05862-6

27. Medina DL, Di Paola S, Peluso I, Armani A, De Stefani D, Venditti R, Montefusco S, Scotto-Rosato A, Prezioso C, Forrester A, Settembre C, Wang W, Gao Q, et al. Lysosomal calcium signalling regulates autophagy through calcineurin and TFEB. Nat Cell Biol. 2015; 17: 288–99.

28. Martina JA, Puertollano R. Protein phosphatase 2A stimulates activation of TFEB and TFE3 transcription factors in response to oxidative stress. J Biol Chem. 2018; 293: 12525–34.

29. Napolitano G, Ballabio A. TFEB at a glance. J Cell Sci. 2016; 129: 2475–81.

30. Pan HY, Alamri AH, Valapala M. Nutrient deprivation and lysosomal stress induce activation of TFEB in retinal pigment epithelial cells. Cell Mol Biol Lett. Cellular & Molecular Biology Letters; 2019; 24: 33.

31. Bao J, Zheng L, Zhang Q, Li X, Zhang X, Li Z, Bai X, Zhang Z, Huo W, Zhao X, Shang S, Wang Q, Zhang C, et al. Deacetylation of TFEB promotes fibrillar Aβ degradation by upregulating lysosomal biogenesis in microglia. Protein Cell. Higher Education Press; 2016; 7: 417–33.

32. Sha Y, Rao L, Settembre C, Ballabio A, Eissa NT. STUB 1 regulates TFEB - induced autophagy–lysosome pathway . EMBO J. 2017; 36: 2544–52.

33. Martini-Stoica H, Cole AL, Swartzlander DB, Chen F, Wan YW, Bajaj L, Bader DA, Lee VMY, Trojanowski JQ, Liu Z, Sardiello M, Zheng H. TFEB enhances astroglial uptake of extracellular tau species and reduces tau spreading. J Exp Med. 2018; 215: 2355–77.

34. Huang J, Wang X, Zhu Y, Li Z, Zhu YT, Wu JC, Qin ZH, Xiang M, Lin F. Exercise activates lysosomal function in the brain through AMPK-SIRT1-TFEB pathway. CNS Neurosci Ther. 2019; 25: 796–807.

35. Evans CS, Holzbaur ELF. Degradation of engulfed mitochondria is rate-limiting in optineurin-mediated mitophagy in neurons. Elife. 2020; 9: 1–30.

36. Fivenson EM, Lautrup S, Sun N, Scheibye-Knudsen M, Stevnsner T, Nilsen H, Bohr VA, Fang EF. Mitophagy in neurodegeneration and aging. Neurochem Int. 2017; 109: 202–9.

37. Fang EF, Hou Y, Palikaras K, Adriaanse BA, Kerr JS, Yang B, Lautrup S, Hasan-Olive MM, Caponio D, Dan X, Rocktäschel P, Croteau DL, Akbari M, et al. Mitophagy inhibits amyloid-β and tau pathology and reverses cognitive deficits in models of Alzheimer's disease. Nat Neurosci [Internet]. Springer US; 2019; 22: 401–12. Available from: http://dx.doi.org/10.1038/s41593-018-0332-9

38. Wong SQ, Kumar A V., Mills J, Lapierre LR. Autophagy in aging and longevity. Hum Genet. Springer Berlin Heidelberg; 2020; 139: 277–90.

39. Escobar KA, Cole NH, Mermier CM, Vandusseldorp TA. Autophagy and aging : Maintaining the proteome through exercise and caloric restriction. 2019; .

40. Fernández ÁF, Sebti S, Wei Y, Zou Z, Shi M, Mcmillan KL, He C, Ting T, Liu Y, Chiang W, Marciano DK, Schiattarella GG, Bhagat G. Disruption of the beclin 1-BCL2 autohpagy regulatory complex promotes logevity in mice. 2018; .

41. Xiao F, Chen X, Yu Q, Ye Y, Liu Y, Yan D, Yang L, Chen G, Lin R, Yang L, Liao X, Zhang W, Zhang W, et al. Transcriptome evidence reveals enhanced autophagy-lysosomal function in centenarians. 2018; : 1601–10.

42. Young ARJ, Narita M. Connecting autophagy to senescence in pathophysiology. Curr Opin Cell Biol [Internet]. Elsevier Ltd; 2010; 22: 234–40. Available from: http://dx.doi.org/10.1016/j.ceb.2009.12.005

43. Domínguez-bautista JA, Acevo-rodríguez PS, Castro-obregón S. Programmed Cell Senescence in the Mouse Developing Spinal Cord and Notochord. 2021; 9: 1–15.

44. Hernandez-Segura A, Nehme J, Demaria M. Hallmarks of Cellular Senescence. Trends Cell Biol [Internet]. Elsevier Ltd; 2018; 28: 436–53. Available from: http://dx.doi.org/10.1016/j.tcb.2018.02.001

45. Yoon M, Kang S, Lee S, Woo T, Oh A, Park S, Ha N, Park B. p53 induces senescence through Lamin A / C stabilization-mediated nuclear deformation. Cell Death Dis [Internet]. Springer US; 2019; . Available from: http://dx.doi.org/10.1038/s41419-019-1378-7

46. Ishikawa S, Ishikawa F. Proteostasis failure and cellular senescence in long-term cultured postmitotic rat neurons. Aging Cell [Internet]. 2019; : 1–15. Available from: https://doi.org/10.1111/acel.13071

47. Moreno-Blas D, Gorostieta-Salas E, Pommer-Alba A, Muciño-Hernández G, Gerónimo-Olvera C, Maciel-Barón LA, Konigsberg M, Massieu L, Castro-Obregón S. Cortical neurons develop a senescence-like phenotype promoted by dysfunctional autophagy. Aging (Albany NY) [Internet]. 2019; 11: 6175–98. Available from: https://doi.org/10.18632/aging.102181

48. Lee BY, Han JA, Im JS, Morrone A, Johung K, Goodwin EC, Kleijer WJ, DiMaio D, Hwang ES. Senescence-associated β-galactosidase is lysosomal β-galactosidase. Aging Cell. 2006; 5: 187–95.

49. Lukášová E, Kovařík A, Bačíková A, Falk M, Kozubek S. Loss of lamin B receptor is necessary to induce cellular senescence. Biochem J [Internet]. 2017; 474: 281–300. Available from: https://doi.org/10.1042/BCJ20160459

50. Yosef R, Pilpel N, Papismadov N, Gal H, Ovadya Y, Vadai E, Miller S, Porat Z, Ben-dor S, Krizhanovsky V. p 21 maintains senescent cell viability under persistent DNA damage response by restraining JNK and caspase signaling. 2017; 36: 2280–95.

51. Jänicke RU, Sohn D, Essmann F, Schulze-Osthoff K. The multiple battles fought by anti-apoptotic p21. Cell Cycle. 2007; 6: 407–13.

52. Criscione SW, Teo YV, Neretti N. The Chromatin Landscape of Cellular Senescence. Trends Genet [Internet]. Elsevier Ltd; 2016; 32: 751–61. Available from: http://dx.doi.org/10.1016/j.tig.2016.09.005

53. Salama R, Sadaie M, Hoare M, Narita M. Cellular senescence and its effector programs Cellular senescence and its effector programs. 2014; : 99–114.

54. Hernandez-Segura A, Nehme J, Demaria M. Hallmarks of Cellular Senescence. Trends Cell Biol [Internet]. Elsevier Ltd; 2018; 28: 436–53. Available from: http://dx.doi.org/10.1016/j.tcb.2018.02.001

55. Munoz-Espin D, Serrano M. Cellular senescence: from physiology to pathology. Nat Rev Mol Cell Biol [Internet]. Nature Publishing Group; 2014; 15: 482–96. Available from: http://dx.doi.org/10.1038/nrm3823

56. Georgakopoulou EA, Tsimaratou K, Evangelou K, Fernandez-Marcos PJ, Zoumpourlis V, Trougakos IP, Kletsas D, Bartek J, Serrano M, Gorgoulis VG. Specific lipofuscin staining as a novel biomarker to detect replicative and stress-induced senescence. A method applicable in cryo-preserved and archival tissues. Aging (Albany NY). 2013; 5: 37–50.

57. von Kobbe C. Cellular senescence: a view throughout organismal life. Cell Mol Life Sci [Internet]. Springer International Publishing; 2018; 75: 3553–67. Available from: https://doi.org/10.1007/s00018-018-2879-8

58. Kang C, Elledge SJ. How autophagy both activates and inhibits cellular senescence. Autophagy [Internet]. Taylor & Francis; 2016; 12: 898–9. Available from: http://dx.doi.org/10.1080/15548627.2015.1121361

59. Rhinn M, Ritschka B, Keyes WM. Cellular senescence in development, regeneration and disease. Dev. 2019; 146.

60. Da S, Álvarez S, Guerra J, Cameán DS, Quelle A, Barreiro A, Laura I, Manuel S. Cell senescence contributes to tissue regeneration in zebrafish. 2020; : 1–5.

61. Baker DJ, Childs BG, Durik M, Wijers ME, Sieben CJ, Zhong J, A. Saltness R, Jeganathan KB, Verzosa GC, Pezeshki A, Khazaie K, Miller JD, van Deursen JM. Naturally occurring p16Ink4a-positive cells shorten healthy lifespan. Nature. Nature Publishing Group; 2016; 530: 184–9.

62. Baker DJ, Wijshake T, Tchkonia T, Lebrasseur NK, Childs BG, Van De Sluis B, Kirkland JL, Van Deursen JM. Clearance of p16 Ink4a-positive senescent cells delays ageing-associated disorders. Nature [Internet]. Nature Publishing Group; 2011; 479: 232–6. Available from: http://dx.doi.org/10.1038/nature10600

63. Kang HT, Lee KB, Kim SY, Choi HR, Park SC. Autophagy impairment induces premature senescence in primary human fibroblasts. PLoS One. 2011; 6: e23367.

64. García-Prat L, Martínez-Vicente M, Perdiguero E, Ortet L, Rodríguez-Ubreva J,

Rebollo E, Ruiz-Bonilla V, Gutarra S, Ballestar E, Serrano AL, Sandri M, Muñoz-Cánoves P. Autophagy maintains stemness by preventing senescence. Nature. Nature Publishing Group; 2016; 529: 37–42.

65. Jurk D, Wang C, Miwa S, Maddick M, Korolchuk V, Tsolou A, Gonos ES, Thrasivoulou C, Jill Saffrey M, Cameron K, von Zglinicki T. Postmitotic neurons develop a p21-dependent senescence-like phenotype driven by a DNA damage response. Aging Cell. 2012; 11: 996–1004.

66. Vazquez-Villaseñor, I., Garwood, C. J., Heath, P. R., Simpson, J. E., Ince, P. G., & Wharton SB (2020). Expression of p16 and p21 in the frontal association cortex of ALS / MND brains suggests neuronal cell cycle dysregulation and astrocyte senescence in early stages of the disease. 2020; : 171–85.

67. Cavazza T, Vernos I. The RanGTP Pathway : From Nucleo-Cytoplasmic Transport to Spindle Assembly and Beyond. 2016; 3.

68. Fu X, Liang C, Li F, Wang L, Wu X, Lu A, Xiao G, Zhang G. The rules and functions of nucleocytoplasmic shuttling proteins. Int J Mol Sci. 2018; 19: 1–17.

69. Ori A, Toyama BH, Harris MS, Ingolia NT, Hetzer MW, Ori A, Toyama BH, Harris MS, Bock T, Iskar M, Bork P. Integrated Transcriptome and Proteome Analyses Reveal Organ-Specific Proteome Deterioration in Old Article Integrated Transcriptome and Proteome Analyses Reveal Organ-Specific Proteome Deterioration in Old Rats. Cell Syst [Internet]. The Authors; 2015; 1: 224–37. Available from: http://dx.doi.org/10.1016/j.cels.2015.08.012

70. Chou CC, Zhang Y, Umoh ME, Vaughan SW, Lorenzini I, Liu F, Sayegh M, Donlin-Asp PG, Chen YH, Duong DM, Seyfried NT, Powers MA, Kukar T, et al. TDP-43 pathology disrupts nuclear pore complexes and nucleocytoplasmic transport in ALS/FTD. Nat Neurosci [Internet]. Springer US; 2018; 21: 228–39. Available from: http://dx.doi.org/10.1038/s41593-017-0047-3

71. Shang J, Yamashita T, Nakano Y, Morihara R, Li X, Feng T, Liu X, Huang Y, Fukui Y, Hishikawa N, Ohta Y, Abe K. Aberrant distributions of nuclear pore complex proteins in ALS mice and ALS patients. Neuroscience [Internet]. IBRO; 2017; 350: 158–68. Available from: http://dx.doi.org/10.1016/j.neuroscience.2017.03.024

72. Zhang K, Donnelly CJ, Haeusler AR, Grima JC, Machamer JB, Steinwald P, Daley EL, Miller SJ, Cunningham KM, Vidensky S, Gupta S, Thomas MA, Hong I, et al. The C9orf72 repeat expansion disrupts nucleocytoplasmic transport. Nature. 2015; 525: 56–61.

73. Kinoshita Y, Ito H, Hirano A, Fujita K, Wate R, Nakamura M, Kaneko S, Nakano S, Kusaka H. Nuclear contour irregularity and abnormal transporter protein distribution in anterior horn cells in amyotrophic lateral sclerosis. J Neuropathol Exp Neurol. 2009; 68: 1184–92.

74. Chillon-marinas C, Goginashvili A, Bang AG, Cleveland DW, Gasset-rosa F, Chillon-marinas C, Goginashvili A, Atwal RS. Polyglutamine-Expanded Huntingtin Exacerbates Age-Related Disruption of Nuclear Integrity and Nucleocytoplasmic

Transport Report Polyglutamine-Expanded Huntingtin Exacerbates Age-Related Disruption of Nuclear Integrity and Nucleocytoplasmic Transport. Neuron [Internet]. Elsevier Inc.; 2017; 94: 48-57.e4. Available from: http://dx.doi.org/10.1016/j.neuron.2017.03.027

75. Grima JC, Daigle JG, Arbez N, Cunningham KC, Zhang K, Ochaba J, Geater C, Morozko E, Stocksdale J, Glatzer JC, Pham JT, Ahmed I, Peng Q, et al. Mutant Huntingtin Disrupts the Nuclear Pore Complex. Neuron [Internet]. Elsevier Inc.; 2017; 94: 93-107.e6. Available from: http://dx.doi.org/10.1016/j.neuron.2017.03.023

76. Haines JD, Herbin O, Hera B De, Vidaurre OG, Moy GA, Sun Q, Yee H, Fung J, Albrecht S, Alexandropoulos K, Mccauley D, Chook YM, Kuhlmann T, et al. Nuclear export inhibitors avert progression in preclinical models of inflammatory demyelination. Nat Publ Gr. Nature Publishing Group; 2015; 18.

77. Lapierre LR, Filho CDDM, Mcquary PR, Chu C, Visvikis O, Chang JT, Gelino S, Ong B, Davis AE, Irazoqui JE, Dillin A. and modulates longevity in Caenorhabditis elegans. Nat Commun. Nature Publishing Group; 2013; .

78. Cunningham KM, Maulding K, Ruan K, Senturk M, Grima JC, Sung H, Zuo Z, Song H, Gao J, Dubey S, Rothstein JD, Zhang K, Bellen HJ, et al. Tfeb/mitf links impaired nuclear import to autophagolysosomal dysfunction in c9-als. Elife. 2020; 9: 1–35.

79. Cheng Z. The FoxO – Autophagy Axis in Health and Disease. Trends Endocrinol Metab [Internet]. Elsevier Ltd; 30: 658–71. Available from: https://doi.org/10.1016/j.tem.2019.07.009

80. Shen S, Niso-Santano M, Adjemian S, Takehara T, Malik SA, Minoux H, Souquere S, Mariño G, Lachkar S, Senovilla L, Galluzzi L, Kepp O, Pierron G, et al. Cytoplasmic STAT3 Represses Autophagy by Inhibiting PKR Activity. Mol Cell. 2012; 48: 667–80.

81. Dickmanns A, Monecke T, Ficner R. Structural Basis of Targeting the Exportin CRM1 in Cancer. Cells. 2015. 538–568 p.

82. Golomb L, Bublik DR, Wilder S, Nevo R, Kiss V, Grabusic K, Volarevic S, Oren M. Importin 7 and exportin 1 Link c-Myc and p53 to regulation of ribosomal Biogenesis. Mol Cell [Internet]. Elsevier; 2012; 45: 222–32. Available from: http://dx.doi.org/10.1016/j.molcel.2011.11.022

83. Debacq-Chainiaux F, Erusalimsky JD, Campisi J, Toussaint O. Protocols to detect senescence-associated beta-galactosidase (SA-βgal) activity, a biomarker of senescent cells in culture and in vivo. Nat Protoc [Internet]. Nature Publishing Group; 2009; 4: 1798–806. Available from: https://doi.org/10.1038/nprot.2009.191

84. Levitsky KL, Toledo-Aral JJ, López-Barneo J, Villadiego J. Direct confocal acquisition of fluorescence from X-gal staining on thick tissue sections. Sci Rep. 2013; 3: 1–6.

85. Brown MW, Aggleton JP. Recognition memory: What are the roles of the perirhinal cortex and hippocampus? Nat Rev Neurosci. 2001; 2: 51–61.

86. Bettio LEB, Rajendran L, Gil-Mohapel J. The effects of aging in the hippocampus and cognitive decline. Neurosci Biobehav Rev [Internet]. 2017; 79: 66–86. Available from: https://doi.org/10.1016/j.neubiorev.2017.04.030

87. Cortes CJ, La Spada AR. TFEB dysregulation as a driver of autophagy dysfunction in neurodegenerative disease: Molecular mechanisms, cellular processes, and emerging therapeutic opportunities. Neurobiol Dis [Internet]. Elsevier Inc; 2019; 122: 83–93. Available from: https://doi.org/10.1016/j.nbd.2018.05.012

88. Ott C, König J, Höhn A, Jung T, Grune T. Macroautophagy is impaired in old murine brain tissue as well as in senescent human fibroblasts. Redox Biol [Internet]. Elsevier; 2016; 10: 266–73. Available from: http://dx.doi.org/10.1016/j.redox.2016.10.015

89. Shen S, Niso-Santano M, Adjemian S, Takehara T, Malik SA, Minoux H, Souquere S, Mariño G, Lachkar S, Senovilla L, Galluzzi L, Kepp O, Pierron G, et al. Cytoplasmic STAT3 Represses Autophagy by Inhibiting PKR Activity. Mol Cell [Internet]. 2012; 48: 667–80. Available from: https://doi.org/10.1016/j.molcel.2012.09.013

90. Cheng Y, Holloway MP, Nguyen K, Mccauley D, Landesman Y. XPO1 (CRM1) Inhibition Represses STAT3 Activation to Drive a Survivin-Dependent Oncogenic Switch in Triple-Negative Breast Cancer. 2014; : 675–87.

91. Rusmini P, Cortese K, Crippa V, Cristofani R, Cicardi ME, Ferrari V, Vezzoli G, Tedesco B, Meroni M, Messi E, Piccolella M, Galbiati M, Garrè M, et al. Trehalose induces autophagy via lysosomal-mediated TFEB activation in models of motoneuron degeneration. Autophagy [Internet]. Taylor & Francis; 2019; 15: 631–51. Available from: https://doi.org/10.1080/15548627.2018.1535292

92. Ishikawa S, Ishikawa F. Proteostasis failure and cellular senescence in long-term cultured postmitotic rat neurons. Aging Cell. 2019; : 1–15.

93. Legartová S, Stixová L, Laur O, Kozubek S, Sehnalová P, Bártová E. Nuclear structures surrounding internal lamin invaginations. J Cell Biochem. 2014; 115: 476–87.

94. Kudo N, Matsumor i N, Taoka H, Fujiwara D, Schreiner E, Wolff B, Yoshida M, Horinouchi S. Leptomycin B inactivates CRM1 ¯exportin 1 by covalent modification at a cysteine residue in the. Proc Natl Acad Sci USA. 1999; 96: 9112–7.

95. Mauthe M, Orhon I, Rocchi C, Zhou X, Luhr M, Hijlkema KJ, Coppes RP, Engedal N, Mari M, Reggiori F. Chloroquine inhibits autophagic flux by decreasing autophagosome-lysosome fusion. Autophagy [Internet]. Taylor & Francis; 2018; 14: 1435–55. Available from: https://doi.org/10.1080/15548627.2018.1474314

96. de Araujo MEG, Liebscher G, Hess MW, Huber LA. Lysosomal size matters. Traffic [Internet]. 2020; 21: 60–75. Available from: https://doi.org/10.1111/tra.12714

97. Leeman DS, Hebestreit K, Ruetz T, Webb AE, McKay A, Pollina EA, Dulken BW, Zhao X, Yeo RW, Ho TT, Mahmoudi S, Devarajan K, Passegué E, et al. Lysosome

activation clears aggregates and enhances quiescent neural stem cell activation during aging. Science (80-) [Internet]. 2018; 359: 1277–83. Available from: https://doi.org/10.1126/science.aag3048

98. Rong Y, Liu M, Ma L, Du W, Zhang H, Tian Y, Cao Z, Li Y, Ren H, Zhang C, Li L, Chen S, Xi J, et al. Clathrin and phosphatidylinositol-4,5-bisphosphate regulate autophagic lysosome reformation. Nat Cell Biol [Internet]. 2012; 14: 924–34. Available from: https://doi.org/10.1038/ncb2557

99. Di Malta C, Cinque L, Settembre C. Transcriptional Regulation of Autophagy: Mechanisms and Diseases. Front Cell Dev Biol. 2019; 7: 1–10.

100. Oberdoerffer P, Sinclair DA. The role of nuclear architecture in genomic instability and ageing. Nat Rev Mol Cell Biol. 2007; 8: 692–702.

101. Eftekharzadeh B, Daigle JG, Kapinos LE, Wegmann S, Rothstein JD, Hyman BT, Eftekharzadeh B, Daigle JG, Kapinos LE, Coyne A, Schiantarelli J, Carlomagno Y, Cook C, et al. Tau Protein Disrupts Nucleocytoplasmic Transport in Alzheimer ' s Disease Article Tau Protein Disrupts Nucleocytoplasmic Transport in Alzheimer ' s Disease. Neuron [Internet]. Elsevier Inc.; 2018; 99: 925-940.e7. Available from: https://doi.org/10.1016/j.neuron.2018.07.039

102. Paonessa F, Evans LD, Solanki R, Larrieu D, Wray S, Hardy J, Jackson SP, Livesey FJ. Microtubules Deform the Nuclear Membrane and Disrupt Nucleocytoplasmic Transport in Tau-Mediated Frontotemporal Dementia. Cell Rep [Internet]. ElsevierCompany.; 2019; 26: 582-593.e5. Available from: https://doi.org/10.1016/j.celrep.2018.12.085

103. Frost B, Bardai FH, Feany MB. Lamin Dysfunction Mediates Neurodegeneration in Tauopathies. Curr Biol. Elsevier Ltd; 2016; 26: 129–36.

104. Adachi Y, Yanagida M. Higher order chromosome structure is affected by cold-sensitive mutations in a Schizosaccharomyces pombe gene crm1+ which encodes a 115-kD protein preferentially localized in the nucleus and its periphery. J Cell Biol. 1989; 108: 1195–207.

105. Cornelison GL, Levy SA, Jenson T, Frost B. Tau-induced nuclear envelope invagination causes a toxic accumulation of mRNA in Drosophila. Aging Cell. 2019; 18: 1–7.

106. Payea MJ, Anerillas C, Tharakan R. crossm Translational Control during Cellular Senescence. 2021; : 1–14.

107. Okamura M, Inose H, Masuda S. RNA Export through the NPC in Eukaryotes. 2015; : 124–49.

108. Watt PJ Van Der, Leaner VD. Biochimica et Biophysica Acta The nuclear exporter , Crm1 , is regulated by NFY and Sp1 in cancer cells and repressed by p53 in response to DNA damage. BBA - Gene Regul Mech [Internet]. Elsevier B.V.; 2011; 1809: 316–26. Available from: http://dx.doi.org/10.1016/j.bbagrm.2011.05.017

109. Wang AY, Liu H. The past, present, and future of CRM1/XPO1 inhibitors. Stem Cell

Investig [Internet]. 2019; 6. Available from:
https://sci.amegroups.com/article/view/24154/html

11. Publicaciones

11.1. *Anexo 1. Connecting chaperon-mediated autophagy dysfunction to cellular senescence*

Ageing Research Reviews 41 (2018) 34–41

Contents lists available at ScienceDirect

Ageing Research Reviews

journal homepage: www.elsevier.com/locate/arr

Review

Connecting chaperone-mediated autophagy dysfunction to cellular senescence

Daniel Moreno-Blas, Elisa Gorostieta-Salas, Susana Castro-Obregón*

Department of Neurodevelopment and Physiology, Institute of Cellular Physiology, National Autonomous University of México (UNAM), Mexico City, Mexico

ARTICLE INFO

Keywords:
Aging
Cellular senescence
Chaperone-mediated autophagy
Macroautophagy
Proteostasis

ABSTRACT

Chaperone-mediated autophagy (CMA) is one of the main pathways of the lysosome-autophagy proteolytic system. It regulates different cellular process through the selective degradation of cytosolic proteins. In ageing, the function of CMA is impaired causing an inefficient stress response and the accumulation of damaged, oxidized or misfolded proteins, which is associated with numerous age-related diseases. Deficient protein degradation alters cellular proteostasis and activates signaling pathways that culminate in the induction of cellular senescence, whose accumulation is a typical feature of ageing. However, the relationship between CMA activity and cellular senescence has been poorly studied. Here, we review and integrate evidence showing that CMA dysfunction correlates with the acquisition of many hallmarks of cellular senescence and propose that loss of CMA function during aging promotes cellular senescence.

1. Introduction

1.1. Hallmarks of cellular senescence

Cellular senescence is a particular phenotype characterized by a permanent cell cycles arrest accompanied by a lack of response to mitotic and apoptotic stimuli. This phenotype is induced by various conditions including telomere dysfunction, reactive oxygen species, DNA damage, oncogene activation and developmental cues (Childs et al., 2015; van Deursen, 2014). Therefore, senescence is often named according to the stimulus inducing it. Replicative senescence occurs in response to telomere shortening during cell proliferation, which triggers the DNA damage response (DDR) and signals to cell cycle inhibition (Blasco et al., 1997; Di Micco et al., 2008). Oncogene-induced senescence (OIS) is triggered by the action of oncogenes such as oncogenic *ras* (Serrano et al., 1997). Stress-induced premature senescence (SIPS) is induced by exposure to different stress signals such as oxidative stress (Mas-Bargues et al., 2017), radiation (Chainiaux et al., 2002) or nonphysiologic culture conditions (including hyperoxia, interruption of cell–cell contacts, loss of interactions between different cell types and plating on plastic) (Sherr and DePinho, 2000). Programmed senescence occurs during embryogenesis and in the placenta, in response to developmental cues (Muñoz-Espín et al., 2013; Storer et al., 2013). Regardless of the induction signal, senescent cells show several common features that together define the senescent state (Fig. 1) reviewed elsewhere, for example (He and Sharpless, 2017; Maciel-Barón et al., 2017). The signaling pathways to activate cellular senescence converge on the expression of the cell cycle inhibitors *p21/Cdkn1a* (Passos et al., 2010) and/or *p16/Cdkn2a* (Baker et al., 2016; Burd et al., 2013), which seem to promote the senescence state in addition to halting the cell cycle. Some of the hallmarks of cellular senescence are a persistent DDR, commonly associated with DNA breaks, activation of ATM and ATR kinases and phosphorylation of the H2A.X histone (γH2AX) (Kang et al., 2015a,b; Wang et al., 2009b). There are noticeable changes in chromatin structure, known as senescence-associated heterochromatin foci (SAHF) associated with altered gene expression (Narita et al., 2003). Lysosomes are enlarged and accumulate non- digestible complexes such as lipofuscin (Georgakopoulou et al., 2013) and have increased senescence-associated β-galactosidase (SA-β-gal) activity (Debacq-Chainiaux et al., 2009). There are also morphological changes, as senescent cells accumulate vesicles and stress granules, and in the nuclear envelope there are patches of Lamin-B1 degradation (Dou et al., 2015; Lukasova et al., 2016).

Both during embryo development and adulthood, senescent cells perform several physiological roles, like promoting tissue remodeling and preventing tumor progression, through the secretion of a large set of molecules such as cytokines, chemokines, growth factors and metalloproteases, which are collectively known as senescence-associated secretory phenotype (SASP). These same secreted factors attract immune effector cells, which actively remove senescent cells (Coppé et al.,

* Corresponding Author: Department of Neurodevelopment and Physiology, Division of Neurosciences, Institute of Cellular Physiology, UNAM. Circuito Exterior, S/N, Ciudad Universitaria 04510, México.
E-mail addresses: dmoreno@email.ifc.unam.mx (D. Moreno-Blas), elisag@email.ifc.unam.mx (E. Gorostieta-Salas), scastro@ifc.unam.mx (S. Castro-Obregón).

https://doi.org/10.1016/j.arr.2017.11.001
Received 21 September 2017; Received in revised form 26 October 2017; Accepted 3 November 2017
Available online 04 November 2017
1568-1637/

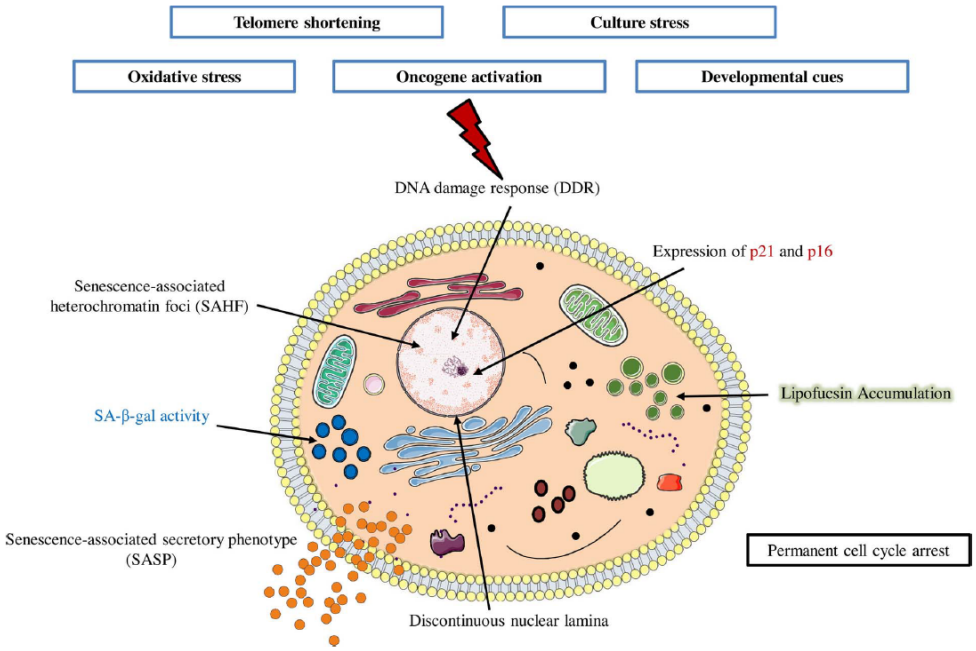

Fig. 1. Hallmarks of cellular senescence. The senescent phenotype is induced by several stiumuli, such as telomere shortening during proliferation, oxidative stress, oncogen activation, culture stress and developmental cues. In these conditions, cells undergo a permanent cell cycle arrest and acquire several characteristics including DDR, lipofuscin accumulation, increased SA-β-gal activity, expression of p21/CDKN1A and/or p16/CDKN2A, senescence-associated heterochromatin foci (SAHF), lamin B1 loss and a senescence-associated secretory phenotype (SASP).

2010a; Coppé et al., 2010b; van Deursen, 2014; Muñoz and Serrano, 2014). As we age, though, senescent cells are not efficiently cleared leading to their accumulation and persistence in various tissues, altering the structure and function of organs and becoming one of the main drivers of ageing and age-related diseases (López-otín et al., 2013). Actually, chemical or genetic interventions that eliminate persistent senescent cells improve organismal health (Baker et al., 2016, 2011; Chang et al., 2015; Jeon et al., 2017). Therefore, understanding the molecular basis of senescence establishment and persistence during aging has a wide biomedical impact.

1.2. Cellular senescence is modulated by autophagy

Autophagy is a catabolic pathway that degrades intracellular components through lysosomes, generating basic biomolecules to be recycled into the cytosol or secreted by the cell and has been extensively reviewed (Bento et al., 2016). In recent years, different functions of autophagy have been discovered, linking anabolic processes with autophagic degradation (Kaur and Debnath, 2015). For example, protein degradation by autophagy preserves the intracellular amino acids pool to be utilized for synthesis of total proteins (Onodera and Ohsumi, 2005). The degradation of lipids by autophagy (lipophagy) provides free fatty acids to be used in the β-oxidation and the tricarboxylic acid (TCA) cycle to produce energy (Singh et al., 2009). And the autophagic degradation of glycogen (glycophagy) releases glucose that can be used by glycolysis for ATP production (Kaur and Debnath, 2015). Furthermore, beyond degradation of cytosolic components, autophagy mediates the unconventional secretion of proteins such as interleukin-1β (IL-1β), IL-18 and the high mobility group protein B1 (HMGB1) (Dupont et al., 2011). Some of those functions can contribute to the establishment of the senescent phenotype.

Based on the different ways to introduce the cytoplasmic material into the lysosomal lumen, three main types of autophagy have been described in mammalian cells: endosomal microautophagy (Sahu et al., 2011), macroautophagy (Ohsumi, 2014) and chaperone-mediated autophagy (CMA) (Cuervo and Dice, 2000).

Macroautophagy is the best characterized type of autophagy, where the cytoplasmic material to be degraded is first engulfed into double-membrane vesicles called autophagosomes. The enclosed material includes proteins and organelles among other cell constituents, and even pathogens. Then, autophagosomes move through the cell to fuse with lysosomes and the engulfed cytoplasmic components, along with the inner membrane of the autophagosome, are degraded by the lysosomal hydrolytic enzymes. The molecular machinery of macroautophagy has been reviewed by others (Klionsky and Schulman, 2014; Mizushima et al., 2011; Xie and Klionsky, 2007).

Macroautophagy has a dual role over the process of cellular senescence. On one hand, interfering the expression of essential genes for the formation of autophagosomes, such as *Atg7* and *Atg12*, induces premature senescence in human fibroblasts (Kang et al., 2011). Accordingly, also in human cells, suppression of the selective degradation of the transcription factor GATA4 by macroautophagy leads to senescence, since GATA4 induces the expression of SASP molecules (Kang et al., 2015a,b). On the other hand, macroautophagy is required in oncogene-induced senescence to form a cytoplasmic compartment known as TOR-autophagy spatial coupling compartment (TASCC), involved in the production of SASP molecules, and hence contributing to senescence transition (Narita et al., 2011). The role of macroautophagy on cellular senescence has been reviewed by others (Capparelli et al., 2012; Kang et al., 2015a,b, 2011; Kang and Elledge, 2016; Luo et al., 2011; Sasaki et al., 2010), whereas the role of endosomal microautophagy and CMA in senescence has been poorly described. In this review we focus on

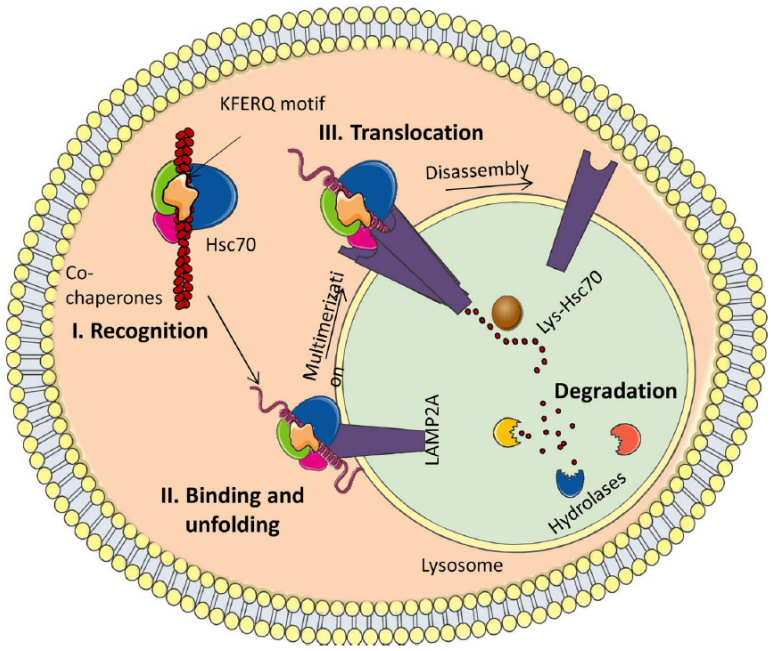

Fig. 2. Core machinery of CMA. **I. Recognition**, proteins targeted for degradation are recognized through an exposed KFERQ motif by the HSC70 chaperone and co-chaperones. **II. Binding and unfolding**, the chaperone complex carries the protein to the lysosomal surface where it is recognized by the transmembrane protein LAMP2A. At this point, the target protein is unfolded assisted by chaperones. **III. Translocation and degradation**, LAMP2A multimerizes to form a pore through which the unfolded protein is internalized to the lysosomal lumen and it is degraded by the hydrolases.

CMA and discuss the evidence that led us to propose that alterations of this pathway during ageing could contribute to the establishment of the senescent phenotype.

2. Core machinery of CMA

During CMA single proteins, assisted by a chaperone complex, are directly translocated across the lysosomal membrane to be degraded by hydrolases. The CMA process can be divided into three steps: 1) Recognition, 2) Binding and unfolding, and 3) Translocation and degradation (Fig. 2).

2.1. Recognition

Each protein targeted for degradation by CMA contains in its amino acid sequence a specific pentapeptide motif known as KFERQ, composed generally of a glutamine residue (Q) either at the beginning or the end of the motif, a positively charged residue that can be lysine (K) or arginine (R), a hydrophobic amino acid, either phenylalanine (F), valine (V), leucine (L) or isoleucine (I), and a negatively charged residue, either glutamic acid (E) or aspartic acid (D). The specific sequence can vary, but the physicochemical properties are maintained. About 30% of the cytosolic proteins contain a KFERQ motif (Chiang et al., 1989), but by post-translational modifications such as phosphorylation and acetylation, KFERQ-like motifs can be generated (Lv et al., 2011; Thompson et al., 2009), increasing the number of target proteins degraded by CMA. The heat shock protein of 70 KDa (HSPA8/HSC70) recognizes and interacts with this motif in the cytosol. Once bound, HSPA8/HSC70 along with co-chaperones carry the target protein to the surface of the lysosomal membrane (Cuervo and Wong, 2014; Dice, 1982; Kaushik and Cuervo, 2012).

2.2. Binding and unfolding

Once at the surface of the lysosome, the target protein/HSC70 complex binds to the transmembrane protein lysosome-associated membrane protein type 2A (LAMP2A). This interaction induces LAMP2A multimerization forming a translocation complex at the lysosomal membrane, which allows the target protein import into the lysosomal lumen (Cuervo and Wong, 2014; Kaushik and Cuervo, 2012; Xilouri et al., 2016). Only unfolded proteins can cross the lysosomal membrane through the LAMP2A complex (Salvador et al., 2000). The unfolded process is likely conducted by the HSPA8/HSC70 and co-chaperones, but it still needs clarification (Xilouri and Stefanis, 2016). Since the availability and function of LAMP2A are fundamental factors for the correct translocation of proteins into the lysosomal lumen, a reduction of LAMP2A is commonly used as a marker for low CMA activity (Bandyopadhyay et al., 2008; Cuervo and Wong, 2014).

2.3. Translocation and degradation

It has been proposed that the lysosomal chaperone HSC70 (lys-HSC70), located in the lysosome lumen, holds and pulls the target protein into the lumen through the LAMP2A complex, leading to the internalization of the target protein. Once internalized, the target protein is degraded by lysosomal enzymes. After translocation, LAMP2A multimer is disassembled into monomers by HSPA8/HSC70 action, allowing LAMP2 monomers to interact with another substrate protein and the CMA cycle starts again (Cuervo and Wong, 2014).

3. CMA impairment induces cellular senescence

Based on several observations we review here, we propose that CMA decline contributes to aging by inducing cellular senescence. First of all, during aging there is a decline in CMA function, primarily due to a decrease in LAMP2A (Cuervo and Dice, 2000; Kiffin et al., 2007; Schneider et al., 2015) and its inefficient multimerization (Rodriguez-Navarro et al., 2012). LAMP2A molecules destined for degradation are mobilized to domains in the lysosome membrane with a specific lipid composition, enriched in proteases like Cathepsin A that degrade

LAMP2A. In old mice, lipid composition of the lysosomal membrane is altered having higher content of cholesterol and ceramides, which causes the formation of wider degradation membrane domains where more LAMP2A molecules accumulate and get degraded, reducing the abundance of LAMP2A. At the same time, higher cholesterol reduces membrane fluidity, which interferes with LAMP2A multimerization to form translocation complexes. Therefore, decreased CMA activity with aging is a combination of less LAMP2A proteins and less translocation complexes (Rodriguez-Navarro et al., 2012).

Several observations indicate that during cellular senescence CMA activity is impaired. For example, in senescent mouse embryonic fibroblasts LAMP2A is reduced (Kiffin et al., 2007) and in senescent IMR-90 human diploid lung fibroblasts, a substantial proportion of HSPA8/HSC70 is modified with advanced glycation end products (Unterluggauer et al., 2009), presumably impairing its function. During replicative senescence there is a reduced rate of degradation of RNase A, a well-known substrate of CMA (Cuervo and Dice, 2000a; Dice, 1982). Interestingly, in neurons derived from Danon disease patients, a pathological condition caused by LAMP2 deficiency, there is an accumulation of lipofucsin (Furuta et al., 2013), as well as in LAMP-2-deficient murine neurons (Rothaug et al., 2015; Xilouri et al., 2016), suggesting an accelerated senescence in the brain. Finally, CMA impairment is sufficient to induce cellular senescence in primary human fibroblasts, as RNAi-knockdown of LAMP2A induces expression of *p21/Cdkn1a* and *p16/Cdkn2a,* cell cycle arrest, an enlarged morphology, increased SA-β-gal activity, ROS and lipofuscin accumulation, (Kang et al., 2011).

3.1. CMA dysfunction generates DNA damage and activates DDR, possibly triggering cellular senescence

As mentioned above, persistent DDR is one of the main features of senescent cells (Rodier and Campisi, 2011; van Deursen, 2014). Failure in CMA activity results in an inefficient degradation and consequently a persistent accumulation of activated checkpoint kinase 1 (CHK1) in the nucleus, which causes increased accumulation of DNA damage and genomic instability after exposure to γ-irradiation and etoposide treatment (Park et al., 2015), both common DNA-damaging stimuli that induce cellular senescence (Lukasova et al., 2016; Nagano et al., 2016). Reduced LAMP2A also increases γH2A.X (Park et al., 2015), a signal that facilitates the focal assembly of checkpoint and DNA repair factors after DNA damage. Therefore, γH2A.X presence is indicative of DDR (Wang et al., 2009a). These findings indicate that failure in CMA function activates DDR, a signaling pathway behind several inducers of cellular senescence (Muñoz-Espín and Serrano, 2014).

An intracellular increase of reactive oxygen species, either by directly exposing cells to hydrogen peroxide or endogenously produced (*i.e.* by mitochondrial dysfunction) can induce DNA damage, activation of DDR and cellular senescence (Correia-Melo et al., 2014; Lu and Finkel, 2008; Passos and Von Zglinicki, 2006). Interestingly, oxidative stress also induces the activation of CMA to contribute to the removal of oxidized proteins and overcome any possible cellular damage (Kaushik et al., 2006; Kiffin et al., 2004; Saha, 2012; Zhang et al., 2014). Considering that in aging CMA function declines, a diminished response to oxidative stress would cause accumulation of oxidized proteins, contributing to an increase of senescent cells in old tissues.

3.2. CMA dysfunction contributes to cell cycle arrest, inducing Cdkn1a expression, p21 protein stabilization and cellular senescence

Permanent cell cycle arrest is a hallmark of cellular senescence and expression of *p21/Cdkn1a*, a cyclin-dependent kinase inhibitor, is a key factor (Jung et al., 2010; Satyanarayana et al., 2008; Childs et al., 2015). Hypoxia-inducible factor 1α (HIF-1α) is a transcription factor that functions as a master regulator of oxygen homeostasis, inducing the expression of most hypoxia-inducible genes. Interestingly, HIF-1α derepresses *p21/Cdkn1a* by displacing MYC from *p21/Cdkn1a* promoter in the absence of a hypoxic signal (Koshiji et al., 2004). Since HIF-1α is a target of CMA (Hubbi et al., 2014; Hubbi and Semenza, 2015), CMA dysfunction during aging could contribute to the expression of *p21/Cdkn1a* by the inefficient degradation of HIF-1α in lysosomes, leading to cellular senescence.

On the other hand, STUB1/CHIP, an E3 ubiquitin ligase that labels proteins for proteasomal degradation (Murata et al., 2003), has also been shown to mediate the degradation of proteins by CMA through the interaction with other chaperones such as HSP90 in addition to HSPA8/HSC70, also through LAMP2A (Arndt et al., 2010; Ferreira et al., 2013; Han et al., 2017). Interestingly, STUB1/CHIP mediates p21 protein degradation assisted by HSPA8/HSC70; RNAi-knocking down of CHIP in A549 cells stabilizes p21 and increases the number of SA-β-Gal-positive cells in response to ionizing radiation (Biswas et al., 2017). Indeed, CMA dysfunction caused by STUB1/CHIP deficiency induces premature senescence *in vivo,* as there is an increase in SA-β-Gal activity in renal cortex of kidneys from *Chip*$^{-/-}$ mice, and *in vitro*, as *Chip*$^{-/-}$ MEFs acquire replicative senescence sooner than wild type MEFs. Accordingly, *Chip*$^{-/-}$ mice exhibit premature aging, displaying osteoporosis, skeletal muscle atrophy, reduced fat and a shortened life span compared to *Chip*$^{+/+}$ mice (Min et al., 2008). Additional evidence supports the notion that STUB1/CHIP mediates CMA degradation of proteins whose accumulation could trigger cellular senescence. For example, STUB1/CHIP depletion by siRNA causes senescence in IMR90 fibroblasts and human foreskin fibroblasts. In this case, STUB1/CHIP is assisted by the chaperone HSP90 to target p14ARF for degradation in a LAMP2A-dependent manner, and hence prevents cellular senescence. Since no HSPA8/HSC70-interacting KFERQ motif was found in p14ARF, this mechanism differs from canonical CMA in that HSP90, rather than HSPA8/HSC70, delivers the target protein to LAMP2A (Han et al., 2017).

3.3. CMA dysfunction contributes to lipid accumulation, which could cause cellular senescence

CMA degrades proteins but not lipids. However, CMA facilitates lipolysis through the degradation of perlepin 2 and perlepin 3 (PLIN2 and PLIN3 respectively). PLIN2 and PLIN3 proteins have a KFERQ motif and function as a scaffold for lipid droplets. Once these proteins are degraded via CMA, then lipid droplets degradation by macroautophagy is allowed. LAMP2A deficient fibroblasts accumulate more and bigger lipid droplets, confirming a role of CMA in lipolysis (Kaushik and Cuervo, 2015). As mentioned before, old organisms have decreased CMA activity with aging caused by an altered lipid composition in the lysosomal membrane, causing a combination of less LAMP2A proteins and inefficient lateral mobilization (Rodriguez-Navarro et al., 2012). In this context, it is relevant to point out that replicative senescence is associated with changes in the lipidome content. Senescent human fibroblasts show an increase in the total content of triacylglycerols, which are the main components of lipid droplets, due to an increase of fatty acid uptake mediated by CD36 and a higher glycerolipid biosynthesis (Lizardo et al., 2017). We suggest that CMA dysfunction also contributes to the accumulation of triacylglycerols reinforcing the senescent phenotype; on the other hand, changes in the lipidome content during cellular senescence could foster CMA dysfunction by altering lysosomal membrane composition and hence interfering with LAMP2A function.

3.4. Dysfunctional CMA could contribute to cellular senescence in neurodegeneration

Some age-related pathologies, in particular neurodegenerative diseases such as Parkinson's diseases (PD), Alzheimer's diseases (AD) and Huntingtoń disease (HD) are characterized by the presence of abnormal accumulated proteins (Sala et al., 2017). The contribution of

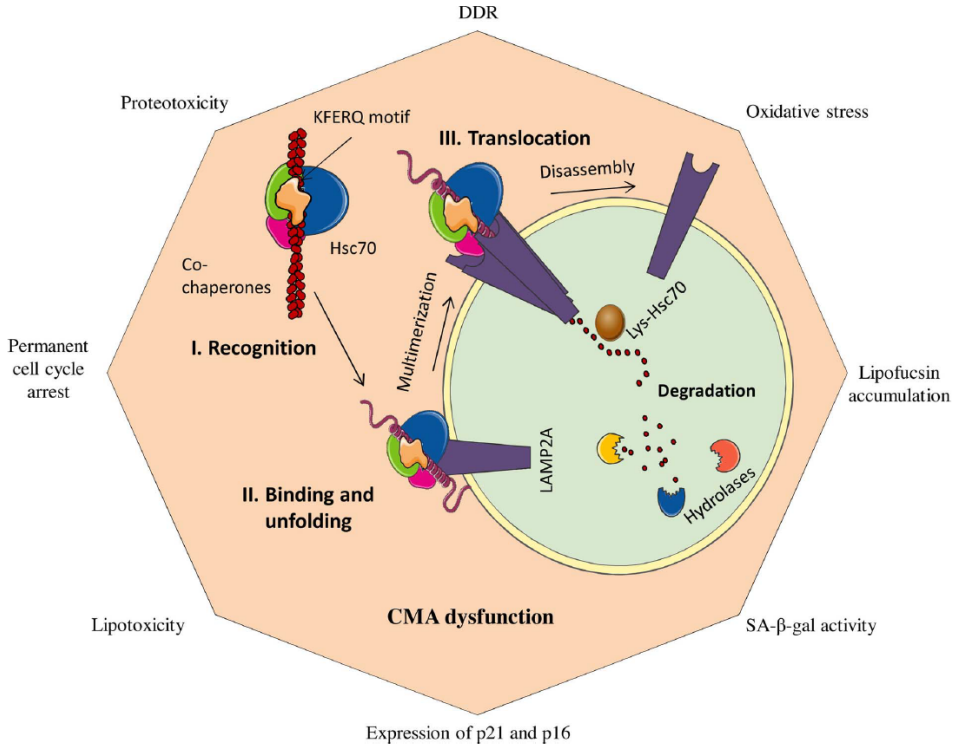

Fig. 3. Integrative connection between CMA and cellular senescence. Impairment of protein degradation by CMA is associated to the acquisition of several hallmarks of the senescent phenotype during both aging and neurodegeneration.

CMA dysfunction to neurodegeneration has been comprehensively reviewed by others (Liu et al., 2015; Xilouri and Stefanis, 2015). Here we focus on evidence supporting the notion that CMA dysfunction could contribute to cellular senescence in neurodegeneration.

In Parkinson's disease abnormal aggregates are known as Lewy bodies, and are composed primarily of α-synuclein and TAU proteins (Ishizawa et al., 2003). α-synuclein acquires multiple conformations including amyloidogenic oligomers (Iwai et al., 1995; Krassnig et al., 2015) and directly alters mitochondrial protein import through its binding to TOM20 receptor, leading to an increase in reactive oxygen species (Di Maio et al., 2016), which is known to induce senescence. α-synuclein is degraded mainly by CMA, so it accumulates when CMA function is impaired, as occurs in PD. For example, there is a decrease in both LAMP2A and HSP8/HSC70 in the *substantia nigra pars compacta* and amygdala of brains from PD patients (Alvarez-Erviti et al., 2010). Accordingly to the proposal that CMA dysfunction triggers cellular senescence, in cerebrospinal fluid from PD patients several features of senescence are found, like an increase in SA-β-gal activity (van Dijk et al., 2013) and the pro-inflammatory cytokines IL6 and IL-β, which are SASP components (Blum-Degena et al., 1995).

In Alzheimeŕs disease there is an extracellular deposition of β-amyloid (Aβ) peptide and intracellular hyper-phosphorylation of TAU. Abnormal aggregates that are formed by amyloid fibrils can be toxic to the cell, damaging cellular membranes and altering mitochondrial function through the inhibition of cytochrome c oxidase subunit 1 (also known as respiratory chain complex CcOX1), promoting an oxidizing environment (Hernandez-Zimbron et al., 2012; Jackson and Hewitt, 2016). Amyloid precursor protein (APP) contains a KFERQ motif, which is necessary for its degradation by CMA; deletion of this motif impairs APP degradation and increases the production of Aβ by the cleavage of APP by α/β secretase (Park et al., 2016). CMA also degrades other pathogenic proteins, such as TAU (Wang et al., 2009b) and Huntingtin (Bauer et al., 2010), supporting the notion that dysfunctional CMA contributes to neurodegeneration, possibly inducing cellular senescence. The latter is supported by the finding that exposure of primary neurons to Aβ induces *p16/Cdkn2a* expression, and in a transgenic model of Alzheimer's disease, 5XFAD mice, there are more senescent hippocampal neurons (identified by the expression of *p16/Cdkn2a*) than in aged match wild type mice (Wei et al., 2016). Cellular senescence in the brain also occurs in humans, as there are more senescent astrocytes, identified by an increase of p16/CDKN2A, the metalloproteinase MMP-1/collagenase (a commonly SASP component), and SA-β-gal activity, in brains from humans 78–90 years compared to young, and in cortex from AD patients compared to cortex from aged match brains. Also in astrocytes, exposure to Aβ induces cellular senescence (Bhat et al., 2012).

We propose that CMA impairment with age contributes to neurodegeneration by causing abnormal protein aggregation and, as a consequence, cellular senescence.

4. Conclusions

So far, advancements in our understanding of the changes that occur in the proteolytic systems during cellular senescence have focused on macroautophagy and the proteasome, leaving aside protein degradation via CMA. Nonetheless, here we present sufficient evidence supporting

the proposal that defects in CMA activity contribute to the onset of cellular senescence, by triggering DDR, SA-β-gal activity, expression of p21/CDKN1A, p16/CDKN2A and lipofuscin accumulation (Fig. 3), both during physiological aging and during pathogenesis such as neurodegeneration. An experimental demonstration of the role of CMA during cellular senescence is necessary, but if proved true, it will contribute to develop suitable strategies to prevent the accumulation of senescent cells and ameliorate physiological ageing and neurodegeneration.

Acknowledgements

Funding was provided by PAPIIT/UNAM IN206015, CONACyT CB2013-220515/F-921, and Fundación Miguel Alemán, A.C. to SCO. CONACyT fellowships were awarded to DMB (588372) and EGS (586932). DMB is student of the "Doctorado en Ciencias Bioquímicas, UNAM". EGS is student of the "Doctorado en Ciencias Biomédicas, UNAM". We acknowledge Dr. Beatriz Aguilar for her technical support.

References

Alvarez-Erviti, L., Rodriguez-Oroz, M.C., Cooper, J.M., Caballero, C., Ferrer, I., Obeso, J.A., Schapira, A.H., 2010. Chaperone-Mediated Autophagy Markers in Parkinson Disease Brains. Arch. Neurol. 67 (12), 1464–1472. http://dx.doi.org/10.1001/archneurol.2010.198.

Arndt, V., Dick, N., Tawo, R., Dreiseidler, M., Wenzel, D., Hesse, M., Fürst, D.O., Saftig, P., Saint, R., Fleischmann, B.K., Hoch, M., Höhfeld, J., 2010. Chaperone-assisted selective autophagy is essential for muscle maintenance. Curr. Biol. 20, 143–148. http://dx.doi.org/10.1016/j.cub.2009.11.022.

Baker, D.J., Wijshake, T., Tchkonia, T., Lebrasseur, N.K., Childs, B.G., Van De Sluis, B., Kirkland, J.L., Van Deursen, J.M., 2011. ageing-associated disorders. Nature 479, 232–236. http://dx.doi.org/10.1038/nature10600.

Baker, D.J., Childs, B.G., Durik, M., Wijers, M.E., Sieben, C.J., Zhong, J.A., Saltness, R., Jeganathan, K.B., Verzosa, G.C., Pezeshki, A., Khazaie, K., Miller, J.D., van Deursen, J.M., 2016. Naturally occurring p16Ink4a-positive cells shorten healthy lifespan. Nature 530, 184–189. http://dx.doi.org/10.1038/nature16932.

Bandyopadhyay, U., Kaushik, S., Varticovski, L., Cuervo, A.M., 2008. The chaperone-mediated autophagy receptor organizes in dynamic protein complexes at the lysosomal membrane. Mol. Cell. Biol. 28, 5747–5763. http://dx.doi.org/10.1128/MCB.02070-07.

Bauer, P.O., Goswami, A., Wong, H.K., Okuno, M., Kurosawa, M., Yamada, M., Miyazaki, H., Matsumoto, G., Kino, Y., Nagai, Y., Nukina, N., 2010. Harnessing chaperone-mediated autophagy for the selective degradation of mutant huntingtin protein. Nat. Biotechnol. 28. http://dx.doi.org/10.1038/nbt.1608.

Bento, C.F., Renna, M., Ghislat, G., Puri, C., Ashkenazi, A., Vicinanza, M., Menzies, F.M., Rubinsztein, D.C., 2016. Mammalian autophagy: how does it work? Annu. Rev. Biochem. 85, 685–713. http://dx.doi.org/10.1146/annurev-biochem-060815-014556.

Bhat, R., Crowe, E.P., Bitto, A., Moh, M., Katsetos, C.D., Garcia, F.U., Johnson, F.B., Trojanowski, J.Q., Sell, C., Torres, C., 2012. Astrocyte senescence as a component of Alzheimer's disease. PLoS One 7, 1–10. http://dx.doi.org/10.1371/journal.pone.0045069.

Biswas, K., Sarkar, S., Du, K., Brautigan, D.L., Abbas, T., Lamer, J.M., 2017. The E3 ligase CHIP mediates p21 degradation to maintain radioresistance. Mol. Cancer Res. 70, 1–10. http://dx.doi.org/10.1158/1541-7786.MCR-16-0466.

Blasco, M., Lee, H.W., Hande, M.P., Samper, E., Lansdorp, P.M., DePinho, R.A., Greider, C.W., 1997. Telomere shortening and tumor formation by mouse cells lacking telomerase RNA. Cell 91, 25–34 S0092-8674(01)80006-4 [pii].

Blum-Degena, D., Müller, T., Kuhn, W., Gerlach, M., Przuntek, H., Riederer, P., 1995. Interleukin-1β and interleukin-6 are elevated in the cerebrospinal fluid of Alzheimerüs and de novo Parkinsonüs disease patients. Neurosci. Lett 202, 17–20. http://dx.doi.org/10.1016/0304-3940(95)12192-7.

Burd, C.E., Sorrentino, J.A., Clark, K.S., Darr, D.B., Krishnamurthy, J., Deal, A.M., Bardeesy, N., Castrillon, D.H., Beach, D.H., Sharpless, N.E., 2013. Monitoring tumorigenesis and senescence in vivo with a p16 INK4a-luciferase model. Cell 152, 340–351. http://dx.doi.org/10.1016/j.cell.2012.12.010.

Capparelli, C., Chiavarina, B., Whitaker-Menezes, D., Pestell, T.G., Pestell, R.G., Hulit, J., Andò, S., Howell, A., Martinez-Outschoorn, U.E., Sotgia, F., Lisanti, M.P., 2012. CDK inhibitors (p16/p19/p21) induce senescence and autophagy in cancer-associated fibroblasts, fueling tumor growth via paracrine interactions, without an increase in neo-angiogenesis. Cell Cycle 11, 3599–3610. http://dx.doi.org/10.4161/cc.21884.

Chainiaux, F., Magalhaes, J.-P., Eliaers, F., Remacle, J., Toussaint, O., 2002. UVB-induced premature senescence of human diploid skin fibroblasts. Int. J. Biochem. Cell Biol. 34, 1331–1339. http://dx.doi.org/10.1016/S1357-2725(02)00022-5.

Chang, J., Wang, Y., Shao, L., Laberge, R.-M., Demaria, M., Campisi, J., Janakiraman, K., Sharpless, N.E., Ding, S., Feng, W., Luo, Y., Wang, X., Aykin-Burns, N., Krager, K., Ponnappan, U., Hauer-Jensen, M., Meng, A., Zhou, D., 2015. Clearance of senescent cells by ABT263 rejuvenates aged hematopoietic stem cells in mice. Nat. Med. 22, 78–83. http://dx.doi.org/10.1038/nm.4010.

Chiang, H., Terlecky, Plant, C., Dice, J., 1989. A role for a 70-kilodalton heat shock protein in lysosomal degradation of intracellular proteins. Science (80-.) 246, 382–385. http://dx.doi.org/10.1126/science.2799391.

Childs, B.G., Durik, M., Baker, D.J., van Deursen, J.M., 2015. Cellular senescence in aging and age-related disease: from mechanisms to therapy. Nat. Med. 21, 1424–1435. http://dx.doi.org/10.1038/nm.4000.

Coppé, J.P., Desprez, P.Y., Krtolica, A., Campisi, J., 2010a. The senescence-associated secretory phenotype: the dark side of tumor suppression. Annu. Rev. Pathol. 5, 99–118. http://dx.doi.org/10.1146/annurev-pathol-121808-102144.

Coppé, J.P., Patil, C.K., Rodier, F., Krtolica, A., Beauséjour, C.M., Parrinello, S., Hodgson, J.G., Chin, K., Desprez, P.Y., Campisi, J., 2010b. A human-like senescence-associated secretory phenotype is conserved in mouse cells dependent on physiological oxygen. PLoS One. http://dx.doi.org/10.1371/journal.pone.0009188. 5.

Correia-Melo, C., Hewitt, G., Passos, J.F., 2014. Telomeres, oxidative stress and inflammatory factors: partners in cellular senescence? Longev. Heal. 3, 1. http://dx.doi.org/10.1186/2046-2395-3-1.

Cuervo, A.M., Dice, J.F., 2000. Age-related decline in chaperone-mediated autophagy. J. Biol. Chem. 275, 31505–31513. http://dx.doi.org/10.1074/jbc.M002102200.

Cuervo, A.M., Wong, E., 2014. Chaperone-mediated autophagy: roles in disease and aging. Cell Res. 24, 92–104. http://dx.doi.org/10.1038/cr.2013.153.

Debacq-Chainiaux, F., Erusalimsky, J.D., Campisi, J., Toussaint, O., 2009. Protocols to detect senescence-associated beta-galactosidase (SA-βgal) activity, a biomarker of senescent cells in culture and in vivo. Nat. Protoc. 4, 1798–1806. http://dx.doi.org/10.1038/nprot.2009.191.

Di Maio, R., Barrett, P.J., Hoffman, E.K., Barrett, C.W., Zharikov, A., Borah, A., Hu, X., McCoy, J., Chu, C.T., Burton, E.A., Hastings, T.G., Greenamyre, J.T., 2016. a-Synuclein binds to TOM20 and inhibits mitochondrial protein import in Parkinsons disease. Sci. Transl. Med. 8, 342ra78. http://dx.doi.org/10.1126/scitranslmed.aaf3634.

Di Micco, R., Cicalese, A., Fumagalli, M., Dobreva, M., Verrecchia, A., Pelicci, P.G., Di Fagagna, F.D.A., 2008. DNA damage response activation in mouse embryonic fibroblasts undergoing replicative senescence and following spontaneous immortalization. Cell Cycle 7, 3601–3606. http://dx.doi.org/10.4161/cc.7.22.7152.

Dice, J.F., 1982. Altered degradation of proteins microinjected into senescent human fibroblasts. J. Biol. Chem. 257, 14624–14627.

Dou, Z., Xu, C., Donahue, G., Shimi, T., Pan, J.-A., Zhu, J., Ivanov, A., Capell, B.C., Drake, A.M., Shah, P.P., Catanzaro, J.M., Daniel Ricketts, M., Lamark, T., Adam, S.A., Marmorstein, R., Zong, W.-X., Johansen, T., Goldman, R.D., Adams, P.D., Berger, S.L., 2015. Autophagy mediates degradation of nuclear lamina. Nature 527, 105–109. http://dx.doi.org/10.1038/nature15548.

Dupont, N., Jiang, S., Pilli, M., Ornatowski, W., Bhattacharya, D., Deretic, V., 2011. Autophagy-based unconventional secretory pathway for extracellular delivery of IL-1β. EMBO J. 30, 4701–4711. http://dx.doi.org/10.1038/emboj.2011.398.

Ferreira, J.V., Fofo, H., Bejarano, E., Bento, C.F., Ramalho, J.S., Girao, H., Pereira, P., 2013. STUB1/CHIP is required for HIF1A degradation by chaperone-mediated autophagy. Autophagy 9, 1349–1366. http://dx.doi.org/10.4161/auto.25190.

Furuta, A., Wakabayashi, K., Haratake, J., Kikuchi, H., Kabuta, T., Mori, F., Tokonami, F., Katsumi, Y., Tanioka, F., Uchiyama, Y., Nishino, I., Wada, K., 2013. Lysosomal storage and advanced senescence in the brain of LAMP-2-deficient Danon disease. Acta Neuropathol. 125, 459–461. http://dx.doi.org/10.1007/s00401-012-1075-4.

Georgakopoulou, E.A., Tsimaratou, K., Evangelou, K., Fernandez-Marcos, P.J., Zoumpourlis, V., Trougakos, I.P., Kletsas, D., Bartek, J., Serrano, M., Gorgoulis, V.G., 2013. Specific lipofuscin staining as a novel biomarker to detect replicative and stress-induced senescence. A method applicable in cryo-preserved and archival tissues. Aging (Albany, N.Y.) 5, 37–50. http://dx.doi.org/10.18632/aging.100527.

Han, S.Y., Ko, A., Kitano, H., Choi, C.H., Lee, M.S., Seo, J., Fukuoka, J., Kim, S.Y., Hewitt, S.M., Chung, J.Y., Song, J., 2017. Molecular chaperone HSP90 is necessary to prevent cellular senescence via lysosomal degradation of p14ARF. Cancer Res. 77, 343–354. http://dx.doi.org/10.1158/0008-5472.CAN-16-0613.

He, S., Sharpless, N.E., 2017. Review senescence in health and disease. Cell 169, 1000–1011. http://dx.doi.org/10.1016/j.cell.2017.05.015.

Hernandez-Zimbron, L.F., Luna-Muñoz, J., Mena, R., Vazquez-Ramirez, R., Kubli-Garfias, C., Cribbs, D.H., Manoutcharian, K., Gevorkian, G., 2012. Amyloid-β peptide binds to cytochrome C oxidase subunit 1. PLoS One 7, 29–31. http://dx.doi.org/10.1371/journal.pone.0042344.

Hubbi, M.E., Semenza, G.L., 2015. An essential role for chaperone-mediated autophagy in cell cycle progression. Autophagy 11, 850–851. http://dx.doi.org/10.1080/15548627.2015.1037063.

Hubbi, M.E., Gilkes, D.M., Hu, H., Kshitiz Ahmed, I., Semenza, G.L., 2014. Cyclin-dependent kinases regulate lysosomal degradation of hypoxia-inducible factor 1α to promote cell-cycle progression. Proc. Natl. Acad. Sci. U. S. A. 111, E3325–34. http://dx.doi.org/10.1073/pnas.1412840111.

Ishizawa, T., Mattila, P., Davies, P., Wang, D., Dickson, D.W., 2003. Colocalization of tau and alpha-synuclein epitopes in Lewy bodies. J. Neuropathol. Exp. Neurol. 62, 389–397. http://dx.doi.org/10.1093/jnen/62.4.389.

Iwai, A., Yoshimoto, M., Masliah, E., Saitoh, T., 1995. Non-AP component of Alzheimer's disease amyloid (NAC) is amyloidogenid. Biochemistry 10139–10145. http://dx.doi.org/10.1021/bi00032a006.

Jackson, M.P., Hewitt, E.W., 2016. Cellular proteostasis: degradation of misfolded proteins by lysosomes. Essays Biochem. 60, 173–180. http://dx.doi.org/10.1042/EBC20160005.

Jeon, O.H., Kim, C., Laberge, R., Demaria, M., Rathod, S., Vasserot, A.P., Chung, J.W., Kim, D.H., Poon, Y., David, N., Baker, D.J., Deursen, J.M., Campisi, Van, Elisseeff, J., 2017. Local clearance of senescent cells attenuates the development of post-traumatic osteoarthritis and creates a pro-regenerative environment. Nat. Publ. Gr. 23, 775–781. http://dx.doi.org/10.1038/nm.4324.

Jung, Y., Qian, Y., Chen, X., 2010. Examination of the expanding pathways for the regulation of p21 expression and activity. Cell. Signal. 22, 1003–1012. http://dx.doi.

org/10.1016/j.cellsig.2010.01.013.
Kang, C., Elledge, S.J., 2016. How autophagy both activates and inhibits cellular senescence. Autophagy 12, 898–899. http://dx.doi.org/10.1080/15548627.2015.1121361.
Kang, H.T., Lee, K.B., Kim, S.Y., Choi, H.R., Park, S.C., 2011. Autophagy impairment induces premature senescence in primary human fibroblasts. PLoS One 6, 1–12. http://dx.doi.org/10.1371/journal.pone.0023367.
Kang, C., Xu, Q., Martin, T.D., Li, M.Z., Demaria, M., Aron, L., Elledge, S.J., 2015a. The DNA damage response induces inflammation and senescence by inhibiting autophagy of GATA4. Science 16, 1–26. http://dx.doi.org/10.1037/emo0000122.
Kang, C., Xu, Q., Martin, T.D., Li, M.Z., Demaria, M., Aron, L., Lu, T., Yankner, B.A., Campisi, J., Elledge, S.J., 2015b. The DNA damage response induces inflammation and senescence by inhibiting autophagy of GATA4. Science (80-.) 349, aaa5612. http://dx.doi.org/10.1126/science.aaa5612.
Kaur, J., Debnath, J., 2015. Autophagy at the crossroads of catabolism and anabolism. Nat. Rev. Mol. Cell Biol. 16, 461–472. http://dx.doi.org/10.1038/nrm4024.
Kaushik, S., Cuervo, A.M., 2012. Chaperone-mediated autophagy: a unique way to enter the lysosome world. Trends Cell Biol. 22, 407–417. http://dx.doi.org/10.1016/j.tcb.2012.05.006.
Kaushik, S., Cuervo, A.M., 2015. Degradation of lipid droplet-associated proteins by chaperone-mediated autophagy facilitates lipolysis. Nat. Cell Biol. 17, 759–770. http://dx.doi.org/10.1038/ncb3166.
Kaushik, S., Massey, A.C., Cuervo, A.M., 2006. Lysosome membrane lipid microdomains: novel regulators of chaperone-mediated autophagy. EMBO J. 25, 3921–3933. http://dx.doi.org/10.1038/sj.emboj.7601283.
Kiffin, R., Christian, C., Knecht, E., Cuervo, A., 2004. Activation of chaperon-mediated autophagy during oxidative stress. Mol. Biol. Cell 16, 4829–4840. http://dx.doi.org/10.1091/mbc.E04.
Kiffin, R., Kaushik, S., Zeng, M., Bandyopadhyay, U., Zhang, C., Massey, A.C., Martinez-Vicente, M., Cuervo, A.M., 2007. Altered dynamics of the lysosomal receptor for chaperone-mediated autophagy with age. J. Cell Sci. 120, 782–791. http://dx.doi.org/10.1242/jcs.001073.
Klionsky, D.J., Schulman, B.A., 2014. Dynamic regulation of macroautophagy by distinctive ubiquitin-like proteins. Nat. Struct. Mol. Biol. 21, 336–345. http://dx.doi.org/10.1038/nsmb.2787.
Koshiji, M., Kageyama, Y., Pete, E.A., Horikawa, I., Barrett, J.C., Huang, L.E., 2004. HIF-1α induces cell cycle arrest by functionally counteracting Myc. EMBO J. 23, 1949–1956. http://dx.doi.org/10.1038/sj.emboj.7600196.
Krassnig, S., Schweinzer, C., Taub, N., Havas, D., Auer, E., Flunkert, S., Schreibmayer, W., Hutter-Paier, B., Windisch, M., 2015. Influence of lentiviral??-synuclein over-expression in the hippocampus of a transgenic mouse model of Alzheimer's disease on amyloid precursor protein metabolism and pathology. Neurodegener. Dis. 15, 243–257. http://dx.doi.org/10.1159/000430952.
López-otín, C., Blasco, M.A., Partridge, L., Serrano, M., 2013. Europe PMC funders group the hallmarks of aging. Cell 153, 1194–1217. http://dx.doi.org/10.1016/j.cell.2013.05.039.
Liu, X., Huang, S., Wang, X., Tang, B., Li, W., Mao, Z., 2015. Chaperone-mediated autophagy and neurodegeneration: connections, mechanisms, and therapeutic implications. Neurosci. Bull. 31, 407–415. http://dx.doi.org/10.1007/s12264-015-1542-8.
Lizardo, D.Y., Lin, Y.-L., Gokcumen, O., Atilla-Gokcumen, G.E., 2017. Regulation of lipids is central to replicative senescence. Mol. BioSyst. 13, 498–509. http://dx.doi.org/10.1039/C6MB00842A.
Lu, T., Finkel, T., 2008. Free radicals and senescence. Exp. Cell Res. 314, 1918–1922. http://dx.doi.org/10.1016/j.yexcr.2008.01.011.
Lukasova, E., Kovařík, A., Bačíková, A., Falk, M., Kozubek, S., 2016. Loss of lamin B receptor is necessary to induce cellular senescence. Biochem. J. http://dx.doi.org/10.1042/BCJ20160459.
Luo, Y., Zou, P., Zou, J., Wang, J., Zhou, D., Liu, L., 2011. Autophagy regulates ROS-induced cellular senescence via p21 in a p38 MAPK?? dependent manner. Exp. Gerontol. 46, 860–867. http://dx.doi.org/10.1016/j.exger.2011.07.005.
Lv, L., Li, D., Zhao, D., Lin, R., Chu, Y., Zhang, H., Zha, Z., Liu, Y., Li, Z., Xu, Y., Wang, G., Huang, Y., Xiong, Y., Guan, K.L., Lei, Q.Y., 2011. Acetylation targets the M2 isoform of pyruvate kinase for degradation through chaperone-mediated autophagy and promotes tumor growth. Mol. Cell 42, 719–730. http://dx.doi.org/10.1016/j.molcel.2011.04.025.
Maciel-Barón, L.Á., Moreno-Blas, D., Morales-Rosales, S.L., González-Puertos, V.Y., López-Diazguerrero, N.E., Torres, C., Castro-Obregón, S., Konigsberg, M., 2017. Cellular senescence, neurological function and redox state. Antioxid. Redox Signal. 7112. http://dx.doi.org/10.1089/ars.2017.7112.
Mas-Bargues, C., Viña-Almunia, J., Inglés, M., Sanz-Ros, J., Gambini, J., Ibáñez-Cabellos, J.S., García-Giménez, J.L., Viña, J., Borrás, C., 2017. Role of p16 INK4a and BMI-1 in oxidative stress-induced premature senescence in human dental pulp stem cells. Redox Biol. 12, 690–698. http://dx.doi.org/10.1016/j.redox.2017.04.002.
Min, J.-N., Whaley, R.A., Sharpless, N.E., Lockyer, P., Portbury, A.L., Patterson, C., 2008. CHIP deficiency decreases longevity, with accelerated aging phenotypes accompanied by altered protein quality control. Mol. Cell. Biol. 28, 4018–4025. http://dx.doi.org/10.1128/MCB.00296-08.
Mizushima, N., Yoshimori, T., Ohsumi, Y., 2011. The role of atg proteins in autophagosome formation. Annu. Rev. Cell Dev. Biol. 27, 107–132. http://dx.doi.org/10.1146/annurev-cellbio-092910-154005.
Muñoz-Espín, D., Serrano, M., 2014. Cellular senescence: from physiology to pathology. Nat. Rev. Mol. Cell Biol. 15, 482–496. http://dx.doi.org/10.1038/nrm3823.
Muñoz-Espín, D., Cañamero, M., Maraver, A., Gómez-López, G., Contreras, J., Murillo-Cuesta, S., Rodríguez-Baeza, A., Varela-Nieto, I., Ruberte, J., Collado, M., Serrano, M., 2013. XProgrammed cell senescence during mammalian embryonic development. Cell 155. http://dx.doi.org/10.1016/j.cell.2013.10.019.
Murata, S., Chiba, T., Tanaka, K., 2003. CHIP: A quality-control E3 ligase collaborating with molecular chaperones. Int. J. Biochem. Cell Biol. 35, 572–578. http://dx.doi.org/10.1016/S1357-2725(02)00394-1.
Nagano, T., Nakano, M., Nakashima, A., Onishi, K., Yamao, S., Enari, M., Kikkawa, U., Kamada, S., 2016. Identification of cellular senescence-specific genes by comparative transcriptomics. Sci. Rep. 6, 31758. http://dx.doi.org/10.1038/srep31758.
Narita, M., Nũnez, S., Heard, E., Narita, M., Lin, A.W., Hearn, S.A., Spector, D.L., Hannon, G.J., Lowe, S.W., 2003. Rb-mediated heterochromatin formation and silencing of E2F target genes during cellular senescence. Cell 113, 703–716. http://dx.doi.org/10.1016/S0092-8674(03)00401-X.
Narita, M., Young, A.R.J., Arakawa, S., Samarajiwa, S.A., Nakashima, T., Yoshida, S., Hong, S., Berry, L.S., Reichelt, S., Ferreira, M., Tavare, S., Inoki, K., Shimizu, S., Narita, M., 2011. Spatial coupling of mTOR and autophagy augments secretory phenotypes. Science (80-.) 332, 966–970. http://dx.doi.org/10.1126/science.1205407.
Ohsumi, Y., 2014. Historical landmarks of autophagy research. Cell Res. 24, 9–23. http://dx.doi.org/10.1038/cr.2013.169.
Onodera, J., Ohsumi, Y., 2005. Autophagy is required for maintenance of amino acid levels and protein synthesis under nitrogen starvation. J. Biol. Chem. 280, 31582–31586. http://dx.doi.org/10.1074/jbc.M506736200.
Park, C., Suh, Y., Cuervo, A.M., 2015. Regulated degradation of Chk1 by chaperone-mediated autophagy in response to DNA damage. Nat. Commun. 6, 6823. http://dx.doi.org/10.1038/ncomms7823.
Park, J.S., Kim, D.H., Yoon, S.Y., 2016. Regulation of amyloid precursor protein processing by its KFERQ motif. BMB Rep. 49, 337–342. http://dx.doi.org/10.5483/BMBRep.2016.49.6.212.
Passos, J.F., Von Zglinicki, T., 2006. Oxygen free radicals in cell senescence: are they signal transducers? Free Radic. Res. 40, 1277–1283. http://dx.doi.org/10.1080/10715760600917151.
Passos, J.F., Nelson, G., Wang, C., Richter, T., Simillion, C., Proctor, C.J., Miwa, S., Olijslagers, S., Hallinan, J., Wipat, A., Saretzki, G., Rudolph, K.L., Kirkwood, T.B.L., von Zglinicki, T., 2010. Feedback between p21 and reactive oxygen production is necessary for cell senescence. Mol. Syst. Biol. 6, 1–14. http://dx.doi.org/10.1038/msb.2010.5.
Rodier, F., Campisi, J., 2011. Four faces of cellular senescence. J. Cell Biol. 192, 547–556. http://dx.doi.org/10.1083/jcb.201009094.
Rodriguez-Navarro, J.A., Kaushik, S., Koga, H., Dall'Armi, C., Shui, G., Wenk, M.R., Di Paolo, G., Cuervo, A.M., 2012. Inhibitory effect of dietary lipids on chaperone-mediated autophagy. Proc. Natl. Acad. Sci. U. S. A. 109, E705–E714. http://dx.doi.org/10.1073/pnas.1113036109.
Rothaug, M., Stroobants, S., Schweizer, M., Peters, J., Zunke, F., Allerding, M., Hooge, R.D., Saftig, P., Blanz, J., 2015. LAMP -2 deficiency leads to hippocampal dysfunction but normal clearance of neuronal substrates of chaperone-mediated autophagy in a mouse model for Danon disease. Acta Neuropathol Commun 1–17. http://dx.doi.org/10.1186/s40478-014-0182-y.
Saha, T., 2012. LAMP2A overexpression in breast tumors promotes cancer cell survival via chaperone-mediated autophagy. Autophagy 8, 1643–1656. http://dx.doi.org/10.4161/auto.21654.
Sahu, R., Kaushik, S., Clement, C.C., Cannizzo, E.S., Scharf, B., Follenzi, A., Potolicchio, I., Nieves, E., Cuervo, A.M., Santambrogio, L., 2011. Microautophagy of cytosolic proteins by late endosomes. Dev. Cell 20, 131–139. http://dx.doi.org/10.1016/j.devcel.2010.12.003.
Sala, A.J., Bott, L.C., Morimoto, R.I., 2017. Shaping proteostasis at the cellular, tissue, and organismal level. J. Cell Biol. 201612111. http://dx.doi.org/10.1083/jcb.201612111.
Salvador, N., Aguado, C., Horst, M., Knecht, E., 2000. Impor of cytosolic portein into lysosomes by chaperone-mediated autophagy depends on its folding state. J. Biol. Chem. 275, 27447–27456.
Sasaki, M., Miyakoshi, M., Sato, Y., Nakanuma, Y., 2010. Autophagy mediates the process of cellular senescence characterizing bile duct damages in primary biliary cirrhosis. Lab. Invest. 90, 835–843. http://dx.doi.org/10.1038/labinvest.2010.56.
Satyanarayana, A., Hilton, M.B., Kaldis, P., 2008. P21 inhibits cdk1 in the absence of cdk2 to maintain the G1/S phase DNA damage checkpoint. Mol. Biol. Cell 19, 65–77. http://dx.doi.org/10.1091/mbc.E07.
Schneider, J.L., Villarroya, J., Diaz-Carretero, A., Patel, B., Urbanska, A.M., Thi, M.M., Villarroya, F., Santambrogio, L., Cuervo, A.M., 2015. Loss of hepatic chaperone-mediated autophagy accelerates proteostasis failure in aging. Aging Cell 14, 249–264. http://dx.doi.org/10.1111/acel.12310.
Serrano, M., Lin, A.W., McCurrach, M.E., Beach, D., Lowe, S.W., 1997. Oncogenic ras provokes premature cell senescence associated with accumulation of p53 and p16(INK4a). Cell 88, 593–602. http://dx.doi.org/10.1016/S0092-8674(00)81902-9.
Sherr, C.J., DePinho, R.A., 2000. Cellular senescence: minireview mitotic clock or culture shock? Cell 102, 407–410. http://dx.doi.org/10.1016/S0092-8674(00)00046-5.
Singh, R., Kaushik, S., Wang, Y., Xiang, Y., Novak, I., Komatsu, M., Tanaka, K., Cuervo, A.M., Czaja, M.J., 2009. Autophagy regulates lipid metabolism. Nature 458, 1131–1135. http://dx.doi.org/10.1038/nature07976.
Storer, M., Mas, A., Robert-Moreno, A., Pecoraro, M., Ortells, M.C., Di Giacomo, V., Yosef, R., Pilpel, N., Krizhanovsky, V., Sharpe, J., Keyes, W.M., 2013. XSenescence is a developmental mechanism that contributes to embryonic growth and patterning. Cell 155, 1119–1130. http://dx.doi.org/10.1016/j.cell.2013.10.041.
Thompson, L.M., Aiken, C.T., Kaltenbach, L.S., Agrawal, N., Illes, K., Khoshnan, A., Martinez-Vincente, M., Arrasate, M., O'Rourke, J.G., Khashwji, H., Lukacsovich, T., Zhu, Y.Z., Lau, A.L., Massey, A., Hayden, M.R., Zeitlin, S.O., Finkbeiner, S., Green, K.N., LaFerla, F.M., Bates, G., Huang, L., Patterson, P.H., Lo, D.C., Cuervo, A.M., Marsh, J.L., Steffan, J.S., 2009. IKK phosphorylates Huntingtin and targets it for

degradation by the proteasome and lysosome. J. Cell Biol. 187, 1083–1099. http://dx.doi.org/10.1083/jcb.200909067.
Unterluggauer, H., Micutkova, L., Lindner, H., Sarg, B., Hernebring, M., Nystrom, T., Jansen-Dürr, P., 2009. Identification of Hsc70 as target for AGE modification in senescent human fibroblasts. Biogerontology 10, 299–309. http://dx.doi.org/10.1007/s10522-008-9193-z.
van Deursen, J.M., 2014. The role of senescent cells in ageing. Nature 509, 439–446. http://dx.doi.org/10.1038/nature13193.
van Dijk, K.D., Persichetti, E., Chiasserini, D., Eusebi, P., Beccari, T., Calabresi, P., Berendse, H.W., Parnetti, L., van de Berg, W.D.J., 2013. Changes in endolysosomal enzyme activities in cerebrospinal fluid of patients with Parkinson's disease. Mov. Disord. 28, 747–754. http://dx.doi.org/10.1002/mds.25495.
Wang, C., Jurk, D., Maddick, M., Nelson, G., Martin-ruiz, C., Von Zglinicki, T., 2009a. DNA damage response and cellular senescence in tissues of aging mice. Aging Cell 8, 311–323. http://dx.doi.org/10.1111/j.1474-9726.2009.00481.x.
Wang, Y., Martinez-Vicente, M., Krüger, U., Kaushik, S., Wong, E., Mandelkow, E.M., Cuervo, A.M., Mandelkow, E., 2009b. Tau fragmentation, aggregation and clearance: the dual role of lysosomal processing. Hum. Mol. Genet. 18, 4153–4170. http://dx.doi.org/10.1093/hmg/ddp367.
Wei, Z., Chen, X.C., Song, Y., Pan, X.D., Dai, X.M., Zhang, J., Cui, X.L., Wu, X.L., Zhu, Y.G., 2016. Amyloid?? protein aggravates neuronal senescence and cognitive deficits in 5XFAD mouse model of Alzheimer???s disease. Chin. Med. J. (Engl.) 129, 1835–1844. http://dx.doi.org/10.4103/0366-6999.186646.
Xie, Z., Klionsky, D.J., 2007. Autophagosome formation: core machinery and adaptations. Nat. Cell Biol. 9, 1102–1109. http://dx.doi.org/10.1038/ncb1007-1102.
Xilouri, M., Stefanis, L., 2015. Molecular and Cellular Neuroscience Chaperone mediated autophagy to the rescue: a new-fangled target for the treatment of neurodegenerative diseases. Mol. Cell. Neurosci. 66, 29–36. http://dx.doi.org/10.1016/j.mcn.2015.01.003.
Xilouri, M., Stefanis, L., 2016. Chaperone mediated autophagy in aging: starve to prosper. Ageing Res. Rev. 32, 13–21. http://dx.doi.org/10.1016/j.arr.2016.07.001.
Xilouri, M., Brekk, O.R., Polissidis, A., Chrysanthou-Piterou, M., Kloukina, I., Stefanis, L., 2016. Impairment of chaperone-mediated autophagy induces dopaminergic neurodegeneration in rats. Autophagy 12, 2230–2247. http://dx.doi.org/10.1080/15548627.2016.1214777.
Zhang, L., Sun, Y., Fei, M., Tan, C., Wu, J., Zheng, J., Tang, J., Sun, W., Lv, Z., Bao, J., Xu, Q., Yu, H., 2014. Disruption of chaperone-mediated autophagydependent degradation of MEF2A by oxidative stress-induced lysosome destabilization. Autophagy 10, 1015–1035. http://dx.doi.org/10.4161/auto.28477.

11.2. *Anexo 2 . Cortical neurons develop a senescence-like phenotype promoted by dysfunctional autophagy*

www.aging-us.com AGING 2019, Vol. 11, No. 16

Research Paper

Cortical neurons develop a senescence-like phenotype promoted by dysfunctional autophagy

Daniel Moreno-Blas[1], Elisa Gorostieta-Salas[1], Alexander Pommer-Alba[1], Gabriel Muciño-Hernández[1], Cristian Gerónimo-Olvera[2], Luis Angel Maciel-Barón[3], Mina Konigsberg[3], Lourdes Massieu[2], Susana Castro-Obregón[1]

[1]Departamento de Neurodesarrollo y Fisiología, División de Neurociencias, Instituto de Fisiología Celular, UNAM, Mexico City 04510, México
[2]Departamento de Neuropatología, División de Neurociencias, Instituto de Fisiología Celular, UNAM, Mexico City 04510, México
[3]Departamento de Ciencias de la Salud, Universidad Autónoma Metropolitana, Unidad Iztapalapa. Mexico City 09340, México

Correspondence to: Susana Castro-Obregón; **email:** scastro@ifc.unam.mx
Keywords: senescence, brain, neuron, autophagy, SASP (senescence-associated secretory phenotype)
Received: March 12, 2019 **Accepted:** August 9, 2019 **Published:** August 30, 2019

ABSTRACT

Senescent cells accumulate in various tissues and organs with aging altering surrounding tissue due to an active secretome, and at least in mice their elimination extends healthy lifespan and ameliorates several chronic diseases. Whether all cell types senesce, including post-mitotic cells, has been poorly described mainly because cellular senescence was defined as a permanent cell cycle arrest. Nevertheless, neurons with features of senescence have been described in old rodent and human brains. In this study we characterized an *in vitro* model useful to study the molecular basis of senescence of primary rat cortical cells that recapitulates senescent features described in brain aging. We found that in long-term cultures, rat primary cortical neurons displayed features of cellular senescence before glial cells did, and developed a functional senescence-associated secretory phenotype able to induce paracrine premature senescence of mouse embryonic fibroblasts but proliferation of rat glial cells. Functional autophagy seems to prevent neuronal senescence, as we observed an autophagic flux reduction in senescent neurons both *in vitro* and *in vivo*, and autophagy impairment induced cortical cell senescence while autophagy stimulation inhibited it. Our findings suggest that aging-associated dysfunctional autophagy contributes to senescence transition also in neuronal cells.

INTRODUCTION

Aging is accompanied by a wide range of symptoms that reduce health span, such as cardiovascular dysfunction, osteoporosis, neurodegeneration and cancer, among other diseases. Amelioration of those symptoms has been achieved after pharmacological interventions using a novel class of drugs termed senolytics. These compounds clear senescent cells that accumulate late in life both in normal tissues and especially in those affected by age-related pathologies [1]. Nevertheless, senescent cells are harmful only when they persist, since transient senescent cells, which are eliminated by effector immune cells, contribute to wound healing, regeneration, immunity and even morphogenesis during development [2]. Therefore, it is fundamental to understand the molecular mechanisms of senescence establishment and maintenance.

Cellular senescence is a phenotype characterized by a durable cell cycle arrest (*i.e.* cells do not respond to mitogens) and a flattened and vacuolated morphology with stress granules collection. Even though there is no single marker of senescence, some of the most common features observed are: activation of the lysosomal enzyme senescence-associated β-galactosidase (SA-β-gal); persistent DNA damage response detected by γH2AX foci; expression of tumor suppressors $p21^{CIP1/WAF1}$ (encoded by *Cdkn1a)* and/or $p16^{INK4A}$ (encoded by *Cdkn2a)*; lipofuscin accumulation [3]; and nuclear deformation associated with nuclear envelop proteins degradation [4]. The most important activity of senescent cells is the secretion of a set of molecules, known as the senescence-associated secretory phenotype (SASP) that, depending on the physiological context, can be either beneficial or harmful. In early stages senescent cells secrete cytokines that promote the migration and infiltration of effector immune cells, as well as growth factors and proteases that facilitate tissue repair and remodeling. Yet, persisting signaling contributes to chronic inflammation, a hallmark of aging and a major contributor to age-related dysfunctions. SASP molecules also have an autocrine role, fostering the senescent phenotype, and a paracrine role inducing senescence in surrounding cells [5], inflammation and tumorigenesis [6, 7].

Autophagy is a catabolic process that degrades intracellular components, like proteins and damaged organelles, including mitochondria, through lysosomes. Similar to senescence, it is induced in response to stressful stimuli, therefore both senescence and autophagy are often observed simultaneously. The interplay between autophagy and senescence requires further investigation, since autophagy has been implicated in both promoting and inhibiting cellular senescence. While autophagy inhibition promotes senescence in normal proliferating cells [8], autophagy inhibition delays oncogene-induced senescence and the synthesis of SASP components [9]. A possible explanation for the opposing role of autophagy over senescence is that it could engulf alternative targets that regulate cellular senescence in opposite manners. For example, the stability of the transcription factor GATA4, a key activator of SASP genes, is regulated by autophagy. Upon senescence induction, GATA4 escapes autophagic degradation because its interaction with p62/SQSTM1 (an autophagy cargo receptor) decreases, leading to GATA4 accumulation [10]. On the other hand, during oncogene-induced senescence, autophagy fosters the SASP through a specialized compartment known as the TOR-autophagy spatial coupling compartment (TASCC), where mTOR localizes at the surface of autolysosomes, which are surrounded by endoplasmic reticulum; a flux of recycled amino acids and metabolites released from the autolysosomes are used by mTORC1 for supporting the synthesis of SASP factors, hence facilitating senescence [11]. Therefore, selective autophagy actively suppresses cellular senescence through the degradation of GATA4, whereas autophagic degradation of other proteins (perhaps long-lived proteins), facilitates the SASP [12].

The traditional view of senescence as a specific phenomenon where a proliferation-competent cell undergoes permanent growth arrest, has limited the study of senescence of post-mitotic cells. Accordingly, the limited studies on cellular senescence in the brain have mostly focused on glial cells [13]. Nonetheless, some senescent markers have been described in several studies of both physiological aging and neurodegenerative diseases [14]. For example, cortical and Purkinje neurons show several senescence features like SA-β-gal activity, lipofuscin accumulation, γH2AX and macro-H2A foci, and IL6 expression, all in a $p21^{CIP1/WAF1}$-dependent manner [15]. Interestingly, human neurons might also senesce, since there is expression of *p16/Cdkn2a* in pyramidal neurons in the prefrontal cortex from human brains of people over 77 years old [10]. We are interested in understanding the molecular basis for neuronal senescence, because we hypothesize that when senescent neurons persist in the brain, they contribute to cognitive decline by impairing synaptic function, inducing paracrine senescence and chronic inflammation.

While cellular senescence of mitotic cells is induced mainly by stressful stimuli (most of them inducing DNA damage), telomere attrition during cell division, oncogene activation or developmental cues [2], the molecular mechanisms that induce post-mitotic cells senescence are less understood. Also, whether autophagy regulates senescence in any direction in post-mitotic cells is completely unknown. Several groups have observed that neuronal cells acquire some senescent features *in vitro*, providing a very helpful system to study the molecular basis of neuronal senescence. For example, primary cortical, hippocampal and cerebellar granule neurons become SA-β-gal-positive over time [16-20]. However, these studies were limited to the detection of SA-β-gal activity, which could be misleading [21]. Recent *in vitro* studies confirmed the presence of additional senescent features, including γH2AX foci in neurons from mouse neuro-glial co-cultures maintained up to 27 days *in vitro* (D*IV*) [22]. Taken together, these reports support the notion that cultured neurons *in vitro* are capable of undergoing cellular senescence with the same features that occur *in vivo*.

For senescent neurons to contribute to chronic inflammation and paracrine senescence, they must establish a senescent phenotype including the SASP. Paracrine senescence has been demonstrated to occur in mouse embryonic fibroblast exposed to conditioned media from senescent fibroblasts [5]. In this work we developed an *in vitro* model of neuronal senescence that recapitulates *in vivo* senescence markers, and secreted molecules able to induce paracrine glial proliferation as well as premature senescence in mouse embryonic fibroblasts, pointing towards a neuronal SASP. We found that senescent cortical cells secrete C-C motif chemokine 2, also known as monocyte chemotactic protein 1 (MCP-1), a known SASP factor able to induce paracrine senescence [23]. Interestingly, we found that rat primary cortical neurons displayed features of cellular senescence before glial cells did. As reported for proliferating cells, functional autophagy, perhaps selective, seems to prevent neuronal senescence, as we observed autophagic flux impairment. Accordingly, we observed more senescent cortical cells when autophagy was impaired and less when it was stimulated. Our findings suggest that a dysfunctional autophagy contributes to senescence transition also in post-mitotic cells.

RESULTS

Primary cortical neurons acquire several senescent features after long-term culture.

To establish an *in vitro* model to study the transition of neurons from a non-dividing terminal differentiation state into senescence *in vitro*, prenatal rat cortical cells were cultured for up to 40 days *in vitro* (D*IV*). Since several reports indicate the presence of senescent glial cells in old brains [13], we considered that glial cells could become senescent and then promote paracrine neuronal senescence; hence, we allowed the proliferation of glial cells during the culture of primary cortical cells. During the first days of culture (6 D*IV*), neurons (expressing βIII-TUBULIN) represented 96.8% (SD 2.2) of the cells with very few glial cells (expressing GFAP); due to proliferation of glial cells and some loss of neurons, by 26 D*IV* there were 51% (SD 6.9) neurons and 31% (SD 11.5) glial cells; and by 40 D*IV* 73% (SD 6.9) of the surviving cells were glial. The cells expressing βIII-TUBULIN did not expressed GFAP. On average, the total number of cells along the culture remained similar (Supplementary Figure 1S). Without any further stressful stimuli, cortical cells became SA-β-gal-positive over time and accumulated lipofuscin detected by autofluorescence and by Sudan Black B staining, a lipophilic dye [24] (Figures 1A-B). SBB staining seems to be more sensitive than SA-β-gal activity. An increment in both SA-β-gal-positive and lipofuscin accumulation was also confirmed in the cortex of old rat brains (Figures 1C-E).

Since different inducers of senescence in mitotic cells converge on the activation of the tumor suppressor $p21^{CIP1/WAF1}$, and indeed $p21^{CIP1/WAF1}$ has been suggested to mediate neuronal senescence in old brains [15], we reasoned that even though post-mitotic cells already express some CDK inhibitors to exit the cell cycle, they could still need to induce its expression for a pro-senescent activity from this protein. Therefore, we analyzed its expression on neurons or glial cells at different times of culture. As shown in Figure 2, in primary culture of cortical cells incubated 26 D*IV*, neurons but not yet glial cells expressed higher levels of $p21^{CIP1/WAF1}$. The number of glial cells with elevated expression of $p21^{CIP1/WAF1}$ increased until 40 D*IV*. This observation suggests that neurons acquire senescent features before glial cells. Interestingly, at 26 D*IV* $p21^{CIP1/WAF1}$ is slightly enriched at the nuclear periphery. This could be related to the recent finding that altered nuclear export is a common hallmark of aging [25]. We confirmed $p21^{CIP1/WAF1}$ expression is induced at transcriptional level in cortical cells at 26 D*IV* by qRT-PCR (Figure 2C).

Another hallmark of senescence is a persistent DNA damage response, commonly detected by the presence of γH2AX foci. As shown in Figure 3A, neuronal cells accumulated γH2AX foci at 26 D*IV*, accompanied by ruptures of DNA detected by Comet assay (Figure 3B). Even though we are not able to distinguish neurons from glial cells with this assay, it is conceivable that the nuclei with broken DNA come from neurons, since we observed that mainly neurons had γH2AX foci; these observations suggest that neurons accumulate DNA damage leading to a persistent DNA damage response. At both 26 and 40 D*IV*, only a small proportion of GFAP expressing cells had γH2AX foci. As expected, cortical neurons from old rat brains also contained more γH2AX foci (Figure 3C).

Finally, since during oncogene-induced senescence, replicative senescence and senescence induced by DNA damaging drugs occur nuclear morphology abnormalities associated with nuclear envelope proteins loss [26], and depletion of Lamin-B1 or Lamin-A/C is sufficient to induce senescent features [4], we wondered whether also senescent post-mitotic cells, such as neurons, would manifest nuclear morphology deformations. As shown in Figure 4, indeed both *in vitro* and *in vivo* senescent neurons had irregular nuclear morphology with folds of the nuclear envelope forming intra-nuclear Lamin-A/C structures that protrude into the nucleoplasm. Very few astrocytes showed abnormal distribution of Lamin-A/C at 26 D*IV*, strengthening the

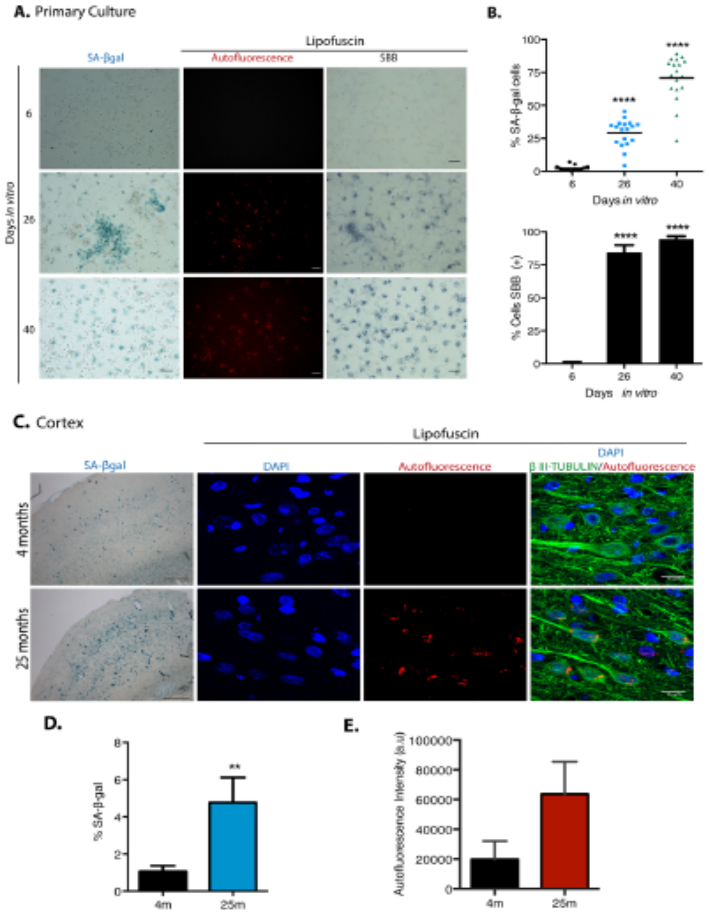

Figure 1. Cortical cells in long-term culture and in old rat brains had higher SA-β-gal activity and accumulated lipofuscin. (A) SA-β-gal activity or lipofuscin accumulation detected by autofluorescence or by Sudan Black B (SBB) staining were detected in primary rat cortical cells cultured for the indicated D*IV*. Notice that cortical cells have higher SA-β-gal activity and lipofuscin from 26 D*IV*. Images are representative of at least three independent experiments. Scales bar represent 100 μm. (B) Percentage of SA-β-gal or SBB positive cells in the cultures incubated at the indicated D*IV*. Quantification was made using NIS Elements software. The mean of three independent experiments, each done by quintupled replicas, is graphed. Bars in graphs represent SEM. Two-way RM ANOVA analysis, with Dunnett´s multiple comparison test. **** $p< 0.0001$ in comparison with 6 D*IV*. (C) Cortical neurons in old brains had higher SA-β-gal activity (scale bars represent 500 μm) and accumulated lipofuscin. Scale bar represents 15 μm. (D) The percentage of SA-β-gal positive area within each brain section is plot. The average of three brains per age is graphed; 15 sections from each brain were quantified. Bars in graphs represent SEM. Unpaired t Test, ** $p< 0.01$. (E) Quantification of autofluorescence intensity per section (arbitrary units). Bars in graphs represent SD. The average of three brains per age is graphed; 15 sections from each brain were quantified. Even though there was an evident increase in autofluorescence, no statistical significance was obtained.

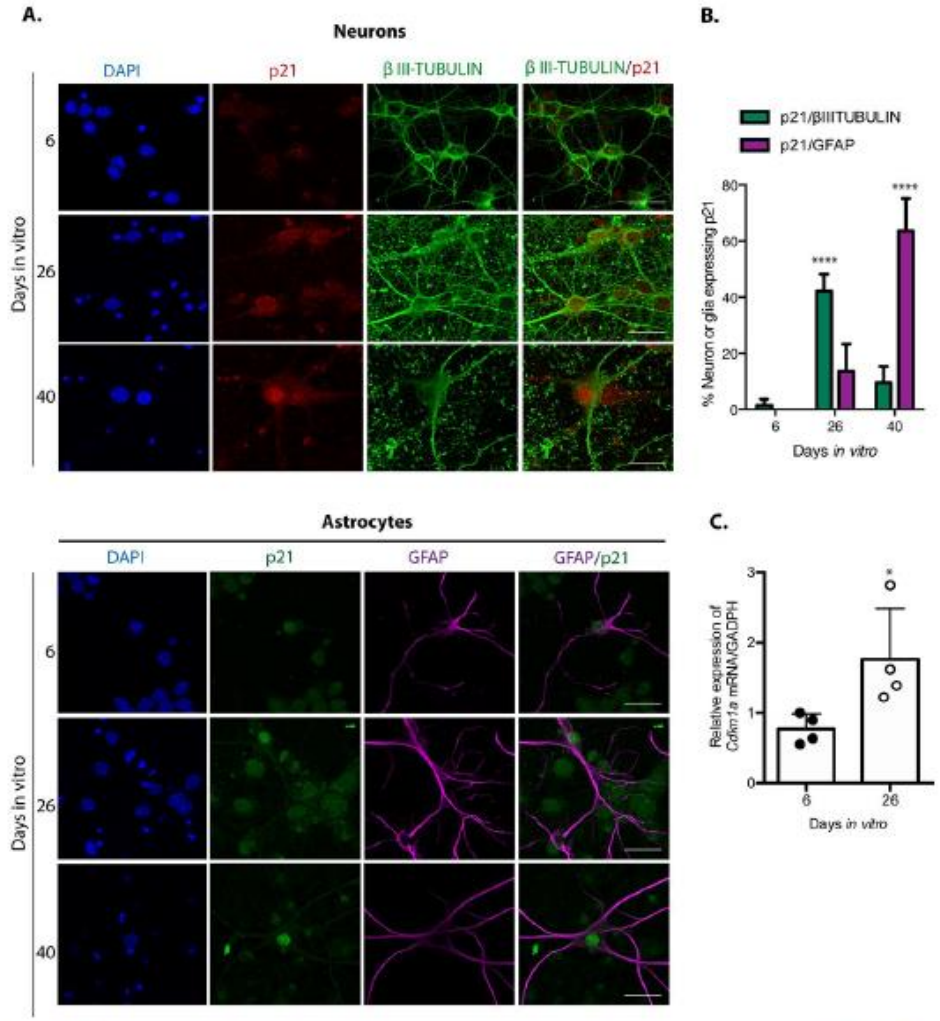

Figure 2. Neuronal cells in cortical long-term culture showed increased expression of p21$^{CIP1/WAF1}$. (**A**) Immunofluorescence to detect p21$^{CIP1/WAF1}$ (p21) in neurons (expressing βIII-TUBULIN) or astrocytes (expressing GFAP) in primary culture of cortical cells incubated during the indicated D/V. Notice that mostly neurons increased the abundance of p21$^{CIP1/WAF1}$ at 26 D/V, indicating that neurons acquired senescent features before glial cells. Scale bar represents 25 μm. Arrows indicate examples of cells with healthy nuclei counted (not all the healthy cells are indicated). (**B**) Percentage of neurons or glial cells expressing p21$^{CIP1/WAF1}$ over all cells. The mean of three independent experiments, each done by duplicate, is plotted. Bars represent standard deviation. Two-way RM ANOVA analysis, with Tukey´s multiple comparison test. **** p<0.0001. (**C**) qRT-PCR from total RNA purified from cortical primary cultures during the indicated days. The relative expression of *Cdkn1a* mRNA was normalized with *Gapdh* mRNA. Bars represent SD. * p=0.039 by unpaired t test two tailed. n=4.

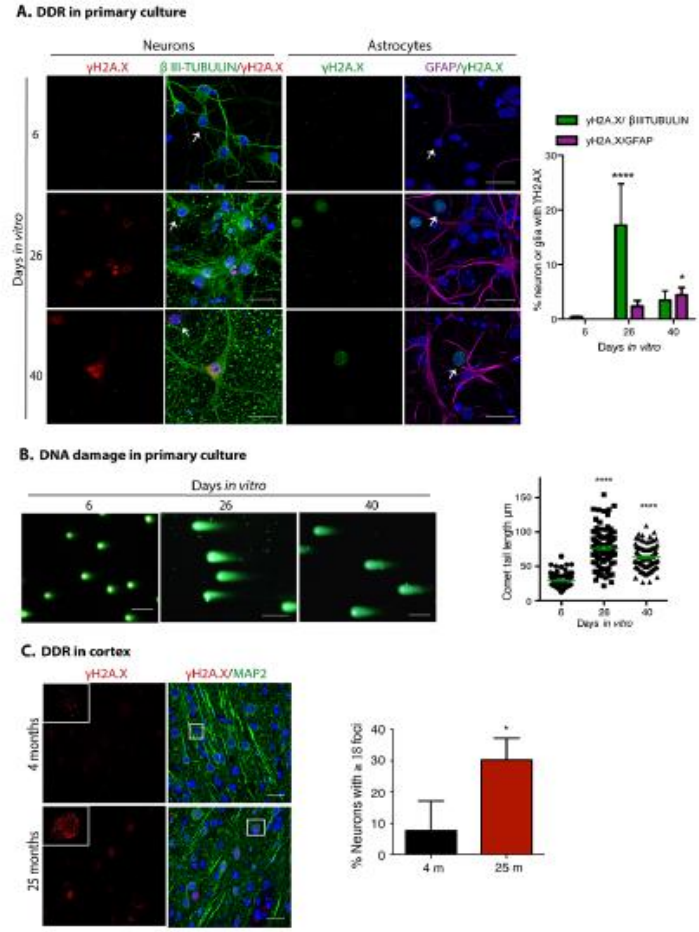

Figure 3. Neuronal cells in cortical long-term culture and in the cortex from old rat brains had a sustained DNA damage response (DDR). (A) Immunofluorescence to detect γH2AX foci in neurons (expressing βIII-TUBULIN) or astrocytes (expressing GFAP) in primary culture of cortical cells incubated during the indicated D*IV*. Notice that mostly neurons have γH2AX foci at 26 D*IV*. Scale bar represents 25 µm. Right, quantification of the percentage of neurons or glial cells with γH2AX foci over all cells. The mean of three independent experiments, each done by duplicate, is plotted. Bars represent SEM. Two-way RM ANOVA analysis, with Dunnett´s multiple comparison test. **** p< 0.0001 26 D*IV vs.* 6 D*IV*; * p<0.05 40 D*IV vs.* 6 D*IV*. Arrows indicate examples of cells with healthy nuclei counted (not all the healthy cells are indicated). (B) Comet assay to detect double strand breaks in genomic DNA from cells collected at the indicated days. Scale bars represent 100 µm. Right, the length of the tail of the comets, indicative of level of DNA damage, is plotted. 50 nuclei from each treatment, from two independent experiments, were analyzed by RM one-way ANOVA with Dennett's´ multiple comparison. **** p< 0.0001 between 26 D*IV* or 40 D*IV* in comparison with 6 D*IV*. (C) Immunofluorescence to detect γH2AX foci in cortical neurons (expressing MAP2) in rat brains from the indicated age. Nuclei were stained with DAPI. Scale bars represent 30 µm. Right, percentage of neurons with more than 18 foci per nucleus. More than 100 neurons were counted from 3 different brains of each age. Bars represent standard deviation. Unpaired t Test * p<0.01.

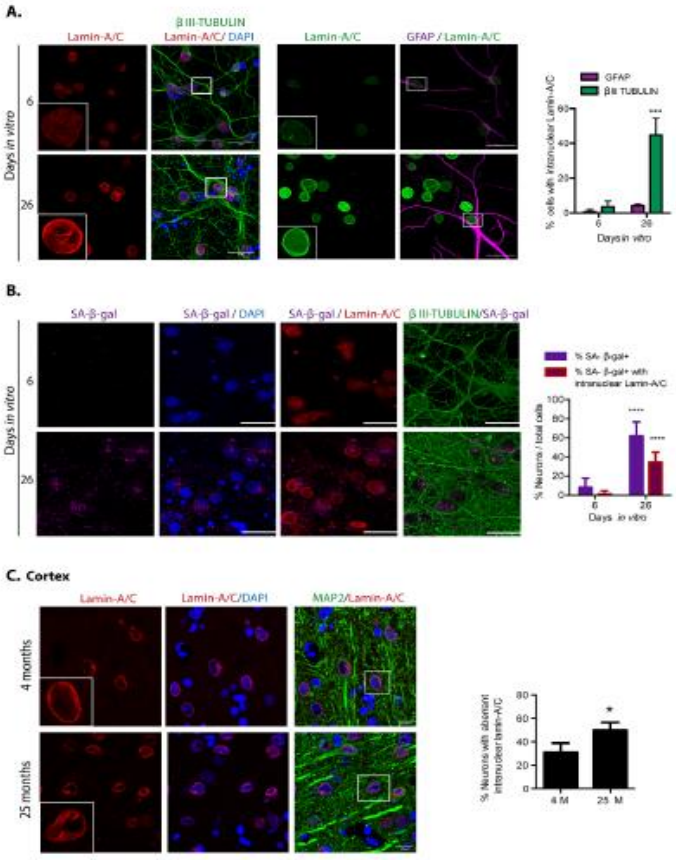

Figure 4. Cortical cells in long-term culture and in old rat brains had nuclear morphology abnormalities. (A) Immunofluorescence to detect Lamin-A/C in neurons (expressing βIII-TUBULIN) or astrocytes (expressing GFAP), in primary culture of cortical cells incubated during the indicated days *in vitro*. Squares indicate the magnified area shown in insets. Representative images of three independent experiments are shown. Scale bars represent 25 μm. Right, percentage of neurons or astrocytes with aberrant nuclear morphology over total cells. Bars represent SEM; two-way RM ANOVA analysis, *** p< 0.001 in comparison with 6 D/V. (B) Simultaneous detection of SA-β-gal activity (by confocal microscopy) and Lamina-A/C (by immunofluorescence) in neurons (expressing βIII-TUBULIN) in primary culture of cortical cells incubated during the indicated days *in vitro*. Representative images of three independent experiments are shown. Scale bars represent 25 μm. Right, percentage of neurons with visible SA-β-gal activity, and with both visible SA-β-gal activity and aberrant intranuclear Lamin-A/C over total cells. Five fields from three independent experiments were quantified. Bars represent SEM. Two-way RM ANOVA analysis, followed by Sidak´s multiple comparison test. **** p< 0.0001 in comparison with 6 D/V. C. Immunofluorescence to detect Lamin-A/C in cortical neurons in the internal pyramidal layer 5 from brain slices of the indicated age. Notice that also *in vivo*, neurons in old brains had nuclear deformations. Squares indicate the magnified area shown in insets. Scale bars represent 30 μm. Right, percentage of neurons in with aberrant nuclear morphology in cortical brain slices of the indicated age, as shown in (C). (n=3). Bars represent SD; unpaired t Test Student * p< 0.01.

notion that neurons become senescent before glial cells in this model. Since every senescent feature, alone, is not sufficient to confirm a senescent state, we simultaneously detected SA-β-gal activity and Lamin-A/C in neurons. As shown in Figure 4B, around half of the neurons with high SA-β-gal activity at 26 D*IV* also had an aberrant nuclear morphology, supporting the notion that neurons in long-term culture acquire senescent features. The observation that some neurons with high SA-β-gal show a normal nuclear morphology, is in agreement with previous observation that SA-β-gal activity alone is not a reliable marker of senescence [21]. We propose that nuclear deformations could be a more reliable marker for neuronal senescence. Since differentiated neurons express low levels of Lamin-B1 [27], we were unable to detect loss of Lamin-B1 in senescent neurons.

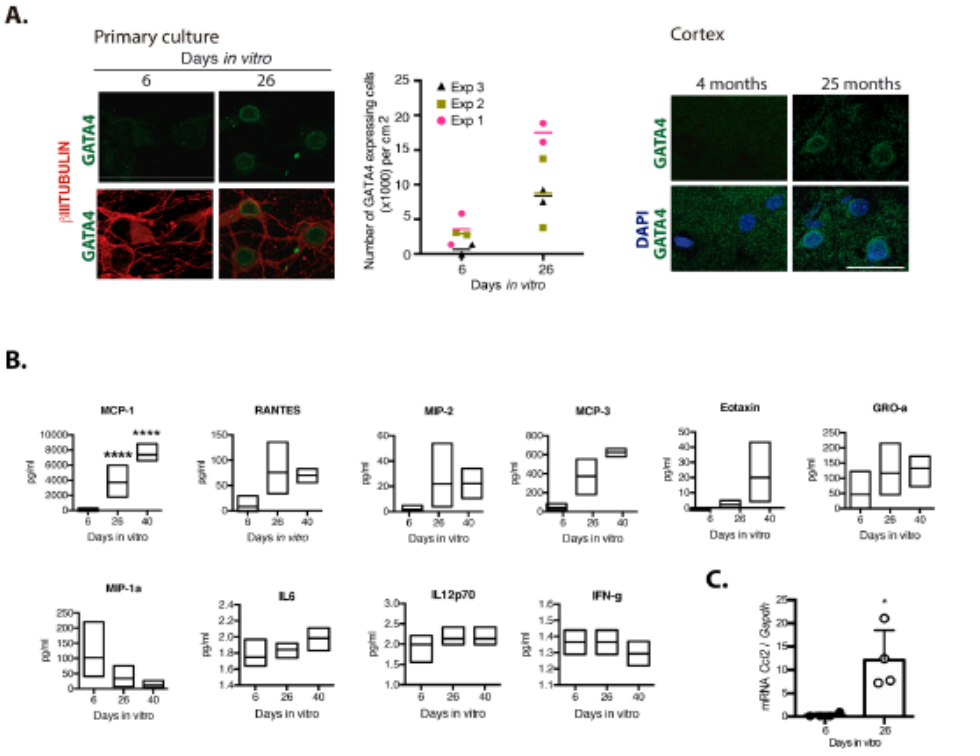

Figure 5. Senescent neurons increased the expression of GATA4 and cortical cells secreted MCP-1. (A) Immunofluorescence to detect GATA4 in neurons (expressing βIII-TUBULIN) in primary culture of cortical cells either incubated during the indicated days *in vitro* or in rat brains of the indicated age. Scale bars represent 25 μm. The number of cells with increased GATA4 abundance from three independent experiments, each performed in duplicate, is graphed. The mean of each experiment is represented by horizontal bars. (B) Quantification by multiplex immunoassay of the indicated cytokines, from conditioned media from cultures of the indicated days from three independent experiments. The maximum and minimum values are graphed. Bars indicate the mean of the three independent experiments. Data were analyzed by two-way ANOVA followed by Tukey's multiple comparisons test analysis, only MCP-1 was significant. **** p<0.0001 relative to 6 D*IV*. (C) qRT-PCR from total RNA purified from cortical primary cultures during the indicated days. The relative expression of *Ccl2* mRNA was normalized with *Gapdh* mRNA. Bars represent SD. * p=0.0106 by unpaired t test two tailed. n=4.

Senescent cortical cells secrete molecules that induce premature paracrine senescence and glial proliferation, suggesting a neuronal SASP

We hypothesize that persistent senescent neurons, through the SASP, contribute to induce paracrine senescence and chronic inflammation in old brains. Therefore, we studied whether neurons would express GATA4, a transcription factor that promotes the expression of SASP factors [10]. As shown in Figure 5A, GATA4 accumulated in neuronal cells cultured for 26 D*IV*, as well in cortical neurons from old brains. To get an insight about the cytokines that senescent cortical cells could be secreting, we analyzed the presence of G-CSF, GM-CSF, IFNγ, IL-1α, IL-1β, IL-10, IL-12p70, IL-13, IL-17A, IL-2, IL-4, IL-5, IL-6, TNFα, EOTAXIN, GRO-α, IP-10, MCP-1, MCP-3, MIP-1α, MIP-2 and RANTES by a multiplex immunoassay. As shown in Figure 5B, MCP-1, RANTES, MIP-2, GRO-1, MCP-3 and EOTAXIN were more abundant in conditioned media from senescent cortical cultures, although only MCP-1 content showed a statistically significant difference at 26 and 40 D*IV* relative to 6 D*IV* cortical cultures; MIP-1a secretion was reduced in older cultures. To our surprise, IL6, a common SASP component, was barely detected and did not increase in conditioned media from senescent cells. Also, IL-12p70 and IFNγ secretion did not change along the time in culture and were secreted in a very small amount, at the threshold limit of detection. G-CSF, GM-CSF, IL-1α, IL-1β, IL-10, IL-13, IL-17A, IL-2, IL-4, IL-5, TNFα, GRO-α, IP-10 and MIP-1α were not detected at any time point. We further confirmed the induction of expression of *Ccl2* (gen coding for MCP-1) by qRT-PCR (Figre 5C).

Since MCP-1 has been shown to induce paracrine senescence [23], and GATA 4 is a mediator regulating MCP-1 expression during senescence induced by Lamin-A defects [28], we reasoned that senescent cortical cells could indeed acquire a functional SASP. To test this hypothesis, we analyzed whether conditioned media from senescent cortical cells could induce premature paracrine senescence (a schematic experimental design is shown in Figure 6A). To obtain conditioned media with accumulated secreted factors, the media was left for intervals of about a week in between fresh media changes over the cells, and it was collected at 6, 26 or 40 days of culture. Conditioned media was then added to young (1 D*IV*) prenatal cortical cells and after 6 D*IV* of treatment all the senescent markers described above were evaluated. Interestingly, conditioned media from cortical cells cultured for 26 D*IV* or 40 D*IV* induced abundant proliferation of glial cells (Figure 6B), suggesting that senescent cortical cells, potentially neurons, could indeed affect tissue organization. Nevertheless, we did not observe significant expression of senescent markers on young neurons (not shown). We reasoned that young neurons could be more resistant to paracrine senescence than mitotic cells; therefore, we tested whether the conditioned media from cortical cells cultured for 26 D*IV*, time at which most of the senescent cells are neurons, would induce paracrine senescence in mouse embryonic fibroblast (MEFs). Indeed, conditioned media from cortical cells cultured for 26 D*IV* induced key senescent features in MEFs, such as increased SA-β-gal activity; inhibition of proliferation (detected by Ki67 expression); DNA damage response identified by γH2AX foci; and increased expression of IL6, although this latter was not statistical different (Figure 6C). In summary, prenatal cortical cells exposed for 6 days to conditioned media from cortical cells cultured for 26 D*IV* or 40 D*IV* did not show senescent features, whereas MEFs did.

Taken together, our results confirm that neurons acquire senescent features potentially including the SASP, interestingly before glial cells. This observation suggests that senescent neurons could affect the function of surrounding cells, such as astrocytes. Intriguingly, young neurons were unresponsive to the SASP produced by senescent cortical cells, since they did not show senescent markers when exposed to the conditioned media from cortical cultures of 26 or 40 *DIV* (not shown).

Dysfunctional autophagy contributes to neuronal senescence

Abundant reports indicate that dysfunctional autophagy accompanies aging, and in the brain it causes neurodegeneration [29]. Accordingly, induction of autophagy ameliorates age-related cognition deficits [30]. Therefore, we evaluated whether dysfunctional autophagy would contribute to neuronal senescence establishment, with a similar mechanism as described for senescence transition of mitotic cells. First, we analyzed in senescent neurons whether autophagic flux is reduced, reflected by accumulation of autophagosomes and proteins associated to them like LC3 and p62/SQSTM1. As shown in Figure 7A, cortical cells at 26 D*IV*, a time point when neurons showed senescent features, had more autophagosomes detected with the specific dye CytoID® and by immunofluorescent detection of LC3. We confirmed the abundance of autophagosomes in senescent neurons by electron microscopy, labeling them with immunogold localization of LC3. As the autophagic receptor p62/SQSTM1 is degraded together with the cargo, it accumulates when the autophagic flux is interrupted. We analyzed the abundance of p62/SQSTM1 by

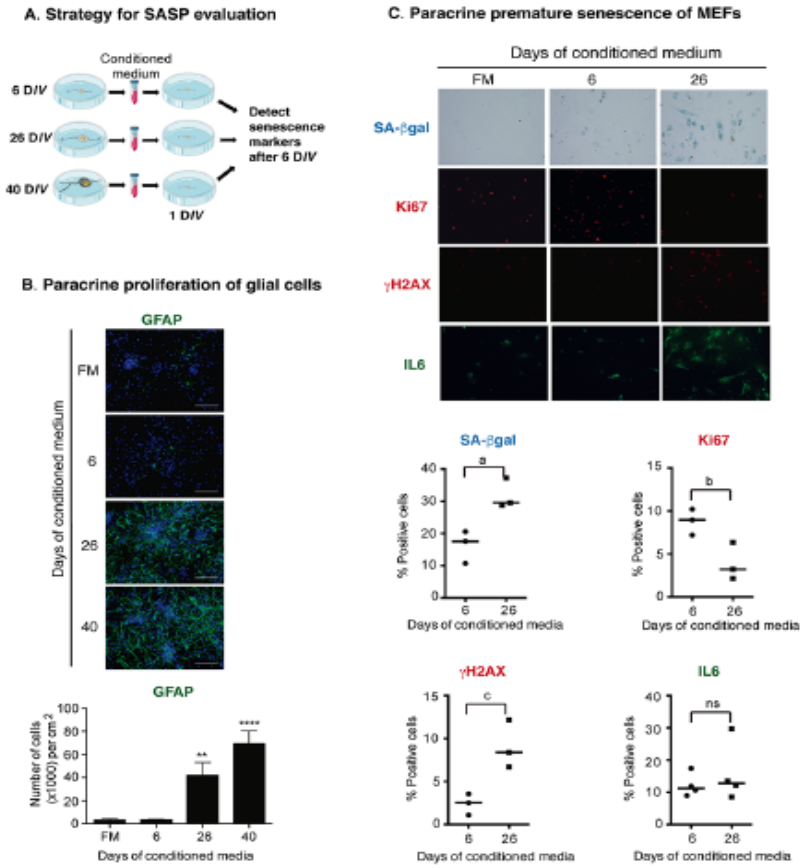

Figure 6. Senescent cortical cells develop a functional SASP. (A) Experimental design to evaluate the presence of secreted molecules with SASP activity from senescent cortical cells. Conditioned media was collected from cortical cells that had been incubated from 1-6 (6), 19-26 (26) or 32-40 (40) D*IV*. Either primary prenatal cortical cells or MEFs were cultured for 24 hr (1 D*IV*) before adding conditioned media; senescence markers were evaluated 6 days later. (B) Conditioned media from senescent cortical cells induced paracrine proliferation of glial cells in primary culture of prenatal cortical cells. Representative immunofluorescences to detect GFAP in cortical cells are shown. Cells were incubated with conditioned media collected from cortical cells that had been incubated during the indicated D*IV*. FM stands for fresh medium. Notice that conditioned media from 26 D*IV* and 40 D*IV* induced high proliferation of glial cells. Scale bars represent 500 μm. The bottom graph is a quantification of the number of GFAP expressing cells in three independent experiments, each done in duplicate. Data were analyzed by one-way ANOVA, with Dunnett´s multiple comparison test. ** p<0.01; ****p<0.0001 compared to FM. (C) Conditioned media from senescent cortical cells induced paracrine premature senescence in MEFs. MEFs were incubated with conditioned media collected from cortical cells that had been incubated during the indicated D*IV*. FM stands for fresh medium. Notice that senescent markers were higher in cells incubated with conditioned media from cortical cells cultured for 26 days. The bottom graphs are quantifications of the percentage of cells with blue or fluorescent signals. The signal (either blue or fluorescent) from cells incubated with 6 D*IV* conditioned media plus one standard deviation was deducted from the signal obtained from the cells treated with 26 D*IV* conditioned media. Three independent experiments, each performed in duplicate were quantified. Data were analyzed by unpaired T test. a, p=0.0175; b, p=.0.0327; c, p=0.0191.

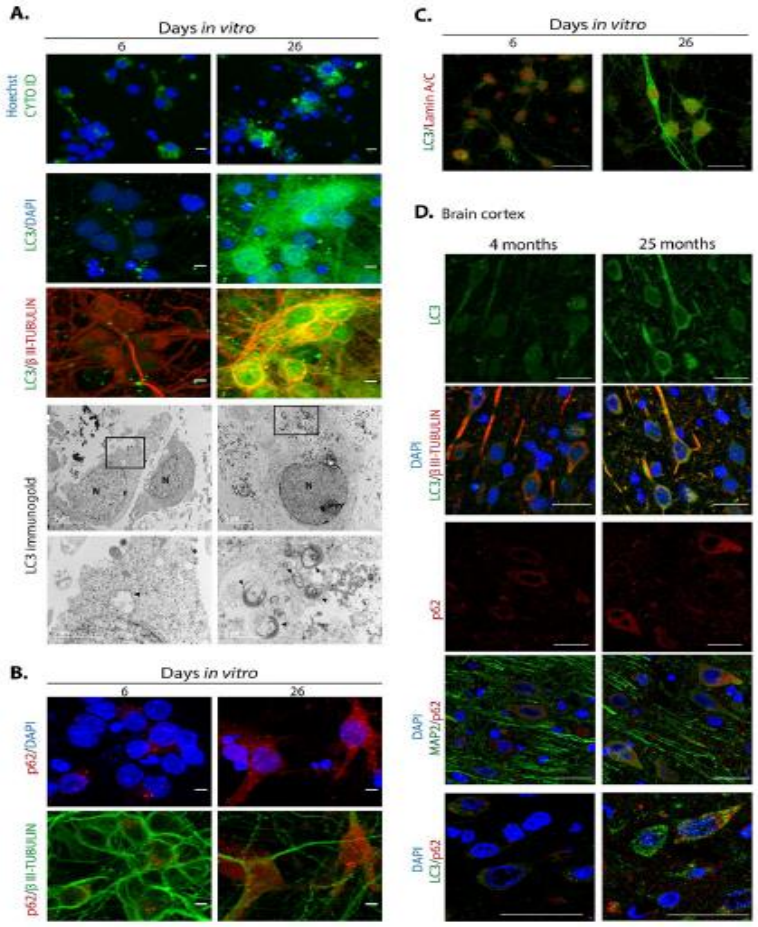

Figure 7. Autophagosomes accumulate during neuronal senescence. (A) Top row, autophagosomes were stained with CytoID® and nuclei with Hoechst in primary culture of cortical cells incubated during the indicated D*IV*; scale bars represent 15 μm. Middle rows, immunofluorescence to detect LC3 in neurons (expressing βIII-TUBULIN) of primary cortical cells cultivated during the indicated D*IV*. Scale bars represent 5 μm. Bottom rows, electron micrographs showing accumulation of autophagosomes in 26 D*IV* cortical cells, detected by immunogold localization of LC3 (arrow heads). Squares indicate the amplified area below. (B) Immunofluorescence to detect p62/SQSTM1 in cortical cells cultured during the indicated D*IV*. Nuclei were stained with DAPI. Notice that p62/SQSTM1 in neurons (expressing βIII-TUBULIN) accumulated at 26 D*IV*. Scale bars represent 5 μm. (C) Immunofluorescence to simultaneously detect LC3 and Lamin-A/C to observe intranuclear folds as a senescence marker, in cortical cells cultured during the indicated D*IV*. Scale bars represent 25 μm. (D) LC3 and p62/SQSTM1 also accumulate in cortical neurons (expressing βIII-TUBULIN or MAP2) form old rat brains. Scale bars represent 30 μm.

immunofluorescence (Figure 7B) and Western blot (Figure 8B), and we found that it was also accumulated in neurons at 26 D*IV*. To determine whether indeed senescent cells had more autophagosomes, we simultaneously detected LC3 and Lamin-A/C. As shown in Figure 7C, the same cells that had intranuclear folds of the nuclear envelop with Lamin-A/C at 26 D*IV* had LC3 accumulation (Figure 7C). Importantly, both LC3 and p62/SQSTM1 also accumulated in cortical neurons of old rat brains (Figure 7D). The accumulation of both autophagosomes and p62/SQSTM1 suggests dysfunctional lysosomes or impairment of the fusion of autophagosomes with lysosomes. We stained lysosomes with Lysotracker® and observed an accumulation of enlarged lysosomes in senescent cortical cells (Figure 8A), as it has been described in another model of neuronal senescence [21]. We confirmed altered lysosomal morphology by localizing the lysosomal protein LAMP1; we noticed that abundant p62/SQSTM1 puncta did not co-localize with LAMP1 at 26 D*IV* (Figure 8A), suggesting limited autolysosome maturation (*i.e.* reduced autophagosome-lysosome fusion), although further studies are needed to corroborate it.

p62/SQSTM1 accumulates when autophagy promotes the SASP through a compartmentalized structure coined TASCC (Tor-autophagy spatial coupling compartment),

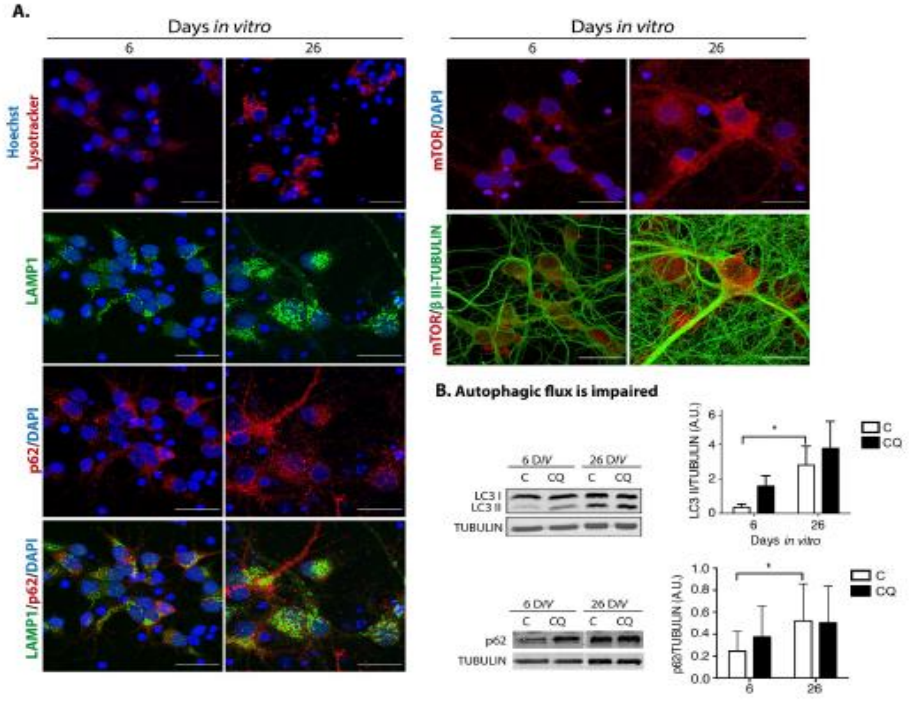

Figure 8. Dysfunctional autophagy contributes to neuronal senescence. (A) There was an accumulation of enlarged lysosomes and undigested p62/SQSTM1 in senescent neurons. Top row, lysosomes were detected with Lysotracker® and nuclei with Hoechst in primary culture of cortical cells incubated during the indicated D*IV*. Bottom rows, immunofluorescence to detect the indicated proteins in cortical cells cultured during 6 or 26 days. Nuclei were stained with DAPI. Notice that even though lysosomes and p62/SQSTM1 accumulated at 26 D*IV*, their intracellular distribution did not overlap. mTOR distribution did not change. Scale bars represent 25 μm. (B) The autophagic flux was impaired in senescent neurons. Western blot of total protein extracts from cortical cells cultured at 6 or 26 days, without (C) or with (CQ) 20 μM Chloroquine for 4 hr. Graphs represent the mean of densitometry analysis of four independent experiments. Bars represent SEM. Two-way RM ANOVA followed by Sidak´s multiple comparison test. *p<0.001.

which is where amino acids released by autolysosomes locally activate mTORC1, facilitating the synthesis of SASP proteins. The TASCC can be distinguished by the polarized co-localization of p62/SQSTM1, mTOR and LAMP2 [11]. Therefore, we analyzed whether during neuronal senescence these proteins were also distributed in a similar polarized intracellular localization (we observed LAMP1 instead of LAMP2). As can be seen in Figure 8A, neither the distribution of p62/SQSTM1 nor mTOR indicated a compartmentalized distribution. Even though lysosomes seemed to be mainly located on one side of the cells, it might reflect only the particular morphology of this type of cells, which have the cytoplasm mostly on one side of the cell. Therefore, we found no evidence of a TASCC during neuronal senescence, indicating that autophagy dysfunction, rather than function, accompanies neuronal senescence. To verify that the observed accumulation of autophagosomes was due to an impaired autophagic flux, instead of an enhanced activation of autophagy, cortical cells were incubated in the presence of Chloroquine, an agent that neutralizes lysosomes pH and impairs autophagosomes fusion with lysosomes. As shown in Figure 8B, the presence of Chloroquine did not increase the amount of LC3-II or p62/SQSTM1 accumulation at 26 D*IV*, indicating that the autophagic flux was already diminished in senescent neurons.

If a limited autophagic flux contributes to neuronal senescence, we would expect more senescent cells when autophagy is inhibited. Since basal autophagy is essential for survival, inhibition of autophagy by genetic means along the time of culture kills the neurons. Therefore, we inhibited autophagy only at distinct time windows (7 days long each) by adding Spautin-1, a molecule that indirectly induces BECN1 and PtdIns-3-kinase type 3/VPS34 (PI3KC3) degradation [31]. As shown in Figure 9B, we found that the number of cells with SA-β-gal activity increased when autophagy was inhibited during the second or third weeks of culture. When Spautin-1 was added at the fourth week of culture or later, it had no effect increasing the number of cells with SA-β-gal activity, suggesting that autophagy was already dysfunctional at this time. On the other hand, stimulating autophagy with trehalose, a disaccharide that mimics caloric restriction by preventing glucose uptake [32], reduced the number of cortical cells with SA-β-gal activity regardless of the time window of exposure, although a more noticeable protection was observed during the second and third weeks of culture. As a control to verify the function of Spautin-1 in neurons, we verified the reduction in the number of autophagosomes in cortical cells at 26 D*IV*, when we had previously observed abundant autophagosomes. We also tested that trehalose stimulates autophagy in neurons by detecting more autophagosomes in cortical cells at 6 D*IV*, which time we had observed neurons have a reduced amount of autophagosomes (Supplementary Figure 2S). To confirm that trehalose induction of autophagy indeed reduced the senescent phenotype and not just SA-β-gal activity, we repeated the experiment now immunodetecting Lamin-A/C to evaluate whether the intranuclear folds were reduced. As shown in Figure 9C, adding trehalose during one week windows statistical significantly reduced the degree of intranuclear Lamin-A/C folds. These results suggest that autophagy induction prevents senescence conversion and potentially reverts the senescent phenotype, although further experiments will be needed to address the latter.

DISCUSSION

Accumulating evidence shows the presence of senescent cells in brains from both physiologically aged subjects and with neurodegeneration [14]. In this work we have characterized an *in vitro* model useful to study the molecular basis for neuronal senescence transition and maintenance, as well as SASP components. We demonstrate that neurons, in spite of being post-mitotic cells, acquire multiple senescent features and notably they do so before glial cells. Every senescent marker we looked at in primary culture of senescent neurons was confirmed in old rat brains (25 months old), validating this *in vitro* neuronal senescence model. We demonstrated, to our knowledge for the first time, that senescent cortical cells develop a functional SASP, secreting components able to induced paracrine senescence in MEFs and glial proliferation. Since most of the senescent cells at 26 D*IV* are neurons, we suggest the existence of a neuronal SASP, although it is still possible that the few senescent astrocytes present in the culture secrete a very potent SASP. Nevertheless, a neuronal SASP is supported by other observations, such as the induction of expression of pro-inflammatory cytokines like TNF-α and CCL2 [33]. Interestingly, dopaminergic neurons with senescent phenotype due to lack of expression of SATB1, a DNA binding protein reduced in the vulnerable region of Parkinson's Disease patients, express several SASP components, including MCP-1 [34], the cytokine we found significantly secreted by senescent cortical cells. MCP-1 is also secreted by senescent human mesenchymal stem cells and induces paracrine senescence; according to our findings, MCP-1 expression is mediated by GATA4 [28], a transcription factor we found increased in senescent cortical neurons. Further experiments are necessary to demonstrate that indeed MCP-1 secreted by senescent cortical neurons is the molecule responsible for the induction of paracrine senescence in MEFs. To our surprise, we did no detect secretions of IL6, as it is a very common SASP component and has

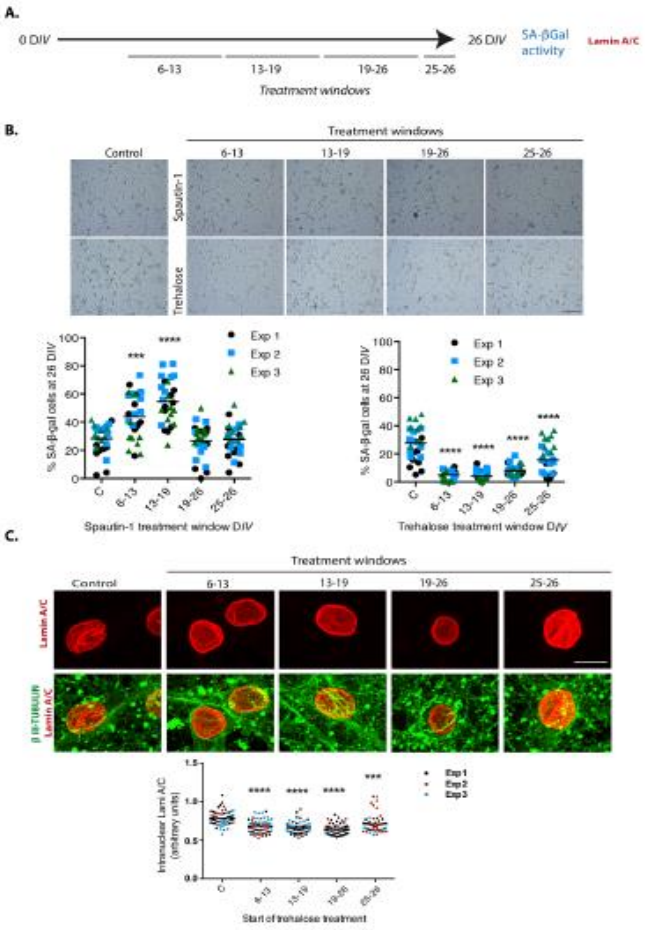

Figure 9. Autophagy modulation alters cortical cells senescence. (A) Experimental design. (B) Early inhibition of autophagy with Spautin1 increased the number of cells with SA-β-gal activity, while early induction of autophagy by adding trehalose reduced them. Spautin1 or trehalose were added during periods of several days, at the indicated time intervals in days of culture (D*IV*); after 26 D*IV* all cultures (including control with no treatment) were fixed to quantify the percentage of cells showing high SA-β-gal activity. Scale bars represent 500 μm. The bars in graphs represent the mean of each independent experiment, each done by triplicates. Three fields from each replica were scored (9 fields per experiment), each dot represent the percentage of SA-β-gal positive cells per field. Data were analyzed by two-way RM ANOVA, followed by Dunnett´s multiple comparison test. ***p<0.001 Spautin1 added during 6-13 D*IV* in comparison with control; **** p< 0.0001 Spautin1 added during 13-19 D*IV* in comparison with control, and Trehalose treatments in comparison with control. (C) Autophagy induction with trehalose reduced the abundance of intranuclear fold with Lamin-A/C. Trehalose were added during periods of several days, at the indicated time intervals in days of culture (D*IV*); after 26 D*IV* all cultures (including control with no treatment) were fixed to detect Lamin-A/C by immunofluorescence. Scale bar represents 5 μm. Representative images of three independent experiments are shown. At least 60 cells per treatment were quantified as described in Methods. Bars in the bottom graph represents mean. Data were analyzed by two-way RM ANOVA, followed by Dunnett´s multiple comparison test. ***p<0.001; **** p< 0.0001 with respect to control.

been found to be secreted in senescent neurons by others [22]. It is worth to note that the paracrine senescence signaling components seem to be conserved between rat and mouse, as the rat neuronal SASP was able to induce premature paracrine senescence in mouse fibroblasts (MEFs).

The finding that conditioned media from senescent cortical cells induced glial cell proliferation, suggests that persistent neuronal senescent cells could alter tissue organization. As opposed to replicative senescence, which is caused by critically short telomeres, premature senescence induced by oncogene activation initiates with hyper-proliferation, followed by a "transition phase" that signals to induce the senescent phenotype [35]. Further experiments are in progress to evaluate whether the increased proliferation of astrocytes we observed reflects a mitotic phase preceding senescence in response to the cortical SASP. Also, the finding that young neurons are resistant to undergo premature paracrine senescence in response to the SASP produced by senescent cortical cells deserves further investigation. It will be interesting to understand the molecular differences that render MEFs susceptible and prenatal cortical neurons resistant to paracrine senescence in response to the cortical SASP. Although we ought to mention that we observed in one out of six experiments an increase of young neurons with high SA-β–gal activity in response to conditioned media from senescent neurons, therefore, it is yet possible that senescent cortical cell secretes molecules able to induce neuronal paracrine senescence, but which are rather labile. We propose that persistent senescent cells in the brain would secrete molecules that induce chronic inflammation and propagate further paracrine senescence to nearby healthy cells within the brain, like astrocytes, microglia or endothelial cells, thereby spreading the senescent phenotype and thus contributing to brain aging and exacerbating neurodegeneration. In fact, chronic and low-grade inflammation (inflammaging) have been associated with neurodegeneration in aging [36, 37] and cellular senescence markers have been observed in brain tissues from Alzheimer's disease patients, such as $p16^{INK4A}$ expression, increased p38MAPK activity, and IL6 and TGFβ mRNA expression [38-41]. Actually, brain overexpression of IL6 in mice induces neurodegeneration [42]. Promising, two recent works demonstrate that eliminating senescent cells in the brain ameliorate Tau-dependent neuropathology in mice transgenic models. Bussian TJ, *et al.* did not find neurons with senescent features (looking for SA-β-gal activity and the mRNA expression of *p16*, *p19*, *p21*, *pai1* and *Il6* in an enriched population of cells expressing Cd56), and propose that senescent microglia and astrocytes induce Tau-containing neurofibrillary tangles (NFT) in neurons by an unknown mechanism [43]. Interestingly, Musi N *et al.* analyzed laser-captured microdissected cortical neurons from human brains with Alzheimer disease and compared their transcriptome signature with adjacent histopathologically normal neurons. NFT-containing neurons had a senescent gene expression profile. The same was observed in NFT-containing neurons in a Tau transgenic mouse line [44]. Therefore, it seems that all cell types in the brain are able to become senescent, but the timing of geroconversion could vary in different contexts. Since in both works senolytics ameliorated Tau-dependent neuropathology, to discover which cell type becomes senescent and how similar are senescent cells from different cell types, will be useful to design targeted therapies.

Considering that it has been widely documented that during aging autophagy becomes dysfunctional [45], that most of the interventions that improve health span and/or lifespan stimulate autophagy [46, 47], and our finding that Spautin-1 treatment increased the number of senescent cortical cells, we propose that dysfunctional autophagy during aging also contributes to cellular senescence in the brain, including neurons, which in turn contributes to synaptic dysfunction. It is fundamental, therefore, to understand the mechanisms of autophagy dysfunction with ageing in the brain. Perhaps the tubular morphology of lysosomes we observed in senescent cortical neurons interferes with lysosomes fusion with autophagosomes. Therefore, treatments that promote autolysosome maturation or prevent lysosomal dysfunction could solve or prevent the onset of neuronal senescence. Interestingly, our observation that trehalose reduced the number of senescent cortical cells suggests that the neuronal senescent phenotype is reversible. Supporting this notion, addition of resveratrol, an autophagy-inducer compound, also decreases senescent hallmarks of long-term neuroglial cocultures [22]. Further experiments are necessary to test the possible reversion of the neuronal senescent phenotype.

Having a molecular understanding of neuronal senescence, new targets for pharmacological intervention could be proposed, with potential impact to prevent or reduce both physiological brain aging and neurodegeneration.

MATERIALS AND METHODS

Animals

Wistar rats of the indicated age in each experiment were obtained from the animal house of the Institute of Cell Physiology at the National University of Mexico (UNAM) and were housed at 22 ^{0}C in 12h light/12h

dark cycle. All procedures were approved by the Internal Committee of Care and Use of Laboratory Animals of the Institute (IFC-SCO51-18). Rats had *ad libitum* access to water and food.

Cell Culture

Cortical primary cultures

Cortical primary cultures were prepared as described before [48], from Wistar rat embryos of 17 days of gestation. Cerebral cortices were isolated and dissociated by 1:1400 Trypsin-EDTA (15400054, INVITROGEN/GIBCO, Grand Island, NY, USA) digestion and trituration with a Pasteur pipette. Cells were suspended in Neurobasal medium (21103049, INVITROGEN/GIBCO, Grand Island, NY, USA) supplemented with 2% B27 (17504044, INVITROGEN/GIBCO, Grand Island, NY, USA), 200 mM GlutaMAX™ Supplement (35050061, GIBCO Life Technologies, Grand Island, NY, USA) and 0.02 mg/ml Gentamicin (15710064, INVITROGEN/GIBCO, Grand Island, NY, USA). Cells were plated at a density of 1.05 x $10^5/cm^2$ in 12-well plates precoated with Poly-L-Lysine (P1524, SIGMA-ALDRICH St. Louis, MO, USA) (0.01 mg/ml). Cells were cultured up to 40 days *in vitro* (40 DIV) at 37°C in a humidified, 5% CO_2 atmosphere. Half the medium was changed every 6 days.

Cell viability

Cell viability was estimated by staining with LIVE/DEAD viability/cytotoxicity kit (INVITROGEN/GIBCO, Grand Island, NY, USA). Alive cells were stained with Calcein, while dead cells were stained with Ethidium homodimer-1, following manufacturer´s instructions. For every experiment, only cells with healthy nuclear morphology (non apoptotic) were quantified.

MEFs culture

Mouse embryonic fibroblasts were isolated from CD1 mouse embryos at E13.5 following the standard protocol [49]. MEFs were seeded at a density of $2.6x10^3$ cells/cm^2 with Dulbecco´s Modified Eagle Medium + GlutaMAX™, 10% FBS and Penicillin/Streptomycin 100 U/ml. Each experiment was performed with MEFs at cell passage 4 to avoid replicative senescence. For conditioned media experiments, one day after seeding, cells were cultured with 25% OptiMEM supplemented with GlutaMAX and 75% of conditioned media. Media and supplements were from GIBCO® Life Technologies™, Grand Island, NY, USA.

SA–β-galactosidase staining

The β-galactosidase activity was analyzed following the protocols described previously [50, 51]. Cells were fixed with 2% formaldehyde + 0.2% glutaraldehyde for 5 min, washed with PBS and stained with the staining solution containing: 20 mg/ml of X-gal (IB02260, IBI SCIENTIFIC, Peosta, IA, USA) in dimethylformamide, 0.2 M citric acid/sodium phosphate buffer pH=6, 100 mM potassium ferrocyanide, 5 M sodium chloride and 1 M magnesium chloride. Cells were incubated for 16 h at 37 °C. For colorimetric analysis, samples were observed in an inverted Nikon ECLIPSE Ti-U microscope, the number of positive cells was counted of at least 500 cells. For SA–β-galactosidase staining and immunofluorescence in the same samples, cells were stained for SA-β-gal as described above and then immunostained. Confocal detection of X-gal was performed as previously described [52].

Lipofuscin accumulation

Autofluorescence Detection

Lipofuscin auto-fluorescence was evidenced by excitation at 450-490 nm of unstained cortical cells using an inverted Nikon ECLIPSE Ti-U microscope.

Sudan Black B (SBB) staining

SBB staining was performed as described [24]. 0.7 g of SBB (199664, SIGMA-ALDRICH, St. Louis, MO, USA) were dissolved in 70% ethanol, covered with Parafilm® and thoroughly stirred overnight at room temperature. Afterwards the solution was filtered (paper filter Whatman™ 1001-110). Cells seeded on coverslips were fixed in 4% (wt/vol) formaldehyde/PBS for 30 min at room temperature and then washed three times at room temperature with PBS. Coverslips with fixed cells were incubated for 2 min in 70% ethanol. A drop of freshly prepared SBB was dropped on a clean slide. The coverslip with the cells was held facing down on the drop of SBB on the slide and was incubated for 10 seconds. The coverslip was carefully lifted and the SBB on the edges of the coverslip was wiped off manually from the back and along the edges of the coverslip with the help of an absorbent paper. The cells were then embedded into 50% ethanol for 1 min, transferred and washed with distilled water. The staining was observed under an inverted Nikon ECLIPSE Ti-U microscope and SBB staining was considered positive when cytoplasmic aggregates of blue-black granules were evident inside the cells. Three independent experiments, each done by quintupled replicas, were analyzed.

Immunofluorescence

Primary culture

Cells were fixed with 4% paraformaldehyde for 30 min, permeabilized with PBS / 0.5% Triton for 5 min, blocked with PBS/5% BSA and incubated at 4 °C with primary antibody overnight. AlexaFluor-conjugated

secondary antibodies were diluted in PBS/2%BSA (1:500, LIFE TECHNOLOGIES, Oregon, USA) and incubated for 1 h at room temperature. Nuclei were stained for 2 min with DAPI (1 μg/ml). Only cells with healthy nuclear morphology (non-apoptotic) were quantified.

Brain section

Wistar rat male brains 4 or 25 months old were isolated following IACUC guidelines. Rats were perfused transcardially with PBS, then with 4% paraformaldehyde. Brains were drop-fixed in 4% paraformaldehyde for 24h; for cryoprotection brains were immersed in PBS/30% sucrose for 24 h. Brain coronal sections (50 μm) from frontal cortex were mounted serially. The sections were permeabilized with PBS/ 0.3% Triton for 15 min, blocked with PBS/5% BSA for 1 hour at room temperature and incubated with primary antibody at 4 °C overnight in PBS/1% BSA. Next, sections were incubated with AlexaFluor-conjugated secondary antibodies (1:350, LIFE TECHNOLOGIES, Oregon, USA) in PBS / 2% BSA 1 h at room temperature; nuclei were stained with DAPI (1 μg/ml). To avoid lipofuscin autofluorescence slices were incubated with Sudan Black B.

The following primary antibodies were used: mouse anti class III β-TUBULIN (1:1000, ABCAM 14545, Cambridge, MA, USA), rabbit anti class III β-TUBULIN (1:1000, ABCAM 18207, Cambridge, MA, USA), rabbit anti- class III β-TUBULIN (1:500, BIOLEGEND, MRB435P-100, San Diego, CA, USA), rabbit anti-GFAP (1:1000, DAKO Z0334, Santa Clara, CA, USA), rat anti-GFAP (1:1000, INVITROGEN 13-0300, Camarillo, CA, USA), rabbit anti-p21 (1:25, ABCAM 7960 or 1:100 ABCAM 109199, Cambridge, MA, USA), mouse anti-γH2AX (1:500, ABCAM 26350, Cambridge, MA, USA), rabbit anti-LC3 (1:500, MBL PD014, Nagoya, Japan), mouse anti-p62 (1:300, ABCAM 56416, Cambridge, MA, USA), rabbit anti-LAMP1 (1:1000, SIGMA-ALDRICH L1418, St. Louis, MO, USA), rabbit anti-mTOR (1:200, CELL SIGNALING 2983, Beverly, MA, USA), rabbit anti-GATA4 (1:500, ABCAM 84593, Cambridge, MA, USA).

Images were acquired using a NIKON ECLIPSE Ti-U microscope or a confocal microscope Zeiss LSM 800. Images were processed using NIS Elements, Basic Research (NIKON INSTRUMENTS Inc ®, NY, USA) software, Version 3.13 or Fiji software.

Immunoelectron microscopy

Cortical cells were fixed with 3% glutaraldehyde. Following fixation, dehydration was performed in an ethanol gradient: 30-40-50-60-70-80-90-100 % ethanol at 4°C. Then, the cells were embedded in a LR White resin and polymerization was carried out at 50 °C. Ultrathin sections of 70-80 nm were cut from the polymer using an Ultracut-Recheirt-Jung and placed on nickel grids for immunogold assay.

The thin sections were washed twice for 2 min with deionized water and two times with PBS with 0.005 % Tween20. Sections were then incubated for 30 min with the blocking solution (50 mM glycine, 0.005 % Tween20, 0.01 % Triton X-100 and 0.1 % BSA in PBS) [53]. After blocking, sections were incubated with the primary antibody: rabbit anti-LC3 (1:500, MBL PD014, Nagoya, Japan). After rinsing three times in PBS with 0.005 % Tween20, the sections were incubated overnight at 4 °C with the secondary antibody: donkey anti-rabbit 25-nm gold conjugate (Electron Microscopy Science Aurion #25708). Samples were washed three times with PBS, 0.005 % Tween20 and post-fixed in 2 % glutaraldehyde in PBS for 10 min. The sections were then rinsed with distilled water twice for 5 min and contrasted with 2 % uranyl acetate, rinsed with water, dried and observed under a JEOL JEM 1200 EXII electron microscope.

Immunoblotting analysis

Cells grown in the presence or absence of 20 □M Chloroquine (C-6628 SIGMA-ALDRICH, St. Louis, MO, USA) for 4 hrs were lysed in an extraction buffer consisting of 25 mM Tris, 50 mM NaCl, 2% Igepal, 0.2% SDS and 2 mg/ml protease inhibitor 18 (Complete, Roche Molecular Diagnostics, pH 7.4). Thirty micrograms of total protein were separated by SDS-PAGE and electroblotted onto polyvinylidene fluoride (PVDF-FL) membranes (Millipore). Membranes were incubated overnight with the primary antibody at 4 °C, rabbit anti-LC3 (1:1000, MBL PD014, Nagoya, Japan), rabbit anti-p62 (1:500, CELL SIGNALING 5114S, Beverly, MA, USA), mouse anti-TUBULIN (1:10000, CELL SIGNALING 3873, Beverly, MA, USA). Following three washes with TTBS secondary antibody IRDye® 680RD goat anti-rabbit (925-68071, LI-COR) or IRDye® 800CW goat anti-mouse (925-32210, LI-COR) was applied at 1:10,000 dilution in TTBS. Membranes were scanned and analyzed using an Odyssey® IR scanner and Odyssey® Image Studio software 5.2.5.

Gene expression analysis

Total RNA was isolated using TRIzol™ reagent (Life Technologies), and cDNA was synthesized from 1 μg of RNA using the High Capacity cDNA Reverse Transcription Kit (Thermo Fisher Scientific #4368814).

The quantitative PCR (qPCR) reaction was performed with the SYBR Green mix (Kapa SYBR® Fast Universal #KK4602) in the Rotor-Gene Qthermocycler (Qiagene, Germantown, MD, USA). All reactions were performed in quadruplicate, and the expression was normalized using the glyceraldehyde-3-phosphate dehydrogenase (*Gapdh*) mRNA. The sequences of the primers used are as follows:

Cdkn1a F 5′-CCGAGAACGGTGGAACTTTGAC-3′;
Cdkn1a R 5′-GAACACGCTCCCAGACGTAGTTG-3′
Ccl2 (*Mcp-1*) F, 5′- ATGCAGTTAATGCCCCACTC;
Ccl2 (*Mcp-1*) R, 5′-TTCCTTATTGGGGTCAGCAC-3′
Gapdh F, 5′-CTCATGACCACAGTCCATGC-3′
Gapdh R, 5′-TTCAGCTCTGGGATGACCTT-3′.

Neutral Comet assay

Cells were resuspended in cold PBS at 10^3 cells/µL density. This suspension was mixed at a 1:5 ratio with 0.75% low-melting point agarose (BIO RAD Certified™ Low Melt Agarose #1613111, Hercules, California, USA) at 37°C. About 50 to 100 µL of the mix were placed on microscope slides pre-coated with 1% normal-melting point agarose (BIO RAD Certified™ PCR Agarose #1613103, Hercules, California, USA), spread with coverslips and incubated at 4° C for 2 min and 10 min more at room temperature. The coverslips were removed and slides were covered with pre-chilled lysis solution (0.03 M EDTA, 1% SDS) for 60 min at 4°C. After that, slides were washed and covered with unwinding/electrophoresis buffer (Tris 60 mM, Acetic acid 90 mM, EDTA 2.5 mM, pH 9.0) for 60 min. Electrophoresis was performed at 25 V for 20 min. Immediately, slides were rinsed and incubated for 10 min in neutralization buffer (Tris-HCl 500 mM, pH 7.5) 3 times. Finally, DNA was stained with SYBR green (SYBR™ green I Nucleic Acid Gel Stain, INVITROGEN™, Eugene, Oregon, USA) 1:10000 in PBS. For each sample 50 comet images were measured, using a Nikon ECLIPSE Ti-U fluorescence microscope. The length and area of the broken DNA were measured with NIS Elements Basic Research software (NIKON INSTRUMENTS Inc ®, NY, USA)-

SASP analysis of cortical cells

Conditioned medium was collected from neuronal cultures at 6, 26 and 40 days *in vitro* (DIV) and was frozen at -20 °C until use. Concentrations (pg/mL) of G-CSF, GM-CSF, IFN gamma, IL-1α, IL-1β, IL-10, IL-12p70, IL-13, IL-17A, IL-2, IL-4, IL-5, IL-6, TNF alpha, Eotaxin, Gro α, IP-10, MCP-1, MCP-3, MIP-1α, MIP-2 and RANTES in media conditioned by cortical cells were measured by ProcartaPlex® Multiplex Immunoassay (BIO RAD # 171K1002M). The conditioned medium was previously concentrated using centrifugal filter units Amicon Ultracel-3 kDa (Millipore # UFC800324) and a total of 50 µL of concentrated conditioned medium were examined following manufacturer's instructions. Data were obtained in a Luminex Instrument and the analytes concentration was measured calibrating with a standard curve for each cytokine provided by the manufacturer.

Cyto-ID autophagosomes detection and Lysotracker staining

The Cyto-ID (ENZO LIFE SCIENCES ENZ-51031-K200, Farmingdale, NY, USA) is an 488 nm-excitable green fluorescent reagent that specifically accumulates in autophagic vesicles. Cells were incubated in Cyto-ID (1 µl Cyto-ID/1ml cell culture medium) for 30 minutes at 37 °C, 5 % CO_2 and washed prior to analysis. Lysotracker dye (DND-99 LIFE TECHNOLOGIES, Oregon, USA) was incubated for 20 min at 37°C. Cells were analyzed by Fluorescence Nikon ECLIPSE Ti-U microscope.

Cortical cells-derived conditioned medium collection and treatment

Conditioned medium was prepared by collecting half the medium from neuronal cultures at 6, 26 and 40 days *in vitro* (DIV) and freezing it at -20°C until use. Conditioned media were diluted 3:1 with fresh medium and added to cells at 1 D*IV* in 12-well plates ($4x10^5$ cortical neurons cells/well; $1x10^4$ MEFs/well). For MEFs, to avoid adding unknown factors from serum, conditioned media were diluted with OptiMEM (GIBCO Life Technologies, Grand Island, NY, USA). Cells were incubated further for 6 days at 37°C and 5 % CO_2. At the end of incubation, the senescent markers were analyzed.

Quantification

The quantifications of cells with a particular phenotype were done using NIS Elements, Basic Research (NIKON INSTRUMENTS Inc ®, NY, USA) Version 3.13 software or Fiji software. The size of the samples analyzed is indicated in every figure legend. We counted at least 100 cells in each graph shown. To quantify data that corresponds to nuclear Lamin A/C invagination (Figure 4), we exploited the observation that internal Lamin A/C invaginations increase the signal intensity of intranuclear Lamin A/C that would otherwise be in the nuclear envelope as follows: Z-Stacked maximum intensity confocal images were utilized. Border ROIs were manually selected with the brush selection tool of FIJI, the brush size corresponded to the pixel number length closest to 500 nm, roughly

the nuclear envelope size (i.e. 101.41 µm x 101.41 µm 1024 pixels x 1024 pixels images required a brush of pixel size 5 and 1437 pixels x 1437 pixels images of the same metric size required a brush of pixel size 7). Border ROIs were selected manually including the most distal from the center of the nucleus signal of DAPI stained nuclei forming ring like ROIs. Central ROIs were selected to be exactly the internal part of the ring excluded from the border ROIs by using the clear outside function on the edit menu followed clicking on the internal part with the wand (tracing) tool of FIJI. The mean fluorescence intensity of these ROIs in Lamin A/C images was measured and the signal of the center was divided by the signal of the border so as to normalize for different Lamin A/C expression. Higher values correspond to more invagination.

Statistical Analysis.
All data were analyzed and graphed with Prism 6 (GraphPad Software Inc. La Jolla, CA, USA). Specific tests were performed according to each experimental design, and are indicated in each figure.

Abbreviations

BECN1: Beclin 1; CQ: Cloroquine; DAPI: 4',6-Diamidine-2'-phenylindole dihydrochloride; DDR: DNA Damage Response; D*IV*: Days *in vitro;* FM: Fresh medium; GFAP: Glial fibrillary acidic protein; IL6: Interleukin-6; LAMP: Lysosomal-associated membrane protein; MEFs: Mouse embryonic fibroblasts; mH2A: Histone macroH2A; mTOR: mechanistic target of rapamycin; N2A: Neuro 2A; PI3KC3: Phosphatidylinositol 3-kinase class 3; p38MAPK: p38 mitogen-activated protein kinase; SA-β-gal: Senescence-Associated β-galactosidase; SAHF: Senescence-associated heterochromatin foci; SAMP8: senescence-accelerated mice prone; SASP: Senescence-associated secretory phenotype; SBB: Sudan Black B; Spautin-1: Specific and potent autophagy inhibitor 1; SQSTM1: Sequestosome 1; TASCC: TOR-autophagy spatial coupling compartment; TGFβ: Transforming growth factor-beta; Tre: Trehalose; 53BP1: p53-binding protein 1; MCP-1: monocyte chemotactic protein 1; official name C-C motif chemokine 2; GATA4: GATA binding protein 4.

AUTHOR CONTRIBUTIONS

DMB carried out most of the experiments and participated in project design. EGS characterized neuronal senescence in the cortex of old rat brains; APA studied the paracrine premature senescence on MEFs; LAM and MK analyzed SASP components; GMH analyzed the double strand DNA brakes in senescent neurons; CGO performed lysotracker staining and contributed to autophagy analysis; LM contributed to experimental design and data analysis. SCO conceived the study and wrote the manuscript. All authors edited and approved the final manuscript.

ACKNOWLEDGMENTS

We are thankful to Dr. Beatriz Aguilar for her technical assistance. We acknowledge the support given by M.Sc. Ana Maria Escalante and Francisco Pérez at the IT Unit and Claudia Rivero at the Animal Facility. We are thankful to Dr. Ruth Rincón for confocal analysis assistance, to M.Sc. Rodolfo Paredes for electron microscopy imaging and to Dr. Abraham Rosas for both confocal analysis and electron microscopy imaging, all at the Imagenology Unit. Data in this work are part of the doctoral dissertation in the "Programa de Doctorado en Ciencias Bioquímicas" at the Universidad Nacional Autónoma de México (UNAM) of DMB and GMH, of the doctoral dissertation of EGS in the "Programa de Doctorado en Ciencias Biomédicas" at UNAM, and of the master dissertation in the "Programa de Maestría en Ciencias Bioquímicas" at UNAM of APA. All are recipients of fellowships from CONACyT.

CONFLICTS OF INTEREST

The authors declare no conflict of interest.

FUNDING

This project was supported by a grant from the Secretaría de Educación, Ciencia, Tecnología e Innovación de la Ciudad de México SECITI/042/2018 (INGER-DI-CRECITES-008-2018) "Red Colaborativa de Investigación Traslacional para el Envejecimiento Saludable de la Ciudad de México (RECITES)"; by CONACyT FC-921 and CB2013-220515; and by UNAM-PAPIIT IN206015-IN206518 to SCO. DMB received CONACyT doctoral fellowship 588372; GMH received CONACyT doctoral fellowship 417724; EGS received CONACyT doctoral fellowship 586932 and APA received CONACyT master fellowship 485243.

REFERENCES

1. Soto-Gamez A, Demaria M. Therapeutic interventions for aging: the case of cellular senescence. Drug Discov Today. 2017; 22:786–95. https://doi.org/10.1016/j.drudis.2017.01.004 PMID:28111332

2. Muñoz-Espín D, Serrano M. Cellular senescence: from physiology to pathology. Nat Rev Mol Cell Biol. 2014; 15:482–96. https://doi.org/10.1038/nrm3823 PMID:24954210

3. Matjusaitis M, Chin G, Sarnoski EA, Stolzing A. Biomarkers to identify and isolate senescent cells. Ageing Res Rev. 2016; 29:1–12. https://doi.org/10.1016/j.arr.2016.05.003 PMID:27212009

4. Lenain C, Gusyatiner O, Douma S, van den Broek B, Peeper DS. Autophagy-mediated degradation of nuclear envelope proteins during oncogene-induced senescence. Carcinogenesis. 2015; 36:1263–74. https://doi.org/10.1093/carcin/bgv124 PMID:26354777

5. Acosta JC, Banito A, Wuestefeld T, Georgilis A, Janich P, Morton JP, Athineos D, Kang TW, Lasitschka F, Andrulis M, Pascual G, Morris KJ, Khan S, et al. A complex secretory program orchestrated by the inflammasome controls paracrine senescence. Nat Cell Biol. 2013; 15:978–90. https://doi.org/10.1038/ncb2784 PMID:23770676

6. Coppé JP, Desprez PY, Krtolica A, Campisi J. The senescence-associated secretory phenotype: the dark side of tumor suppression. Annu Rev Pathol. 2010; 5:99–118. https://doi.org/10.1146/annurev-pathol-121808-102144 PMID:20078217

7. Sieben CJ, Sturmlechner I, van de Sluis B, van Deursen JM. Two-Step Senescence-Focused Cancer Therapies. Trends Cell Biol. 2018; 28:723–37. https://doi.org/10.1016/j.tcb.2018.04.006 PMID:29776716

8. Kang HT, Lee KB, Kim SY, Choi HR, Park SC. Autophagy impairment induces premature senescence in primary human fibroblasts. PLoS One. 2011; 6:e23367. https://doi.org/10.1371/journal.pone.0023367 PMID:21858089

9. Young AR, Narita M, Ferreira M, Kirschner K, Sadaie M, Darot JF, Tavaré S, Arakawa S, Shimizu S, Watt FM, Narita M. Autophagy mediates the mitotic senescence transition. Genes Dev. 2009; 23:798–803. https://doi.org/10.1101/gad.519709 PMID:19279323

10. Kang C, Xu Q, Martin TD, Li MZ, Demaria M, Aron L, Lu T, Yankner BA, Campisi J, Elledge SJ. The DNA damage response induces inflammation and senescence by inhibiting autophagy of GATA4. Science. 2015; 349:aaa5612. https://doi.org/10.1126/science.aaa5612 PMID:26404840

11. Narita M, Young AR, Arakawa S, Samarajiwa SA, Nakashima T, Yoshida S, Hong S, Berry LS, Reichelt S, Ferreira M, Tavaré S, Inoki K, Shimizu S, Narita M. Spatial coupling of mTOR and autophagy augments secretory phenotypes. Science. 2011; 332:966–70. https://doi.org/10.1126/science.1205407 PMID:21512002

12. Kang C, Elledge SJ. How autophagy both activates and inhibits cellular senescence. Autophagy. 2016; 12:898–99. https://doi.org/10.1080/15548627.2015.1121361 PMID:27129029

13. Chinta SJ, Woods G, Rane A, Demaria M, Campisi J, Andersen JK. Cellular senescence and the aging brain. Exp Gerontol. 2015; 68:3–7. https://doi.org/10.1016/j.exger.2014.09.018 PMID:25281806

14. Walton CC, Andersen JK. Unknown fates of (brain) oxidation or UFO: close encounters with neuronal senescence. Free Radic Biol Med. 2019; 134:695–701. https://doi.org/10.1016/j.freeradbiomed.2019.01.012 PMID:30639615

15. Jurk D, Wang C, Miwa S, Maddick M, Korolchuk V, Tsolou A, Gonos ES, Thrasivoulou C, Saffrey MJ, Cameron K, von Zglinicki T. Postmitotic neurons develop a p21-dependent senescence-like phenotype driven by a DNA damage response. Aging Cell. 2012; 11:996–1004. https://doi.org/10.1111/j.1474-9726.2012.00870.x PMID:22882466

16. Chernova T, Nicotera P, Smith AG. Heme deficiency is associated with senescence and causes suppression of N-methyl-D-aspartate receptor subunits expression in primary cortical neurons. Mol Pharmacol. 2006; 69:697–705. https://doi.org/10.1124/mol.105.016675 PMID:16306232

17. Bhanu MU, Mandraju RK, Bhaskar C, Kondapi AK. Cultured cerebellar granule neurons as an in vitro aging model: topoisomerase IIβ as an additional biomarker in DNA repair and aging. Toxicol In Vitro. 2010; 24:1935–45. https://doi.org/10.1016/j.tiv.2010.08.003 PMID:20708677

18. Dong W, Cheng S, Huang F, Fan W, Chen Y, Shi H, He H. Mitochondrial dysfunction in long-term neuronal cultures mimics changes with aging. Med Sci Monit. 2011; 17:BR91–96. https://doi.org/10.12659/MSM.881706 PMID:21455101

19. Geng YQ, Guan JT, Xu XH, Fu YC. Senescence-associated beta-galactosidase activity expression in aging hippocampal neurons. Biochem Biophys Res Commun. 2010; 396:866–69. https://doi.org/10.1016/j.bbrc.2010.05.011 PMID:20457127

20. Xu T, Sun L, Shen X, Chen Y, Yin Y, Zhang J, Huang D, Li W, Li W. NADPH oxidase 2-mediated NLRP1 inflammasome activation involves in neuronal senescence in hippocampal neurons in vitro. Int Immunopharmacol. 2019; 69:60–70. https://doi.org/10.1016/j.intimp.2019.01.025 PMID:30677569

21. Piechota M, Sunderland P, Wysocka A, Nalberczak M, Sliwinska MA, Radwanska K, Sikora E. Is senescence-associated β-galactosidase a marker of neuronal senescence? Oncotarget. 2016; 7:81099–109. https://doi.org/10.18632/oncotarget.12752 PMID:27768595

22. Bigagli E, Luceri C, Scartabelli T, Dolara P, Casamenti F, Pellegrini-Giampietro DE, Giovannelli L. Long-term Neuroglial Cocultures as a Brain Aging Model: Hallmarks of Senescence, MicroRNA Expression Profiles, and Comparison With In Vivo Models. J Gerontol A Biol Sci Med Sci. 2016; 71:50–60. https://doi.org/10.1093/gerona/glu231 PMID:25568096

23. Jin HJ, Lee HJ, Heo J, Lim J, Kim M, Kim MK, Nam HY, Hong GH, Cho YS, Choi SJ, Kim IG, Shin DM, Kim SW. Senescence-Associated MCP-1 Secretion Is Dependent on a Decline in BMI1 in Human Mesenchymal Stromal Cells. Antioxid Redox Signal. 2016; 24:471–85. https://doi.org/10.1089/ars.2015.6359 PMID:26573462

24. Georgakopoulou EA, Tsimaratou K, Evangelou K, Fernandez-Marcos PJ, Zoumpourlis V, Trougakos IP, Kletsas D, Bartek J, Serrano M, Gorgoulis VG. Specific lipofuscin staining as a novel biomarker to detect replicative and stress-induced senescence. A method applicable in cryo-preserved and archival tissues. Aging (Albany NY). 2013; 5:37–50. https://doi.org/10.18632/aging.100527 PMID:23449538

25. García-Aguirre I, Alamillo-Iniesta A, Rodríguez-Pérez R, Vélez-Aguilera G, Amaro-Encarnación E, Jiménez-Gutiérrez E, Vásquez-Limeta A, Samuel Laredo-Cisneros M, Morales-Lázaro SL, Tiburcio-Félix R, Ortega A, Magaña JJ, Winder SJ, Cisneros B. Enhanced nuclear protein export in premature aging and rescue of the progeria phenotype by modulation of CRM1 activity. Aging Cell. 2019:e13002. [Epub ahead of print] https://doi.org/10.1111/acel.13002 PMID:31305018

26. Freund A, Laberge RM, Demaria M, Campisi J. Lamin B1 loss is a senescence-associated biomarker. Mol Biol Cell. 2012; 23:2066–75. https://doi.org/10.1091/mbc.e11-10-0884 PMID:22496421

27. Takamori Y, Tamura Y, Kataoka Y, Cui Y, Seo S, Kanazawa T, Kurokawa K, Yamada H. Differential expression of nuclear lamin, the major component of nuclear lamina, during neurogenesis in two germinal regions of adult rat brain. Eur J Neurosci. 2007; 25:1653–62. https://doi.org/10.1111/j.1460-9568.2007.05450.x PMID:17432957

28. Lee JY, Yu KR, Lee BC, Kang I, Kim JJ, Jung EJ, Kim HS, Seo Y, Choi SW, Kang KS. GATA4-dependent regulation of the secretory phenotype via MCP-1 underlies lamin A-mediated human mesenchymal stem cell aging. Exp Mol Med. 2018; 50:63. https://doi.org/10.1038/s12276-018-0092-3 PMID:29760459

29. Rubinsztein DC, Mariño G, Kroemer G. Autophagy and aging. Cell. 2011; 146:682–95. https://doi.org/10.1016/j.cell.2011.07.030 PMID:21884931

30. Yang F, Chu X, Yin M, Liu X, Yuan H, Niu Y, Fu L. mTOR and autophagy in normal brain aging and caloric restriction ameliorating age-related cognition deficits. Behav Brain Res. 2014; 264:82–90. https://doi.org/10.1016/j.bbr.2014.02.005 PMID:24525424

31. Liu J, Xia H, Kim M, Xu L, Li Y, Zhang L, Cai Y, Norberg HV, Zhang T, Furuya T, Jin M, Zhu Z, Wang H, et al. Beclin1 controls the levels of p53 by regulating the deubiquitination activity of USP10 and USP13. Cell. 2011; 147:223–34. https://doi.org/10.1016/j.cell.2011.08.037 PMID:21962518

32. Mayer AL, Higgins CB, Heitmeier MR, Kraft TE, Qian X, Crowley JR, Hyrc KL, Beatty WL, Yarasheski KE, Hruz PW, DeBosch BJ. SLC2A8 (GLUT8) is a mammalian trehalose transporter required for trehalose-induced autophagy. Sci Rep. 2016; 6:38586. https://doi.org/10.1038/srep38586 PMID:27922102

33. Song J, Lee B, Kang S, Oh Y, Kim E, Kim CH, Song HT, Lee JE. Agmatine Ameliorates High Glucose-Induced Neuronal Cell Senescence by Regulating the p21 and p53 Signaling. Exp Neurobiol. 2016; 25:24–32. https://doi.org/10.5607/en.2016.25.1.24 PMID:26924930

34. Riessland M, Kolisnyk B, Kim TW, Cheng J, Ni J, Pearson JA, Park EJ, Dam K, Acehan D, Ramos-Espiritu LS, Wang W, Zhang J, Shim J, et al. Loss of SATB1 Induces a p21 Dependent Cellular Senescence Phenotype in Dopaminergic Neurons. bioRxiv. 2018; 452243. 10.1101/452243

35. Narita M, Young AR, Narita M. Autophagy facilitates oncogene-induced senescence. Autophagy. 2009;

5:1046–47. https://doi.org/10.4161/auto.5.7.9444 PMID:19652542

36. Golde TE, Miller VM. Proteinopathy-induced neuronal senescence: a hypothesis for brain failure in Alzheimer's and other neurodegenerative diseases. Alzheimers Res Ther. 2009; 1:5. https://doi.org/10.1186/alzrt5 PMID:19822029

37. Franceschi C, Campisi J. Chronic inflammation (inflammaging) and its potential contribution to age-associated diseases. J Gerontol A Biol Sci Med Sci. 2014 (Suppl 1); 69:S4–9. https://doi.org/10.1093/gerona/glu057 PMID:24833586

38. McShea A, Harris PL, Webster KR, Wahl AF, Smith MA. Abnormal expression of the cell cycle regulators P16 and CDK4 in Alzheimer's disease. Am J Pathol. 1997; 150:1933–39. PMID:9176387

39. Lüth HJ, Holzer M, Gertz HJ, Arendt T. Aberrant expression of nNOS in pyramidal neurons in Alzheimer's disease is highly co-localized with p21ras and p16INK4a. Brain Res. 2000; 852:45–55. https://doi.org/10.1016/S0006-8993(99)02178-2 PMID:10661494

40. Luterman JD, Haroutunian V, Yemul S, Ho L, Purohit D, Aisen PS, Mohs R, Pasinetti GM. Cytokine gene expression as a function of the clinical progression of Alzheimer disease dementia. Arch Neurol. 2000; 57:1153–60. https://doi.org/10.1001/archneur.57.8.1153 PMID:10927795

41. Sun A, Liu M, Nguyen XV, Bing G. P38 MAP kinase is activated at early stages in Alzheimer's disease brain. Exp Neurol. 2003; 183:394–405. https://doi.org/10.1016/S0014-4886(03)00180-8 PMID:14552880

42. Campbell IL, Abraham CR, Masliah E, Kemper P, Inglis JD, Oldstone MB, Mucke L. Neurologic disease induced in transgenic mice by cerebral overexpression of interleukin 6. Proc Natl Acad Sci USA. 1993; 90:10061–65. https://doi.org/10.1073/pnas.90.21.10061 PMID:7694279

43. Bussian TJ, Aziz A, Meyer CF, Swenson BL, van Deursen JM, Baker DJ. Clearance of senescent glial cells prevents tau-dependent pathology and cognitive decline. Nature. 2018; 562:578–82. https://doi.org/10.1038/s41586-018-0543-y PMID:30232451

44. Musi N, Valentine JM, Sickora KR, Baeuerle E, Thompson CS, Shen Q, Orr ME. Tau protein aggregation is associated with cellular senescence in the brain. Aging Cell. 2018; 17:e12840. https://doi.org/10.1111/acel.12840 PMID:30126037

45. Martinez-Lopez N, Athonvarangkul D, Singh R. Autophagy and aging. Adv Exp Med Biol. 2015; 847:73–87. https://doi.org/10.1007/978-1-4939-2404-2_3 PMID:25916586

46. Gelino S, Hansen M. Autophagy - An Emerging Anti-Aging Mechanism. J Clin Exp Pathol. 2012 (Suppl 4); Suppl 4:006. PMID:23750326

47. Madeo F, Zimmermann A, Maiuri MC, Kroemer G. Essential role for autophagy in life span extension. J Clin Invest. 2015; 125:85–93. https://doi.org/10.1172/JCI73946 PMID:25654554

48. Gerónimo-Olvera C, Montiel T, Rincon-Heredia R, Castro-Obregón S, Massieu L. Autophagy fails to prevent glucose deprivation/glucose reintroduction-induced neuronal death due to calpain-mediated lysosomal dysfunction in cortical neurons. Cell Death Dis. 2017; 8:e2911. https://doi.org/10.1038/cddis.2017.299 PMID:28661473

49. Xu J. Preparation, culture, and immortalization of mouse embryonic fibroblasts. Curr Protoc Mol Biol. 2005; Chapter 28:Unit 28.1. https://doi.org/10.1002/0471142727.mb2801s70 PMID:18265366

50. Dimri GP, Lee X, Basile G, Acosta M, Scott G, Roskelley C, Medrano EE, Linskens M, Rubelj I, Pereira-Smith O. A biomarker that identifies senescent human cells in culture and in aging skin in vivo. Proc Natl Acad Sci USA. 1995; 92:9363–67. https://doi.org/10.1073/pnas.92.20.9363 PMID:7568133

51. Debacq-Chainiaux F, Erusalimsky JD, Campisi J, Toussaint O. Protocols to detect senescence-associated beta-galactosidase (SA-betagal) activity, a biomarker of senescent cells in culture and in vivo. Nat Protoc. 2009; 4:1798–806. https://doi.org/10.1038/nprot.2009.191 PMID:20010931

52. Levitsky KL, Toledo-Aral JJ, López-Barneo J, Villadiego J. Direct confocal acquisition of fluorescence from X-gal staining on thick tissue sections. Sci Rep. 2013; 3:2937. https://doi.org/10.1038/srep02937 PMID:24121824

53. Rosas-Arellano A, Villalobos-González JB, Palma-Tirado L, Beltrán FA, Cárabez-Trejo A, Missirlis F, Castro MA. A simple solution for antibody signal enhancement in immunofluorescence and triple immunogold assays. Histochem Cell Biol. 2016; 146:421–30. https://doi.org/10.1007/s00418-016-1447-2 PMID:27188756

SUPPLEMENTARY MATERIAL

Supplementary Figures

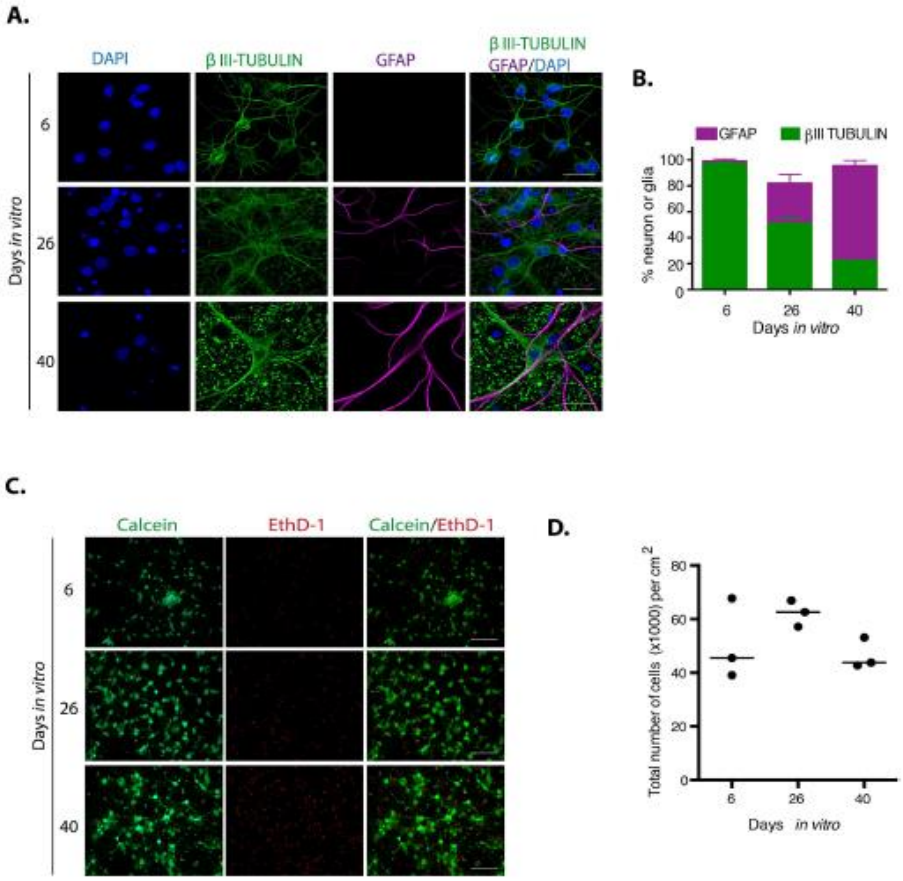

Supplementary Figure 1S. Rat prenatal cortex primary culture is viable up to 40 days *in vitro* (D*IV*). (A) Representative immunofluorescence used to quantify neurons (βIII-TUBULIN) and glial cells (GFAP) at 6, 26 or 40 D*IV* as indicated. Nuclei were stained with DAPI. Scale bars represent 25 μm. (B) The percentage of neurons or glial cells along the culture is graphed. It changes along the time of culture due to both neuronal death and glial proliferation. Bars represent SEM, n=3. (C) Cell viability was estimated by staining with LIVE/DEAD viability/cytotoxicity kit. Alive cells were stained with Calcein, while dead cells were stained with Ethidium homodimer-1 (EthD-1). Scale bars represent 500 μm. (D) The total number of cells per square cm remained similar along the culture. Each dot represents the average of three wells per experiment. Bars represent the average of three independent experiments. Although there was an increment in the average number of cells at 26 D*IV*, it was not statistically significant analyzed by two-way RM ANOVA, with Dunnett´s multiple comparison test.

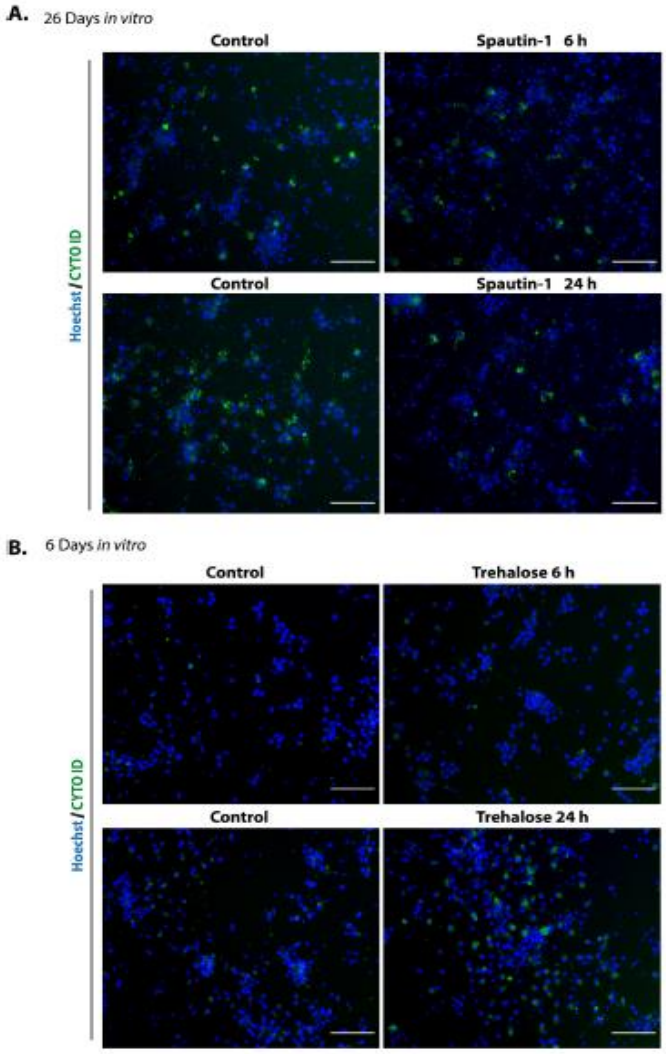

Supplementary Figure 2S. Spautin-1 inhibited autophagy and Trehalose induced autophagy on cortical primary cells. (A) Autophagosomes were stained with CytoID® to verify Spautin1 inhibition of autophagy on cortical cells cultured for 26 D*IV*, since at this time cells have abundant autophagosomes. Controls were treated with vehicle only. (B) Trehalose induction of autophagy was verified by adding it to cortical cells cultured for 6 D*IV*, since at this time cortical cells have only few autophagosomes. Controls were treated with vehicle only. Nuclei were stained with Hoechst. Scale bars represent 500 μm.

11.3. *Anexo 3. Enchanced activity of exportin-1/CRM1 in neurons contributes to autophagy dysfunction and senescent features in old mouse brain.*

Hindawi
Oxidative Medicine and Cellular Longevity
Volume 2021, Article ID 6682336, 22 pages
https://doi.org/10.1155/2021/6682336

Research Article

Enhanced Activity of Exportin-1/CRM1 in Neurons Contributes to Autophagy Dysfunction and Senescent Features in Old Mouse Brain

Elisa Gorostieta-Salas,[1] **Daniel Moreno-Blas**,[1] **Cristian Gerónimo-Olvera**,[2] **Bulmaro Cisneros**,[3] **Felipe A. Court**,[2,4,5] **and Susana Castro-Obregón**[1]

[1]*Departamento de Neurodesarrollo y Fisiología, División de Neurociencias, Instituto de Fisiología Celular, Universidad Nacional Autónoma de México (UNAM), Mexico City, Mexico*
[2]*Center for Integrative Biology, Faculty of Sciences, Universidad Mayor, Santiago, Chile*
[3]*Department of Genetics and Molecular Biology, Center of Research and Advanced Studies (CINVESTAV-IPN), Mexico City, Mexico*
[4]*Fondap Geroscience Center for Brain in Health and Metabolism, Santiago, Chile*
[5]*Buck Institute for Research on Aging, Novato, USA*

Correspondence should be addressed to Susana Castro-Obregón; scastro@ifc.unam.mx

Received 17 December 2020; Revised 3 April 2021; Accepted 24 June 2021; Published 16 August 2021

Academic Editor: Jan Gebicki

Brain aging is characterized by dysfunctional autophagy and cellular senescence, among other features. While autophagy can either promote or suppress cellular senescence in proliferating cells, in postmitotic cells, such as neurons, autophagy impairment promotes cellular senescence. CRM1 (exportin-1/XPO1) exports hundreds of nuclear proteins into the cytoplasm, including the transcription factors TFEB (the main inducer of autophagy and lysosomal biogenesis genes) and STAT3, another autophagy modulator. It appears that CRM1 is a modulator of aging-associated senescence and autophagy, because pharmacological inhibition of CRM1 improved autophagic degradation in flies, by increasing nuclear TFEB levels, and because enhanced CRM1 activity is mechanistically linked to senescence in fibroblasts from Hutchinson–Gilford progeria syndrome patients and old healthy individuals; furthermore, the exogenous overexpression of CRM1 induced senescence in normal fibroblasts. In this work, we tested the hypothesis that impaired autophagic flux during brain aging occurs due to CRM1 accumulation in the brain. We found that CRM1 levels and activity increased in the hippocampus and cortex during physiological aging, which resulted in a decrease of nuclear TFEB and STAT3. Consistent with an autophagic flux impairment, we observed accumulation of the autophagic receptor p62/SQSTM1 in neurons of old mice, which correlated with increased neuronal senescence. Using an in vitro model of neuronal senescence, we demonstrate that CRM1 inhibition improved autophagy flux and reduced SA-β-gal activity by restoring TFEB nuclear localization. Collectively, our data suggest that enhanced CRM1-mediated export of proteins during brain aging perturbs neuronal homeostasis, contributing to autophagy impairment, and neuronal senescence.

1. Introduction

Aging is defined as a time-dependent functional decline that increases the likelihood to die [1], although it affects different species at variable rates [2, 3]. The aging process involves the combined action of a set of different molecular and cellular mechanisms including genomic instability, mitochondrial dysfunction, proteostasis failure, and cellular senescence, collectively coined the hallmarks of aging [4]. Dysfunctional autophagy is associated with numerous age-related diseases including metabolic and neurodegenerative disorders [5]. Particularly in the brain, autophagy failure and the accumulation

of senescent cells are strongly associated with brain deterioration and lose of cognitive abilities, both in physiological and pathological aging [6, 7].

Macroautophagy (referred to as autophagy) is a catabolic process whereby cytoplasmic components and damaged organelles like mitochondria and misfolded proteins are engulfed in a double membrane vesicle called autophagosome and transported then to lysosomes for degradation [8]. Since autophagy is involved in the regulation of different cellular process including protein turnover and energy metabolism, it is considered as a quality control mechanism of the cell [9]. Increasing evidence indicates that a deficient autophagic degradation promotes cellular senescence in proliferating and postmitotic cells [10–13].

Senescent cells are characterized by a lack of response to mitotic and apoptotic stimuli, leading to a perdurable cell cycle arrest accompanied by the expression of the tumor suppressors *Cdkn1a* (coding for $p21^{CIP/WAF}$) and/or *Cdkn2a* (coding for $p16^{INK4A}$) and antiapoptotic *Bcl2* family members, as well as activation of the lysosomal enzyme senescence-associated β-galactosidase (SA-β-gal) [14]. The most important feature of cellular senescence is the acquisition of a senescence-associated secretory phenotype (SASP) which depending on the physiological context can be either beneficial or harmful. In early stages of senescence, cells secrete growth factors and proteases that facilitate tissue repair and remodeling, as well as cytokines that promote infiltration of effector immune cells. Yet, persisting signaling is tumorigenic and causes chronic inflammation, a major contributor to age-related dysfunction. SASP molecules also have an autocrine role that enhances the senescent phenotype and a paracrine role that induces senescence in surrounding cells, altering thereby the tissue where they reside [15]. Therefore, it is fundamental to understand the molecular basis underlying the establishment and maintenance of senescence. Senescent cells have an aberrant nuclear morphology and alterations of proteins that conform the nuclear envelope, which contribute, at least in part, to trigger cellular senescence. For example, lamin A/C stabilization leads to the degradation of polycomb repressive complex 1 (PCR1), which promotes the *Cdkn2a* expression [16], while loss of lamin B1 and its receptor LBR1 induces senescence [17]. LBR1 reduction causes changes in the chromatin structure that upregulate in turn the expression of SASP factors, such as IL-6, IL-8, and MMP1 [18]. Relevant to brain aging, treatments with rapamycin or trehalose that restore dysfunctional autophagy in long-term cultured neurons ameliorate senescent features, including SA-β-gal activity, nuclear envelope alterations, and $p16^{INK4A}$ expression [13, 19, 20].

A previously unrecognized feature of aging is an enhanced CRM1 (exportin-1/XPO1)-driven nuclear protein export mechanism [21], which was recently observed in skin fibroblasts from both Hutchinson–Gilford progeria syndrome (HGPS) patients and old healthy individuals [21]. It is though that enhanced nuclear protein export, due to increased activity of CRM1, impacts protein homeostasis by altering nucleocytoplasmic partitioning of critical proteins (transcription factors, enzymes, and structural proteins). Supporting this hypothesis, pharmacological attenuation of CRM1 activity in HGPS fibroblast was sufficient to prevent premature senescence, while the CRM1 overexpression in normal human skin fibroblasts induces them to senesce [21]. CRM1 binds to cargo proteins through the recognition of a hydrophobic nuclear export sequence (NES) to regulate the nucleocytoplasmic transport of hundreds of proteins [22], including the transcription factor EB (TFEB), the main inducer of autophagy, and lysosomal biogenesis gene expression [23, 24]. In line with this, reduction of the CRM1 expression promotes autophagy, via TFEB nuclear enrichment, which ultimately extends lifespan in worms and protects from neurodegeneration in flies [24]. STAT3, other regulator of autophagy, is also a CRM1 target. Cytoplasmic STAT3 suppresses autophagy by binding to PKR, which interferes then with eIF2α phosphorylation, a necessary step for autophagy induction [25].

Previously, we described that autophagy dysfunction causes neuronal senescence [13]; however, the molecular mechanisms underlying autophagy dysfunction during aging and the consequent induction of cellular senescence are still poorly understood. In this study, we explored the idea that the age-associated perturbation of the autophagic flux, with the concomitant induction of neuronal senescence, might be mechanistically linked to the increased expression and activity of CRM1 that could occur during aging. We found indeed that the CRM1 protein level and activity increased in the mouse hippocampus and cortex during physiological aging, provoking then a decrease of nuclear TFEB and STAT3. The physiological consequence of this alteration is an impaired autophagic flux, as shown by accumulation of p62/SQSTM1 in neurons of old mice and increased neuronal senescence. Remarkably, CRM1 inhibition increased nuclear TFEB and restored thereby the autophagic flux in cultured neurons, as demonstrated by reduced p62/SQSTM1 and LC3 accumulation, increased functional lysosomes, and reduced SA-β-gal activity. Taken together, our data imply that enhanced CRM1-mediated export of proteins during brain aging perturbs neuronal homeostasis, contributing to autophagy impairment and potentially to neuronal senescence.

2. Materials and Methods

2.1. Animals. Wild-type (WT) C57BL/6J [International Mouse Strain Resource (IMSR) catalog #JAX: 000664, RRID: IMSR_JAX: 000664] was obtained from Jackson Laboratory and maintained in the Universidad Mayor animal facility. Autophagy reporter GFP-LC3 transgenic mice C57BL/6 J were kindly shared by Dr. Sandra Cabrera and kept at the animal house of the Institute of Cellular Physiology at the National University of Mexico (UNAM), housed at 22°C in 12 h light/12 h dark cycle with ad libitum access to water and food. Mice used in the present study were handled and cared according to the animal care and ethics legislation. All procedures were approved by the Internal Committee of Care and Use of Laboratory Animals of the Institute (IFC-SCO51-18) and the SAG Chile (RUP: 13.1.07.0018).

2.2. Cortical Primary Cultures and Leptomycin B Treatment. Cortical primary cultures were prepared as previously

described (Moreno-Blas et al. 2019). Cerebral cortices from Wistar rat embryos of 17 days of gestation were isolated and dissociated by digestion and trituration with a Pasteur pipette in a solution of 1 : 1400 Trypsin-EDTA (15400054, Invitrogen/Gibco, Grand Island, NY, USA). Cells were suspended in neurobasal medium (21103049, Invitrogen/Gibco, Grand Island, NY, USA) supplemented with 2% B27 (17504044, Invitrogen/Gibco, Grand Island, NY, USA), 200 mM GlutaMAX™ Supplement (35050061, GIBCO Life Technologies, Grand Island, NY, USA), and 0.02 mg/ml gentamicin (15710064, Invitrogen/Gibco, Grand Island, NY, USA). Cells were plated at a density of $1.05 \times 10^5/cm^2$ in 12-well plates precoated with poly-L-lysine (P1524, Sigma-Aldrich St. Louis, MO, USA) (0.01 mg/ml). Cultures were maintained up to 26 days in vitro (26 DIV) at 37°C in a humidified, 5% CO_2 atmosphere. Half of the medium was changed every 6 days. Cortical cells were treated with 5 nM leptomycin B (LMB; Sigma-Aldrich) for 24 h (at 25 DIV) or 4 days (at 22 DIV) diluted in ethanol (vehicle) and 20 μM chloroquine (C-6628 Sigma-Aldrich , St. Louis, MO, USA) for 4 h.

2.3. Immunoblotting Analysis

2.3.1. Brain. Animals were euthanized via an overdose of pentobarbital. Hippocampus and cerebral cortex from six young (3 to 6 months), six adult (14 to 17 months), and three-old (24 to 28 months) wild-type mice were homogenized in an extraction buffer containing (Tris-HCl pH 8.0 50 mM, NaCl 150 mM, Triton X-100 1%, sodium deoxycholate 0.5% and SDS 2%). Thirty micrograms of total protein was separated by SDS-PAGE and electroblotted onto polyvinylidene (PVDF) membranes (Millipore). Membrane was blocked with 3% Blotting-Grade blocker (BIO-RAD Cat. #170-6404) and incubated overnight with the primary antibody at 4°C, rabbit anti-CRM1 (1 : 1000, Novus 100-79802, Centennial-CO, USA), rabbit anti-lamin B1 (1 : 1000, Abcam 32454, Cambridge, MA, USA), mouse anti-lamin A/C (1 : 1000, Santa Cruz Biotechnology 376248, Dallas, TX, USA), and mouse anti-β-actin (1 : 5000, Santa Cruz Biotechnology 47778, Dallas, TX, USA), diluted in TTBS/BSA 3%. After three washes with TTBS, secondary antibody goat anti-mouse IgG (1 : 5000, Sigma A3682, Saint, Louis, USA) or goat anti-rabbit IgG (1 : 5000, Sigma A0545, Saint, Louis, USA) was prepared in TTB/blocker 3%. Following by three washes, immunoreactivity was detected by chemiluminescent HRP substrate (Milipore Cat. WBKLS0100, Billerica, Ma, USA). Membranes were scanned using C-DiGit Blot Scanner (LI-COR).

For subcellular fractions, the collected tissue was homogenized using a hypotonic buffer (Hepes 10 mM, $MgCl_2$ 1.5 mM, KCl 10 Mm, pH 7.4), incubated for 5 min at 4°C and centrifuged at 11,000 rpm for 1 min at 4°C. To collect cytoplasmic proteins, supernatant was collected and centrifuged again at 4,000 rpm for 10 min at 4°C. The supernatant was collected again; to precipitate cytoplasmic proteins, a 1 : 1 proportion of methanol/chloroform mix (5 : 1) was added and centrifuged at 14,000 rpm for 5 min. The pellet obtained was resuspended in lysis buffer (Tris-HCl pH 8.0 50 mM, NaCl 150 mM, Triton X-100 1%, sodium deoxycholate 0.5%, and SDS 2%). To collect nuclear proteins, the pellet of the first centrifugation was resuspended in hypotonic buffer and centrifuged at 4,000 rpm for 5 min at 4°C. Supernatant was discarded, and the pellet was resuspended on lysis buffer.

Thirty micrograms of cytosolic and nuclear fractions was separated by SDS-PAGE and electroblotted onto polyvinylidene (PVDF) membranes (Millipore). Membranes were blocked with 3% Blotting-Grade blocker (BIO-RAD Cat. #170-6404) and incubated overnight with the primary antibody at 4°C, anti-TFEB (1 : 1000, Mybiosure MBS716265, San Diego, CA, USA), anti-GADPH (1 : 8000, Cell Signaling Technology Gapdh 14c10 anti-rb mAb 2118), and rabbit anti-fibrillarin (1 : 1000, Abcam 5821 Cambridge, MA, USA), diluted in TTBS/BSA 3%. Secondary antibody goat anti-mouse IgG (1 : 5000, Sigma A3682, Saint, Louis, USA) or goat anti-rabbit IgG (1 : 5000, Sigma A0545, Saint, Louis, USA) was prepared in TTB/blocker 3%. Immunoreactivity was detected by chemiluminescent HRP substrate (Milipore Cat. WBKLS0100, Billerica, Ma, USA). Membranes were scanned using C-DiGit Blot Scanner (LI-COR).

2.3.2. Primary Culture. Cells were lysed in an extraction buffer consisting of 62.5 mM Tris, 2% SDS, and 2 mg/ml protease and phosphatase inhibitors 18 (Complete, Roche Molecular Diagnostics, pH 7.4). Thirty micrograms of total protein was separated by SDS-PAGE and electroblotted onto polyvinylidene fluoride (PVDF-FL) membranes (Millipore). Membranes were incubated overnight with the primary antibody at 4°C, rabbit anti-LC3 (1 : 2000, MBL PD014, Nagoya, Japan), rabbit anti-lamin B1 (1 : 1000, Abcam 32454, Cambridge, MA, USA), mouse anti-lamin A/C (1 : 1000, Santa Cruz Biotechnology 376248, Dallas, TX, USA), and mouse anti-β-actin (1 : 10000, Santa Cruz Biotechnology 47778, Dallas, TX, USA) diluted in TTBS/BSA 3%. Following three washes with TTBS secondary antibody IRDye® 680RD goat anti-rabbit (925-68071, LI-COR) or IRDye® 800CW goat anti-mouse (925-32210, LI-COR) that was applied at 1 : 5000 dilution in TTBS, membranes were scanned and analyzed using an Odyssey® IR scanner and Odyssey® Image Studio software 5.2.5.

2.4. Immunofluorescence

2.4.1. Brain Section. GFP-LC3 transgenic mice under anesthesia with pentobarbital sodium were perfused transcardially with PBS 1×, then with 4% paraformaldehyde. Brains were drop fixed in 4% paraformaldehyde for 24 h; cryoprotection brains were immersed in PBS/30% sucrose for 24 h. Brain coronal sections (40 μm) from the hippocampus and perirhinal cortex were mounted serially. The sections were permeabilized and blocked with PBS 1×/0.5% Tween/BSA 5% for 30 min at RT. After three washes, primary antibody was incubated at 4°C overnight in PBS/0.05% Tween/0.1% Triton. Next, sections were incubated with Alexa Fluor-conjugated secondary antibodies (1 : 400, Life Technologies, Oregon, USA) in PBS/0.05% Tween/0.1% Triton for 12 h at 4°C; nuclei were stained with DAPI (1 μg/ml). To avoid

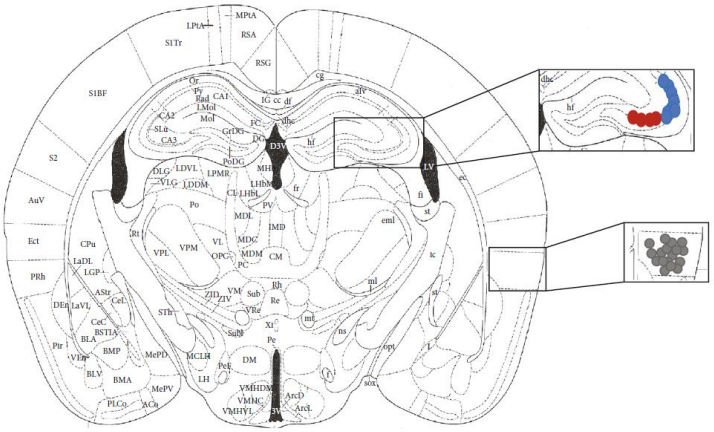

(a)

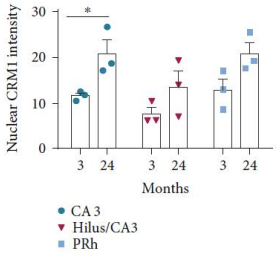

(b)

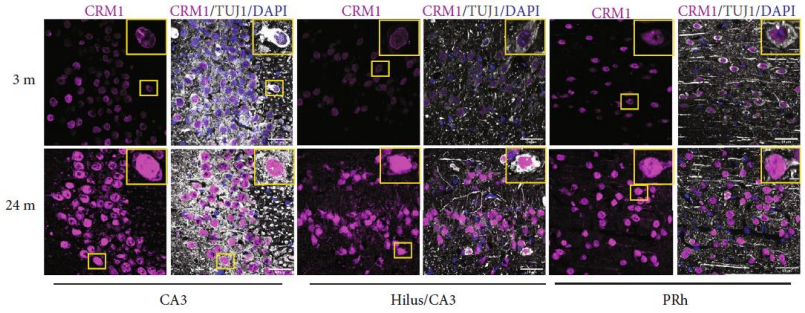

(c)

Figure 1: CRM1 accumulates in neurons during brain aging. (a) Anatomic diagram to locate the regions analyzed along the work. (b) Graph shows pixel density of nuclear CRM1 in neurons of mice at the indicated ages and brain regions. Bars represent the mean ± SEM from three independent experiments, with significant differences determined by unpaired t-test Student; $^*p < 0.05$. Three or four fields per region were analyzed, and 70-100 neurons per region per animal were counted. (In total, we counted for CA3, $n = 300$ neurons of each age; for hilus, $n = 274$ neurons from 3 months old and $n = 263$ neurons from 24 months old; and for PRh, $n = 115$ neurons from 3 months old and $n = 139$ neurons from 24 months old). (c) Representative images of immunofluorescences to detect CRM1 in neurons (expressing TUJ1), in the hippocampus (CA3 and hilus) ,and perirhinal cortex (PRh) from young (3 months-old) and old (24 months-old) mice used for the quantification shown in (b). Scale bars represent 30 μm. Nuclei were stained with DAPI. Squares indicate the magnified area shown in insets.

lipofuscin, autofluorescence slices were incubated with Sudan Black B. The following primary antibodies were used: rabbit anti-CRM1 (1 : 500, Novus NB100-79802, Centennial-CO, USA), rabbit anti-TFEB (1: 400, Mybiosure MBS716265, San Diego, CA, USA), mouse anti-p62 (1 : 300, Abcam 56416, Cambridge, MA, USA), mouse anti-lamin A/C (1 : 1000, Santa Cruz Biotechnology 376248, Dallas, TX, USA), rabbit anti-p21 (1 : 200, abcam 109199 Cambridge, MA, USA), mouse anti-p16 (1 : 200, Santa Cruz Biotechnology sc1661, Dallas, TX, USA), mouse anti-class III β-tubulin (1 : 1000, Abcam 14545, Cambridge, MA, USA), rabbit anti-class III β-tubulin (1 : 1000, abcam 18207, Cambridge, MA, USA), and rabbit anti-MAP2 (1 : 500 abcam 32454 Cambridge, MA, USA), mouse anti-GFAP (1 : 400, Sigma-Aldrich G3893, St. Louis, MO, USA), and mouse anti-STAT3 (1 : 100 Santa Cruz Biotechnology 482, Dallas, TX, USA). Images were acquired using a confocal microscope Zeiss LSM 800; in all cases, images were processed and quantified using Fiji software. Pseudocolors were assigned to gray images. Corrected fluorescence intensity was obtained as the result of raw fluorescence intensity minus background fluorescence in every case.

2.4.2. Primary Culture. Cells were fixed with 100% methanol on ice for 20 min and then rinsed with PBS blocked with PBS/5% BSA, and incubated at 4°C with primary antibody overnight. Alexa Fluor-conjugated secondary antibodies were diluted in PBS/2% BSA (1 : 500, LIFE TECHNOLOGIES, Oregon, USA) and incubated for 1 h at room temperature. Nuclei were stained for 5 min with DAPI (1 μg/ml). The antibodies used and dilutions were as follows: rabbit anti-CRM1 (1 : 400, Novus NB100-79802, Centennial-CO, USA), rabbit anti-TFEB (1: 500, Mybiosure MBS716265, San Diego, CA, USA), mouse anti-p62 (1 : 500, Abcam 56416, Cambridge, MA, USA), rabbit anti-LAMP1 (1 : 1000, Sigma-Aldrich L1418, St. Louis, MO, USA), mouse anti-lamin A/C (1 : 1000, Santa Cruz Biotechnology 376248, Dallas, TX, USA), rabbit anti-lamin B1 (1 : 1000, Abcam 32454, Cambridge, MA, USA), mouse anti-p16 (1 : 1000, Santa Cruz Biotechnology sc1661, Dallas, TX, USA), mouse anti-class III β-tubulin (1 : 1000, Abcam 14545, Cambridge, MA, USA) and rabbit anti-class III β-tubulin (1 : 1000, abcam 18207, Cambridge, MA, USA). Images were acquired using a confocal microscope Zeiss LSM 800 and processed using Fiji software. LAMP1 immunofluorescence images were processed simultaneously for each experiment using Fiji software, to generate binarized masks that were subjected to particle analysis. Particles with 10 μm^2 or lower area and a circularity index of 0.60 or more were considered as small lysosomes. Particles with values higher than 10 μm^2 of area and a circularity index of 1 or less were considered as enlarged lysosomes.

2.5. SA–β-Galactosidase Staining. The β-galactosidase activity was analyzed following the protocol described previously [26]. Cells fixed with 2% formaldehyde+0.2% glutaraldehyde and brain sections previously fixed with 4% paraformaldehyde were washed with PBS 1× and stained with the staining solution containing 20 mg/ml of X-gal (IB02260, IBI SCIENTIFIC, Peosta, IA, USA) in dimethylformamide, 0.2 M citric acid/sodium phosphate buffer pH = 6, 100 mM potassium ferrocyanide, 5 M sodium chloride, and 1 M magnesium chloride. Sections were incubated for 12 h and cells for 24 h at 37°C.

2.5.1. Brain Sections. To corroborate staining, the complete regions of the hippocampus and cerebral cortex were imaged at 10× using an inverted Nikon Eclipse Ti-U microscope and accompanying NIS Elements, Basic Research (Nikon Instruments Inc. ®, NY, USA) software. In order to obtain better resolution images of each focal plane, CA3 and hilus of hippocampus and perirhinal cortex were imaged at 40× using transmitted light illumination of a confocal microscope Zeiss LSM 800. Images were processed and quantified using Fiji software. The percentage of SA–β-gal positive was quantified using images of each hippocampal region and perirhinal cortex from both hemispheres of three different animals per group. All images were analyzed using binarized masks, IsoData threshold, and particle analysis in the Fiji software.

2.5.2. Primary Culture. Confocal detection of X-gal in cultured neurons was performed as previously described (Levitsky et al. 2013) and quantified using confocal images acquired with 63× objective. All images were processed simultaneously for the three independent experiments using Fiji–ImageJ, to generate binarized masks and define the IsoData threshold. Then, these masks were subjected to particle analysis of the ImageJ macro. Finally, the percentage of the SA–β-gal-positive area was divided by the total number of nuclei of each experiment.

2.6. Statistics. All data were analyzed and graphed with Prism 6 (GraphPad Software Inc. La Jolla, CA, USA). Specific tests were performed according to each experimental design.

Western blot analysis for in vivo samples was performed using one-way ANOVA and Dunnet as the posthoc test. Western blot analysis for in vitro samples was performed using two-way ANOVA followed by Holm-Sidak's posthoc test. In vivo pixel density analysis and SA-β-gal-positive area were performed using unpaired t-test student or one-way ANOVA analysis, followed by Sidak's multiple comparison tests, as indicated in each figure. Pearson's correlation coefficient was included. In vitro pixel density of cortical neurons was analyzed with one-way ANOVA analysis, followed by Tukey's or Sidak's multiple comparison test as indicated in each figure. Lysosome morphologies were compared using ordinary one-way ANOVA analysis, followed by Sidak's multiple comparison test.

3. Results

3.1. CRM1 Accumulates in Aged Neurons in the Hippocampus and Perirhinal Cortex. To ascertain whether CRM1 level increases during aging in the mouse brain, we compared CRM1 expression in the hippocampus and cortex of young and old mice. We chose those regions because they play an important role in learning and memory and undergo functional and structural alterations during physiological aging and age-related neurodegenerative diseases, like Alzheimer's

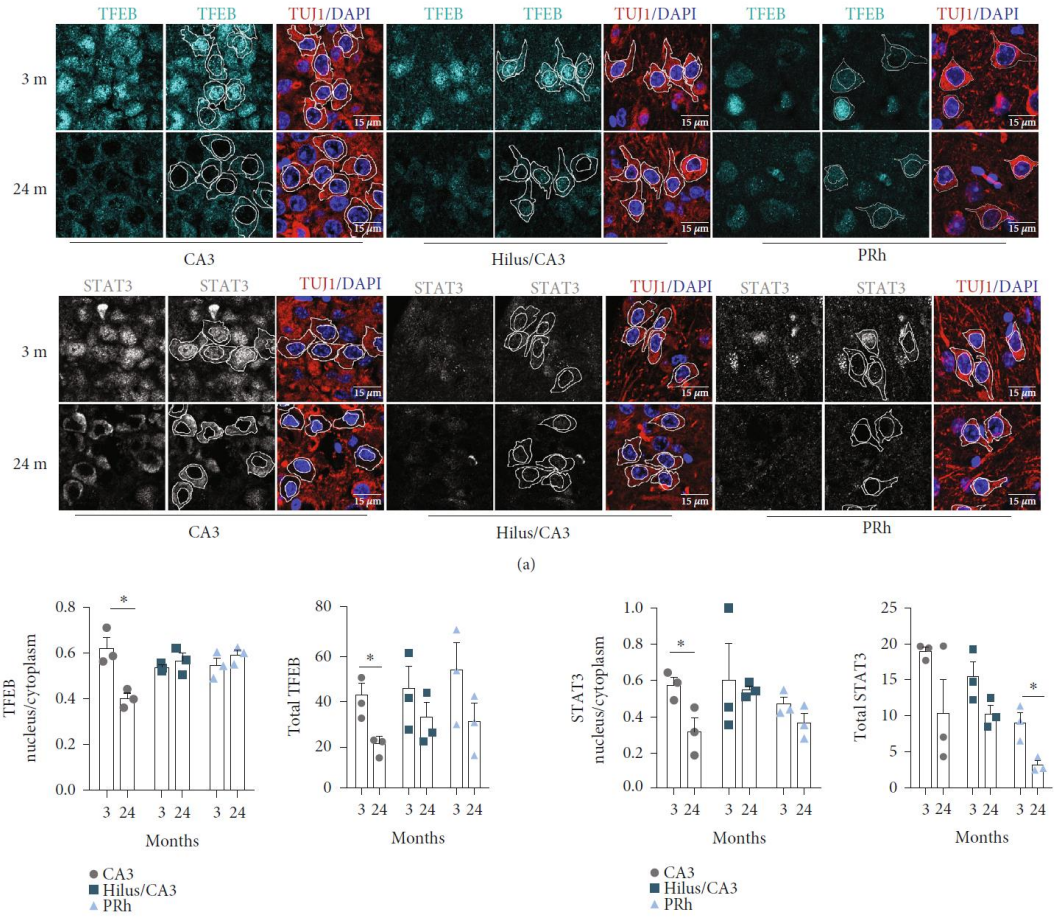

Figure 2: Continued.

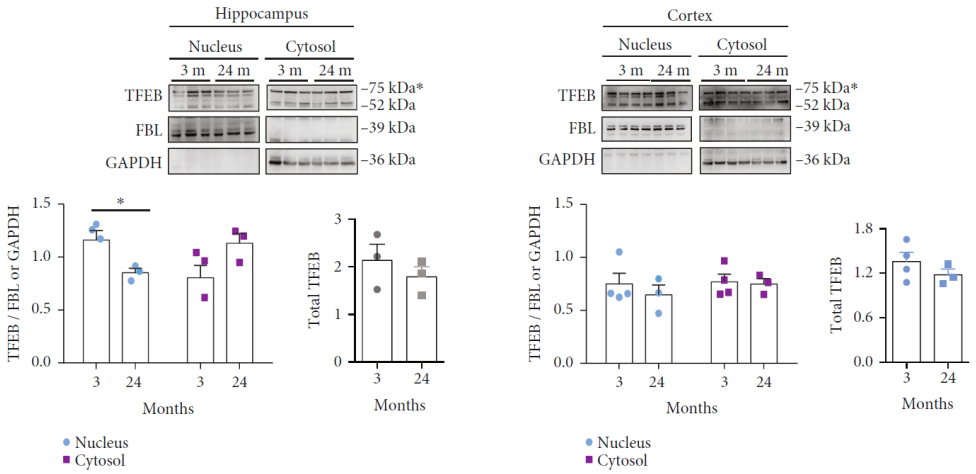

(c)

Figure 2: Enhanced TFEB and STAT3 nuclear export in CA3 neurons during brain aging. (a) Immunofluorescence analysis was carried out to detect TFEB and STAT3 in neurons (expressing TUJ1) of the indicated brain regions, collected from 3 and 24 months old mice. Scale bars, 15 μm. Nuclei were stained with DAPI. (b) Pixel density of TFEB or STAT3 signals in nuclear and cytoplasmic areas was quantified; white lines in panel (a) exemplify delineated areas. Left graphs represent the nuclear/cytoplasmic ratio found in each region and age; right graphs represent the total signal (nuclear plus cytoplasmic signal); bars represent the mean ± SEM. Three or four fields per region per animal were analyzed. The collective number of neurons counted was CA3, $n = 150$ neurons from 3 months old and $n = 120$ neurons from 24 months old; for hilus, $n = 86$ neurons from 3 months old and $n = 70$ neurons from 24 months old; and for PRh, $n = 75$ neurons from 3 months old and $n = 77$ neurons from 24 months old. Significant differences were determined by unpaired t-test Student $^*p < 0.05$. (c) Subcellular distribution of TFEB was analyzed by western blot of cytoplasmic and nuclear fractions from the hippocampus and cortex of mice at the indicated ages. GAPDH and fibrillarin (FBL) detection was used as cytoplasmic and nuclear markers, respectively. Left graphs represent the mean of densitometry analysis of the 75 KDa band of TFEB, and right graphs represent total TFEB (nuclear plus cytoplasmic densitometry) from at least three animals per age group, expressed in arbitrary units. Bars correspond to the mean ± SEM from three independent experiments, with significant differences determined by unpaired t-test Student; $^*p < 0.05$.

disease [27, 28]. We observed an increase of CRM1 in neurons in the CA3 region and hilus/CA3 areas of the hippocampus, as well as in neurons in the perirhinal cortex (PRh), when brains from 24 months old mice were compared with those of 3 months old mice (Figure 1). To rule out that the increase of CRM1 observed was due just to an increase in the size of old neurons, we measured the area of both nucleus and cytoplasm of neurons from 3 and 24 months old brains. As show in Supplementary Figure 1, the average size of neurons does not change significantly with age. The age-associated increased level of CRM1 was confirmed by western blot analysis by comparing whole hippocampus and cortex lysates from 24-28, 14-17, and 3-6 months old mice (Supplementary Figure 2).

3.2. Neurons Expressing High Level of CRM1 in Old Brains Display Enhanced Nuclear Export of TFEB and STAT3 and Accumulate p62/SQSTM1. To determine whether elevated CRM1 level in old brains is reflected in increased CRM1 activity, we analyzed the subcellular distribution of TFEB and STAT3, proteins whose nuclear export depend on CRM1 [24, 25, 29]. A decrease in the nuclear labeling of both TFEB and STAT3 was observed in CA3 and PRh neurons from 24 months old mice, compared with 3 months mice (Figure 2). We quantified the partition of nuclear vs. cytoplasmic signal and found in the CA3 region an increased export of TFEB statistically significant and a trend of increased export of STAT3 in the PRh region (Figure 2(b)).

Consistently, a reduction of TFEB in the nuclear fraction of the hippocampus, with its concomitant increase in the cytoplasmic fraction, was found by western blot analysis in 24 months old mice. Such enrichment in the cytoplasm was not observed in the cytoplasmic fraction from the cortex (Figure 2(c)). The overall reduction of the TFEB expression noticed previously during the analysis per cel by immunofluorescence was not detectable by western blot, when the whole hippocampus is lysed (Figure 2(c)).

Collectively, our data imply that increased the CRM1 level corresponds to its enhanced activity in CA3.

Since we had previously observed that the autophagic flux is impaired in senescent neurons in vivo and in vitro [13], we next wondered whether decreased nuclear localization of TFEB and STAT3 in old neurons might impair the autophagic flux [30]. Consistent with this idea, we observed accumulation of the autophagy adaptor protein p62/SQSTM1 in 24 months old brain regions (Figure 3(a)), being statistically significant in PRh cortex neurons (Figure 3(b)). A positive correlation between p62/SQSTM1 accumulation and increased CRM1

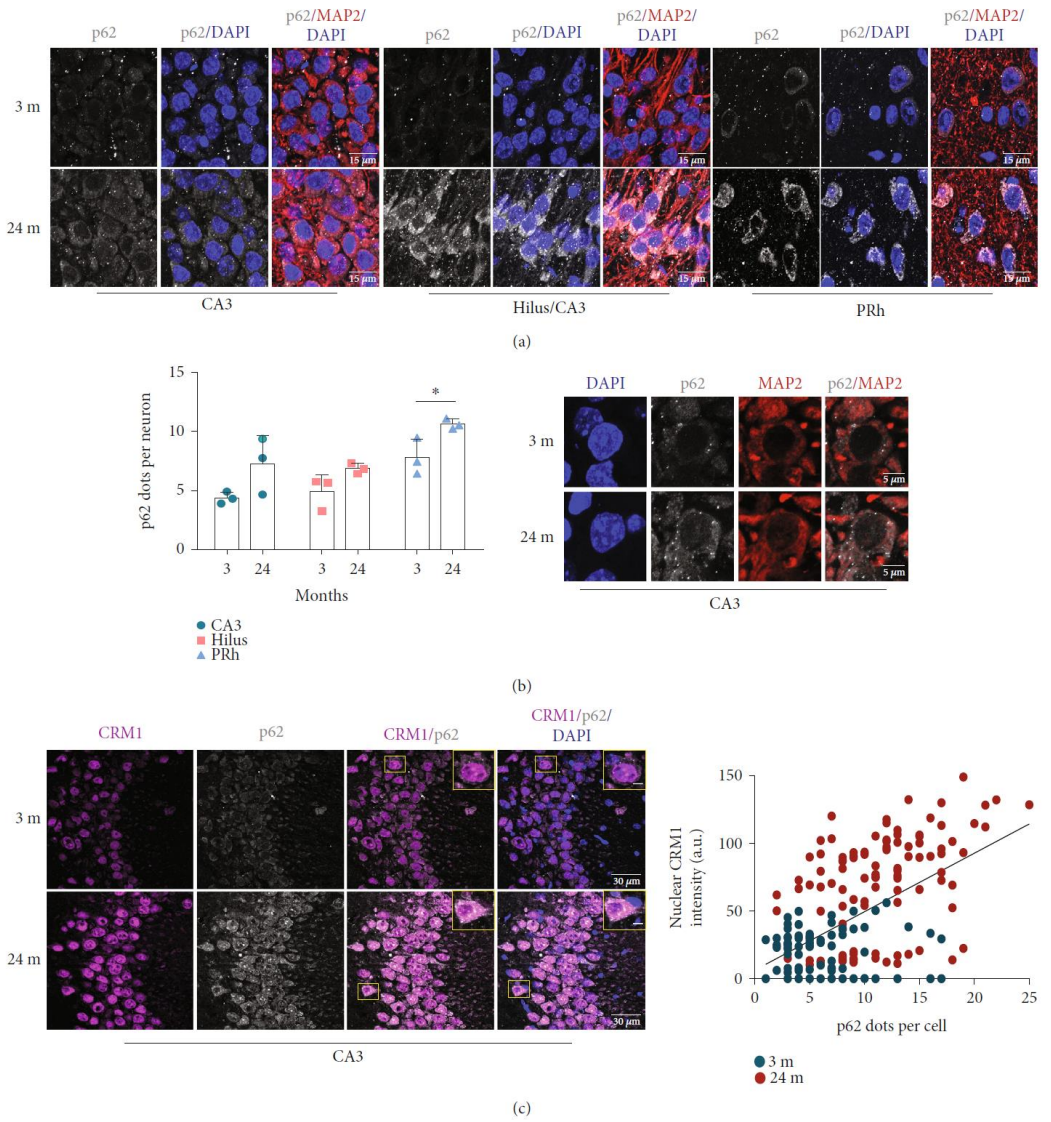

Figure 3: Accumulation of p62/SQSTM1 correlated with high nuclear level of CRM1 in neurons of 24 months old mice. (a) Immunofluorescence analysis to detect p62/SQSTM1 in neurons (expressing MAP2) at the indicated brain regions from 3 or 24 months old mice. Scale bars, 15 μm. Nuclei were stained with DAPI. (b) Graph shows quantification of p62/SQSTM1 dots per neuron. Bars correspond to the mean ± SEM from three independent experiments, with significant differences determined by unpaired t-test Student; $^*p < 0.05$. Three or four fields per region per animal were analyzed. The total number of neurons counted was CA3, $n = 187$ from 3 months old and $n = 201$ from 24 months old; hilus, $n = 161$ from 3 months old and $n = 285$ from 24 months old; and PRh, $n = 113$ from 3 months old and $n = 124$ from 24 months old. Right, an amplified image representative of the neurons was counted. (c) Coimmunodetection of CRM1 and p62/SQSTM1 in the CA3 region of the hippocampus from 3 or 24 months old mice. Scale bars, 30 μm. Nuclei were stained with DAPI. The plot shows a linear regression analysis that positively correlates the nuclear CRM1 intensity with p62/SQSTM1 dots in cells ($r = 0.5985$, $n = 100$ neurons from 3 months; $n = 102$ neurons from 24 months, $p < 0.0001$). Squares indicate the magnified area shown in insets.

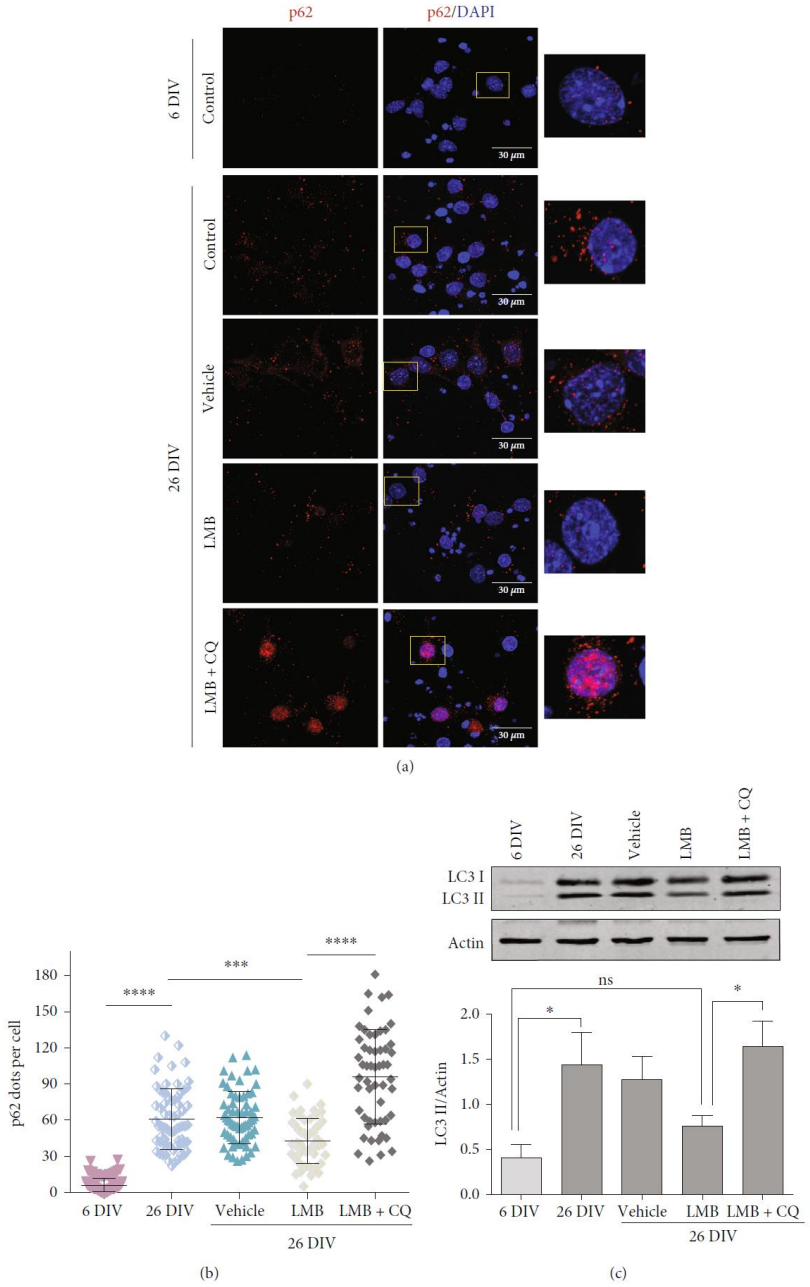

Figure 4: Continued.

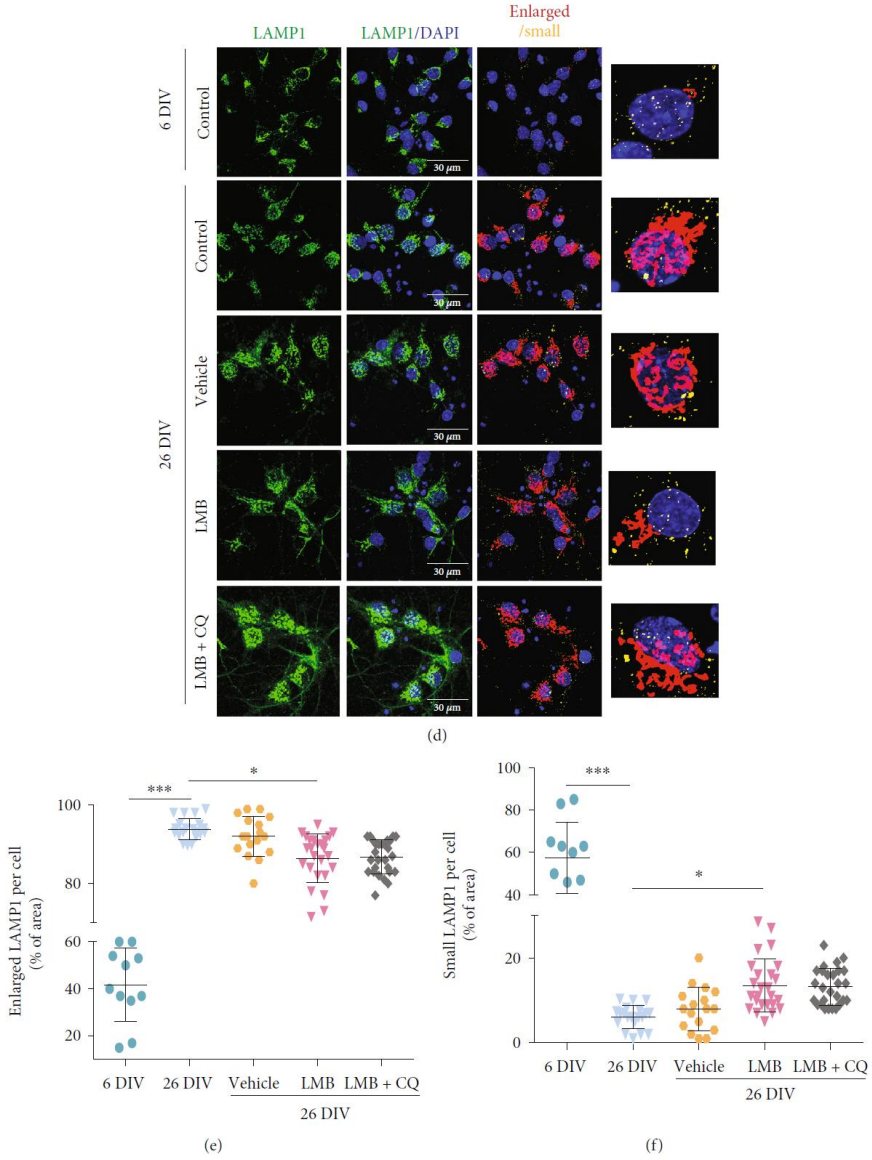

Figure 4: CRM1 inhibition restored the autophagic flux in cultured 26 DIV neurons. Cortical neurons cultured during 6 and 26 DIV were treated for 4 days (starting at 22 DIV) with 5 nM LMB, or with the vehicle alone, or with 5 nM LMB and 20 μM chloroquine (CQ) for 4 h. (a) Immunofluorescence analysis to detect p62/SQSTM1. Scale bars, 30 μm. Squares indicate the magnified area shown in insets. (b) Graph shows quantification of p62/SQSTM1 dots per cell. Bars correspond to the mean ± SD from three independent experiments, with significant differences calculated by ordinary one-way ANOVA analysis, with Tukey's multiple comparison test; ***$p < 0.001$; ****$p < 0.0001$. (c) Western blot detects LC3 and ACTIN. Graph shows the densitometric quantification of LC3-II normalized against ACTIN. Bars represent the mean ± SEM from three independent experiments, with significant differences determined by two-way ANOVA followed by Holm-Sidak's multiple comparison test; *$p < 0.05$; ns: no significant. (d) Immunofluorescence analysis to detect LAMP1. (e) The number of enlarged lysosomes per cell is shown. (f) The number of small lysosomes per cell is plotted. The quantification method is described in the methods section. Bars represent the mean ± SD, with significant differences calculated by ordinary one-way ANOVA analysis, with Sidak's multiple comparison test; *$p < 0.05$; ****$p < 0.0001$.

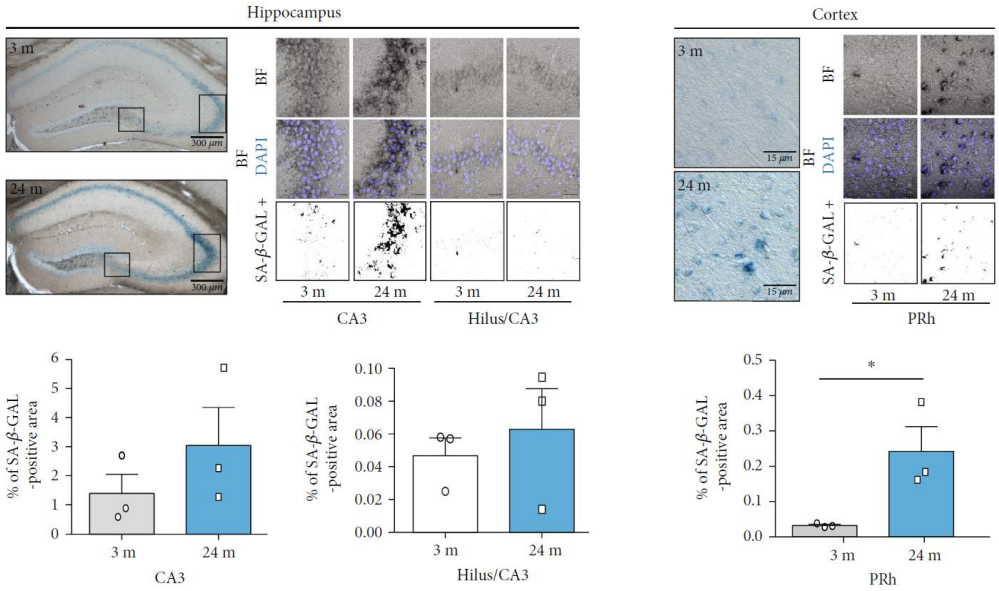

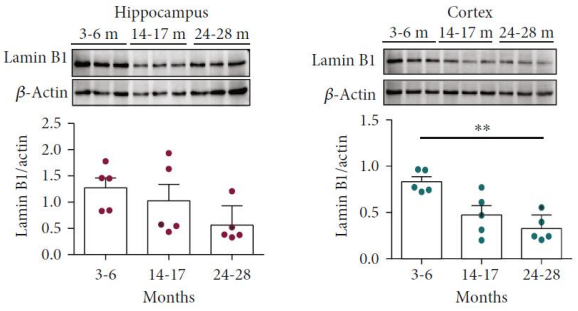

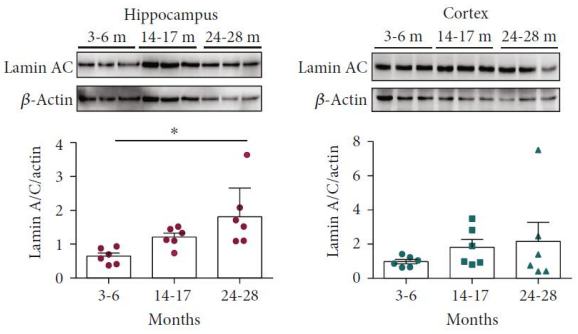

Figure 5: Continued.

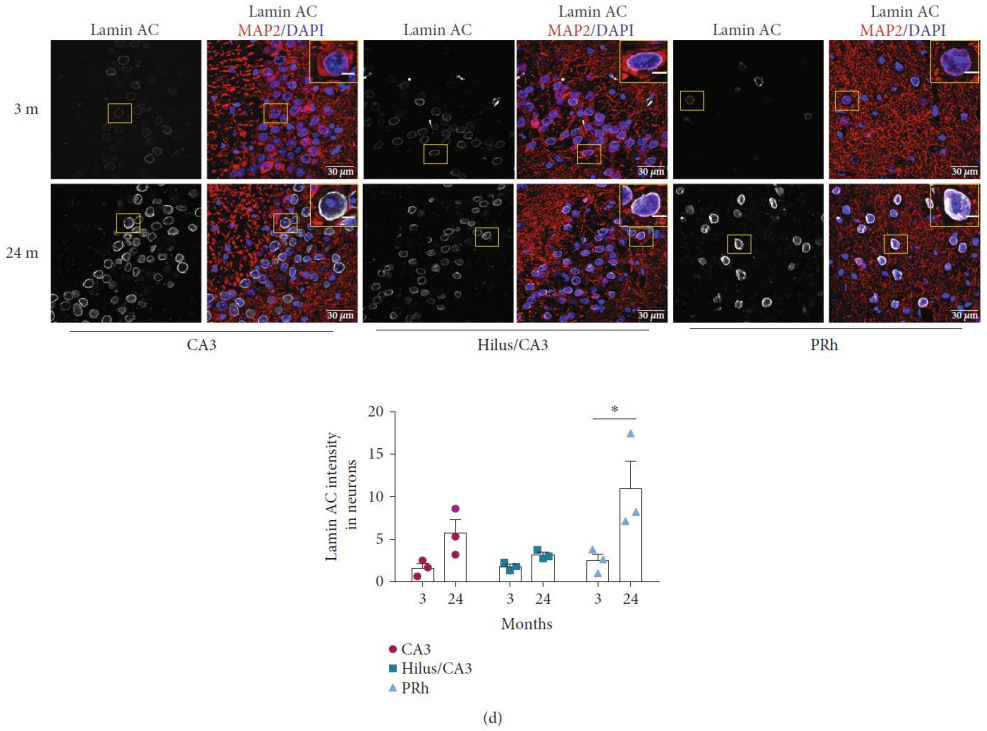

FIGURE 5: Neurons with senescence features accumulate in the hippocampal and cortical regions in 24 months old mice. (a) SA-β-gal activity was quantified in the hippocampal and cortical regions of 3 and 24 months old mice as indicated in the methods section. Graphs show the percentage of the SA-β-gal-positive area in each brain region at the indicated mice ages. Bars correspond to the mean ± SEM from three independent experiments, with significant differences determined by unpaired t-test Student; $^{*}p < 0.05$. (b) Western blot analysis showing the expression of lamin B1 and (c) lamin A/C in the hippocampus and cortex of the indicated mice ages. Graphs show the densitometric analysis of immunoblot autoradiograms to determine lamin B1 and lamin A/C protein expression from five or six animals per age group (each dot represents an animal). Data represent the mean ± SEM, with significant differences calculated by one-way ANOVA and Dunnet's posthoc test; $^{*}p < 0.05$; $^{**}p < 0.01$. (d) Immunofluorescence analysis to detect lamin A/C in neurons (expressing MAP2) of the indicated brain regions from 3 and 24 months old mice. Scale bars, 30 μm. Nuclei were stained with DAPI. Squares indicate the magnified area shown in insets. Graph shows pixel density of lamin A/C in the indicated brain regions and mice ages. Bars represent the mean ± SEM from three independent experiments, with significant differences calculated by two-way ANOVA analysis, with Sidak's multiple comparison test; $^{*}p < 0.05$.

expression was corroborated by double-labeling immunofluorescence assays in CA3 neurons of 24 months old brains (Figure 3(c)). Although no statistically significant change was observed for GFP-LC3 intensity (Supplementary Figure 3), we confirmed that autophagy dysfunction occurs in senescent neurons in vitro, as we observed that they accumulate p62/SQSTM1, LC3, and enlarged lysosomes (Figure 4). Taken together, these findings imply that cytoplasmic localization of TFEB and STAT3 in aged neurons, due likely to enhanced CRM1 activity, could lead to autophagic flux impairment.

3.3. Neurons with Senescent Features Increase in Old Mice and Correlate with Increased CRM1 Expression. Since CRM1 overexpression promotes cellular senescence in normal fibroblasts [21], we wondered whether enhanced CRM1 activity might also contribute to neuronal senescence during physiological aging. To this end, we examined senescent features in neurons of old mice brains. We detected an increased number of SA-β-gal-positive neurons in the hippocampus and PRh cortex of 24 months old mice brains (Figure 5(a)). Senescent cells have aberrant nuclear morphology and altered distribution of nuclear envelope proteins [21]; loss of lamin B1 and its receptor LBR1 induces senescence [17], while lamin A/C stabilization leads to polycomb repressive complex 1 (PRC1) degradation, which allows *Cdkn2a* expression [16]. In line with this, we found a significant decrease of lamin B1 in both the hippocampus and PRh cortex of 14-17 and 24-28 months old mice brains (Figure 5(b)), as well as an increase of lamin A/C in the hippocampus neurons of 24-

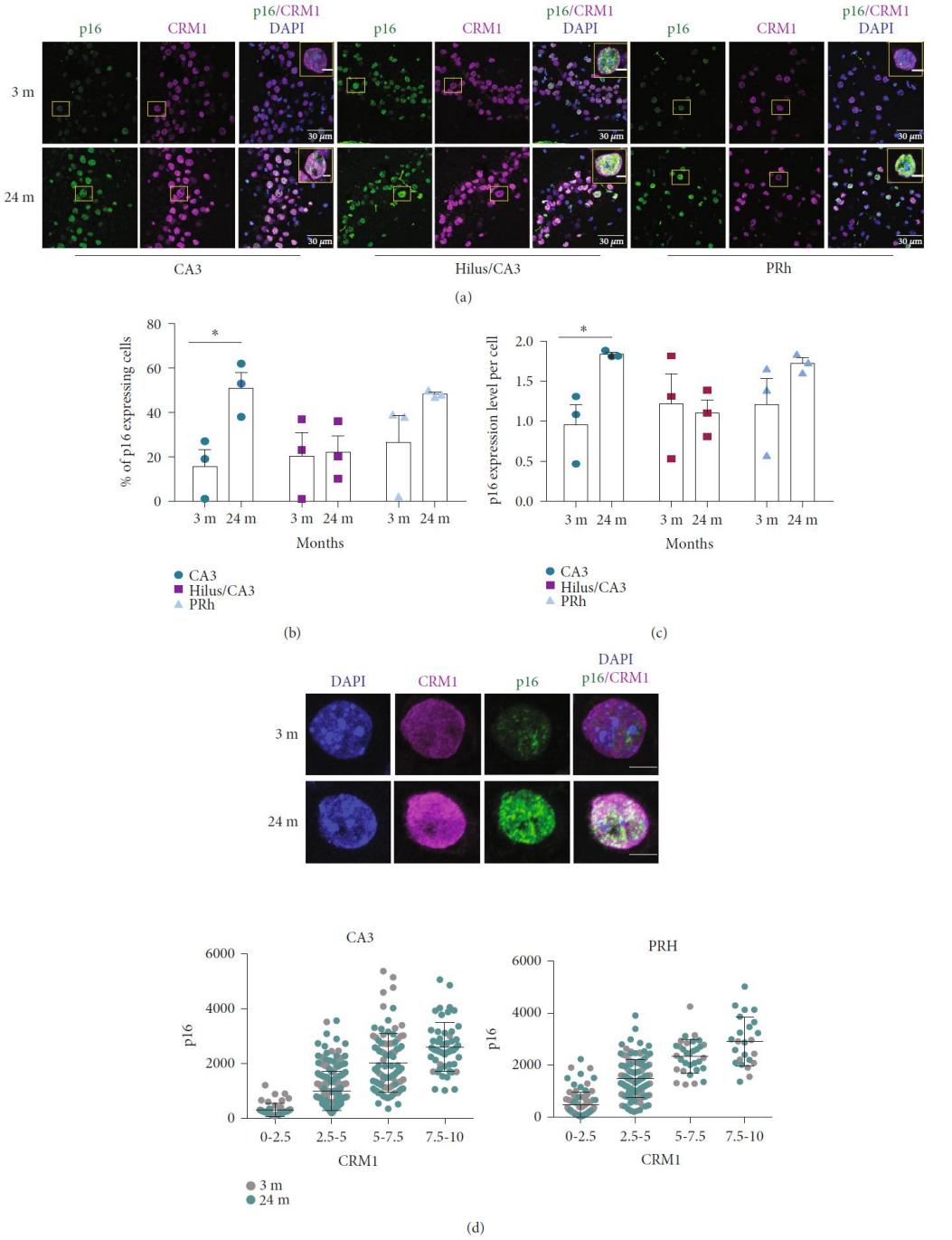

Figure 6: Continued.

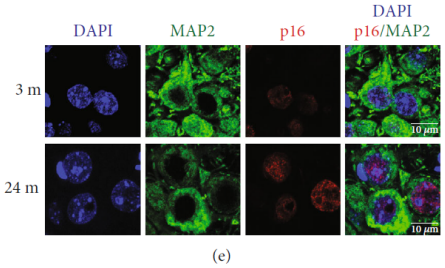

Figure 6: Brain cells with increased expression of $p16^{INK4A}$ also express elevated levels of CRM1 in the CA3 and PRh cortex of 24 months old mice. (a) Immunofluorescence analysis to detect $p16^{INK4A}$ and CRM1 in the hippocampus (CA3 and hilus) and PRh cortex of young (3 months old) and old (24 months old) mice brains. Nuclei were stained with DAPI. Squares indicate the magnified area shown in insets. Scale bars represent 30 μm. (b) Graph shows the percentage of cells expressing detectable levels of $p16^{INK4A}$. Data correspond to the mean ± SEM, with significant differences calculated by t-test Student; $^*p < 0.05$. (c) Graph shows the pixel density of nuclear $p16^{INK4A}$. Results show the mean ± SEM from three separate experiments, with significant differences calculated by t-test Student; $^*p < 0.05$. For (b) and (c), the number of cell counted from 3 brains was CA3, $n = 233$ from 3 months old and $n = 221$ from 24 months old; hilus, $n = 134$ from 3 months old and $n = 159$ from 24 months old; and PRh, $n = 168$ from 3 months old and $n = 151$ from 24 months old. (d) Representative magnified images to visualize immunostaining of $p16^{INK4A}$ and CRM1 are shown. Scale bars represent 5 μm. Bottom, quantification of the nuclear $p16^{INK4A}$ pixel density was plotted against the nuclear CRM1 pixel density in the CA3 and PRh cortex cells of the indicated mice ages. Bars represent the mean ± SEM (from 3 brains, the number of cell counted was CA3, $n = 190$ from 3 months old and $n = 200$ from 24 months old and PRh, $n = 125$ from 3 months old and $n = 132$ from 24 months old). (e) Immunofluorescence analysis to detect $p16^{INK4A}$ in neurons (expressing MAP2) in the CA3 region of 3 and 24 months old brains. Scale bars represent 10 μm.

28 months old mice brains (Figure 5(c)). In concordance, increased lamin A/C immunolabeling was observed in the CA3 and PRh neurons of aged mice (Figure 5(d)).

We then analyzed whether the same cells that express $p16^{INK4A}$, a mediator of cellular senescence [31], also have high CRM1 expression. Interestingly, increased immunostaining of $p16^{INK4A}$ and CRM1 concurred in the CA3 and PRh neurons of aged mice (Figures 6(a) and 6(b)). Even though there were some cells expressing $p16^{INK4A}$ at 3 months old, they had lower expression level than cells expressing $p16^{INK4A}$ in 24 months old brains, particularly in the CA3 region (Figure 6(c)). We found indeed a direct correlation between the immunolabeling intensity of $p16^{INK4A}$ and CRM1 in the CA3 and PRh brain cells of 24 months old mice (Figure 6(d)). We verified that neurons in particular express high levels of $p16^{INK4A}$ in the CA3 region at 24 months old brains (Figure 6(e)). These findings led us to speculate that enhanced CRM1 activity might trigger neuronal senescence.

3.4. Pharmacological Inhibition of CRM1 Improves Autophagic Flux and Reduces SA-β-GAL Activity in Senescent Neurons In Vitro. To analyze whether enhanced CRM1 activity contributes to neuronal senescence through perturbation of the autophagic flux, we used a long-term culture of rat primary cortical neurons. Neurons at 26 days in vitro (DIV) display autophagy dysfunction and cellular senescence characteristics, recapitulating then features of physiological aging [13, 19]. We observed that neurons at 26 DIV accumulated CRM1, and that around half of them displayed nuclear envelope invaginations, a senescent feature, compared with 6 DIV neurons (Figures 7(a)–7(c)). Consistent with enhanced CRM1 activity, reduced nuclear immunolabeling of TFEB (a CRM1 target) was specifically observed in 26 DIV senescent neurons (Figures 7(d) and 7(e)). As TFEB is a main positive modulator of autophagy, we hypothesized that treatment of neuron cultures with the CRM1-specific inhibitor leptomycin B (LMB) may accumulate TFEB in the nucleus and consequently restore proper autophagic flux in 26 DIV neurons. Supporting this notion, a significant nuclear enrichment of TFEB was found in the 6 DIV and 26 DIV neuronal cultures upon treatment with LMB, compared with cultures treated with the vehicle alone in 26 DIV neurons (Figures 7(f) and 7(g)). Remarkably, pharmacological inhibition of CRM1 prevented the accumulation of p62/SQSTM1 and LC3-II levels in 26 DIV neurons, compared with control 6 DIV neurons and vehicle-treated 26 DIV neurons (Figures 4(a)–4(c)). The LMB-mediated decrease of p62/SQSTM1 and LC3-II was blocked in the presence of chloroquine, an inhibitor of autophagolysosome maturation. We next analyzed lysosome morphology, a critical parameter of autophagy function. As shown in Figures 4(d)–4(f), senescent neurons exhibited enlarged LAMP1-stained lysosomes, which are characteristic of low degradation rate and accumulation of protein aggregates [32–34], while LMB-treated senescent neurons showed significant decrease of enlarged lysosomes, with concomitant increase of functional, small-size lysosomes, compared with vehicle-treated senescent neurons. Collectively, our results imply that pharmacological CRM1 inhibition restored the autophagy flux through improvement of TFEB activity.

Next, we explored the notion that enhanced CRM1 activity might be mechanistically linked to neuronal senescence. To approach this, we analyzed the response of 6 DIV and 26 DIV neuron cultures to LMB treatment and evaluated four markers of cellular senescence, namely, $p16^{INK4A}$ induction, lamin A/C stabilization, lamin B1 depletion, and SA-β-

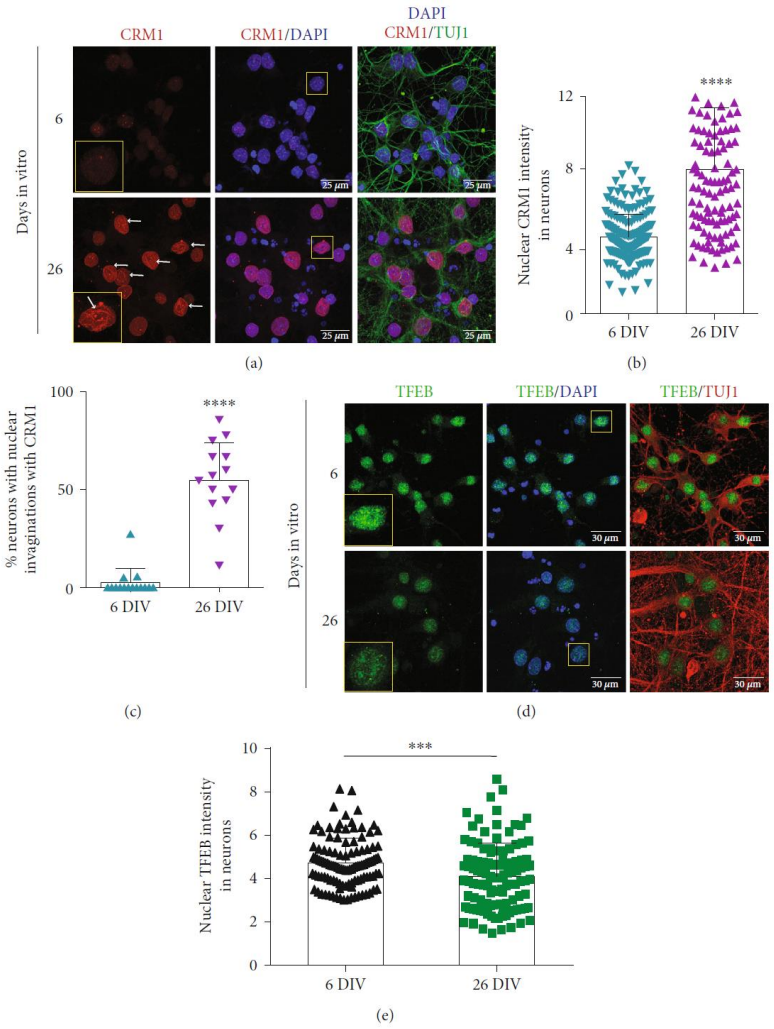

FIGURE 7: Continued.

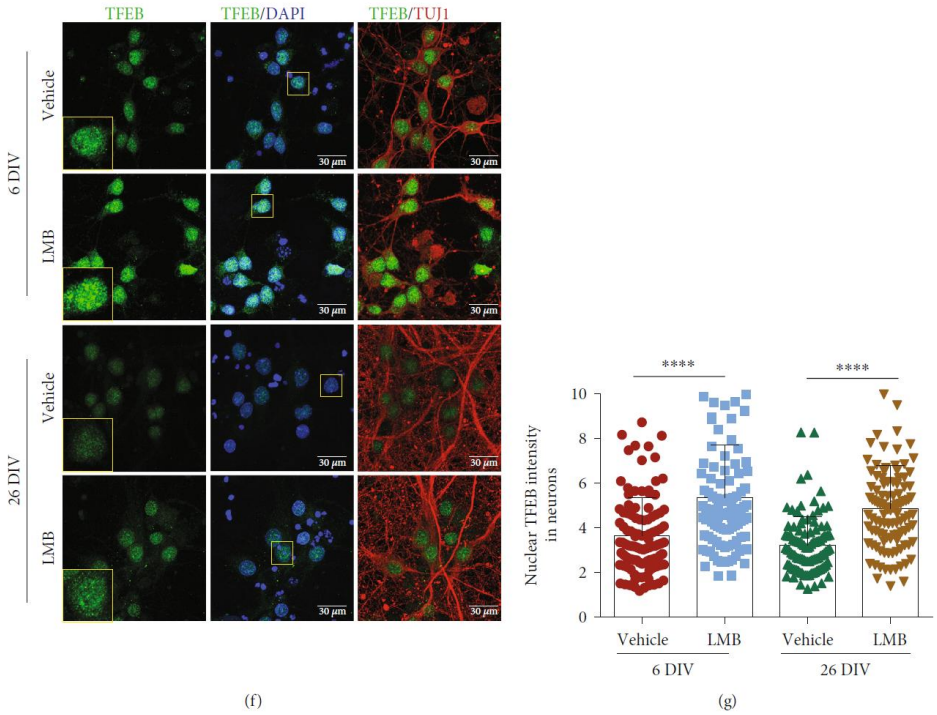

Figure 7: CRM1 accumulates in cultured senescent neurons and its pharmacological inhibition restored TFEB nuclear localization. (a) Immunofluorescence analysis was carried out to detect CRM1 in primary cortical neurons (expressing TUJ1) cultured during the indicated DIV. Arrows indicate CRM1 enrichment in nuclear envelope invaginations. Scale bars, 25 μm. (b) Graph shows pixel density of nuclear CRM1 in cortical neurons incubated during the indicated DIV. (c) Graph shows the percentage of neurons with CRM1-containing nuclear invaginations over total cells. Bars represent the mean ± SD ($n = 100$ cells per experimental group, from three independent experiments) with significant differences determined by unpaired t-test Student; $^{****}p < 0.0001$. (d) Immunofluorescence analysis to detect TFEB in neurons (expressing TUJ1) in primary cortical cells cultured during the indicated DIV. Scale bars, 30 μm. (e) Graph shows the pixel density of nuclear TFEB in cortical neurons incubated during the indicated DIV. Bars represent the mean ± SD ($n = 100$ cells per experimental group, from three independent experiments), with significant differences determined by unpaired t-test Student; $^{***}p < 0.001$. (f) Primary cortical cells cultured during 6 or 26 DIV were treated for 24 h with 5 nM LMB or the vehicle alone and immunolabeled to detect TFEB. (g) Graph represents the pixel density of nuclear TFEB. Bars correspond to the mean ± SD ($n = 100$ cells per experimental group, from three independent experiments), with significant differences determined by unpaired t-test Student; $^{****}p < 0.0001$. Squares indicate the magnified area shown in insets (a, d, f).

Gal activity. As observed above in vivo, the immunostaining of $p16^{ink4a}$ and lamin A/C increased in correlation with that of CRM1 in 26 DIV cortical neurons (Figures 8(a) and 8(b)). Furthermore, we observed also a decrease of lamin B1 immunolabeling (Figure 8(c)) and high of SA-β-gal activity (Figure 9(a)), confirming the senescent phenotype of the 26 DIV neuronal culture. A CRM1 increase concomitant with lamin B1 depletion in 26 DIV neuronal culture was confirmed by western blot (Figure 8(d)).

Interestingly, attenuation of CRM1 activity using LMB treatment for the last four days of culture (from 23 DIV to 26 DIV) reduced SA-β-gal activity (Figure 9(a)) in 26 DIV neurons; however, no changes in lamin A/C and lamin B1 levels were observed by immunofluorescence (Figure 9(b)) nor by western blot (Figure 9(d)).

4. Discussion

This work was aimed at determining whether aging-associated enhanced activity of CRM1 is the mechanism that functionally connects autophagy dysfunction with neuronal senescence. Trafficking of proteins between the nucleus and cytoplasm is modulated by the nuclear pore complex (NPC) and karyopherins that transport proteins in and out of the nucleus. Importins drive the nuclear import of proteins with nuclear localization sequences, while exportins mediate the nuclear export of NES-containing proteins, being CRM1 the major mammalian export protein. As TFEB is a master modulator of autophagy and lysosomal biogenesis [23, 24], whose nuclear export is mediated by CRM1 via recognition of the NES localized in the N-terminal domain of TFEB

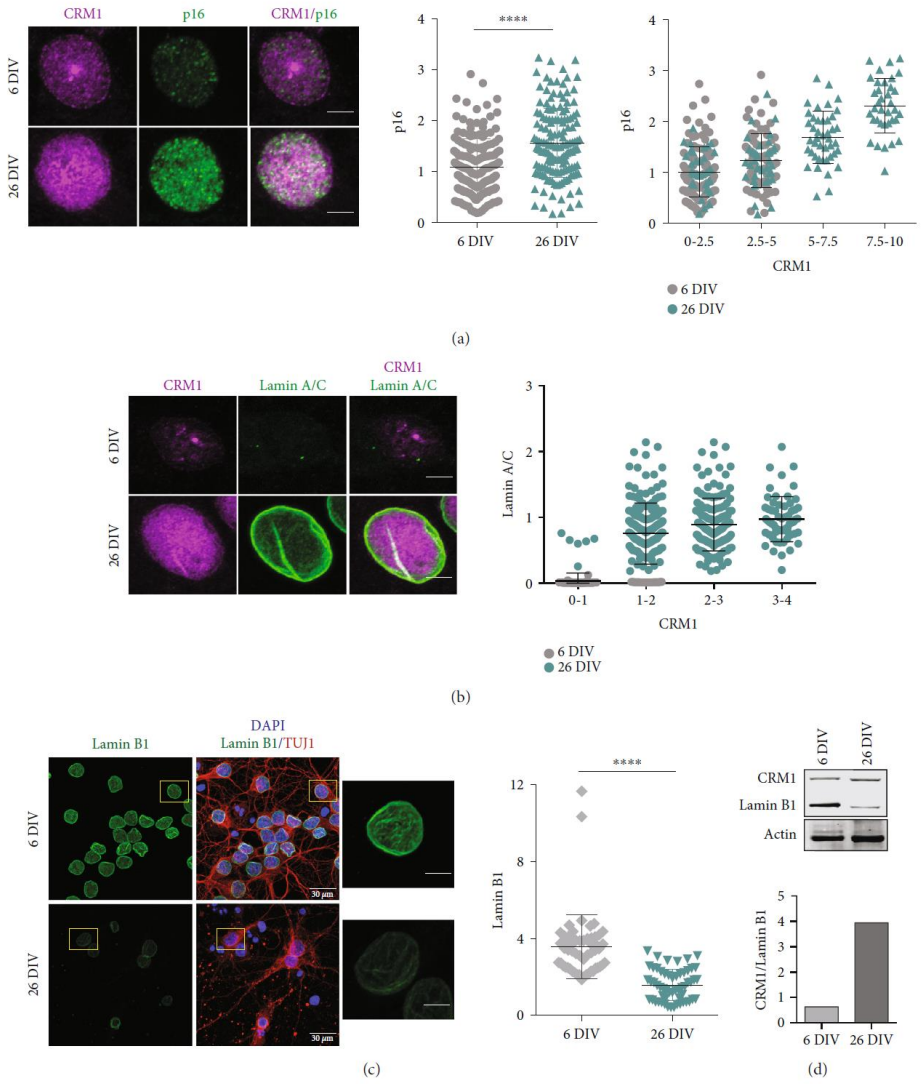

FIGURE 8: Elevated level of CRM1 correlated with neuronal senescence markers in vitro. (a) Immunofluorescence analysis to detect $p16^{INK4A}$ and CRM1 in primary cortical cells cultured during 6 and 26 DIV. Scale bars represent 30 μm. Nuclei were stained with DAPI. Left graph shows the pixel density of nuclear $p16^{INK4A}$ in cortical cells; right graph shows a correlation between $p16^{INK4A}$ and CRM1 expression levels. Bars represent the mean ± SD from three independent experiments, with significant differences determined by unpaired *t*-test Student; $^{****}p < 0.0001$. Notice that cells at 26 DIV have higher expression of CRM1 and $p16^{INK4A}$ compared with 6 DIV. (b) Immunofluorescent double staining for CRM1 and lamin A/C. Scale bars represent 5 μm. Quantification of lamin A/C intensity versus the CRM1 intensity is plotted. Notice that cells at 26 DIV have higher expression of CRM1 and lamin A/C. Bars represent the mean ± SD from 3 independent experiments. (c) Immunofluorescence to detect lamin B1 in primary cortical neurons (expressing TUJ1) of 6 and 26 DIV. Scale bars, 30 μm. Squares indicate the magnified area shown at the right; scale bars 5 μm. Graph represents the signal fluorescence intensity of nuclear lamin B1. Bars represent the mean ± SD from 3 independent experiments with significant differences determined by unpaired *t*-test Student; $^{****}p < 0.0001$. Each dot in each graph represents a cell measured from 3 independent experiments. (d) Western blot of total protein extracts from cortical cells cultured for 6 or 26 DIV. The ratio of CRM1 over the lamin B1 expression (both previously normalized by actin expression) is compared in the graph below, $n = 2$.

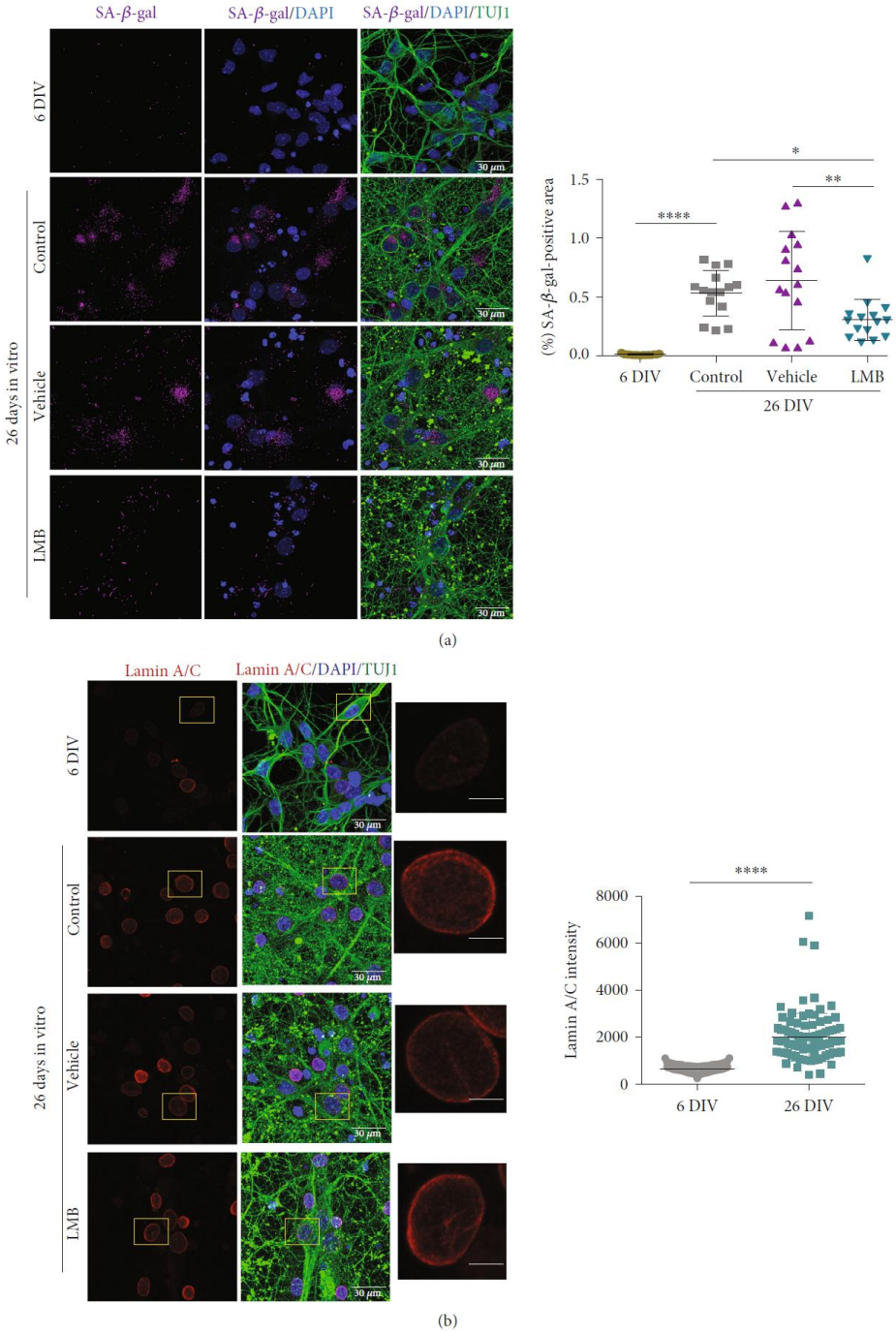

FIGURE 9: Continued.

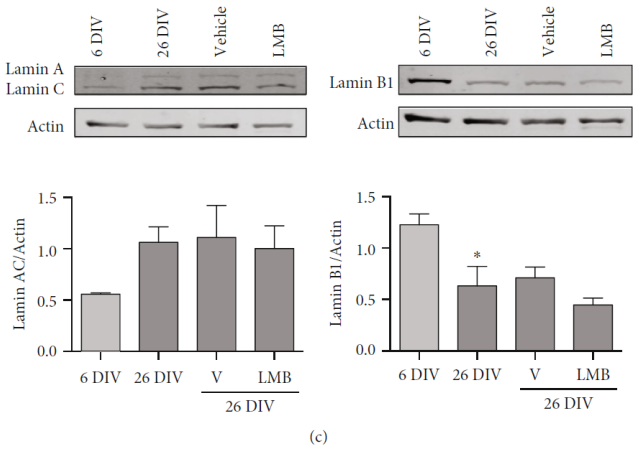

Figure 9: CRM1 inhibition reduced SA-β-gal activity but did not restored nuclear lamin alterations in senescent neurons in vitro. (a) Detection of SA-β-gal activity (by confocal microscopy) in neurons (expressing TUJ1) in primary culture of cortical cells of 26 DIV, treated for 4 days (starting at 22 DIV) with 5 nM LMB or the vehicle alone. Scale bars, 30 μm. Graph shows the percentage of the SA-β-gal-positive area. Five fields from three independent experiments were quantified. Bars represent the mean ± SD from 3 independent experiments with significant differences determined by ordinary one-way ANOVA analysis, with Holm-Sidak's multiple comparison test; $^{*}p < 0.05$; $^{**}p < 0.01$; $^{****}p < 0.0001$. Notice that LMB treatment significantly reduced SA-β-gal-positive area. (b) Immunofluorescence to detect lamin A/C in neurons (expressing TUJ1) in primary culture of cortical cells of 26 DIV, treated for 4 days (starting at 22 DIV) with 5 nM LMB or the vehicle alone. Scale bars, 30 μm. Squares indicate the magnified area shown in insets, scale bars 5 μm. Graph shows fluorescence intensity of nuclear lamin A/C in neurons cultured 6 or 26 DIV. Bars represent the mean ± SD from three independent experiments, with significant differences determined by unpaired t-test Student; $^{****}p < 0.0001$. (c) Western blot analysis showing the expression of lamin A/C or lamin B1 in primary culture of cortical cells of 6 or 26 DIV treated or not with LMB or the vehicle alone. Bars represent the mean ± SEM from three independent experiments, with significant differences determined by ordinary one-way ANOVA and Holm-Sidak's multiple comparison test; $^{*}p < 0.05$.

[35], we reasoned that enhanced CRM1 activity might cause depletion of nuclear TFEB, which in turn can perturb autophagy and ultimately drive neurons to senescence. Consistently, we found that CRM1 protein levels increased in the hippocampus and cortex of aged mice, concomitantly with a decrease of nuclear TFEB, implying that increased CRM1 activity improved nuclear export of TFEB. The CRM1-mediated nuclear depletion of TFEB resulted in impaired autophagic flux in the CA3 region of 24 months old mice brains, as shown by accumulation of p62/SQSTM1 in neurons that overexpressed CRM1. Strengthening our hypothesis, CRM1-driven decrease of nuclear TFEB occurred in conjunction with the accumulation of p62/SQSTM1 and the presence of LAMP1-stained enlarged lysosomes in 26 DIV cultured neurons as well.

Alterations in nuclear shape and nuclear membrane function are associated with several deleterious changes such as disrupted nucleocytoplasmic function and commonly occur in physiological aging [36]. Tau-mediated dementias are also accompanied by dysfunction in neuronal nucleocytoplasmic transport [37], and alterations of the nuclear lamina have been observed in postmortem Alzheimer's disease brain [38] and several models of Huntington's disease [39]. We observed that CRM1 is enriched in nuclear envelope invaginations of senescent neurons, which might potentially compartmentalize NPC and increase then the kinetics of CRM1-driven nuclear export, as has been observed for mRNA export in tau-induced nuclear envelope invaginations [40]. Furthermore, dysfunctional autophagy contributes to the formation of neuronal aggregates and characteristic of neurodegeneration, which are known to damage NPC [41], with the obvious effect on protein trafficking across the NPC. Nonetheless, enhanced activity of CRM1 in skin fibroblasts of HGPS patients is carried out by transcriptional upregulation of CRM1 [21]. Further experiments to analyze CRM1 gene regulation during brain aging are required to approach this question.

Pharmacological interventions that attenuate CRM1 activity reduce neuronal death and restore nucleocytoplasmic transport in either a model of Huntington's disease [39], a model of amyotrophic lateral sclerosis and frontotemporal dementia [42], and a *Drosophila* model of tauopathies [40]. Thus, in this work, we counteracted the increased activity of CRM1 by treating 26 DIV cultured neurons with LMB1 (a specific CRM1 inhibitor), as an attempt to accumulate TFEB in the nucleus and consequently activate its transcriptional function. Strikingly, pharmacological inhibition of CRM1 restored proper autophagic flux in 26 DIV neurons, as shown by reduced p62/SQSTM1 and LC3 accumulation in LMB-treated cells, and the presence of small lysosomes. Improving autophagy by modulating CRM1 activity appears to delay senescence, because a decrease in SA-β-gal activity

was observed in LMB-treated 26 DIV neurons. Repartitioning of other CRM-target proteins in the nucleus, such as STAT3, may also contribute to improve autophagy and delay senescence. We found no restoration of lamin A/C nor lamin B levels in response to LMB, suggesting that the senescent phenotype was not fully reverted in neurons once it was established. This finding seems to be in contrast with the previous observation that LMB treatment restores the lamin B1 expression in HGPS senescent fibroblasts [21]. We argue that a reduction in the number of senescent fibroblasts upon LMB treatment could be explained by their proliferative nature, which is in contrast with neurons. Since a subpopulation of fibroblasts are not yet senescent at the moment LMB is added, the reduction in the number of senescent fibroblasts could be due to a prevention of new geroconversion of proliferating cells, instead of a reversion of the senescent phenotype. Further experiments are needed to distinguish between prevention and reversion of cellular senescence.

DNA damage induces a regulated enhanced nucleocytplasmic export to promote genome stability; our findings suggest that it might become dysfunctional with aging. When DNA is damaged, some DNA repair proteins such as BRCA1, MRE11, RAD50, and NBS, as well as damaged DNA itself, are translocated from the nucleus to the cytoplasm by a CRM1-mediated nuclear export [43–46]. Cytoplasmic DNA is degraded by autophagy; otherwise, it induces cellular senescence [46]. Since DNA damage occurs continually, our findings of an age-associated exacerbated CRM1 activity and autophagy dysfunction could cause persistent cytoplasmic DNA promoting cellular senescence.

Taken together, our study demonstrates that age-associated enhanced activity of the CRM1-mediated nuclear export mechanism perturbs neuronal homeostasis by contributing to autophagy impairment, which in turn triggers neuronal senescence. Therefore, CRM1 may serve as a therapeutic target to prevent/ameliorate all these effects found in physiological brain aging and neurodegeneration.

Data Availability

All data is included in the manuscript, either in the main text and figures, as well as in the Supplementary Information files that are submit alongside our manuscript.

Conflicts of Interest

The authors declare that they have no conflict of interest.

Authors' Contributions

EGS and DMB conceived the work, acquired most of the data, and drafted the manuscript. CGO contributed in collecting biological samples and acquiring data. BC and FAC contributed with analysis and interpretation of the data and revised critically the manuscript. SCO contributed with experimental design, analysis, and interpretation of the data, revised critically the manuscript, and proofed it. All authors approved the version to be published and agreed to be accountable for all aspects of the work.

Acknowledgments

We are thankful to Dr. Beatriz Aguilar and Biol. Teresa Montiel for their technical assistance. We acknowledge the technical advice given by Dr. Abraham Rosas and Dr. Ruth Rincón at the Imagenology Unit for confocal microscopy analysis; we are thankful to Claudia Rivero at the Animal Facility and to M.C. Ana Maria Escalante and Francisco Pérez at the IT Unit, as well as to Aurey Galvan and Manuel Ortínez at the Equipment Maintenance Workshop, all at the Instituto de Fisiología Celular, UNAM. We thank Dr. Macarena Arrazola from Universidad Mayor for facilitating mice tissue. Funding: EGS had a CONACyT doctoral fellowship (586932) and data in this work is part of her doctoral dissertation in the Posgrado en Ciencias Biomédicas de la Universidad Nacional Autónoma de México. DMB had a CONACyT doctoral fellowship (588372) and data in this work is part of his doctoral dissertation in the "Programa de Doctorado en Ciencias Bioquímicas de la Universidad Nacional Autónoma de México." This work was supported partially by grants CONACyT FC921, UNAM-PAPIIT IN206518-IN209221, and a grant from the Secretaria de Educación, Ciencia, Tecnología e Innovación de la Ciudad de México SECTEI/008/2018 "Red Colaborativa de Investigación Traslacional para el Envejecimiento Saludable de la Ciudad de México (RECITES)" to SCO; CONACyT CF2019-514879 to BC; FONDECYT-1190518, Geroscience Center for Brain Health and Metabolism (FONDAP-15150012) to FC, and FONDECYT Postdoctoral fellowship Nº 3190608 to CGO. The publication of this paper was supported by a grant from the Secretaria de Educación, Ciencia, Tecnología e Innovación de la Ciudad de México CM-SECTEI/200/2020 "Red Colaborativa de Investigación Traslacional para el Envejecimiento Saludable de la Ciudad de México (RECITES)".

Supplementary Materials

Supplementary Figure 1: the cellular area of neurons in young and old mice is similar. The nuclear (a) and cytoplasmic (b) areas (expressed in μm^2) of neurons (identified by MAP2 expression) were quantified in the hippocampal and cortical regions of brains from 3 and 24 months old mice. The graph below each representative image expresses the mean ± SEM. No significant differences were found, analyzed by unpaired t-test Student. From 3 brains, the total number of neurons counted was CA3, $n = 248$ from 3 months old and $n = 203$ from 24 months old; hilus, $n = 148$ from 3 months old and $n = 132$ from 24 months old; and PRh, $n = 133$ from 3 months old and $n = 133$ from 24 months old. Representative neurons of the CA3 regions are shown. Scale bars represent 15 μm. Supplementary Figure S2: CRM1 accumulates in the hippocampus and cortex with age. Western blot analysis showing the expression of the CRM1 protein in hippocampus and cortex of wild-type mice at the indicated ages. Graph represents the mean of densitometry analysis of western blot analysis from six animals per age group expressed in arbitrary units. Bars correspond to the mean ± SEM from six independent experiments, with significant differences determined by one-way ANOVA and Dunnet as posthoc test; $^{***}p < 0.001$. Supplementary Figure S3: pattern

distribution and expression level of GFP-LC3 did not change during brain aging. (a) Confocal images showing GFP-LC3 signal in neurons (expressing MAP2) of the hippocampus and perirhinal cortex (PRh) from 3 and 24 months old GFP-LC3 transgenic mice. (b) Graph represents pixel density of GFP-LC3 signal in the different brain regions analyzed in three brains per age. We noticed an increment of GFP-LC3 along axons in the PRh region, but quantifying GFP-LC3 intensity, we found no significant difference. Bars represent the mean ± SEM. *(Supplementary Materials)*

References

[1] B. K. Kennedy, S. L. Berger, A. Brunet et al., "Geroscience: linking aging to chronic disease," *Cell*, vol. 159, no. 4, pp. 709–713, 2014.

[2] P. Stenvinkel and P. G. Shiels, "Long-lived animals with negligible senescence: clues for ageing research," *Biochemical Society Transactions*, vol. 47, no. 4, pp. 1157–1164, 2019.

[3] C. E. Finch, "Variations in senescence and longevity include the possibility of negligible senescence," *The Journals of Gerontology. Series A, Biological Sciences and Medical Sciences*, vol. 53A, no. 4, pp. B235–B239, 1998.

[4] C. López-Otín, M. A. Blasco, L. Partridge, M. Serrano, and G. Kroemer, "The hallmarks of aging," *Cell*, vol. 153, no. 6, pp. 1194–1217, 2013.

[5] S. Y. Cheon, H. Kim, D. C. Rubinsztein, and J. E. Lee, "Autophagy, cellular aging and age-related human diseases," *Experimental Neurobiology*, vol. 28, no. 6, pp. 643–657, 2019.

[6] T. J. Bussian, A. Aziz, C. F. Meyer, B. L. Swenson, J. M. van Deursen, and D. J. Baker, "Clearance of senescent glial cells prevents tau-dependent pathology and cognitive decline," *Nature*, vol. 562, no. 7728, pp. 578–582, 2018.

[7] E. Sikora, A. Bielak-Zmijewska, M. Dudkowska et al., "Cellular senescence in brain aging," *Frontiers in Aging Neuroscience*, vol. 13, 2021.

[8] H. Nakatogawa, "Mechanisms governing autophagosome biogenesis," *Nature Reviews. Molecular Cell Biology*, vol. 21, no. 8, pp. 439–458, 2020.

[9] R. T. Netea-Maier, T. S. Plantinga, F. L. van de Veerdonk, J. W. Smit, and M. G. Netea, "Modulation of inflammation by autophagy: consequences for human disease," *Autophagy*, vol. 12, no. 2, pp. 245–260, 2016.

[10] M. O. Grootaert, P. A. da Costa Martins, N. Bitsch et al., "Defective autophagy in vascular smooth muscle cells accelerates senescence and promotes neointima formation and atherogenesis," *Autophagy*, vol. 11, no. 11, pp. 2014–2032, 2015.

[11] L. García-Prat, M. Martínez-Vicente, E. Perdiguero et al., "Autophagy maintains stemness by preventing senescence," *Nature*, vol. 529, no. 7584, pp. 37–42, 2016.

[12] X. Han, H. Tai, X. Wang et al., "AMPK activation protects cells from oxidative stress-induced senescence via autophagic flux restoration and intracellular NAD+ elevation," *Aging Cell*, vol. 15, no. 3, pp. 416–427, 2016.

[13] D. Moreno-Blas, E. Gorostieta-Salas, A. Pommer-Alba et al., "Cortical neurons develop a senescence-like phenotype promoted by dysfunctional autophagy," *Aging (Albany NY)*, vol. 11, no. 16, pp. 6175–6198, 2019.

[14] M. Matjusaitis, G. Chin, E. A. Sarnoski, and A. Stolzing, "Biomarkers to identify and isolate senescent cells," *Ageing Research Reviews*, vol. 29, pp. 1–12, 2016.

[15] J. P. Coppé, P. Y. Desprez, A. Krtolica, and J. Campisi, "The senescence-associated secretory phenotype: the dark side of tumor suppression," *Annual Review of Pathology*, vol. 5, no. 1, pp. 99–118, 2010.

[16] M. H. Yoon, S. M. Kang, S. J. Lee et al., "p53 induces senescence through Lamin A/C stabilization-mediated nuclear deformation," *Cell Death & Disease*, vol. 10, no. 2, p. 107, 2019.

[17] E. Lukášová, A. Kovarˇík, A. Bacˇíková, M. Falk, and S. Kozubek, "Loss of Lamin B receptor is necessary to induce cellular senescence," *The Biochemical Journal*, vol. 474, no. 2, pp. 281–300, 2017.

[18] A. En, Y. Takauji, D. Ayusawa, and M. Fujii, "The role of lamin B receptor in the regulation of senescence-associated secretory phenotype (SASP)," *Experimental Cell Research*, vol. 390, no. 1, p. 111927, 2020.

[19] S. Ishikawa and F. Ishikawa, "Proteostasis failure and cellular senescence in long-term cultured postmitotic rat neurons," *Aging Cell*, vol. 19, no. 1, article e13071, 2020.

[20] E. Bigagli, C. Luceri, T. Scartabelli et al., "Long-term neuroglial cocultures as a brain aging model: hallmarks of senescence, microRNA expression profiles, and comparison with in vivo models," *The Journals of Gerontology. Series A, Biological Sciences and Medical Sciences*, vol. 71, no. 1, pp. 50–60, 2016.

[21] I. García-Aguirre, A. Alamillo-Iniesta, R. Rodríguez-Pérez et al., "Enhanced nuclear protein export in premature aging and rescue of the progeria phenotype by modulation of CRM1 activity," *Aging Cell*, vol. 18, no. 5, article e13002, 2019.

[22] A. Y. Wang and H. Liu, "The past, present, and future of CRM1/XPO1 inhibitors," *Stem Cell Investigation*, vol. 6, p. 6, 2019.

[23] C. Settembre, C. di Malta, V. A. Polito et al., "TFEB links autophagy to lysosomal biogenesis," *Science*, vol. 332, no. 6036, pp. 1429–1433, 2011.

[24] M. J. Silvestrini, J. R. Johnson, A. V. Kumar et al., "Nuclear export inhibition enhances HLH-30/TFEB activity, autophagy, and lifespan," *Cell Reports*, vol. 23, no. 7, pp. 1915–1921, 2018.

[25] S. Shen, M. Niso-Santano, S. Adjemian et al., "Cytoplasmic STAT3 represses autophagy by inhibiting PKR activity," *Molecular Cell*, vol. 48, no. 5, pp. 667–680, 2012.

[26] F. Debacq-Chainiaux, J. D. Erusalimsky, J. Campisi, and O. Toussaint, "Protocols to detect senescence-associated beta-galactosidase (SA-βgal) activity, a biomarker of senescent cells in culture and _in vivo_," *Nature Protocols*, vol. 4, no. 12, pp. 1798–1806, 2009.

[27] M. W. Brown and J. P. Aggleton, "Recognition memory: what are the roles of the perirhinal cortex and hippocampus?," *Nature Reviews. Neuroscience*, vol. 2, no. 1, pp. 51–61, 2001.

[28] L. E. B. Bettio, L. Rajendran, and J. Gil-Mohapel, "The effects of aging in the hippocampus and cognitive decline," *Neuroscience and Biobehavioral Reviews*, vol. 79, pp. 66–86, 2017.

[29] Y. Cheng, M. P. Holloway, K. Nguyen et al., "XPO1 (CRM1) inhibition represses STAT3 activation to drive a survivin-dependent oncogenic switch in triple-negative breast cancer," *Molecular Cancer Therapeutics*, vol. 13, no. 3, pp. 675–686, 2014.

[30] P. Rusmini, K. Cortese, V. Crippa et al., "Trehalose induces autophagy via lysosomal-mediated TFEB activation in models of motoneuron degeneration," *Autophagy*, vol. 15, no. 4, pp. 631–651, 2019.

[31] H. Rayess, M. B. Wang, and E. S. Srivatsan, "Cellular senescence and tumor suppressor gene p16," *International Journal of Cancer*, vol. 130, no. 8, pp. 1715–1725, 2012.

[32] Y. Rong, M. Liu, L. Ma et al., "Clathrin and phosphatidylinositol-4,5-bisphosphate regulate autophagic lysosome reformation," *Nature Cell Biology*, vol. 14, no. 9, pp. 924–934, 2012.

[33] D. S. Leeman, K. Hebestreit, T. Ruetz et al., "Lysosome activation clears aggregates and enhances quiescent neural stem cell activation during aging," *Science*, vol. 359, no. 6381, pp. 1277–1283, 2018.

[34] M. E. G. de Araujo, G. Liebscher, M. W. Hess, and L. A. Huber, "Lysosomal size matters," *Traffic*, vol. 21, no. 1, pp. 60–75, 2020.

[35] G. Napolitano, A. Esposito, H. Choi et al., "mTOR-dependent phosphorylation controls TFEB nuclear export," *Nature Communications*, vol. 9, no. 1, p. 3312, 2018.

[36] P. Oberdoerffer and D. A. Sinclair, "The role of nuclear architecture in genomic instability and ageing," *Nature Reviews. Molecular Cell Biology*, vol. 8, no. 9, pp. 692–702, 2007.

[37] F. Paonessa, L. D. Evans, R. Solanki et al., "Microtubules deform the nuclear membrane and disrupt nucleocytoplasmic transport in tau-mediated frontotemporal dementia," *Cell Reports*, vol. 26, no. 3, pp. 582–593.e5, 2019, e5.

[38] B. Frost, F. H. Bardai, and M. B. Feany, "Lamin dysfunction mediates neurodegeneration in tauopathies," *Current Biology*, vol. 26, no. 1, pp. 129–136, 2016.

[39] J. C. Grima, J. G. Daigle, N. Arbez et al., "Mutant Huntingtin disrupts the nuclear pore complex," *Neuron*, vol. 94, no. 1, pp. 93–107.e6, 2017, e6.

[40] G. L. Cornelison, S. A. Levy, T. Jenson, and B. Frost, "Tau-induced nuclear envelope invagination causes a toxic accumulation of mRNA in Drosophila," *Aging Cell*, vol. 18, no. 1, article e12847, 2019.

[41] G. Bitetto and A. Di Fonzo, "Nucleo-cytoplasmic transport defects and protein aggregates in neurodegeneration," *Translational Neurodegeneration*, vol. 9, no. 1, p. 25, 2020.

[42] K. Zhang, C. J. Donnelly, A. R. Haeusler et al., "The _C9orf72_ repeat expansion disrupts nucleocytoplasmic transport," *Nature*, vol. 525, no. 7567, pp. 56–61, 2015.

[43] Z. Feng, L. Kachnic, J. Zhang, S. N. Powell, and F. Xia, "DNA Damage Induces p53-dependent BRCA1 Nuclear Export," *The Journal of Biological Chemistry*, vol. 279, no. 27, pp. 28574–28584, 2004.

[44] J. D. Seno and J. R. Dynlacht, "Intracellular redistribution and modification of proteins of the Mre11/Rad50/Nbs1 DNA repair complex following irradiation and heat-shock," *Journal of Cellular Physiology*, vol. 199, no. 2, pp. 157–170, 2004.

[45] Y. Y. Lan, D. Londoño, R. Bouley, M. S. Rooney, and N. Hacohen, "Dnase2a deficiency uncovers lysosomal clearance of damaged nuclear DNA via autophagy," *Cell Reports*, vol. 9, no. 1, pp. 180–192, 2014.

[46] Y. Y. Lan, J. M. Heather, T. Eisenhaure et al., "Extranuclear DNA accumulates in aged cells and contributes to senescence and inflammation," *Aging Cell*, vol. 18, no. 2, article e12901, 2019.